Outburst Floods from High-Mountain Lakes: Risk Analysis of Cascading Processes under Present and Future Conditions

---

Dissertation
zur
Erlangung der naturwissenschaftlichen Doktorwürde
(Dr. sc. nat.)
vorgelegt der
Mathematisch-naturwissenschaftlichen Fakultät
der
Universität Zürich
von

Yvonne Schaub
von
Andelfingen ZH

Promotionskomitee
Prof. Dr. Andreas Vieli (Vorsitz)
PD Dr. Christian Huggel (Leitung der Dissertation)
Prof. Dr. em. Wilfried Haeberli
Dr. Michael Bründl
Prof. Dr. Jan Seibert

Zürich, 2015

SUMMARY

Climate change has been causing the complex and sensitive high-mountain systems to move considerably away from past conditions, and it will continue to do so. Lake formation as a consequence of glacier recession can currently be observed all over the world and is modelled to continue. Many of these new lakes are found below hanging glaciers and seracs or at the foot of oversteepened and destabilised rock slopes and are thus prone to impacts from rapid mass movements. If a rock/ice avalanche impacts a lake, an outburst flow can be the consequence. This disadvantageous situation is likely to persist for a long time, because larger lakes will exist for extended time periods and climate change also affects slope stability in the long term. Such process chains, related to lakes, glaciers and permafrost, can have large socioeconomic impacts. Even though the probability of such cascading processes is currently small, it is systematically increasing and requires fundamental process understanding and anticipatory risk management. There persists an urgent need for detailed investigations and assessment methods regarding triggering events, causal relations, probabilities, or other specific characteristics of high-mountain lake outburst flows under full consideration of spatiotemporal aspects and developments. This thesis attempts a holistic contemplation of the subject with an in-depth investigation responding to two main objectives.

The first objective was to improve the systematic analysis and anticipation of hazard potentials emerging from high-mountain lakes within the framework of integrated risk management. A rock-avalanche impact disposition model considering the topographic potential as well as the additional disposition parameters lithology, deglaciation and permafrost degradation, was elaborated and implemented into a spatially-explicit deterministic approach and into a probabilistic Bayesian Network for a regional inter-comparison of the rock-avalanche impact disposition in the catchments of high-alpine lakes in Switzerland. The results indicated a general increase in the rock-avalanche impact susceptibility of lakes and allowed for first-order prioritization of hazards, also for future conditions. For the deglaciated Alps, the disposition area is expected to raise by a factor 2.8 from approx. 264 to 763km^2, while the disposition intensity is assumed to raise by a factor 3.3. As such, hotspots of rock-avalanche impact disposition into lakes above densely populated valleys have to be expected in several regions in the Swiss Alps, with a spe-

cial focus in the Valais (e.g. in the Aletsch Region, in the southern Valais) but also in the upper Engadin or the Bernese Alps.
Once a hazardous situation or a risk hotspot is detected, a detailed hazard analysis might be required. A wide range of techniques – from empirical equations and analytical methods to (semi-) physically-based numerical simulations – are available for assessing the single processes involved in the chain. As hazard assessment of the process chain with physically-based, fully coupled simulations is not yet possible, other combinations have to be applied. But the assessment of cascading processes by means of a model chain inevitably comprises assumptions and manual adjustments at the cutting points. The influence of uncertainties and their propagation throughout the numerical simulation of the process chain of a rock/ice avalanche-triggered impact wave were assessed by means of an analysis of variance of 54 simulation runs with RAMMS and IBER. The coupling of simulations delivered reasonable results of an overtopping wave, despite the inherent, large uncertainties, which did have considerable effects on the results. The largest uncertainties inherent in the simulation of the wave, which overtops the dam, emerge from avalanche-scenario definition rather than from manual coupling of the models. Hazard analyses based on a single simulation run were therefore assumed to be highly difficult. The application of a simulation chain to a set of scenarios, however, allows one to draw valuable conclusions on the overall hazard situation. This was illustrated with the numerical simulation of an outburst-flow scenario triggered by ice avalanches, at Mount Hualcán, Peru. The RAMMS ice-avalanche simulations suggested that all potential ice avalanches might reach Lake 513, independent of their detachment locations or initial volumes, but that only two large scenarios and the extreme scenario contained an overtopping of the Lake 513. The effect of the outburst event was simulated perceptibly until the confluence with the Río Santa in all three scenarios. But a hazard analysis is not an ending point; rather, it is the base and input for a risk analysis, which was the topic addressed in the second objective.

The second objective of this thesis was the improvement and expansion of consequence analyses and risk calculation approaches with regard to high-mountain outburst flows, also under consideration of future conditions. As lake-outburst events can have consequences reaching farther than in the directly affected areas, secondary and tertiary damage potential should also be considered in a risk analysis. Results show that it is possible to estimate and quantify costs caused by a chosen lake-outburst event in Grindelwald, Switzerland, from 2008 almost entirely, especially regarding touristic infrastructures. The resulting secondary (36 million CHF) and tertiary damage potential (at least 25 million CHF) amounted to additional costs as high as two-thirds of the primary damage potential (92 million CHF) and thereby easily justified the costs spent on risk-reduction measures (28 million CHF).
One of the main challenges of anticipatory risk management is integrating spatiotemporal developments. A three-step methodology, to integrate future physical hazards with future damage potential given future socioeconomic conditions, was elaborated and presented on the case of a modelled glacier-bed overdeepening (which was assumed to be a potential location of a future lake) above Naters, Switzerland. Even though uncertainties were substantial with respect to future damage potential in 2045, the socioeconomically-driven land-use scenarios were assumed to represent a relatively robust range of possible future outcomes. They allowed for

identification of future risk hotspots, such as the school, a hotel and the church. This study further corroborated the fundamental importance of land-use policies and governance for risk reduction.

This thesis expanded the knowledge basis and process understanding and showed potential hotspots for lake hazards in Switzerland. The direction and time scales of the changes in high mountains are known, and methodologies for assessing causal relations and outcomes are available. This is a first step towards risk management of low-probability and high-magnitude events. The evaluation of these risks remains subject to social and political discourse, which is difficult, especially as large uncertainties remain regarding detailed hazard assessment of local cases. Multi-purpose solutions, which reduce risks and simultaneously benefit from the advantages provided by high-mountain lakes, have the potential to facilitate these dialogues. Decisions should nevertheless be taken promptly and with broad support, since many stakeholders are present, and degrees of freedom in decision-making decrease with proceeding time.

ZUSAMMENFASSUNG

Hochgebirgslandschaften verändern sich stark unter dem Einfluss des Klimawandels. Zurzeit kann weltweit die Bildung von neuen Seen als eine Folge des Gletscherschwundes beobachtet werden - eine Entwicklung, die auch in Zukunft weitergehen wird. Viele dieser neuen Seen befinden sich unter Hängegletschern, Seracs oder am Fusse von übersteilen und destabilisierten Felshängen. Sie liegen damit in Reichweite von Eislawinen oder Felsstürzen. Prozessketten, die Seen, Gletscher und Permafrost umfassen, können schwer wiegende sozio-ökonomische Konsequenzen verursachen, vor allem wenn ein Seeausbruch bewirkt wird. Diese gefährlichen Situationen können für lange Zeit Bestand haben, da grössere Seen über einen längeren Zeitraum existieren werden und weil der Klimawandel auch die Hangstabilität langfristig beeinflusst.
In der Schweiz ist die Wahrscheinlichkeit des Eintretens einer solchen Prozesskette zurzeit gering. Sie steigt aber systematisch an und erfordert deshalb vorausschauendes Risikomanagement und grundlegendes Verständnis der beteiligten Prozesse. Es besteht ein dringender Bedarf für detaillierte Untersuchungs- und Bewertungsmethoden unter voller Berücksichtigung der räumlich-zeitlichen Aspekte und Entwicklungen in Bezug auf auslösende Ereignisse, Kausalbeziehungen, Wahrscheinlichkeiten oder andere spezifische Eigenschaften von Flutwellen aus Hochgebirgsseen. Die vorliegende Arbeit strebt eine ganzheitliche Betrachtung des Themas an, wobei zwei Hauptziele vertieft bearbeitet wurden.

Das erste Ziel beinhaltet die Verbesserung der systematischen Analyse und Antizipation von Gefahrenpotentialen, die sich aus Hochgebirgsseen ergeben, im Rahmen des integralen Risikomanagement. Zur Analyse der Anfälligkeit der Schweizer Hochgebirgsseen für den Einschlag eines Felssturzes wurde ein Modell erarbeitet, welches in einen räumlich-expliziten deterministischen Ansatz und in ein probabilistisches Bayes-Netzwerk implementiert wurde. Das Modell berücksichtigt das topographische Potenzial von Stürzen, sowie die zusätzliche Dispositionsparameter Lithologie, Gletscherschwund und Permafrostdegradation. Die Ergebnisse zeigten einen generellen Anstieg der Anfälligkeit der Seen gegenüber Sturzereignissen und ermöglichten erste Lokalisierungen und Bewertungen von Gefahren, auch für zukünftige Bedingungen. Für die stark entgletscherten Alpen wird die Fläche, von der sich ein Sturz lösen und einen See treffen kann, um einen Faktor 2.8 von ca. 264 auf 763km^2 wachsen, wobei die Intensität der

Sturzdisposition um eine Faktor 3.3 ansteigen wird. Gefahrenhotspots oberhalb von dicht besiedelten Tälern sind in mehreren Gegenden der Schweizer Alpen zu erwarten, insbesondere aber im Wallis (z.B. in der Aletsch-Region, im südlichen Wallis) aber auch im Oberengadin oder in den Berner Alpen.
Wo ein erhöhtes Gefahrenpotential oder ein erhöhtes Risiko erkannt wird, kann eine detaillierte Gefahrenanalyse der Prozesskette erforderlich sein. Eine breite Palette von Techniken zur Beurteilung der involvierten Einzelprozesse existiert - von empirischen Gleichungen über analytische Methoden bis zu (semi-)physikalischen numerischen Simulationen. Eine Gefahrenbeurteilung der gesamten Prozesskette basierend auf vollständig gekoppelten, physikalischbasierten Simulationen ist zur Zeit nicht möglich; es müssen andere Kombinationen angewandt werden. Die Beurteilung von Prozessketten mithilfe von Modellketten umfasst aber zwangsläufig Annahmen und manuelle Anpassungen an den Schnittpunkten. In dieser Arbeit wurde deshalb mithilfe einer Varianzanalyse von 54 Simulationsläufem der Einfluss von Unsicherheiten und von deren Entwicklung in der numerischen Simulation einer Stosswelle untersucht, welche durch ein Sturzereignis ausgelöst wurde. Die Kopplung eines Felssturz- (RAMMS) und eines Tsunamimodells (IBER) lieferte realistische Simulationen der Überschwappwelle auf dem Damm, obwohl die inhärenten Unsicherheiten erhebliche Auswirkungen auf die Ergebnisse ausübten. Die grössten Unsicherheiten in der Simulation der Überschwappwelle entstanden dabei eher durch die Sturzdefinition als durch die manuelle Verbindung der Programme. Gefahrenanalysen von Prozessketten sollten deshalb nicht auf einer Einzelsimulation beruhen, doch Szenariensimulationen ermöglichen Aussagen auf die Gesamtgefahrensituation. Dies wurde am Beispiel einer Flutwelle dargestellt, welche sich durch den Einschlag einer Eislawine in den See 513 am Berg Hualcán, in Peru, ereignen könnte. Die Eislawinensimulationen mit RAMMS zeigten, dass alle potenzielle Eislawinen den See 513 erreichen würden, unabhängig von der Lage ihrer Anrisszone oder ihres Anrissvolumens. Ein Überschwappen des Sees wurde aber nur durch zwei Szenarien mit grossen Volumina und einem extremen Szenario modelliert. Der Effekt dieser Stosswelle konnte in allen drei Fällen bis ins Tal zum Zusammenfluss mit dem Santa Fluss modeliert werden.

Dieses zweite Ziel bestand in der Verbesserung der Konsequenzen- und Risikoanalyse von Seeausbrüchen im Hochgebirge, ebenfalls unter Berücksichtigung von zukünftigen Bedingungen. Da die Folgen von Flutwellen nach Seeausbrüchen weiterreichend sein können, sollten auch das sekundäre und das tertiäre Schadenpotenzial berücksichtigt werden. Für ein Fallbeispiel von 2008 in Grindelwald, Schweiz, konnten die gesamten Kosten eines Seeausbruches abgeschätzt und quantifiziert werden, vor allem hinsichtlich der Einbussen im Tourismusbereich. Die sekundären (36 Mio. CHF) und tertiären Kosten (mind. 25 Mio. CHF) betrugen zwei Drittel des primären Schadenpotentials (92 Mio. CHF) und rechtfertigen damit die Kosten der getroffenen Massnahmen zur Risikoreduktion (28 Mio. CHF).
Eine der grössten Herausforderungen im Risikomanagement besteht aber in der Integration von räumlich-zeitlichen Entwicklungen, auch hinsichtlich des Schadenpotenzials. Eine dreiteilige Methode wurde erarbeitet, um künftige Gefahren dem Schadenpotenzial gegenüber zu stellen, unter Berücksichtigung von zukünftigen sozio-ökonomischen Bedingungen. Die Methode wurde für Naters, Wallis, angewandt, im Hinblick auf eine modellierte Übertiefung im

Aletschgletscherbett, welche als potenzieller Standort eines künftigen Sees im 2045 angenommen wurde. Obwohl das resultierende Schadenpotenzial grosse Unsicherheiten aufwies, ergaben die sozio-ökonomisch definierten Landnutzungsszenarien relativ robuste Ergebnisse. Darauf basierend konnten zukünftige Risikohotspots identifiziert werden, wie die Schule, ein Hotel und die Kirche. Diese Studie bestätigte ferner die grundlegende Bedeutung der Landnutzungspolitik und der Steuerung des Risikoreduktion.

Die vorliegende Arbeit erweitert die Wissensbasis sowie das Prozessverständnis hinsichtlich eines Sturzereignisses in einen Hochgebirgssee und zeigt potenzielle Problemzonen in der Schweiz auf. Die Abläufe und die Zeitskalen der Veränderungen im Hochgebirge sind bekannt und Methoden zur Analyse von kausalen Zusammenhängen sowie zur Abschätzung der zu erwartenden Ergebnisse sind vorhanden. Dies ist ein erster Schritt in Richtung Risikomanagement von Ereignissen mit zwar geringen Eintretenswahrscheinlichkeiten, aber grossen potenziellen Auswirkungen. Die Bewertung dieser Risiken bleibt Gegenstand eines schwierigen politischen und gesellschaftlichen Diskurses, zumal in der lokalen Gefahrenbeurteilung vielerorts noch grosse Unsicherheiten bestehen. Mehrzwecklösungen, welche Risikoreduktion mit der Nutzung von Seen kombinieren, können diesen Dialog erleichtern. Diskussionen sollten zeitnah und breit abgestützt geführt werden, da verschiedene Interessengruppen eingebunden werden müssen und Freiheitsgrade bei der Entscheidungsfindung mit fortschreitender Zeit abnehmen.

ACKNOWLEDGEMENTS

I would like to express my gratitude to all those people who enabled this study and who enduringly encouraged, supported and accompanied me.

My greatest thanks go to Wilfried Haeberli and Christian Huggel for giving me the opportunity to work on this fascinating topic. Wilfried always had full confidence in me regarding management of my thesis and of the project, it was settled in. He thus provided me enormous freedom and scope for creativity in composition and realization of my thesis. Christian furthermore enabled and promoted the integration of my activities into other projects at the institute. He thereby created many more opportunities and facilitated exciting encounters, which were essential for the success of my thesis, and which furthermore allowed me to combine personal interests with work. I am very grateful for these privileges. Sometimes it was nevertheless hard for me, not to sink into these endless possibilities. Yet Wilfried and Christian helped me back on track every time I was in danger to get lost.
I equally highly acknowledge the effort and contributions of the other members of my PhD-committee, Michael Bründl, Jan Seibert and Andreas Vieli. Michael always provided me with expertise in risk management and ensured an exterior view. Jan not only eased the troubled period of transition by bridging the gap between the two professorships, but also continued his engagement until completion of the thesis. Andreas unconditionally supported the final phase of my thesis.

The active integration of my thesis within the NELAK-project was a crucial precondition for the success of this interdisciplinary thesis, not only thanks to the generous funding provided by the Swiss National Science Foundation and UNISCIENTIA STIFTUNG within the framework of the National Research Programme 61 on sustainable water management. I was strongly inspired and motivated by the interchange, the support, the collaborations and the enthusiasm within the team. My sincere thanks belong also to Nico Mölg, Matthias Künzler, Therese Lehmann Friedli, Anton Schleiss, Michael Bütler, Frédéric Jordan and Hansruedi Müller.
The broad content of my thesis was only rendered possible thanks to essential supports from numerous people, which I am very grateful for. The diploma, master's and bachelor's theses of Souria Nussbaumer, Marco Epp, Sara Würmli, Domenika Bucher-Sanchez and Pascal Senn

were not only a pleasure to supervise, but also formed an integral part of my work and I appreciate their dedication and their carefully elaborated contributions. Enrico Celio and Martina Sättele revealed the world of Bayesian networks to me and always helped me out once the probability of being confused raised towards one. Mattia Molinaro patiently and competently introduced statistics to me. Demian Schneider and Sebastián Guillén Ludeña were my sheet anchors concerning simulation issues. Roland Schaub solved all my programming troubles with high personal commitment. Carol McDonald carefully edited my thesis for language usage and grammar. I am also thankful to Philipp Rastner, Michaela Teich and Sina Schneider, who shared their experiences and provided valuable advices and comments, especially in the final phase of the thesis. Many thanks also belong to members of CARE PERU (esp. Cesar Gonzales and David Ocaña), to members of the Unidad de Glaciología y Recursos Hídricos, Peru (esp. Judith Torres, Daniel Colonia, Alejo Cochachin, Cesar Checa) and to Cesar Portocarrero an Fabian Drenkhan on whose support I could rely in all my expeditions to Peru.

The atmosphere and the support was also extraordinary in house. I appreciated working under the banana tree in the greenest office of the institute and would like to thank Michael Hilf and Anett Hofmann for their enjoyable company. The entire team of 3G infected me with their passion for the working area and I highly appreciate the uncountable pieces of daily assistance - be it in form of R-scripts, of inspiring discussions, of assistance for field work, of pieces of cakes, of after-work beers or even of (extended) weekend trips. Listing all of you would simply go beyond the scope of this section, but be assured, I would not have wanted to miss a single one of you!
Balance is key. It was my employment in the team of the university's vice-president, which kept me from loosing the balance in the troubled starting phase of my PhD. Beatrice Brunner, Eline Embrechts, Florian Kempter, Blanca Keller and Daniel Wyler are thanked for the exciting, unique and social working environment.
Having a safe retreat from work is crucial to success. I shared flat with many people but I have never felt as much home as with Jonas Schwaab and Michaela Teich. And then, there were those friends or families, I could have simply not done it without. They unconditionally supported me in more than one way and in all circumstances; listing their assistances is simply impossible. Michaela, Nico, Philipp, Thomas, Souria, Nicole, Sina, Claudia, Mami, Papi, Roland - Danke!

TABLE OF CONTENTS

LIST OF FIGURES

LIST OF TABLES

CHAPTER 1

INTRODUCTION

1.1 High-mountain lakes in a changing environment

High mountains are dynamic systems consisting of different regimes, which are ruled by interactions of manifold processes and elements. This complexity makes high-mountain systems sensitive to external impacts. Currently, climate-related alterations are of great concern (Bender et al., 2011; Gądek, 2014). The rise in atmospheric temperature is a global phenomenon that concerns all major systems, such as the ocean or the cryosphere, and has been observed unequivocally and is projected to continue to rise in the future (IPCC, 2013). The increase in temperature implies enhanced melting of snow and ice (UNEP, 2011), which is evidenced by the accelerated, worldwide shrinking of glaciers (IPCC, 2013; Zemp et al., 2008). One consequence of this glacier recession is the formation of new lakes, which can be observed all over the world (e.g. Byers et al., 2013; Haeberli and Linsbauer, 2013; Loriaux and Casassa, 2013).

Many of these new lakes are and will be located underneath hanging glaciers and seracs or at the feet of oversteepend and destabilizing rock slopes (Haeberli et al., 2010a). This can be problematic, as slope stability is also assumed to be affected by climate change. The changing, warmer conditions in high mountains are likely to promote large rock slides (Stoffel and Huggel, 2012). Often, these new lakes are prone to impacts from rapid mass-movements. The danger of ice avalanches is a serious, but most likely transient situation because glaciers are vanishing. The disadvantageous situation with regard to unstable rock slopes is equally dangerous and it is very likely to persist for a very long time, because climate change affects slope stability, not only for the short term (days) but also for the long term (millennia) (Huggel et al., 2012), and because the lakes usually remain for a very long time, too. If a rock/ice avalanche impacts a lake, the overtopping of the dam and an outburst flow triggered thereby can be the consequence. In the worst case, a lake can be completely emptied. Such process cascades, related to lakes, glaciers and permafrost, can have large socioeconomic impacts (Iribarren Anacona et al., 2014), especially in areas with densely populated valleys, such as the Callejón de Huaylas in the Peruvian Cordillera Blanca (Lliboutry et al., 1977; Zapata Luyo, 2002).

The Callejón de Huaylas is populated by approximately 267,000 people, many of them concentrated in cities in the valley bottom (Carey et al., 2012). The adjacent Cordillera Blanca is considered the largest tropical mountain chain worldwide, containing around 24% of the global tropical ice mass (Racoviteanu et al., 2008). These glaciers lost approximately 30% of their area between the Little Ice Age in the mid-19^{th} century and the end of the 20^{th} century (Georges, 2004; Rabatel et al., 2013), enabling the formation of numerous lakes (Carey et al., 2012; Lliboutry et al., 1977). Many catastrophic outburst floods have occurred from these lakes, which claimed several thousand fatalities by devastating large areas of land and some of the major cities in the affected valleys (e.g. Carey, 2005; Lliboutry et al., 1977; Zapata Luyo, 2002). The inhabitants of the Callejón de Huaylas adapted to these changing hazards through the implementation of a large number of risk-reduction measures (Lliboutry et al., 1977; Portocarrero, 2013b). Some of them were already effective and prevented casualties, as evidenced by the most recent outburst flow of the Lake 513, which was triggered by a rock/ice avalanche impact in 2010 (Carey et al., 2012; Haeberli et al., 2010b).

The Swiss Alps belong to the high mountains that feature densely populated valley bottoms, which have a long history regarding glacier hazards (Glaciorisk, 2003). In the past decade, problems emerging from newly formed lakes increased and required the implementation of risk-reduction measures. The drainage of the lake at the lower Grindelwald glacier (Gletschersee, 2012; Werder et al., 2010) or the early warning system at lake Trift (Dalban Cannassy et al., 2011) are examples. These lakes were formed as a consequence of glacier recession.
The volume of the Alpine glaciers is now annually decreasing by 2 - 3% (Haeberli et al., 2007), and climate scenarios suggest that the ice will have vanished by the middle of this century for 75% of the area in the Swiss Alps, which was glacierised by the end of the 20^{th} century (Linsbauer et al., 2013; OcCC, 2007; Zemp et al., 2006). Models, which allow the digital calculation of the terrain without glaciers (Farinotti et al., 2009; Huss et al., 2008; Linsbauer et al., 2012; Paul and Linsbauer, 2012), suggest the appearance of numerous overdeepenings in the newly exposed glacier beds. Based on the observed current developments, these locations are assumed to represent sites of potential future lake formation (Linsbauer et al., 2013). Hazardous situations emerging from high-alpine lakes, which are prone to impacts from mass movements, are therewith indicated to become an even more frequent scenario in the Swiss Alps. Even though the probability of such cascade processes is currently small, it is systematically increasing and requires fundamental process understanding and anticipatory risk management (Haeberli et al., 2010a; Schaub et al., 2013).

Switzerland is in a leading position worldwide (Bischof et al., 2008) regarding risk-based management of natural hazards instead of purely technical defence (PLANAT, 2002). This is mainly due to the development of hazard assessment guidelines (e.g BFL and SLF, 1984; Lateltin, 1997; Petrascheck and Loat, 1997), process simulation software (e.g. Christen et al., 2010b; Feah et al., 2011) and the implementation of risk management concepts (Bründl, 2009) into practice-oriented tools (e.g. BABS and BAFU, 2007; BAFU, 2010). The main focus of integrated risk management with respect to natural hazards in Switzerland has so far been on a selection of single processes, which are hail, floods, storms, earthquakes, landslides, rock falls, debris flows, snow avalanches and extreme temperatures (Bründl, 2009). Some attempts

to elaborate integrated risk management techniques for glacier hazards haven been carried out (Glaciorisk, 2003; Wegmann et al., 2004). These hazard and risk assessment approaches, based on historical documentation of events, assess the current socioeconomic situation and are designed for single processes. Multi-hazard and multi-risk assessment is still an arising research field (Kappes, 2011).

Rapid mass movements from destabilised slopes interacting with lakes, especially in relation with permafrost degradation and glacier retreat, however, require integrated assessment of the entire process chain. There persists an urgent need for detailed investigations and assessment methods regarding triggering events, causal relations, probabilities or other specific characteristics of high-mountain lakes (Schaub et al., 2013), especially with regard to future conditions and developments (Haeberli et al., 2010a).

The integration of spatiotemporal aspects in risk management is a general necessity (Aubrecht et al., 2013), which is even more pronounced in risk management in high-mountain regions. The Cryosphere system was and will continue to be considerably taken away from past experiences through the climate-introduced changes. Contemporaneously, land use in the valley bottoms has changed (Bender et al., 2011) and will most likely continue to change (Perlik et al., 2008). It is therefore fundamentally important to adequately consider recent, ongoing and future changes and related implications in terms of hazards and risks.

1.2 Objectives and research questions of the thesis

This study is a contribution to advance hazard assessment, risk analysis and management of high-mountain lakes, especially with regard to the process chain of a lake-outburst flow triggered by impact waves, and under full integration of future conditions. Priority is therefore given to an integrated, holistic contemplation of the subject with in-depth investigations responding to two main objectives and addressing the following research questions (RQ).

The first objective is to improve systematic analysis and anticipation of hazard potentials emerging from high-mountain lakes within the framework of integrated risk management (Chapters 2, 3 and 16). Special focus will therewith be put on five specific questions, addressing gaps on different temporal and spatial scales.

RQ 1: How can the lake-outburst potential, also due to impact waves, be systematically analysed and anticipated and what is the current state of knowledge and corresponding assessment methods (Chapter 4)?

RQ 2: Which of the present and potential future high-mountain lakes in the Swiss Alps are most susceptible to rock-avalanche impacts (Part II)?

RQ 3: How can the process chain of a lake-outburst flow due to an impact wave triggered by a rock/ice avalanche be analysed for the purpose of a risk analysis (Chapter 10)?

RQ 4: How do uncertainties propagate in the numerical simulation of the process chain of a lake-outburst flow due to an impact wave triggered by a rock/ice avalanche (Chapter 12)?

RQ 5: How can ice-avalanche scenarios be developed and their effects on a lake be simulated and evaluated (Chapter 13)?

The second objective is to improve and to expand consequence analyses and risk calculation approaches with regard to high-mountain lake-outburst flows, which are under consideration of future conditions. Two specific aspects will be treated.

RQ 6: Can a complete costs assessment be carried out as part of a practical application to a lake-outburst event (Grindelwald) (Chapter 14)?

RQ 7: How can future risks be estimated by incorporating future-oriented land-use changes and outburst flow scenarios for a local case (Naters) (Chapter 15)?

1.3 Structure of the thesis

This thesis is structured according to the subject, spatial and temporal scale, which the single research questions and the related chapters cover. The thesis is thus composed of five semantic parts (Fig. 1.1) rather than strictly following the standard arrangement of scientific publications.

In **Part I** high-mountain lake-outburst events are introduced, framed and explained. The introductory *Chapter 2* contains an overview on worldwide occurrences, consequences and terminologies of high-mountain lake-outburst flows. The event of a high-mountain lake-outburst is then embedded into the risk concept in *Chapter 3* to enable systematic treatment of the cascading processes. The current knowledge on hazard assessment of high-mountain lake-outburst events is summarized in *Chapter 4*. This involves the definition of lake-outburst mechanisms, identification of the related disposition and trigger parameters, as well as the presentation of corresponding hazard assessment techniques that are currently available. Special attention is thereby given to process chains and their treatment within in the elaborated theoretical framework.

In **Part II** the relevance of rock avalanche-induced impact waves for the entire Swiss Alps is assessed on a regional scale and discussed as much for current as for future conditions by identifying areas of special concern. A rock-avalanche impact disposition model was elaborated (*Chapter 5*), to assess the long-term rock-avalanche impact disposition for Swiss high-mountain lakes in a spatially-explicit deterministic approach (*Chapter 6*) and in a probabilistic approach (*Chapter 7*). A detailed reliability and robustness analysis of the model was carried out (*Chapter 8*) before the relevance of rock-avalanche impact disposition into Swiss high-alpine lakes was elaborated through comparison to current settlements in the Alps as well as to national scenarios of spatial development (*Chapter 9*).

Detailed hazard analyses have to be carried out on a local scale for every lake individually, which is the topic of **Part III**. The current knowledge on the effects of a slope failure in a lake and on the techniques available for hazard assessment of the single process involved in the resulting process chain are summarized and discussed in *Chapter 10*. The discussion focuses on the possibility of coupling the assessment techniques for the purpose of a hazard analysis of the entire process chain. The approach chosen to represent the effects of the 2010 rock/ice-avalanche impact into, and the propagation of the wave through, Lake 513 in Peru, is presented in *Chapter 11*. This case study serves as a basis for the following two chapters. *Chapter 12* assesses the propagation of the uncertainties in the coupled hazard simulation approach. In *Chapter 13*, the case study serves an example for a complete hazard analysis of a lake outburst through ice-avalanche induced impact waves, bringing together the thus-far elaborated knowledge.

Hazard analysis is a component of risk analysis, together with damage potential. This is the content of **Part IV**, in which two selected issues of damage potential and risk estimations regarding high-mountain lake-outburst events will be treated. Firstly, quantification of all costs incurred by the 2008 lake-outburst event in Grindelwald, Switzerland is presented (*Chapter 14*). Secondly, a method to conduct future-oriented risk estimations considering future hazards and land-use changes is presented with the help of a modelled overdeepening (which is assumed a potential location of a future lake) above the town of Naters, Switzerland (*Chapter 15*).

The final **Part V** brings together the achievements within discussion of integrated risk and lake management (*Chapter 16*), and it also considers questions regarding probabilities, risk evaluation and feasible risk reduction measures. The final *Chapter 17* contains the main conclusions of this thesis and an outlook on further opportunities and challenges.

Appendices are attached after the literature references, the personal bibliography and the curriculum vitae.

Content							Part	Chapter
Subject			*Temporal scale*		*Spatial scale*			
Hazard	Damage potential	Risk	Present	Future	Local	Regional		
x	x	x	x	x	x	x		1 High-mountain lakes in a changing environment
x							I	2 Occurrence, consequences and terminologies
x	x	x	x	x	-	-		3 Embedding high-mountain lake-outburst events into the theoretical background of risk
x			x	x	x	x		4 Identifying and analysing high-mountain lake-outburst hazards
x			x	x	x	x	II	5 Developing a model of rock-avalanche impact disposition into high-mountain lakes in Switzerland
x			x	x	x	x		6 Spatially-explicit, deterministic assessment of the rock-avalanche impact disposition
x			x	x	(x)	x		7 Probabilistic rock-avalanche impact disposition assessment considering parameter uncertainties
x			x	x	(x)	x		8 Reliability and robustness assessment of the rock-avalanche impact disposition model (Appendix A)
x	(x)	(x)	x	x		x		9 Relevance of rock-avalanche impact susceptibility of high-alpine lakes in Switzerland
x			x		x		III	10 Effect analysis of rapid mass movements triggering impact waves
x					x			11 2010 outburst event of Lake 513: Case-study and event descriptions (Appendix B)
x			x		x			12 Uncertainty propagation in coupled impact-wave simulations (Appendices C, D, E)
x			x	x	x			13 Hazard analysis of potential ice avalanches at Mount Hualcán
(x)	x	(x)	x		x		IV	14 Cost assessment of a lake-outburst flow in Grindelwald with regard to touristic infrastructure
x	x	x		x	x			15 Damage potential and risk estimation for future conditions with the example of Naters
x	x	x	x	x	x	x	V	16 Integrated risk management of high-mountain lakes
x	x	x	x	x	x	x		17 Conclusions and outlook
							VI	Appendices A-E

Figure 1.1: Structure of the thesis. x = chapter refers strongly to the topic. (x) = chapter refers partly to the topic.

Part I

An application-oriented framework for treatment of outburst flows from high-mountain lakes

The aim of this thesis is to improve systematic analysis of high-mountain lakes, especially with regard to outburst flows triggered by impact waves. This introduction will discuss the processes for understanding and modelling such situations, so that they may be framed and analyzed.
The thesis starts with an overview in Chapter 2 on worldwide occurrence of high-mountain lake-outburst flows, consequences reported and terminologies applied. The event of a high-mountain lake outburst is then embedded into the risk concept in Chapter 3 to enable systematic treatment of the cascading processes. The current knowledge on hazard assessment of high-mountain lake-outburst events is summarized in Chapter 4. This includes the definition of lake-outburst mechanism, identification of the related disposition and trigger parameters, as well as the presentation of corresponding hazard assessment techniques currently available. This section pays special attention to process chains and their treatment within the elaborated theoretical framework.
This framework provides the basis for the entire thesis.

CHAPTER 2

OCCURRENCE, CONSEQUENCES AND TERMINOLOGIES

2.1 Occurrence and consequences

High-mountain lake-outburst flows can potentially be disastrous. Peru experienced 6000 fatalities in the town of Huaraz in 1941 (Lliboutry et al., 1977), 500 deaths at Ayhuinyaraju Lake in 1945 and another 500 at Jancarurish Lake in 1950 (Flubacher et al., 2007). 19 million m^3 of water released within 60 minutes from Lake Dig Tsho destroyed two highway sections, a hydropower project and two bridges, resulting in damages of 3 million US dollars for Nepal (Mool, 1995). 126 km of railways, a small village and some bridges in the main international route between Argentina and Chile were demolished by an outburst of the Río del Plomo in 1934, which was impounded behind the surging Plomo glacier (Flubacher et al., 2007). In Täsch, Switzerland, 150 people were forced to be evacuated and damage of around 18 million Swiss francs was caused to buildings and other infrastructure from an outburst of Lake Weingarten in 2001 (Huggel et al., 2003). Eventually 400 fatalities in two devastated cities and on 57 km^2 of farmland were counted in Tibet in 1954 after the impact of a glacier avalanche into the Sangwang lake (Ives et al., 2010). These are just a few examples of the consequences of high-mountain lake-outburst flows.

In fact, lake-outburst flows are a worldwide phenomenon (Mergili and Schneider, 2011; Vuichard and Zimmermann, 1987). Some regional documentation is available for Peru (Lliboutry et al., 1977), Patagonia (Dussaillant et al., 2010; Iribarren Anacona et al., 2014), the Yukon territory (Clarke, 1982), the Pakistani (Karakoram) Himalayas (Ashraf et al., 2012; Hewitt, 1982), Alaska (Post and Mayo, 1971), the European Alps (Chiarle et al., 2007; Haeberli, 1983; Röthlisberger, 1978), Nepal (Bajracharya and Mool, 2010; Mool, 1995; Yamada and Sharma, 1993), New Zealand (Hancox et al., 2005) and British Columbia (Blown and Church, 1985; Clague and Evans, 2000). Their occurrence in all major mountain regions is documented (Fig. 2.1) in a compilation of 566 records (Vilímek et al., 2014). The disproportionately high number of

events recorded in the European Alps and in the Rocky Mountains is most likely due to sporadic reporting, as lake-outburst flows often happen in remote areas (Würmli, 2012). In these cases, damage is mostly caused to landscape and roads. In areas featuring densely populated valleys, however, loss of life frequently occurs. The examples mentioned at the beginning of this chapter illustrate that lake-outburst flows can be very destructive. Outburst mechanisms such as overtopping, sudden dam breaching, or piping often feature high peak discharges up to several 1,000 m^3/s or even several 10,000 m^3/s are common (Cenderelli and Wohl, 2001; Würmli et al., 2013). As a result of the large amounts of water involved, up to tens of millions of cubic meters, lake-outburst flows can cause damage over a length of few kilometres up to more than 100 km (Würmli, 2012). Lake-outburst flows can flow rapidly; velocities between 3-9 m/s have been reported (Cenderelli and Wohl, 2001).
The reported causes for these lake-outburst events have been manifold (Fig. 2.2). Reports describe lake outburst from sudden mechanical breaching, piping (Lliboutry et al., 1977), progressive breaching, overtopping by impact waves (Eisbacher and Clague, 1984; Lliboutry et al., 1977; Richardson and Reynolds, 2000; Schneider et al., 2014) or retrogressive erosion (Würmli et al., 2013). The stability of lakes is therefore an outcome of the dam characteristics but also of the surrounding processes impacting the dam.

2.2 Terminologies

Lake-outburst floods have been described by Carrivick (2007) as "subaerial high-magnitude outburst floods", which are characterized as "a sudden release of water and sediment with discharges that are several orders of magnitude greater than perennial flows". According to this definition, lake-outburst floods belong to the same class as flows from volcano-glacier interac-

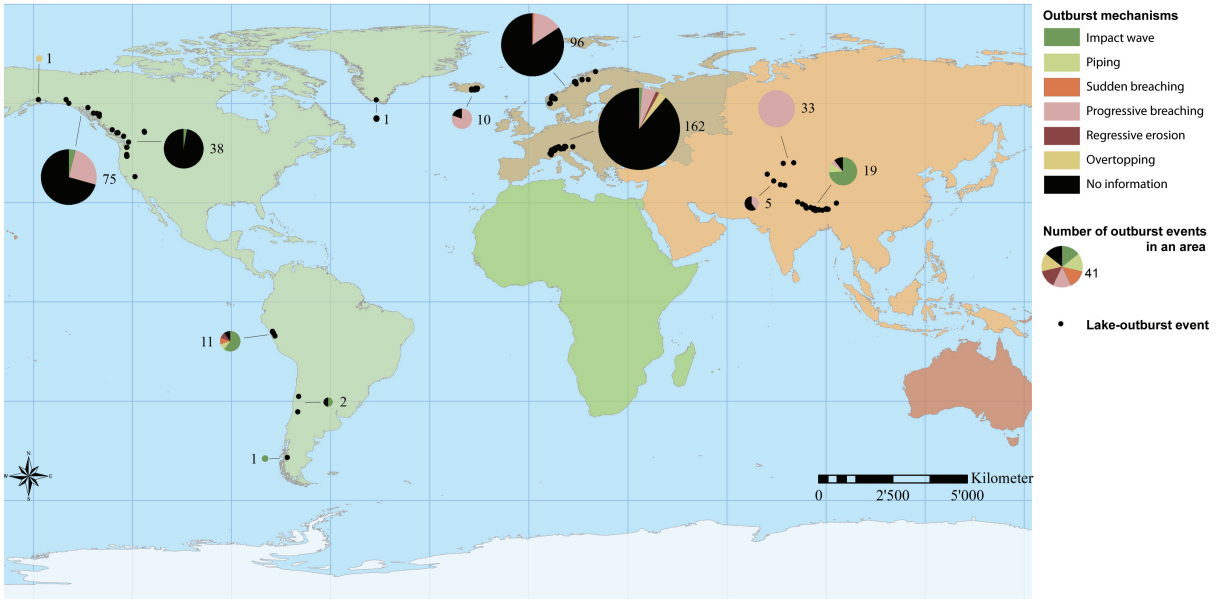

Figure 2.1: A worldwide compilation of 566 lake-outburst events (Vilímek et al., 2014).

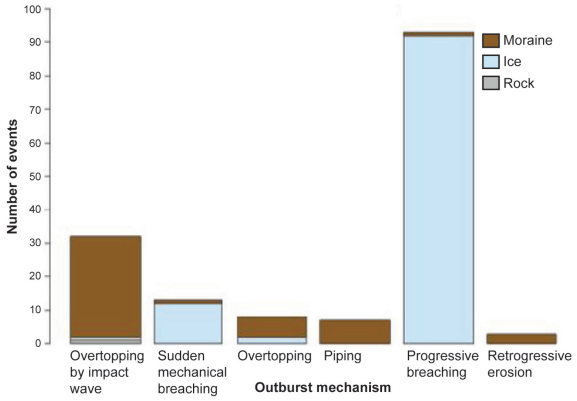

(a) Number of events recorded per outburst mechanism as a function of the dam type.

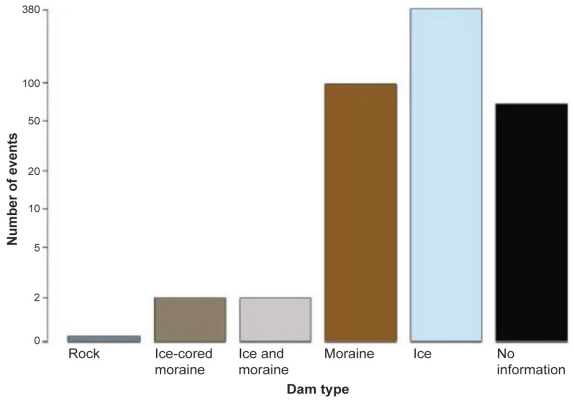

(b) Number of events that were recorded per dam type (material).

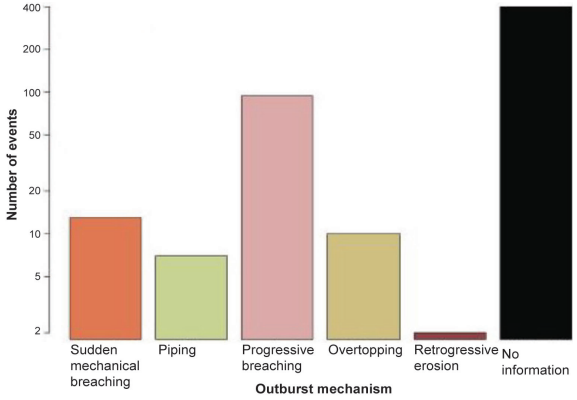

(c) Number of events that were recorded per outburst mechanism.

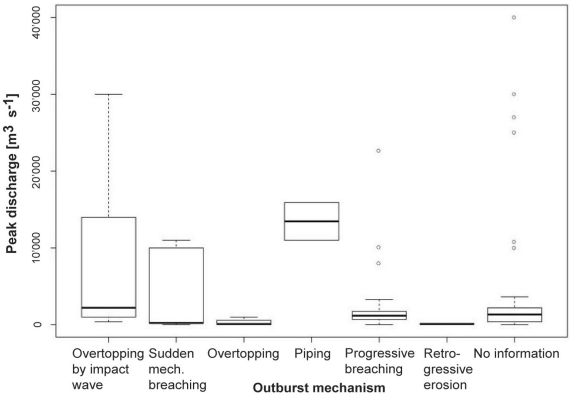

(d) Magnitude of peak discharges per outburst mechanism.

Figure 2.2: Some insights into lake-outburst mechanism from a compilation of a worldwide inventory of 566 lake-outburst flows (Würmli et al., 2013).

tions (so-called lahars) or directly glacier-related floods from sub-, en- or supra-glacier flows (Richardson and Reynolds, 2000).

The terminology describing these events is not consistently used across the literature, due to the historical development of expressions and also due to the sometimes inconsistent use of popular expressions. The term Jökulhlaup – adopted from Icelandic – is applied in glacier science to describe the sudden release of water impounded within or behind a glacier (Thorarinsson, 1953). This definition was later expanded to include moraine-dammed lakes, which led to defining up to seven different types of Jökulhlaups (Roberts, 2005): (1) drainage of an ice-marginal, ice-dammed lake, (2) drainage of a supraglacial lake, (3) volcanically induced Jökulhlaup, (4) drainage of a subglacial lake, (5) drainage of an intraglacial cavity, (6) drainage of a moraine-dammed lake, including those dammed by ice-cored moraines, (7) meltwater release during surge termination.

The ambiguous term "glacial lake outburst floods" (GLOF) has been introduced from studies in mountainous regions. Mergili and Schneider (2011) describe a GLOF as the sudden release from lakes in glacially shaped landscapes or which are dammed by a glacier. Different glacier

lake types are described by Raymond et al. (2003). They distinguish among (a) subglacial lakes, which can also form as water pockets in the ice (and which will not be further considered in the present study), (b) supraglacial lakes, which form in depressions on the surface of a glacier, (c) periglacial lakes, which are dammed by moraines, dead-ice, sediments or permafrost and are no longer in contact with the glacier, (d) ice-marginal lakes, which are in touch with the glacier and are often dammed by it and (e) proglacial lakes, which are located in depressions in formerly glaciated areas and which are often dammed by moraines. The expression GLOF is also applied as a synonym for Jökulhlaups (Hewitt, 1982, e.g.). Other authors, however, define the expressions differently; the classification of Richardson and Reynolds (2000) on glacier and related hazards describes glacier outbursts as a catastrophic discharge of water under pressure from a glacier, while they associate Jökulhlaups with floods triggered by subglacial volcanic activities. According to them, the term GLOF describes outbursts from usually moraine-dammed proglacial lakes.

Natural lakes in mountainous areas, however, also contain other types of dams, formed, for example, by landslide deposits, or bedrock-dams (Costa and Schuster, 1988), which are not necessarily a consequence of (former) glacial activity. Mergili and Schneider (2011) therefore introduced the term lake outburst floods, LOF, which accounts as much for glacial as for non-glacial lakes. A broad overview about the terminology in use is given by Korup and Tweed (2007). Without presenting them in detail, the conclusion of this compilation is that the terminology currently applied regarding LOFs, especially the expression GLOF, is not consistent. Depending on the author, the term GLOF refers either to the flow characteristics of a high-magnitude outburst flood or to the formation of the lake in glacially shaped landscapes. This ambiguity makes a structured approach for hazard assessment difficult. Therefore none of the terms introduced in this paragraph will be used in the present study.

The present part, entitled "An application-oriented framework for treatment of outburst flows from high-mountain lakes", refers to the environment in which the lakes of concern are currently situated rather than the formation history or the outburst flow magnitude. Hence, the high-mountain environment has to be demarcated, as this term is also used ambiguously. Barsch and Caine (1984) summarized several definitions, e.g. by means of vegetation (above timberline) or elevation and relief (differing by more than 1000 m of altitude over a 5-km distance), amongst others. For the purpose of the present study, a high-mountain lake is defined by its catchment. Following in principle Barsch and Caine (1984), the catchment should be located above the timberline and exhibit steep (>35°) and even precipitous gradients, rocky terrain, and the presence of snow as well as of (potential) contemporaneous or recent past ice-occurrence.
This definition is intentionally not formulated too specifically. This implies ongoing reflection for every lake assessment, to determine whether this definition applies and how the boundaries of the study areas have to be defined. This study is aligned towards mountain ranges featuring a glacial regime, which are currently impacted by strong climate-induced changes and towards lakes, and which feature paraglacial environments in their catchment. Two main definitions of a paraglacial environment are currently in use (Ballantyne, 2002; Slaymaker, 2009). McColl (2012) combined them with regard to slope failure assessment, defining paraglacial as an environment or processes, which "are part of or influenced by, the transition from glacial conditions

to non-glacial conditions". The advantage of this relatively open definition applied to high-mountain lakes is, however, that all kinds of lakes affected by the same outburst trigger factors can be assessed in an equal manner independent of the lake classification into glacial, non-glacial or even artificially dammed lakes. The general description of the outburst as a flow (in accordance with Korup and Tweed (2007)) further prevents preconceptions of assumptions on the flow characteristics, since anything from pure water floods up to heavy debris flows are feasible. This point of view allows for more precise conclusions regarding the probability of occurrence and potential magnitude of lake outbursts, which are crucial for hazard assessment.

This overview on the variety of occurrence, causes and consequences of worldwide lake-outburst events illustrates the destructive nature of such incidents and their classification as high-magnitude, low-probability events. The terminologies used in literature to describe variable aspects of these events were presented, and the term "high-mountain lake-outburst flow" was introduced as a starting point for hazard assessment of the respective phenomenon, which will be examined more closely in the next chapter.

CHAPTER 3

EMBEDDING HIGH-MOUNTAIN LAKE-OUTBURST EVENTS INTO THE THEORETICAL BACKGROUND OF RISK

The basis of any management activity with regard to a potential danger is a profound hazard and risk analysis, as risk allows for comparing and rating different hazards within integrated risk management. The analysis has to meet four main criteria, if it is to be performed to empower decision makers in efficient risk reduction (Chen et al., 2010): the analysis has to enable (1) the prioritization of hazard/risk by (2) identifying hotspots, critical components or locations and (3) recognizing and analysing interconnections between causes and consequences of hazardous processes in order to (4) establish hazard scenarios, which serve as a basis for vulnerability and risk estimations as well as for mitigation planning. To satisfy these criteria, the analysis is best conducted within a risk management framework, which will be outlined in the next section.

3.1 The risk concept

Risk is not clearly defined: disagreement currently prevails regarding its nature. Risk can be understood as a subjective construct rather than a real fact (e.g. Becker et al., 1993), while another school of thought perceives risk as an objective state of the world, which exists independent of our perceptions (e.g. Rosa, 1998, 2003). The definition of risk further depends on the perspective. Common point of views are traditional engineering and Bayesian views, or economic, social, and anthropological perspectives (see Aven and Kristensen (2005) for more precise explanations). These definitions can be merged into two categories (Aven and Renn, 2009a). Definitions in the first category express risk by means of probabilities and expected values (e.g Crozier and Glade, 2005; WMO, 2014), while the second category describes risk

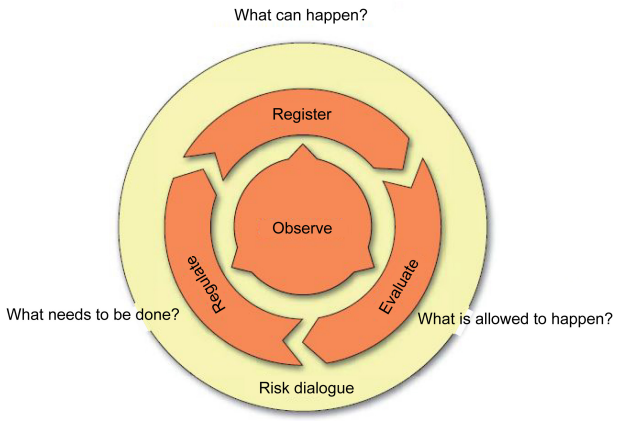

Figure 3.1: The cycle of integrated risk management (PLANAT, 2013). The three leading questions (Kaplan and Garrick, 1981) are assigned to the respective activities.

through events or consequences and uncertainties in the second category (see (Aven and Renn, 2009a) for a summary of corresponding definitions).

The present thesis will focus on the first, engineering-based, category of risk, following Kaplan and Garrick (1981), as they aim at supporting decision-making (Aven and Kristensen, 2005). The focus, understanding and management of risk, also, however, depends on its social and political context (Huggel, 2010).
The understanding of disasters is indeed always a product of social, political and economic environments (Hewitt, 1983). To include this principle, risk is here defined according to the widely accepted and applied approach of the United Nations International Strategy for Disaster Reduction (UNISDR, 2009) as "the combination of the probability of an event and its negative consequences", which is also the basis for the IPCC (2012, 2013) Reports.

In line with the geographical focus of the present study, risk management as applied in Switzerland (Bründl et al., 2009; PLANAT, 2004) will serve as a reference, which will moreover be compared and discussed with further approaches in some aspects. Here, integrated risk management is understood as continuous observation, capturing, and evaluation of risks in order to derive the need for action, set priorities and anticipatorily regulate development with the help of risk-reduction measures (Fig. 3.1). According to the concept of Kaplan and Garrick (1981), the three leading questions "What can happen?", "What is allowed to happen?" and "What needs to be done?" have to be considered in three steps.
In the risk analysis (described in detail in Section 3.2), the question "What can happen?" is answered and refers to both the environmental, hazardous element as well as to its potential impacts. The resulting scenarios are the premise for the risk estimation.
The meaning of the estimated risk can only be recognized in comparison to societal accepted risk levels, answering the second question of "What is allowed to happen?" (Kaplan and Garrick, 1981). In this risk evaluation, the risk is classified as acceptable, tolerable or intolerable (Fell et al., 2005). This assessment reflects mainly the culture of a society, especially its values, history and ideology (Weinstein, 1980). Risk acceptance also varies, however, within a society, as a function of gender and age (Slovic, 2000). Discussions on risk acceptances are therefore generally lively (e.g Aven, 2007; Bell et al., 2006; Lentz and Rackwitz, 2004; Smith, 2013). The evaluation of the risk emerging from a high-mountain lake-outburst flow poses the further

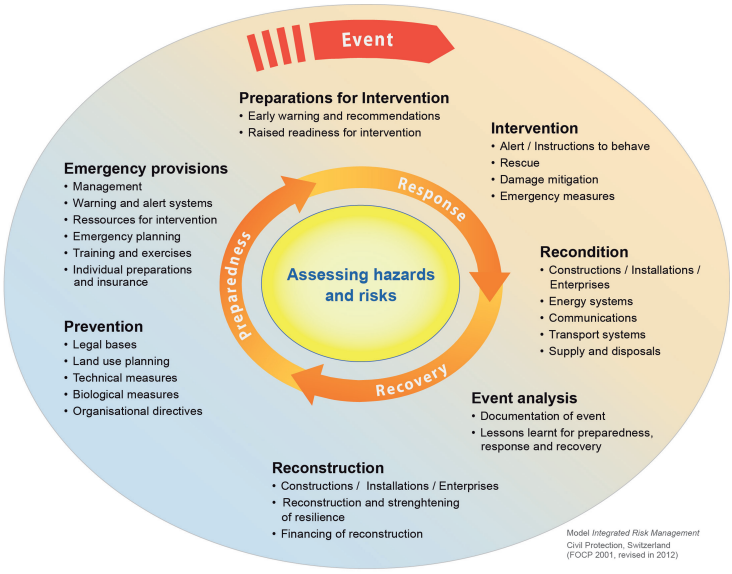

Figure 3.2: The range of possible risk-reduction measures in the framework of integrated risk management, which can be taken at certain stages in an event. The choice of the measure(s) is made based on hazard and risk assessments (BABS, 2013).

challenge of a low-frequency, high-magnitude event, which will be more closely discussed in Chapter 16.
In a third step, possible risk-reduction measures are planned in order to reach the aspired level of safety (PLANAT, 2013), by assessing "What needs to be done?" based on the evaluated risk. In line with integrated risk management, all kind of measures have to be treated on a par (BABS, 2003). The variety of measures is huge and depends strongly on the hazard type and the context of the possible event; a general overview on possible risk-reduction measures is summarized in Figure 3.2. A more focused compilation and discussion of measures with regard to high-mountain lake-outburst flows is established in Chapter 16.

The main two objectives of this thesis defined in the introduction (Section 1.2) are related to the first step of risk analysis. The risk analysis procedure of high-mountain lake-outburst events is presented in more detail in the following sections, where challenges and open questions are also identified. Furthermore, challenges with regard to application of the analysis to different temporal or spatial scales are addressed, and chapters that deal with specific aspects as defined in the introduction are referred to.

3.2 Risk analysis

In the risk analysis, the question "What can happen?" is answered in three parts, presented in this section, referring to a detailed risk analysis on a local scale. Firstly, the procedure of hazard analysis is introduced (Section 3.2.1). Secondly, the assessment of potential impacts in the consequence analysis is presented (Section 3.2.2). These findings are combined in the final step of risk estimation, which is explained in Section 3.2.3.

3.2.1 Hazard analysis

The hazard analysis is carried out in the first step of a risk analysis, defining the event and its effect, which results in intensity maps for each hazard scenario. The short overview in the previous chapter on past lake-outburst events already revealed that they can be caused by several different outburst mechanisms as well as by complicated interactions. To account for this complexity, high-mountain lake-outburst events have to be treated as multi-hazard situations.

Multi hazards
The framework of multi-hazard and multi-risk assessments is relatively recent. A review of definitions, concepts and assessment methods of multi hazards and risks was provided by Kappes et al. (2012). The most recent advances were compiled in the EU-project MATRIX (2013), whose results were, however, not yet fully available when this thesis was written. The following explanations of the multi-hazard concept are therefore mainly based on the review of and references in Kappes et al. (2012).

Multi hazards are defined as the totality of relevant hazards in a defined area (Kappes, 2011), for which the hazard potential is amplified due to a possible coincidence of two or more different hazards in space and time. When two processes occur simultaneously or one shortly after the other, the potential damage impact is greater than the simple sum of the two processes (Kappes et al., 2010; Tarvainen et al., 2006). This is true for processes interacting with high-mountain lakes, because the lake acts as a reservoir, providing much more water than would otherwise be available to the hazard process and thereby intensifies the effect of the event.
The classification of the interactions between hazards is not that straightforward: the relationships between hazardous processes are as diverse as the interactions between them (Kappes et al., 2012). An undisputed type of interaction refers to so-called cascading processes, domino effects or process chains, which consist of a sequence of hazard events and are defined as "a failure in a system of interconnected parts, where the service provided depends on the operation of a preceding part, and the failure of a preceding part can trigger the failure of successive parts" (Delmonaco et al., 2006a). This definition applies to the case for a lake-outburst flow triggered by a rock/ice avalanche-induced impact wave. The classification of remaining types of relationships between hazards is still missing, and they are defined differently in each study (e.g. Hewitt and Burton, 1971; Kappes et al., 2010; Tarvainen et al., 2006). However, these distinctions are not of relevance for the present thesis. Multi-hazard analyses aim at "implementation of methodologies and approaches aimed at assessing and mapping the potential occurrence of different types of natural hazards in a given area. Analytical methods and mapping have to take into account the characteristics of the single hazardous events [...] as well as their mutual interactions and interrelations", according to Delmonaco et al. (2006b).

The study area stretches over the lake, the catchment and the downstream valley for hazard analysis of a high-mountain lake-outburst event. In the following, the two steps of event and effect analysis are described in more detail for a lake-outburst event, with special focus on the process chain of an outburst event triggered by a rock/ice avalanche-induced impact wave.

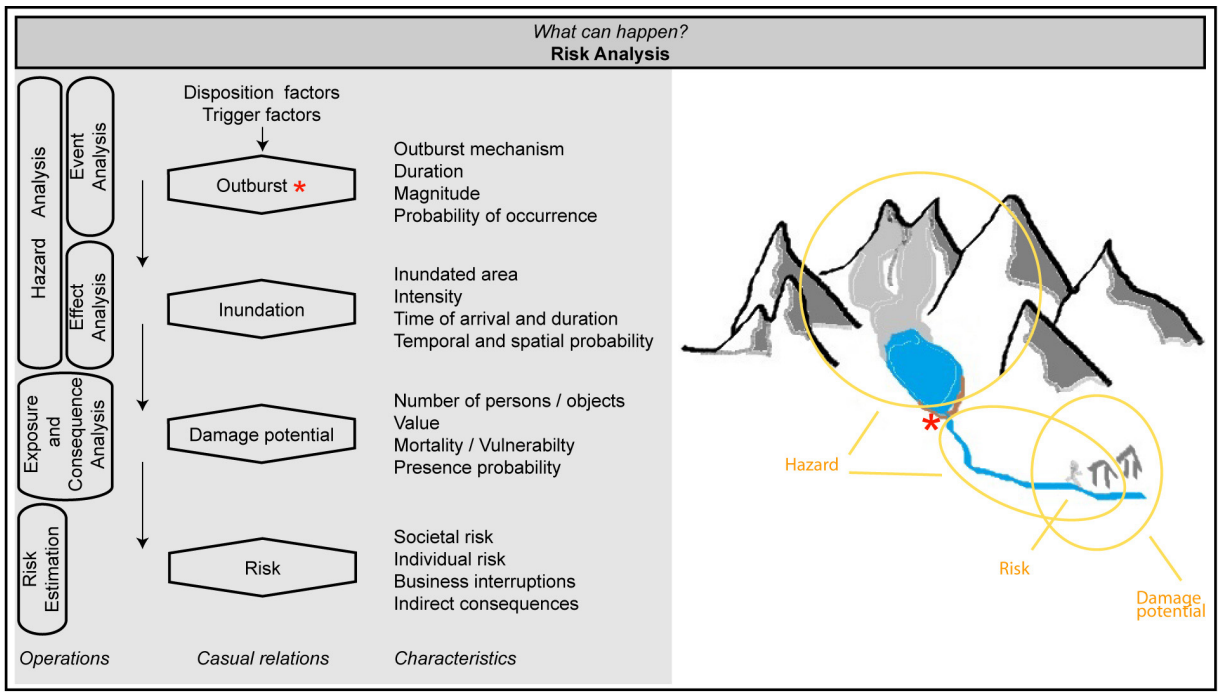

Figure 3.3: Risk assessment of a lake-outburst event (*) in the framework of the risk concept. The assessment of the characteristics of the casual relations involves the operations hazard analysis, exposure and consequence analysis and risk estimations. A hazard analysis begins with an event analysis, which aims at identification and localization of hazards by means of observations, records or analyses of the terrain. The intensity of the hazard is assessed in the effect analysis, which completes the hazard analysis. The negative consequences are assessed within an exposure and consequence analysis, before the risk is estimate based on the hazard and the damage potential.

Event analysis

The starting point of any hazard analysis is the event analysis, in which hazards are identified and localized. Realistic release scenarios are established by means of analysis of inventories either basing on observations of past events or on geomorphologic features in the terrain, or on basis of analysis of the terrain and natural processes occurring in the area (Bründl, 2013). The development of a natural process into a hazard can be described by means of disposition and trigger factors (Heinimann et al., 1998). Disposition indicates the ability of a location to produce a dangerous process, while a trigger factor causes the release of the hazardous process and the initiation of the movement once a certain threshold is exceeded in an area featuring the disposition. One can further distinguish between basic and variable disposition: the basic disposition is defined by Zimmermann et al. (1997) as the static and inherent setting of the environment, e.g. geology. The variable disposition, in contrast, is composed of factors varying over time, such as temperature or hydrology, which bring the system from stable into marginally stable conditions (Glade and Crozier, 2005). Some authors label these two disposition categories as preconditioning and preparatory parameters (e.g Glade and Crozier, 2005).

In hazard analyses of high-mountain lakes, the event is defined as the outburst (Fig. 3.3). The leading question (according to Kaplan and Garrick (1981)) is then reformulated as, "What can happen, if a lake bursts out?". The aim of the event analysis is to define the outburst mecha-

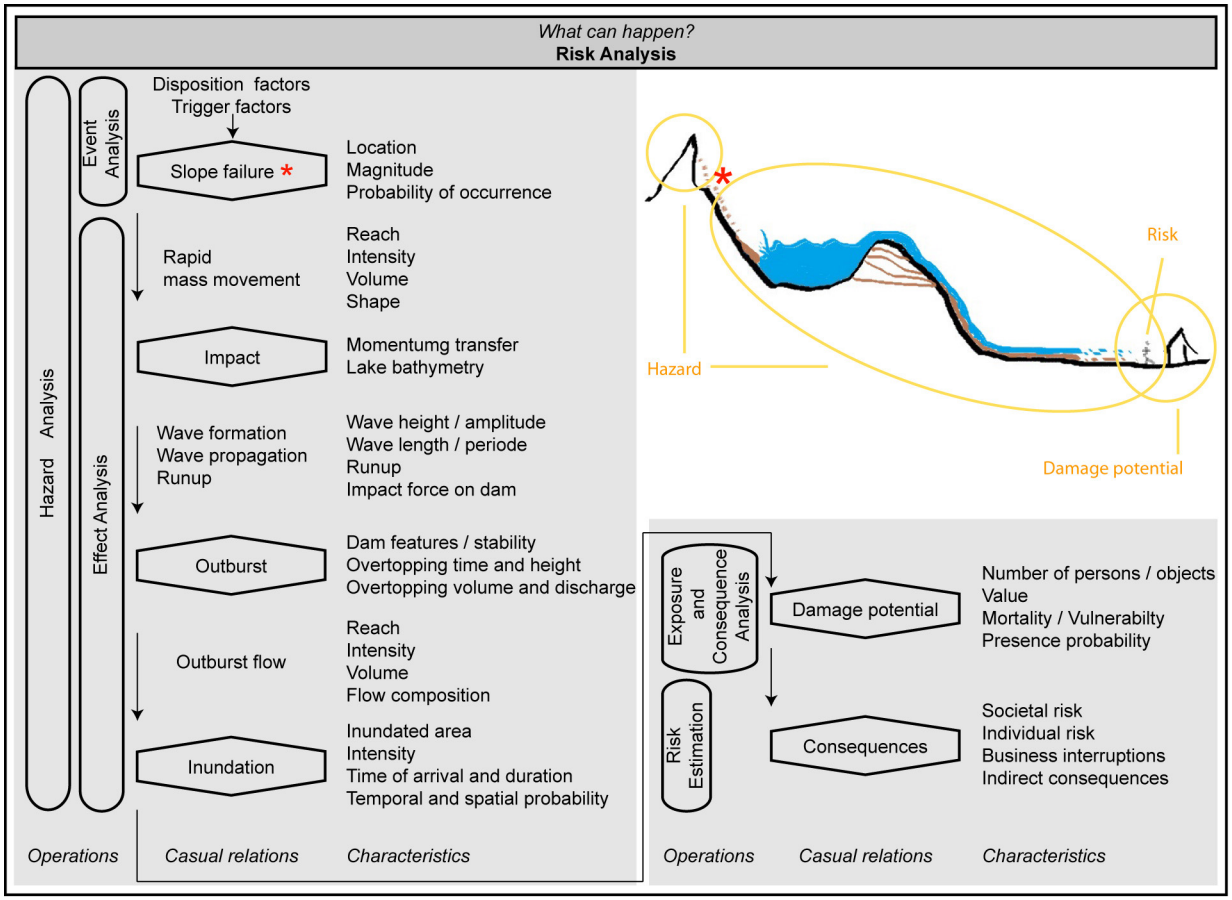

Figure 3.4: Analysing the risk of a lake-outburst flow triggered by an impact wave in the framework of the risk concept. The event (*) is here defined as the slope failure, whose effect has to be assessed considering cascading processes. The other operations are carried out as described in Figure 3.3.

nism, the characteristics of the outburst hydrograph and the probability of occurrence based on observations, records or analysis of the terrain. The most likely outburst mechanism has to be derived in a multi-hazard assessment considering all possible interactions. The state-of-the-art in identification and assessment of the most likely outburst mechanisms and the corresponding trigger and disposition parameters is revealed in Chapter 4.
For the hazard assessment of a lake outburst triggered by an impact wave, the scheme presented in Figure 3.3 has to be adapted ,as illustrated in Figure 3.4, to define the triggering event as a slope failure. The leading question has to be reformulated to "What can happen, if a slope failure occurs?". The event analysis hence aims at assessment of location, magnitude and probability of a slope failure, which is more closely treated in Chapter 4.

Ideally, the event analysis also produces the probability of hazard occurrence, which is highly relevant for spatial planning. A probability in form of a quantitative return period or probability of occurrence, however, is highly difficult to obtain or even not applicable, especially for non-stochastic events (Kappes et al., 2011) or for processes occurring in high mountains. In the latter case, fundamental climate-induced, cumulative changes in the environment (Beniston et al., 2007) imply changes in frequency, magnitude and interactions of processes which can

hardly be assessed by means of retrospective event analyses (Fuchs et al., 2013; Kron, 2002). Furthermore, the dates of past events are often not known exactly due to missing observations, and often the events can only occur once (McKillop and Clague, 2007b). This is, for example, the case for a moraine-dammed lake-outburst flow, where the dam is destroyed irreparably during the event.
The challenge of defining the probability of occurrence of a low-probability or non-stochastic event is again addressed within the discussion on integrated risk management of high-mountain lakes in Chapter 16. One proposed solution is briefly presented, as this concept is in the present thesis applied in Chapter 4 and in Part II.
One possibility for circumventing this obstacle is the identification of hazard occurrence susceptibility, which is feasible for present and partly for future conditions. The term "susceptibility" is here understood as the probability of occurrence (here of the hazard) by virtue of intrinsic characteristics of the territory and its elements (Carpignano et al., 2009). The occurrence susceptibility can be assigned to the basic disposition as defined by Zimmermann et al. (1997) (see previous paragraph).
An effect analysis can be carried out subsequent to the event analysis, whether the probability was defined or not.

Effect analysis
The effect of an identified and localized potential hazardous event is in a second step assessed regarding reach, spatial dispersal and intensity. The respective methods for local scale effect assessment are numerous and depend on the type of hazard process (Chapter 10). In any case, the resulting hazard potential is recorded in intensity maps for each scenario.
In the case of a lake-outburst event (Fig. 3.3), the assessment of the hazard potential is completed with the analysis of the effects of the outburst flow. The runout distance, the intensity and spreading are assessed and detained in intensity maps. Available methods are discussed in Chapter 10.
The effects of a slope failure triggering an outburst event have to be assessed as a cascading multi-hazard, where the inundation also depends on the impact in the lake and on the outburst mechanism (Fig. 3.4). These relations and interactions are described in detail in Chapter 10.

Multi-hazard assessments feature the challenge of comparability of multiple hazards (Kappes et al., 2012), because hazards are usually described by means of reference units and intensity indicators, which best fit to the respective process characteristics. An extensive overview on multi-hazard assessment systems currently in practice is given by Delmonaco et al. (2006b). Such a classification scheme is always elaborated in reference to a certain objective (Kappes et al., 2010). One solution proposed (Delmonaco et al., 2006b) is to apply classification of all hazards into a consistent intensity-scale matrix consisting of low, medium and high intensities. An example is the Swiss planning system, in which hazard zones are defined according to process characteristics and to probability (Heinimann et al., 1998). Further examples of assessment of lake-outburst susceptibility are presented in Chapter 4. The effect of a process chain can, however, hardly be defined using such a classification scheme.
The problem of comparability can also be addressed by means of indices. They allow a semi-

quantitative comparison of the hazard levels, instead of a qualitative ranking. To this purpose, the hazard score is derived as the product of a frequency score with an area-impact score and an intensity score (Kappes et al., 2012). Scale is important in this context (Delmonaco et al., 2006b). This method is picked up in comparison of rock-avalanche impact susceptibility of high-mountain lakes in Switzerland in Part II.

To summarize, high-mountain lakes have to be assessed as complex multi-hazard situations, independent of the outburst mechanism. The event and the effect analysis have to be adapted to the outburst mechanism assumed. Most complex interactions are probably outburst events induced through impact waves triggered by rock/ice avalanches.
The assessed natural process acts as a hazard if it "may cause loss of life, injury or other health impacts, property damage, loss of livelihoods and services, social and economic disruption, or environmental damage" (UNISDR, 2009). Therefore an exposure and consequence analysis has to be carried out in a next step, to estimate the negative consequences.

3.2.2 Exposure and consequence analysis

The second part of the risk analysis consists of the exposure and consequence analysis, in which the damage potential is identified and the expected loss is estimated (Bründl et al., 2009). Four important, general parameters should be considered, which are explained in detail in this section, referring to the following numbers: (1) the number and value of (material) assets and the number of persons exposed; (2) the exposure probability of an object/person while a scenario is occurring; (3) the spatial probability that an object/person is directly encountered by the scenario and (4) the vulnerability of an object/the lethality of a person against the impact of the event.

Exposure analysis
In the exposure analysis, (1) the number, type and value of potentially endangered objects and persons are identified and (2) the probability of their presence in the hazard area assessed. The choice of which endangered objects are to be considered depends on the scale and on the social or cultural evaluation of loss (as explained in Section 3.1). This information is commonly elevated for current conditions, also distinguishing between permanent (e.g. houses) and mobile assets (e.g. cars on the road) (Bründl et al., 2009). A very detailed analysis, also differentiates between different exposure scenarios, such as, e.g. a normal working day vs. a football match with many spectators in the sports ground.
In Switzerland, only the direct damage potential is considered in risk analyses, consisting of the number and value of the exposed objects and the number of persons exposed (Bründl et al., 2009). This is a very simplified definition, because the loss due to natural hazards can be much broader, as shown in a recent review on costs incurred by natural hazards (Meyer et al., 2013). Five categories of cost were distinguished: loss, which is caused by direct physical impact of the hazard, is assigned to the (a) direct costs. The directly affected area might also suffer from (b) business-interruption costs, which arise, for example, through destruction or inaccessibility of workplaces. All further category (a) or (b) losses occurring inside as well as outside of the di-

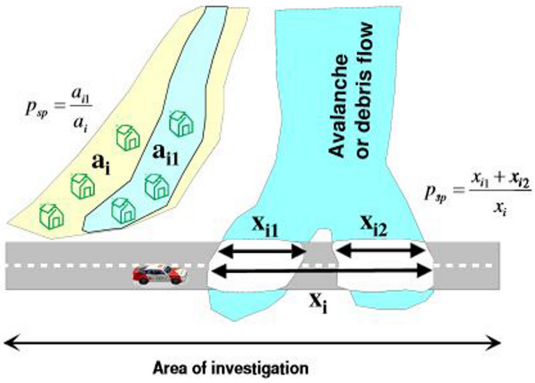

Figure 3.5: Schematic illustration of the spatial probability (P_{sp}) of a process. The areas considered in the intensity maps are indicated with a_i and x_i, respectively. The left part shows that only a part of the potential run out area (yellow area) is assumed to be affected (a_{i1}); the right shows that only a part of the road section is hit by the process (x_{i1}, x_{i2}). Figure and caption from Romang (2009).

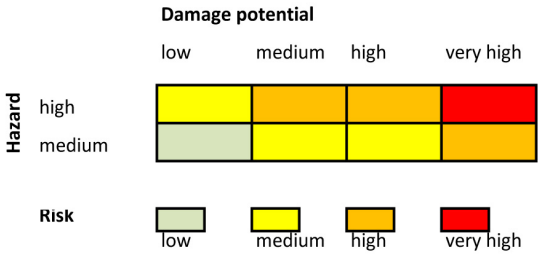

Figure 3.6: Schematic illustration of a matrix, which can be applied to qualitative risk estimations or for multi-hazard assessment (Kappes et al., 2012). A closer description of the matrix elaboration is given in Chapter 15.

rectly affected area, occurring immediately or with a delay are summarized as (c) indirect costs. The (d) intangible costs comprise goods and services, such as impacts on environment, health or cultural heritages which are difficult to measure in terms of money. A last category of costs caused by natural hazards is (e) risk-reduction costs, which are, however, not included in the risk analysis process but rather assessed for risk-reduction measurement planning. A complete assessment of costs caused by a lake-outburst event is provided in Chapter 14.
The spatiotemporal developments of land use are currently little integrated in exposure analyses (Cammerer and Thieken, 2013; Cammerer et al., 2013). A method to conduct future-oriented risk estimations considering future hazards and land-use changes is presented in Chapter 15.

Consequence analysis

In the consequence analysis, the hazard scenarios are set in relation to the exposure with the help of the intensity maps, to estimate the expected damage or loss for all considered scenarios. To prevent overestimation of damage potential, (3) spatial probability is included for processes such as snow-avalanches or rock-falls, whose spatial distribution might vary with every event and not extend over the entire area considered in the intensity maps (Fig. 3.5). Empirical estimations for hazardous processes in Switzerland are well established and can also be applied to other regions (BAFU, 2010).

The definition and use of (4) vulnerability varies substantially between different research disciplines or societies (Hufschmidt, 2011), but recent global efforts define it as the propensity to be adversely affected, or the characteristics of a person or system that make it susceptible to damaging effects of hazards (IPCC, 2012; UNISDR, 2009). The different, detailed concepts of vulnerability can roughly be summarized by the two categories physical and social vulnerability

(Bara, 2010; Hegglin and Huggel, 2008), which again are quite diverse. Social vulnerability can, for example, be understood as the ability of a person or a group to cope with loss, which can be assessed with the help of proxies. The aspects most stated in the literature are socioeconomic status, age, gender, race, ethnicity and populations with special needs (Cutter et al., 2009). Physical vulnerability usually characterizes the degree of physical impairment an object can expect to experience if affected by a particular hazard process (BAFU, 2010), which is related to the type of hazard and its magnitude (Bründl et al., 2009) and is captured in loss functions (Rheinberger et al., 2013; Totschnig and Fuchs, 2013).
The exact methods for implementation of vulnerability into the risk analysis procedure vary considerably. In Switzerland, physical vulnerability only is considered and included in risk analysis as a factor between zero (low) and one (very high), where zero means no impairment and one means total destruction. These values are even incorporated into software tools such as EconoMe (BAFU, 2010). Social vulnerability is not yet a fixed assessment variable in the established risk analysis approach (Bründl, 2009); recommendations on how to integrate this aspect have nevertheless been formulated (Bara, 2010). In other societies and nationalities, vulnerability is understood differently, depending on the respective situation and needs (e.g. Bara, 2010; GoC, 2007).
The Peruvian Civil Protection Agency INDECI (2006) has created its own manual for risk estimation, in which risk is the product of hazard and vulnerability, even though INDECI also refers to the UNISDR (2009) vocabulary and terminology. In this sense, the consequences are equated with vulnerability as the degree of weakness or exposure of an element against the occurrence of a hazard of given magnitude, which is expressed as a probability in percent from zero to 100. While the understanding and classifications of hazard are congruent with the Swiss concept, the consequences are defined differently. In addition, the consequence analysis is assessed on behalf of a different set of indicators that are relevant to the sensibility and the resilience of the Peruvian society: (i) The level of scientific and technological knowledge local people have about the dangers in their region. (ii) The degree of political and institutional organization is assumed to influence the capacity for disaster management or for fulfilling prevention and relief measures. (iii) The formal education of students regarding prevention and relief issues is assumed to impact the entire society's capacity for disaster management. (iv) Social vulnerability considers that the level of social trauma resulting from a disaster is inversely proportional to the level of organization in the affected community. (v) Economic vulnerability describes access to economic assets – meaning the level of income and the ability to meet basic needs – and is also considered. (vi) Physical vulnerability is related to the type of construction and material used as well as to the exposure to the hazard. This is the factor most similar to the Swiss system. (vii) Environmental and ecological vulnerability is the degree of resistance of the natural environment and the living things that make up a particular ecosystem, in the presence of climate variability.

The outcome of all consequence analysis is, independent of the exact procedure or terminology, a compilation of the expected loss for the given hazard scenarios, which serve as a main input for the final risk estimation.

3.2.3 Risk estimation

In the final step of the risk analysis, the probability of a scenario and its damage potential are brought into relation with each other with the help of the intensity maps. Again, a wide variety of approaches are proposed, depending on the framework of the analysis, which embraces scale, data availability and quality, as well as the purpose of the study (Kappes et al., 2012). Two strongly differing examples applying diverse metrics of risk description will be briefly outlined. In Switzerland, two quantitative risk indicators are calculated (Bründl et al., 2009). A given individual's risk of dying within a given reference period is calculated as the individual risk. The societal risk is calculated by summing up the risks for each individual person and object for every given scenario, resulting in the annual expected damage. This approach requires monetization of the entire loss, which pokes the discussions on risk evaluation, especially in regard to valuation of human lives (e.g. Lentz and Rackwitz, 2004). If the fatalities shall also be monetized, the willingness to pay for reducing mortality has to be taken into account (see e.g. Leiter and Pruckner (2009)). The willingness to pay allows for valuation the risk to the entire group of persons or objects in the potentially affected area in terms of Swiss francs per year.
Such quantitative risk analyses are only possible for well-investigated study areas. If the necessary information on societal structure and hazardous processes is not available, or if the scale of the study area is too large, qualitative approaches have to be applied, such as risk rating or risk-scoring systems (Fell et al., 2005). A widely recognized technique is a matrix-based risk estimation, in which risk levels are allocated to the matrix cells, whose axes are composed of the hazard and damage potential (an example is illustrated in Figure 3.6). This method was, for example, applied to a regional hazard study in the Pamir (Mergili and Schneider, 2011) and is also established in the national Peruvian risk assessment strategy (INDECI, 2006). The principle behind this risk-estimation method is comparable to the intensity-scale matrix-based techniques recommended for multi-hazard assessment in Section 3.2.1. This strategy is explained in more detail and applied to a local case in Chapter 15.

The risk, independent of the metric of its description, is the basis for any management activity. The theoretical framework for risk analyses of high-mountain lakes (especially with regard to process chains of outburst-events triggered by impact waves) was established in this chapter following the concept of integrated risk management. The assessment of such multi hazards requires detailed understanding of the processes as well as their interactions and relations. This process-specific knowledge basis is established in the next chapter with regard to identification, localization and assessment of outburst events (triggered by impact waves from rock or ice avalanches).

CHAPTER 4

IDENTIFYING AND ANALYSING HIGH-MOUNTAIN LAKE-OUTBURST HAZARDS

High-mountain lake-outburst events were introduced in the previous chapter as multi-hazard events, because of the variety of possible outburst mechanisms, which can again be a product of interactions between a number of disposition parameters and trigger mechanisms. This chapter treats the research question, "How can the lake-outburst potential, also due to impact waves, be systematically analysed and anticipated and what is the current state of knowledge and corresponding assessment methods?". The current knowledge basis in identification of hazards and the corresponding assessment techniques are gathered in this chapter.
Event analyses of high-mountain lakes aim to define the most likely outburst mechanism, the characteristics of the outburst hydrograph and the probability of occurrence. Correspondingly, schematic outburst hydrographs are presented in Section 4.1, to enable better assigning of the lake-outburst mechanism. The related disposition parameters, triggers and process interactions are explained in Section 4.2. The available hazard assessment techniques are presented in Section 4.3. Special focus is put on slope failures, as trigger mechanisms of a process chain causing overtopping (Section 4.3.4).

4.1 Lake-outburst hydrographs

Lake-outburst events can roughly be divided into four types, which are illustrated schematically in Figure 4.1, according to the magnitude and characteristics of the outflow hydrographs. The hydrographs of type I represent overtopping only, while type II and III assume a complete emptying of the lake, representing the probable maximum flows. Type IV hydrographs represent so called dam-crest floods.
The form of type I hydrographs caused by overtopping resembles the one of type II hydrographs;

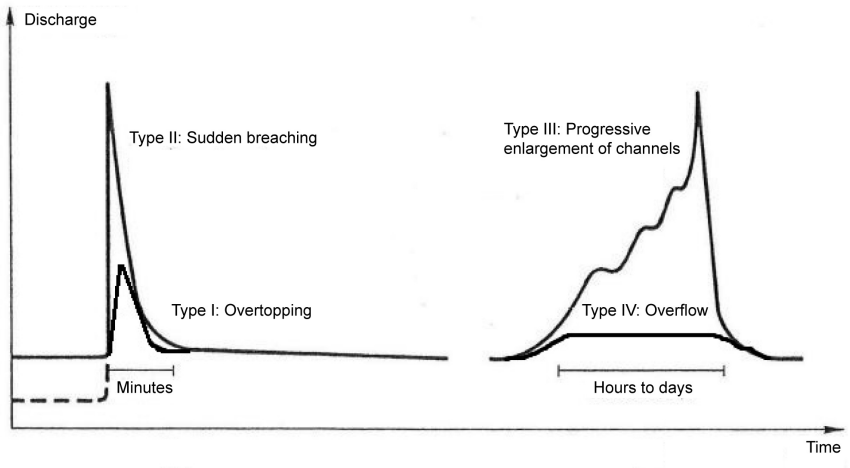

Figure 4.1: Idealized hydrographs representing overtopping (I), sudden breaching (II), progressive lake drainage (III) and overflow (IV). The form of type I hydrograph resembles type II; it does not, however, necessarily involve the entire lake volume. The idealized hydrographs II and III were originally published by Haeberli (1983) and also explained in Walder and Costa (1996).

they usually differ, however, with regard to the volume involved in the outburst event. Type II hydrographs are rather short, but feature a high intensity characterized by a high peak discharge, which usually occurs in case of sudden dam failures. Type III hydrographs are characterized by longer-lasting flows with lower peak discharges, which are features of progressive dam failure. Dam-crest floods (Type IV) can be assumed to be continuous, but not necessarily dangerous, overflows of the dam due to a rise in the reservoir water level (Wang and Bowles, 2006a).
This schematic is oversimplified, as many intermediate forms are possible in real outburst events. It nevertheless allows us to draw some first-order estimates on the severity of the consequences of a lake-outburst event as a function of the most likely outburst mechanism.

To determine the most feasible characteristics of the outburst flow, the most likely outburst mechanism has to be defined through identification and localization of disposition and trigger parameters as well as interactions, as illustrated in Figure 4.2. This illustration is the basis of the explanations on lake-outburst mechanism in the next section.

4.2 Lake-outburst mechanism and related disposition and trigger parameters

The main disposition parameter of dam instability is the compositions of the lake and of the dam themselves. The literature on forms, formation and failure of (natural) dams is wide and several compilations are available (e.g Cenderelli, 2000; Costa, 1994; Haeberli et al., 2010a; Iribarren Anacona et al., 2014; Korup and Tweed, 2007), whereby the compilation established by Costa and Schuster (1988) is probably the most frequently applied one. With regard to high-mountain lakes, the relevant dams are mainly ice, landslide, moraine and bedrock dams (Korup

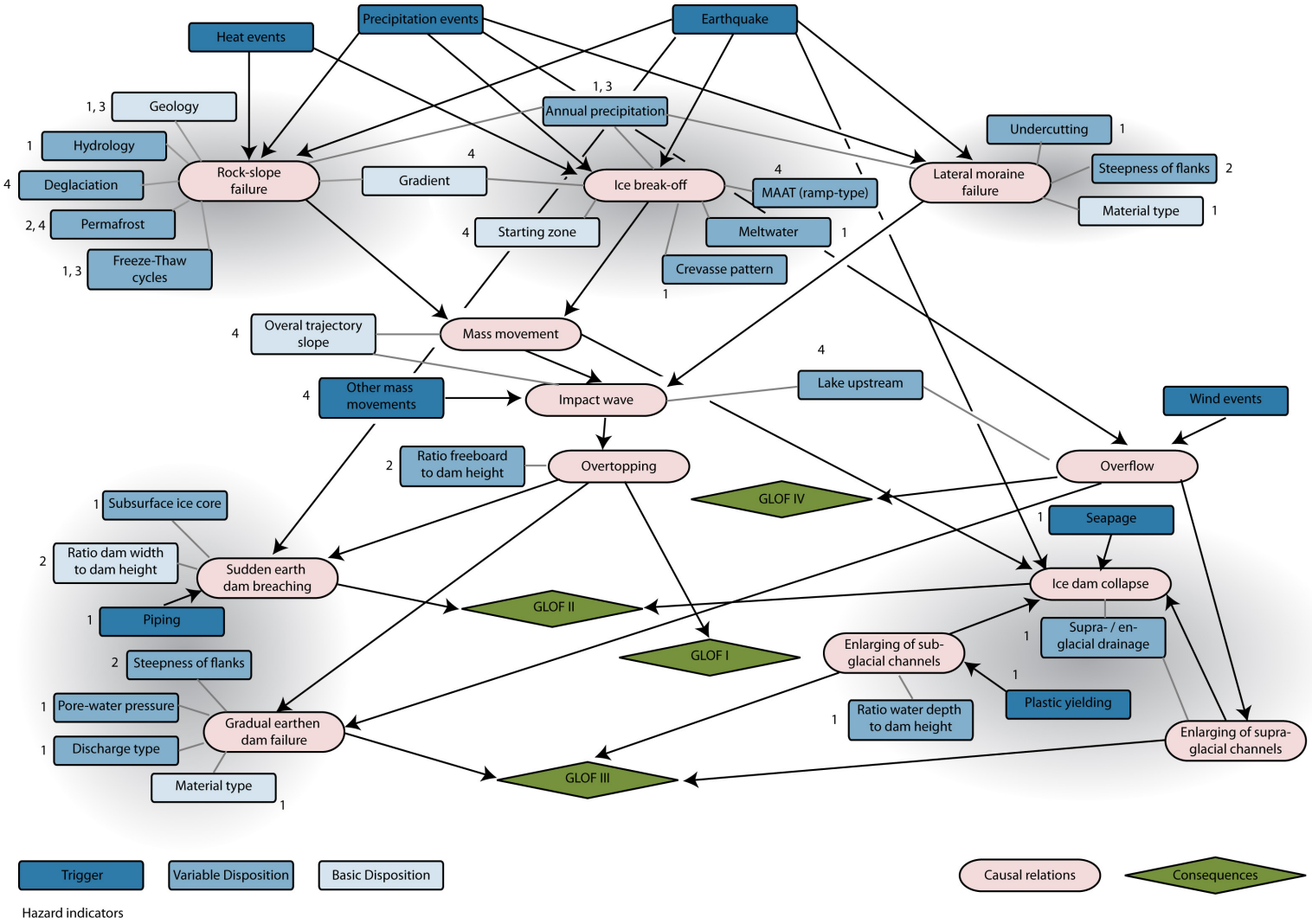

Figure 4.2: This lake hazard assessment scheme relates disposition and trigger parameters with outburst mechanism, interactions and hydrograph types. The hydrograph types overtopping (GLOF I), sudden breaching (GLOF II), progressive drainage (GLOF III) and overflow (GLOF IV) are illustrated in Figure 4.1. The starting zones of ice avalanches refer to ramp or cliff situations, which are illustrated in Figure 4.4. The numbers indicate the assessability of the respective parameter: 1 = assessability for current conditions on local scale; 2 = assessability for current conditions on regional scale; 3 = assessability for future conditions also on local scale; 4 = assessability for future conditions also on regional scale. See section 3.2.1 for differentiation of the disposition and trigger parameters.

and Tweed, 2007) rather than volcanic, fluviatile, eolian, coastal or organic dams (Costa and Schuster, 1988). Amongst these, ice dams are highly probable to fail, while earthen dams in general feature a medium to high and bedrock dams a low failing probability (Huggel et al., 2004). The different modes of failure, illustrated in Figure 4.2, are explained in the following section according to the dam type they concern (Section 4.2.1). Further, overflow and overtopping are dealt with; these are relevant to all dam types (Section 4.2.2).

4.2.1 Dam-type specific outburst mechanism

Earthen-dam failure

Moraine and landslide dams are in this thesis summarized as earthen dams, because both are characterized as a heterogeneous mixture of a variety of particle sizes (Costa, 1994). Moraine and landslide dams differ, however, with regard to their mode of formation and as to their shape (Korup and Tweed, 2007). Further, landslide dams are, contrary to moraine dams, reported to mostly fail within the first year after their formation (Ermini and Casagli, 2003). After having reached a stable state, however, the failure mechanism of landslide dams is similar to the ones that can affect moraine dams.

Disposition and trigger factors of earthen-dam failures have been summarized several times (e.g. Haeberli, 1992; Huggel et al., 2004; Iribarren Anacona et al., 2014; Wang et al., 2008). The stability of an earthen dam and the likelihood of an outburst depend on the geometry, internal characteristics and the probability of a triggering event (Richardson and Reynolds, 2000). A set of factors that define the disposition are indicated in Figure 4.2. The parameter's attributes and the associated failure probability are summarized in Table 4.1 for every failure mechanism.

Failure mechanisms specific to earthen dams are sudden mechanical breaching or gradual earthen-dam failure (e.g. Costa, 1994; Westoby et al., 2014). Gradual earthen-dam failure embraces two processes, retrogressive erosion and the more frequent progressive erosion. Retrogressive erosion, also called headcut erosion (Morris et al., 2009), begins at the outer dam flank. Progressive erosion starts at the upstream flank. Gradual earth-dam failure is mostly triggered by overflow, by overtopping, or by a combination of the disposition parameters (summarized in Table 4.1), which strongly reduce the dam stability until breach through high pore-water pressure.

Outburst flows from gradual earthen-dam failure usually resemble a hydrograph type III, while sudden earthen-dam breaching result in an outburst flow of type II.

Ice-dam failure

Ice dams are unstable as a matter of principle. Their susceptibility to failure can nevertheless be approached by qualitative description of a set of disposition parameters, as summarized in Table 4.1. Ice-dam failure mechanisms are reported in great detail (Costa, 1994; Iribarren Anacona et al., 2014; Post and Mayo, 1971) and can be summarized in three main categories.

The first category consists of enlarging of subglacial channels. This is not the most dangerous, but it is the most common failure mechanism (Walder and Costa, 1996), because several subprocesses are summarized within this description. These are (a) sub-glacial drainage through ice-dam flotation, which usually takes place in temperate ice once the water level reaches 90% of the height of the ice dam due to the difference between the densities of ice and water (Herget,

Dam type	Outburst mechanism	Disposition parameter		Attribute	Probability	Source
All	Overtopping	Ratio freeboard to dam height	V	low medium high	high medium low	Huggel et al. (2004)
Earthen	Sudden breaching	Ratio dam width to dam height	B	small (0.1-0.2) medium (0.2-0.5) high (> 0.5)	high medium low	Huggel et al. (2004)
		Ice core	V	present not present	high none	Clague and Evans (2000)
	Progressive failure	Material type	B	Ice in dam silt, sand, gravel rock, clay	high medium low	Clague and Evans (2000)
		Steepness of flanks	V	$< 35°$ $> 35°$	low high	Costa and Schuster (1988) Hubbard et al. (2005)
		Discharge type	V	Subterranean drainage Overflow channel	high low	Clague and Evans (2000)
Ice	Sudden and progressive failure	Ratio water depth to dam height	V	< 0.5 0.5-0.7 > 07	low medium high	Costa and Schuster (1988)
		Supra-/englacial drainage	V	none minimal moderate large	none low medium high	Reynolds (2003)
		Seapage	V	none minimal moderate large	none low medium high	Reynolds (2003)

Table 4.1: Disposition parameters mentioned in literature defining the stability of different natural dams. B = basic disposition parameter; V = variable disposition parameter. See Section 3.2.1 for differentiation of the disposition parameters.

2005; Thorarinsson, 1953); (b) subglacial channel building through plastic yielding, which depends on the hydrostatic-cryostatic pressure ratio and starts to become critical from lake depths around 200 m on (Iribarren Anacona et al., 2014); (c) formation of subglacial channels via increase in water supply and melting that produces flowing water; or (d) syphoning and drainage of the lake through the internal glacial drainage system. The second type of ice dam failures occur through enlarging of supraglacial channels, which is usually a consequence of overflowing lakes or impact waves (Post and Mayo, 1971). A rare but dangerous ice-dam failure mechanism is the third category of the sudden breaching or collapse of ice dams, which can be triggered by crack progression due to shear stresses (e.g. in the case of a surging glacier), by an earthquake or by the direct impact of a mass movement. An ice dam can also collapse as a consequence of subglacial drainage (Haeberli, 1983; Post and Mayo, 1971), e.g. in case of a blockage of channels (Reynolds, 2003).

Analogous to earthen-dam failures, enlarging of sub- and supraglacial channels leads to outflow hydrographs of type III, while ice-dam collapses generally cause hydrographs of type II.

Next to the just-presented lake-outburst mechanism specifically concerning earthen or ice dams, overflowing or overtopping can cause a lake-outburst event independent of the dam characteristics. These mechanisms are introduced in the following section.

4.2.2 Overtopping and overflow of dams

Overtopping and overflow are dam-type independent outburst mechanisms and thus the only processes which can also affect bedrock-dammed lakes. The ratio of the freeboard to the dam height is the most important disposition indicator in respect to both processes. The lower the ratio, the higher the probability of overtopping (Huggel et al., 2004).

Overflow
Overflow can be triggered by hydrometeorological events (such as strong precipitation or snow melt (Huggel et al., 2004)), by waves constructed through wind action (Wang and Bowles, 2006a), or as a consequence of the emptying of another lake located upstream (Haeberli et al., 2010a).
The probability of extreme hydrometeorological events could be described qualitatively (frequent, sporadic, unlikely (Huggel et al., 2004)), e.g. based on percentile values of long-term precipitation or temperature records (Valiente, 2001).
Overflowing of a dam can either constitute a dam-crest outburst flood of type IV, which is usually not dangerous. Or it can act as an element in a process chain leading to complete failure of an earthen or an ice dam, as illustrated in Figure 4.2.

Overtopping
Another process chain involves overtopping, which is the consequence of an impact wave (Fig. 4.2). Triggers of impact waves are usually rapid mass movement (Huggel et al., 2004), outburst flows from another lake located upstream (Haeberli et al., 2010a), or the failure of a lateral moraine.
The primary disposition factor for such an event is the steepness of the flank, which is assumed to be critical if it exceeds 35° (Costa and Schuster, 1988; Huggel et al., 2005). Undercut moraine parts are also highly prone to sliding into the lake. The moraine failure disposition further depends on the material type. Exposed moraine and debris material is more susceptible to failure than if it is already covered by vegetation (Clague and Evans, 2000). The annual precipitation rate is considered a further failure disposition parameter; feasible susceptibility classes are for example suggested by Santi et al. (2009). Feasible triggering events of lateral moraine collapse are an earthquake or a strong precipitation event.
Many other types of mass movements (see Section 10.1 for more details on classification of rapid mass movements) can impact a lake. The overtopping probability is related to the ratio of the volume of the impacting mass to the lake volume ((Huber, 1980; Müller, 1995; Walder et al., 2003) summarized in Huggel et al. (2004)). Complete emptying of the lake is assumed, if this ratio measures between 1:1 and 1:10 and a high probability (given a rather low freeboard) of overtopping is assumed for ratios between 1:10 and 1:100. The threshold of critical impact mass has to be defined for every lake individually as a function of the lake volume. Larger mass

movements inhibiting volumes greater than approx. 10,000 m^3 are generally of larger concern than small-scale slides.

High-mountain lake-outburst events triggered by impact waves induced by rapid mass movements like rock/ice avalanches belong to the most complex process chains, and have to be assessed in an event analysis (Fig. 4.2). This process chain is further relevant to all kinds of lakes, independent of the nature of the dyke. Correspondingly varied are the magnitude and characteristics of the outburst flows. The event analysis of a high-mountain lake is also demanding, because the respective outburst mechanism has to be defined for each lake individually as a function of the most probable trigger.
Subsequent to this overview on relations and interactions between process in connection with high-mountain lakes, efforts and advances in assessment methods and techniques are presented in the following section.

4.3 Methods for recognizing and analysing hazards

Huggel et al. (2002b) introduced the hazard assessment of lakes as a three-level procedure, the available methods for which are presented in this section. Firstly, any given lake has to be detected (Section 4.3.1), including determination of its volume (Section 4.3.2). Secondly, the outburst susceptibility of the lake has to be estimated (Section 4.3.3) before, thirdly, detailed event analyses may be carried out. The third step is here presented with regard to ice- and rock-slope instabilities (Section 4.3.4).

4.3.1 Lake detection methods

Probably the most fundamental step in the event analysis is the detection of lakes in time or even in anticipation of their formation. Remote sensing is a powerful discipline for lake detection (Ashraf et al., 2014). An overview on lake inventories established by means of remote sensing is provided in Table 4.2. The applied optical systems, data availability, resolution and applications to glacial hazards are for example summarized by Quincey et al. (2005).
Formation of lakes can also be anticipated for future conditions. A multi-level strategy to anticipate lakes in glacier beds with the help of simple criteria derived from the glacier surface and slope was developed by Frey et al. (2010a), which also includes first-order hazard estimations of lake outbursts. Other approaches digitally calculate the terrain of mountains without glaciers (Farinotti et al., 2009; Huss et al., 2008; Linsbauer et al., 2013). A GIS-based simulation of the recession of the Swiss glacier uncovers overdeepenings at certain locations. These overdeepenings are considered as potential sites of lake formation (Linsbauer et al., 2012).

Inventory basis	Inventoried region and source
Landsat	*Swiss Alps* (Frey, 2007; Huggel et al., 2002b), *Himalaya* (Wessels et al., 2002), *Nepal* (Mool, 1995; Bajracharya and Mool, 2005), *Hindukush* (Ashraf et al., 2012; Gardelle et al., 2011)
Landsat and Aster	*Tien Shan* (Bolch et al., 2012), *Nepal* (Bolch et al., 2008), *Patagonia* (Harrison et al., 2006), *Pamir* (Mergili and Schneider, 2011), *Afghanistan* (Molnia, 2009)
ALOS	*Bhutan* (Ukita et al., 2011), *Kirgistan* (Narama et al., 2010), *Tibet* (Wang et al., 2011)
SAR	*Switzerland* (Strozzi et al., 2012)

Table 4.2: A compilation of some lake detection studies and lake inventories established by means of remote sensing images.

4.3.2 Lake-volume estimation

Another important piece of information with regard to lake-outburst hazard is the lake volume. Different empirical equations exist to estimate the volume based on the lake area and depth; the most commonly applied ones were suggested by Huggel et al. (2002b) (Eq. 4.1) and by O'Connor et al. (2001) (Eq. 4.2):

$$V = 0.104A^{1.42} \tag{4.1}$$

$$V = 3.114A + 0.00016853A^2 \tag{4.2}$$

These equations can be applied on a regional level on a basis of remote-sensing lake area estimations. However, they neglect the fact that volume is never directly measured, which results in an undesired self-correlation. Furthermore the variability in the measurements is also disregarded. It is therefore more advisable – if only feasible for local-scale assessment – to directly measure lake depth and bathymetry.

Direct measurement of lake depths can be gained by echo sounding. During echo sounding, an acoustic signal is sent from a pulse emitter towards the lake bottom, where it is reflected to be received again by the same emitter upon its return. The lake depth is then derived as half of the product of the signal run-time with the impulse velocity. Currently, two main echo sounding systems are available. A multi-beam emitter enables accurate and detailed mapping of large areas in relatively short time by sending several hundred beams at a time. A single-beam emitter sends one impulse at a time, which requires interpolation of the resulting point lake depths in a second step (Schimel et al., 2010). Single-beam emitters are applicable in high-mountain lakes, as they are relatively easy to transport. Applications are described in reports from Peru, (Cochachin, 2011), from Greenland (Tedesco and Steiner, 2011) or from the Himalayas (Yao et al., 2012).
In Switzerland, first measurements of high-mountain lake depths were carried out by means of a single-beam emitter installed on a remote-controlled boat. The resulting lake depths were judged appropriate as first-order measurements, despite several factors influencing measurement accuracy, such as water temperature, density increase with depth or suspended load. The influence of further factors having an effect in high mountains, such as wind and wave action, causing roll-

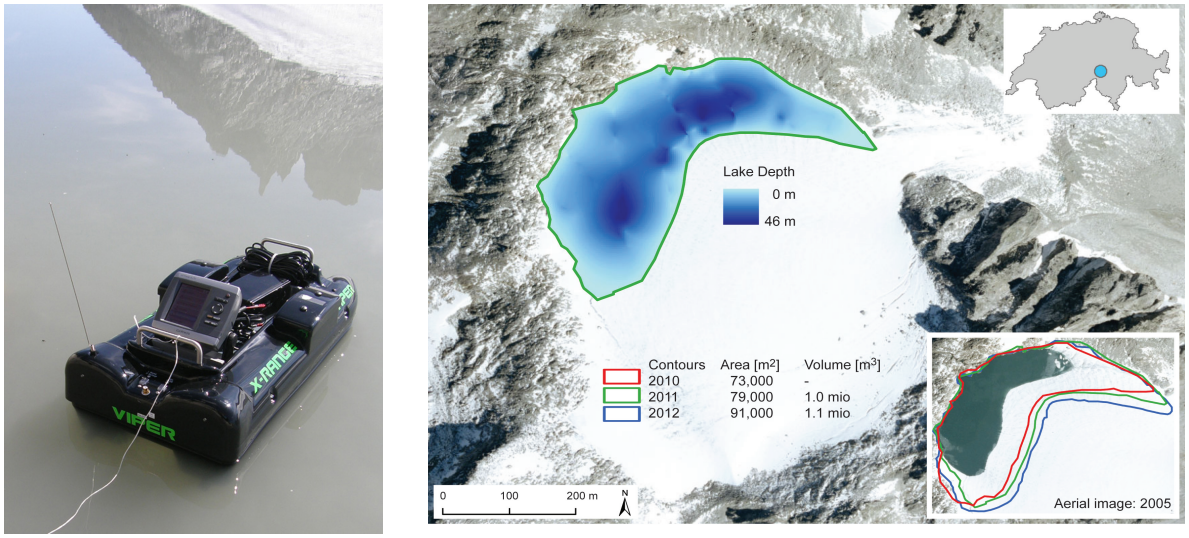

(a) The remote-controlled boat.

(b) Development of Lake Geeren, Switzerland.

Figure 4.3: Depth measurement and derivation of bathymetries for lakes in Switzerland. Aerial image 2005 from Swisstopo.

and pitch-effects, or different reflectance of different lake floors, are not yet investigated (Epp, 2013).
Lake volume and lake bathymetry can be calculated on basis of these point-depth measurements. The choice of interpolation is another crucial element for the quality of the resulting lake bathymetry (Epp, 2013). Such data is, despite all uncertainties, crucial and suitable for local hazard assessment, e.g. by means of numerical process simulation (which will be presented in detail in Chapter 10). Once a lake is detected, its susceptibility to failure is in a first step better assessed more generally before carrying out such detailed assessments.

4.3.3 Lake-outburst susceptibility assessment

The use of less extensive, more general and therewith also regionally applicable procedures is recommended for first-order hazard assessment. Emmer et al. (2014) provide an overview over existing lake-outburst assessment schemes (Table 4.3). Many of them are empirically based and therefore often only applicable to a specific type of lake or a certain geographic region. The principles of five selected procedures will be shortly outlined in the following pages; the process and interactions they refer to were already explained in detail in Section 4.2.

- The most recent procedure to assess the susceptibility of a lake-outburst flow was presented by Emmer et al. (2014) for lakes in the Peruvian Cordillera Blanca. It assesses five outburst-triggering mechanisms by means of decision trees considering 18 hazard characteristics. The outburst scenarios include (a) overtopping caused by an impact wave or (b) overtopping caused by a water inflow of a lake located upstream, as well as (c) dam fail-

Author(s)	Regional focus	LT	N	Method description
Bolch et al. (2012)	Tien Shan	GL	11	Partly objective semi-automatic assessment procedure
Clague and Evans (2000)	British Columbia (versatile)	MDL	6	Subjective manual assessment of factors indicating increased hazard
Costa and Schuster (1988)	versatile	MDL	4	Subjective manual assessment of factors indicating increased hazard
Grabs and Hanisch (1993)	versatile	MDL	11	Subjective manual assessment of factors indicating increased hazard
Gruber and Mergili (2013)	Pamir	GL,LD	8	Objective semi-automatic assessment procedure
Huggel et al. (2002b, 2004)	Swiss Alps	GL	5	Partly objective automatic assessment procedure
McKillop and Clague (2007b,a)	British Columbia	MDL	4	Objective statistical remote sensing based procedure (calculation)
Mergili and Schneider (2011)	Pamir	GL,LD	8	Objective semi-automatic assessment procedure
O'Connor et al. (2001)	Cascade Range (versatile)	MDL	2	Subjective manual assessment procedure
Reynolds (2003)	Cordillera Blanca	MDL	8	Subjective manual assessment procedure
Wang et al. (2008)	Himalaya	MDL	9	Partly objective manual assessment procedure
Wang et al. (2011)	Tibetian Plateau	MDL	5	Objective manual assessment procedure
Wang et al. (2012)	Himalaya	MDL	9	Partly objective semi-automatic assessment
Yamada (1993)	Himalaya	MDL	4	Subjective manual assessment of factors indicating increased hazard

Table 4.3: An overview of existing lake-outburst susceptibility assessments (Table shortened from Emmer et al. (2014)). LT = assessed lake types: MDL = moraine-dammed lakes, GL = all types of glacial lakes, LD = landslide-dammed lakes. N = Number of assessed characteristics.

ure caused by an impact wave, (d) dam failure caused by a water inflow of a lake located upstream or (e) a dam failure caused by an earthquake.

- Reynolds (2003) developed a hazard and a vulnerability assessment procedure. The hazard evaluation procedure represented a first-order assessment scheme, in which factors influencing magnitude and probability of an event each get a score. The total score per lake is then given based on an empirical scoring system (recommended for assessment of multi hazards in Section 3.2.1), with the help of which the lake-outburst hazard can be qualitatively described. Reynolds (2003) considered the volume of the stored water. The lake level relative to the freeboard, seepage through dam and ice-cored moraine and/or thermokarst features are called threshold parameters, while ice calving, rock/ice-avalanche risk and supra-/englacial drainage were considered lake-outburst triggers. The corresponding guidelines for techniques used within glacial hazard and risk assessments are also summarized with regard to engineering geological descriptions and mapping, slope stability analysis, geophysical methods and geomorphological mapping.

- Huggel et al. (2004) proposed a general assessment scheme in form of a decision tree starting with the detection of the lake and aiming at estimating the lake volume, the probable maximum discharge as a function of the dam type, the probable flow volume under consideration of entrainment, as well as the probable maximum travel distance (for debris flows). The probability of a lake-outburst event was in this scheme derived by attributing qualitative probabilities to five disposition parameters, which contained the dam type, the ratio of the freeboard to dam height, the ratio of dam width to dam height, the occurrence of impact waves triggered by rock/ice-avalanches into the lake, and extreme meteorological events.

- A similar setup was proposed by McKillop and Clague (2007a) to assess potential peak discharge, maximum travel distance, maximum flow volume and maximum area of inundation for moraine-dammed lakes. Contrary to the previous assessment schemes, a logistic regression model is implemented in their scheme as a predictor of the outburst probability of moraine-dammed lakes, which is based on statistical evaluation of 186 lakes in British Columbia (McKillop and Clague, 2007b). This model took into account parameters assessable with the help of remote sensing only, which are geology, ice-core of the moraine, lake area and the moraine height-to-width ratio.
- Lake hazard assessment approaches were also established for Asian mountain ranges. Wang et al. (2011) presented first-order assessment schemes for Tibetan mountains. Overtopping triggered through ice avalanches was observed to be the most frequent outburst mechanism. Their method considered two parameters with regard to the adjacent glaciers' characteristics (mother glacier area, mother glacier snout steepness), two parameters characterizing the lake-glacier relationship (distance between lake and glacier terminus, slope between lake and glacier) and mean slope of the moraine dam. The parameters were further weighted with the help of a fuzzy consistent matrix to define thresholds for classification of the parameters.

Remote sensing is also a very helpful tool in detecting the features needed to identify and localize disposition and trigger processes over a large area (Bolch et al., 2008, 2012; Huggel et al., 2002b; Quincey et al., 2005; Richardson and Reynolds, 2000). Correspondingly, automatic lake detection procedures based on remote sensing can be combined with first-order assessment of, e.g. ice-avalanche impact potential (Frey et al., 2010b).
Most of these approaches consider the scenario of an outburst triggered by an impact wave in a very generalized manner only, e.g. by distance relationships between lakes and glaciers or rock walls. To really assess the event of an outburst flow generated by an impact wave, the disposition and trigger parameters of the rapid mass movement have to be identified and localized.

4.3.4 Slope-instability assessments

In principle, any kind of rapid mass movement exhibits the potential to cause a lake outburst. As mentioned in the introduction (Section 1.1), many of the new lakes are and will be located underneath hanging glaciers and seracs or at the foot of oversteepend and destabilised rock slopes (Haeberli et al., 2010a). This situation can be problematic, as slope stability is also assumed to be affected by climate change. The focus of the present section is therefore put on ice break-offs and failures in rock-slopes. In these cases, the event is defined as the slope failure (Fig. 3.4), for which the disposition and trigger parameters (summarized in Table 4.4) have to be assessed.

Ice break-off
Three crucial disposition factors of ice avalanches are the slope, the glacier type and the thermal regime (Alean, 1985; Huggel et al., 2004), which are illustrated in Figure 4.4. A distinction can be identified between cliff-type and ramp-type ice-avalanche starting zones (Alean, 1985),

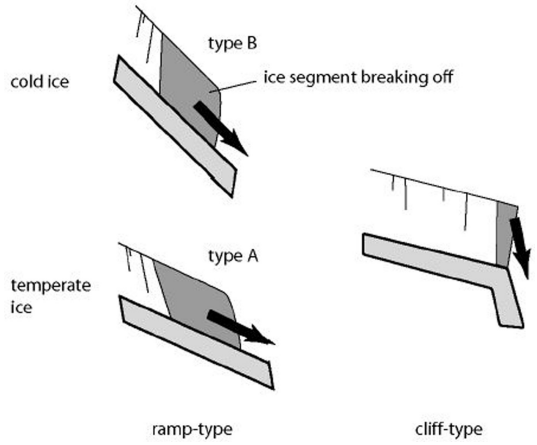

Figure 4.4: Idealized types of ice-avalanche starting zones. A and B exhibit different slope angles. Most or all of the ice in the type B starting zone is frozen to the bedrock (high altitude); most or all of the ice near the bedrock of the type A starting zone is at the pressure melting-point (lower altitude). Figure from Salzmann et al. (2004), caption after Alean (1985).

which differ in volume and probability. As a first and very general assumption, cliff-type situations can be credited with smaller but more frequent events, while ramp-type situations are observed to produce fewer but larger ice avalanches. Glaciers can further be classified into cold and polythermal (Haeberli, 1976), according to the temperature at the bottom, which can be approached by means of the mean annual air temperature (MAAT) (Huggel et al., 2004). While ice avalanches are possible from a gradient of ca. 25° in temperate glaciers, the minimal slope angle has to be much steeper (45°) for cold glaciers (Haeberli et al., 1989). Depending on the temperature regime, failure of ramp-type hanging glaciers can occur as mechanical break-off or as sliding (Faillettaz and Funk, 2013). It has to be considered in hazard assessments, that thermal regimes might alter as a consequence of climatic changes (Huggel et al., 2013; Stoffel and Huggel, 2012).
Ice avalanches can also detach from other topographic situations; therefore areas featuring many crevasses or changing crevasse patterns should be of concern, especially if the catchment behind the zone is of large size (Fig. 4.2). The size of the catchment indicates the amount of meltwater available, which can reinforce instabilities, especially in combination with strong precipitation events.

A systematic first-order, three-level approach for identification of potential ice-avalanche release areas for broad regions was presented by Salzmann et al. (2004). But the localization of potential ice-avalanche detachment zones on a local scale remains a challenging task (Margreth and Funk, 1999). Evidences of failure, e.g. in form of a slowly opening transverse crevasse, can often not be observed long in advance, which complicates volume estimations, which further vary depending on the season (summer, winter). Therefore, continuous monitoring with the help of aerial photographs and remote sensing is indispensable for detecting problematic developments of the glacier. The probability of failure of already recognized stability problems in ice on a local scale, can be defined e.g. by means of aerial survey (Dalban Cannassy et al., 2011), by observation of seismic shaking (Faillettaz and Funk, 2013) or by means of finite time models (Pralong et al., 2005).

Rock-slope failure
Rock-slope failures are reported to detach at a slope angle of ca. 30° (Fischer et al., 2012; Gruber and Haeberli, 2007), which is probably the most important basic disposition parameter. Despite

Rock-slope failure Parameter			**Sources (Selection)**
Topography	Gradient	B	Fischer et al. (2012); Frattini et al. (2008); Gruber and Haeberli (2007)
	Elevation	B	Fischer et al. (2012); Gruber and Haeberli (2007); Noetzli et al. (2003)
Geology	Transition zones	B	Fischer et al. (2012); Frattini et al. (2008); Gruber and Haeberli (2007)
	Lithology	B	Fischer et al. (2012); Frattini et al. (2008)
	Rock strength/quality	B	Marinos et al. (2005); McColl (2012); Jaboyedoff et al. (2004b)
Hydrology	Fluid pressure	V/T	Fischer et al. (2012); McColl (2012)
	Chemical weathering	V	McColl (2012)
Glacier	Proximity	B	Fischer et al. (2012); Haeberli et al. (1997); Wegmann et al. (2004); Allen et al. (2011)
	Glacial erosion	V/T	McColl (2012); Augustinus (1995)
	Debuttressing	V/T	Ballantyne (2002); McColl et al. (2010); McColl (2012)
Permafrost	Distribution	B/V	Fischer et al. (2012); Gruber and Haeberli (2007); Boeckli et al. (2012a)
	Surface temperature	V	Gruber et al. (2004); Noetzli et al. (2003)
	Rock temperature	V	Davies et al. (2001); Gruber et al. (2004); Noetzli and Gruber (2009)
	Rock-ice mechanics	V/T	Krautblatter et al. (2013)
Vegetation cover	Absence of vegetation	V	Frattini et al. (2008)
Climate	Hydrometeorological events	T	Hasler et al. (2011); Huggel et al. (2004)
	Freeze-thaw cycles	V/T	Matsuoka (2008)
Ice break-off Parameter			**Source (Selection)**
Topography	Gradient	B/V	Alean (1985); Huggel et al. (2004); Rothenbuehler (2006)
Glacier-permafrost	Interaction	V	Huggel (2009)
Climate	Thermal regime (MAAT)	V	Haeberli (1976); Huggel et al. (2004)
	Hydrometeorological events	T	Huggel et al. (2004)

Table 4.4: Factors mentioned in literature, which define the location of possible detachment zones of rock, ice and rock/ice avalanches. Classification into B = basic disposition parameter; V = variable disposition parameter; T = trigger; based on McColl (2012) and this study.

that criterion, slope stability assessment is very complex, especially in paraglacial environments (McColl, 2012). The exact processes, interactions, time-scales of action or reaction are not yet fully understood. A comprehensive review on the state of the knowledge was given by McColl (2012), and is touched on briefly here.

Basic geological rock conditions, such as lithology (Fischer et al., 2012; McColl, 2012), together with joint characteristics or structure (Gruber and Haeberli, 2007; Jaboyedoff et al., 2004) define rock mechanics and are continuously preconditioning slope stability (Marinos et al., 2005). Joints provide channels for water and corrosion surfaces for weathering processes (Holm et al., 2004; Jaboyedoff et al., 2004b). They are important in relation with hydrometeorological predisposition or triggering events such as rainfall or melting of snow and ice, which might lead to an increase of pore water pressure triggering the slope failure (Hasler, 2011).
The stability can be altered by further preparatory and trigger parameters, which are related to climate, weather or paraglacial processes. Freeze-thaw cycles are usually connected to continuous erosion. Annual cycles might, however, at some point also destabilize even large rock masses (Matsuoka, 2008). Paraglacial processes can introduce changes into geomechanical rock-properties (Fischer et al., 2006, 2010) and have the potential to act as variable disposition parameters as well as immediate triggers (McColl et al., 2010; McColl, 2012).

Glacial erosion leads to steepening, deepening or undercutting of rock slopes, which favours debuttressing during and after the retreat. Debuttressing indicates the loss of support that glaciers provide to adjacent rock slopes. It is assumed unlikely to act as a direct trigger (Ballantyne et al., 2014); it might, however, cause paraglacial stress-release, a thesis which is currently under investigation (McColl et al., 2010). The action of paraglacial stress-release is widely recognized and redistributions of stresses are known to alter the jointing, which implies changes in rock strength and in failure surfaces (Hencher et al., 2011).
Permafrost degradation was also considered in relation to slope instabilities (Davies et al., 2001), e.g. by thawing of ice-rich layers at the bottom of permafrost through extra-hot summers or strong rainfall (Gruber and Haeberli, 2007). Both slow subcritical destabilization of rock slopes, enabling large slope failures, as well as rapid responses to warming, potentially resulting in small slope failures, are assumed connected to the mechanics of permafrost rock (Krautblatter et al., 2013).

Comprehensive hazard assessment schemes are available with regard to rather small-scale rockfall processes (e.g. Agliardi and Crosta, 2003; Frattini et al., 2008; Santi et al., 2009), which aim at defining the factor of safety. These procedures can be taken as an assessment starting point; they are, however, not designed for larger events and do not explicitly take into account paraglacial processes.
Geometrical characteristics of discontinuities indicating potential sliding zones, however, can be detected on a regional scale by means of a digital elevation model (Jaboyedoff et al., 2004c). The rock mass properties of individual slopes can e.g. be estimated by means of the Geological Strength Index (GSI), which is based on qualitative observations of rock-mass characteristics, the material, structure and the geological history (Hoek and Brown, 1997; Marinos et al., 2005). Further methods characterizing joints are available (Priest, 1993).
Most of the processes assigned to deglaciation can hardly be directly observed and have to be considered in a more general way. Holm et al. (2004) attributed deglaciation to glacial retreat since the Little Ice Age (LIA) and provided a corresponding decision flowchart assisting with identification of associated landslide hazards for British Columbia. Allen et al. (2011) assumed the area affected by deglaciation in New Zealand within distances beyond 300 m from glaciers. Permafrost distribution can be estimated based on simulations of surface and subsurface thermal conditions (Noetzli and Gruber, 2009; Noetzli et al., 2007). A permafrost index map (APIM) was elaborated for debris-covered surfaces and for steep bedrocks in the Alps (Boeckli et al., 2012a). The APIM is based on a statistical model explaining the mean annual rock-surface temperature by means of the mean annual air temperature (MAAT), the potential incoming solar radiation, the sum of precipitation and a seasonal precipitation index (Boeckli et al., 2012b). A global permafrost distribution map is also available at a scale of 1 km, which is based on the MAAT only, but also includes other effects stochastically (Gruber, 2012). Methods for exact detection of permafrost are summarized in Harris et al. (2009).

The potential sliding volume can be approached by means of the "Sloping Local Base Level" technique, which estimates the potential geometry of a failure surface for an unstable area (Jaboyedoff et al., 2004). More precise volume determination of the unstable mass are achieved by means of combined field and remote surveys, applying terrestrial laser scanning, and terres-

trial infra-red thermography (Gigli et al., 2014). Monitoring methods, which apply for local slope instabilities, contain InSAR (Jaboyedoff et al., 2012) or SAR interferometry in combination with differential GPS, airborne digital photogrammetry and airborne photography interpretation (Strozzi et al., 2010).

Synthesis

This chapter treated the research question "How can the lake-outburst potential, also due to impact waves, be systematically analysed and anticipated and what is the current state of knowledge and corresponding assessment methods?". In summary, the analysis of a high-mountain lake-outburst event is extensive because of the complexity of the environment and the multitude of interactions. Methods for assessment of the lake-outburst susceptibility are available, but most of them do not account for process chains in detail. The most complex and therefore probably the least investigated outburst mechanism is the process chain of an impact wave induced through a rock or an ice avalanche. The related disposition and trigger events are mostly recognized, but the exact processes and interactions are not yet fully understood. Correspondingly, assessment of slope-failure susceptibility in paraglacial environments remains challenging and approved assessment procedures are missing. With regard to the climate sensitivity of many of the involved disposition and trigger parameters and the ongoing changes in the high-mountain environment, the possibility especially of rock-avalanche impacts has to be considered to be increasingly significant. The relevance of the rock-avalanche impact susceptibility of high-alpine lakes in Switzerland is assessed more precisely in the next chapter.

Part II

Long-term rock-avalanche impact susceptibility of high-alpine lakes in Switzerland

As outlined in the previous chapter, the process chain of rock avalanche-induced impact waves triggering an outburst flow from high-mountain lakes is so far barely investigated. With regard to the climate sensitivity of many of the involved disposition and trigger parameters and the ongoing changes in the high-mountain environment, this scenario has to be considered to be ever more significant, also because of the appearance of numerous overdeepenings in the newly exposed glacier beds, which are assumed to represent sites of potential future lake formation (Linsbauer et al., 2013).
The relevance of the subject to Switzerland is in this part assessed for current and future conditions. The research question treated is "Which of the present and future lakes in the Swiss Alps are most susceptible to rock-avalanche impacts?".

To this purpose a regional intercomparison of the rock-avalanche impact disposition in the catchment of high-alpine lakes in Switzerland is attempted. This study is divided into five chapters. In the next chapter 5, a model for rock-avalanche impact disposition assessment is developed, which is applied in a deterministic approach to derive the spatial distribution of the disposition in the catchments of lakes (Chapter 6). In Chapter 7 this model is implemented into a probabilistic framework to assess the quantitative rock-avalanche impact disposition under consideration of the inherent uncertainties. In the Chapter 8 the robustness and the reliability of the model and its implementations is assessed, before discussion of the relevance of the topic for Switzerland with regard to the potential damages (Chapter 9).

CHAPTER 5

DEVELOPING A MODEL OF ROCK-AVALANCHE IMPACT DISPOSITION INTO HIGH-MOUNTAIN LAKES IN SWITZERLAND

The model developed in the present chapter aims at assessment of the rock-avalanche impact disposition for high-alpine lakes in Switzerland for current and for future conditions. This model shall in the following chapters be applied to prioritize hazards and risks by identifying hotspots and critical locations, which is a requirement for risk management (as mentioned in Chapter 3). The reality must be represented in a simplified way in order to understand complex processes (Bossel, 2004). The application of quantity-oriented (physical) models, which aim at predicting the value of an observable quantity, such as, e.g. flow velocity, is not feasible on the regional scale of the Swiss Alps. Therefore the relations among sets of factors have to be described by event-oriented models, which consist of logical terms describing the conditions under which events occur (Nilsen and Aven, 2003).

5.1 Model concept

This section outlines the development of the model. The principles (Section 5.1.1), the considered parameters (Sections 5.1.1 and 5.1.2), the aspired results (Section 5.1.3), and established terminologies (Sections 5.1.2 and 5.1.3) are introduced.

5.1.1 Principles of the model

To derive the potential of a rock-avalanche impact in a lake, three elements have to come together as illustrated in Figure 5.1: most basically, an existing lake is identified. Secondly, slopes that are potentially unstable on a large scale – characterizing the rock-avalanche disposition – have to be within the catchment of the lake. And thirdly, the lake has to be situated within the runout distance of the potential rock avalanche. Only if all requirements are fulfilled does a catchment feature a rock-avalanche impact disposition for the lake.
Disposition and trigger parameters characterizing slope instability have been outlined in the previous Chapter 4. Not all parameters are assessable for future condition and on regional scale, as required by the aim of this chapter. Assessments of some parameters require direct measurements and are correspondingly only realisable for local investigations under current conditions. Only those disposition parameters were considered for the model which were introduced in Figure 4.2 as assessable long-term and on a regional scale. These are slope, lithology, deglaciation, permafrost and the overall trajectory slope. The latter is assumed to be an appropriate estimate of the runout distance of a mass movement (for further options of runout estimates see the upcoming Chapter 10).
All these parameters are intrinsic characteristics of the territory and its elements and contribute to the susceptibility of occurrence of a rock-avalanche impact in a lake, as it was defined in Section 3.2.1. The rock-avalanche impact disposition (RAID) into the lake is synonymous with the rock-avalanche impact susceptibility (RAIS) of the lake. The expressions marked italic in the Sections 5.1.2 and 5.1.3 will be reused often within this part of the thesis and are highlighted to guarantee better understanding of the upcoming analyses.

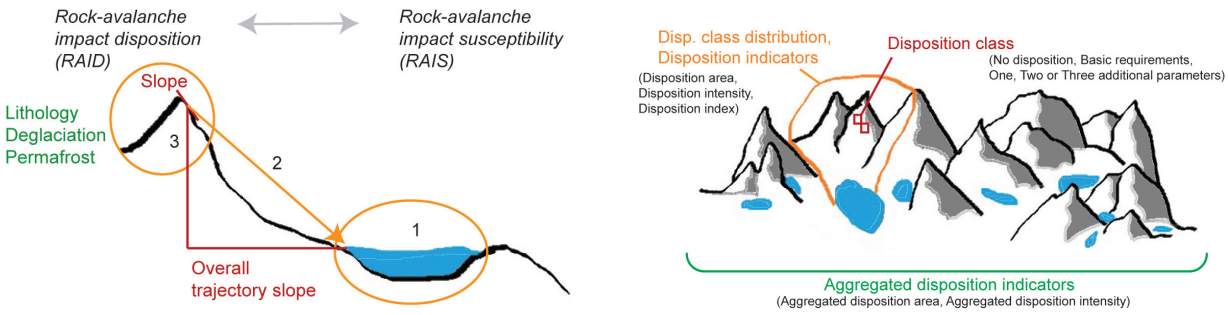

(a) The concept of the RAID model.

(b) The results of the RAID model.

Figure 5.1: The concept and the results of the rock-avalanche impact disposition model. Concept (a): the numbers indicate the basic elements required to be present: (1) A lake has to be situated within (2) the runout distance of (3) a potential unstable slope in its catchment. The decisive disposition parameters are written in red, while the green elements refer to the non-decisive disposition parameters. Aspired results (b): The aspired results on scale of the smallest unit (red), at catchment scale (orange) and at regional scale (green).

5.1.2 Classification of the disposition parameters

This section contains the description of the model development. Not all parameters were given equal weights for the RAID assessment. Differentiation was made between *decisive* and *non-decisive parameters* (indicated in Figure 5.1a in red and green). The attributes of the disposition parameters were classified on whether they or not contribute to slope instability and impact disposition by means of *classification rules*, which are summarized in Table 5.1. The details are explained in the following.

The topographic potential, composed of (a) slope and (b) overall trajectory slope, was assumed to be a decisive requirement for a rock avalanche to (a) detach (see Section 4.2.2 for the reasoning) and to (b) reach a lake (Romstad et al., 2009). The basic requirements for rock-avalanche impact disposition were only fulfilled if a location featured as much of a slope angle $> 30^{\circ}$ as an overall trajectory slope to the lake $> 25\%$. If one or both conditions were not met, no RAID was assumed present.

The other parameters (deglaciation, lithology and permafrost) were considered non-decisive parameters, as their influence on slope stability was assumed, but not yet conclusively shown in literature (see also Section 4.2.2 for the reasoning). The evaluation of a dataset of the release zones of 69 rock avalanches in the Swiss Alps by Fischer et al. (2012) indicated the following classification rules: effects of deglaciation were considered present in the area deglaciated since the LIA around 1850. With the exception of conglomerate and schist, all lithology categories suggested by Fischer et al. (2012) – mafic metamorphic, granite/diorite, gneiss, limestone – were present in the catchments of past rock avalanches in the Swiss Alps and were therefore assumed to contribute to rock-avalanche disposition. The effect of permafrost was ambiguous in the dataset of Fischer et al. (2012). In the present study, the presence of permafrost was assumed

Disposition parameters	**Categories**	**Classification (rules)**	**Disposition elements**
Decisive Parameters			
Slope	$< 30^{\circ}$	slope $< 30^{\circ}$ and/or ov. tr.	
	$> 30^{\circ}$	slope $< 25\%$ = not fulfilled	No disposition
Overall trajectory	$< 25\%$	slope $> 30^{\circ}$ and ov. tr.	
slope (ov. tr. slope)	$> 25\%$	slope $> 25\%$ = fulfilled	Basic requirements
Non-decisive parameters			
Permafrost	API < 0.5	not fulfilled	No add. parameter
	API > 0.5	fulfilled	Additional parameter
Lithology	Conglomerate, Schist	not fulfilled	No add. parameter
	Gneiss, Limestone, Granite/ Diorite, Mafic Metamorphic	fulfilled	Additional parameter
Deglaciation	No glacier recession since 1850	not fulfilled	No add. parameter
	glacier recession since 1850	fulfilled	Additional parameter

Table 5.1: Overview on the rock-avalanche impact disposition model: Categorization of the chosen disposition parameters and the corresponding classification into disposition elements. API = Alpine Permafrost Index (introduced in Section 5.2.2).

as an additional parameter, where its occurrence is widely probable. These areas feature an enhanced potential of alterations in the rock mechanics as a consequence of temperature-induced permafrost degradation, which might lead to a subcritical destabilization of rock slopes.
According to these classification rules, the categories of the disposition parameters were classified into *disposition elements* (named "no disposition", "basic requirement", "no additional parameter" and "additional parameter"), depending on whether or not they contribute to slope instability and impact disposition (Table 5.1).

5.1.3 Aspired results

The outcomes aspired to by the model differ as a function of the scale at which the assessment is carried out. These scales and the respective results sought are illustrated in Figure 5.1b and are explained in the following.
The disposition elements can be compiled for the smallest analysed unit (e.g. for each location or catchment), which results in five possible *disposition classes* (RAID class): if a location does not fulfil the classification criteria of the basic requirements, no disposition is present. Certain areas feature the basic requirements only, while other areas further exhibit one, two or three additional parameters respectively. The model results therefore in a RAID class per location.
Based on this information, spatially non-explicit products describing the RAIS can be derived. A first product is the percentage each disposition class covers of the entire catchment area, summarized in the *disposition class distribution*. From this information three *indicators* of the RAID per catchment can be derived, which served for the regional intercomparison of the RAIS of high-alpine lakes in Switzerland. One indicator is the extent of the area exhibiting RAID in km^2, called *disposition area*. Another indicator accounts for the magnitude and intensity of the RAID (e.g. the number of additional parameters present), called *disposition intensity*. The disposition intensity is an artificial construct and does therefore not exhibit a unit. These two indicators are a function of the catchment size and are in this way only of limited suitability for comparison of the RAIS of different lakes. To make the RAID comparable between different catchments, an *impact index* was further built, consisting of the product of the disposition area with the disposition intensity per catchment or lake.
It is not feasible to discuss the changes in disposition area or intensity for each catchment or lake, due to the large number of analysed lakes. To nevertheless analyse the changes in the RAID between the two considered time steps (current conditions and under conditions of deglaciated Alps), the values of the RAID indicators can be aggregated over the entire study area (here the Swiss Alps) per time step, resulting in the *aggregated disposition area* and the *aggregated disposition intensity* on a regional scale.

This theoretical framework was implemented into a working environment in a next step. The applied datasets representing the disposition parameters in the Swiss Alps for current and future conditions, as well as for their categorization according to the classification rules (Table 5.1), are presented in the following section.

5.2 Implementation of the model in the Swiss Alps

The implementation of the model into a Geographic Information System (GIS) is presented in this section. The datasets chosen to represent the lakes and the disposition parameters for current and future conditions are presented, together with an explanation of the categorization of these parameters according to the classification into the disposition element as defined in Table 5.1.

5.2.1 Choice of lake, catchment and topographic datasets

A first choice had to be taken regarding the lake datasets. For the purpose of this study, high-alpine lakes were defined as natural or artificial lakes located above 1,500 m above sea level (a.s.l.). For present conditions only lakes represented in the 25-m digital elevation model (DEM) (Swisstopo, 2010) were considered. For future conditions this lake dataset was extended by the overdeepenings modelled in the rockbeds underneath today's glaciers (Linsbauer et al., 2012), which were assumed to be locations of potential future lakes. This second dataset represents the conditions after deglaciation of the Swiss Alps, which were modelled approximately towards the end of this century.
The catchments of the lakes had already been defined by Serraino (2011) for both time steps. For present conditions, this information was derived from the 25-m DEM (Swisstopo, 2010), while the modelled DEM of the entirely deglaciated Alps (Paul and Linsbauer, 2012) was used as a basis for the assessment of future catchments. Serraino (2011) also calculated the topographic potential based on these datasets for all catchments. These datasets were directly adopted for the present study. The datasets representing the non-decisive parameters are presented in the next section.

5.2.2 Choice of datasets and categorization of additional disposition parameters

Different datasets were applied to the analyses of present and future conditions. They are presented separately.

Current conditions
The datasets representing the non-decisive disposition parameters and their categories for present conditions were compiled as follows: the deglaciated area was derived from subtraction of the glacier outline of the LIA (Maisch et al., 1999) with the glacier outline in the year 2000 (Paul, 2007). The entire deglaciated area was classified as a contributing category, fulfilling the requirements of an additional parameter (Table 5.1).
Lithology categories were compiled according to Fischer et al. (2012) into the categories conglomerate, gneiss, granite/diorite, limestone, mafic metamorphic and schist by means of the Geotechnical Map of Switzerland (BWG and SGTK, 2000). Lithology categories were strongly

generalized, also combining similar lithologies, which can have different geotechnical and geomechanical characteristics. Conglomerate and schist were the only categories not fulfilling the classification rules, as summarized in Table 5.1.
Permafrost distribution was estimated according to the APIM (Boeckli et al., 2012a,b), which features four categories of permafrost occurrence probability. Detailed information on permafrost occurrence assessment was given by Boeckli et al. (2012a). Here the relevant points regarding the API are summarized only. An index value between zero and 0.25 indicates areas not covered by permafrost. Index values between 0.25 and 0.5 indicate permafrost presence only in very favourable conditions. In areas featuring indices from 0.5 to 0.75, permafrost is assumed present mostly in cold conditions. Higher values up to one indicate permafrost presence in nearly all conditions. The threshold classifying the disposition parameter into a disposition element was set at an API of 0.5. This cautious decision took into account that permafrost research is recent and that process understanding and modelling are only relatively reliable. Therefore only where permafrost is assumed reliably modelled, at least in cold conditions, could areas be classified as contributing to rock-slope instability disposition.

Classification of the disposition parameters into disposition elements was carried out according to the same rules (Table 5.1) for both time steps, current and future conditions. The datasets were, however, chosen differently or adapted to expected future conditions as justified next.

Future conditions
For future conditions assuming deglaciated Alps, the following datasets were chosen for representation of the non-decisive disposition parameters: effects of deglaciation were assumed to occur in the entire area where deglaciation occurred beginning after the LIA in 1850.
No models of future permafrost distribution are available. Therefore the APIM (Boeckli et al., 2012a) was applied unaltered. For permafrost conditions in the exposed glacier beds, assumptions on the evolution were leaned on the assumption of APIM, that permafrost nowadays is mostly distributed over the area deglaciated since the LIA. Consequently, an index value of 0.5 was allocated to today's glacier beds. Similarly, the glacier bed's lithology had to be estimated based on the surrounding lithology and topography, as measurements or observations were missing.

Synthesis
The development of a RAIS-model for high-alpine lakes in Switzerland was presented in this chapter. The following chapters contain assessments based upon this model. Chapter 6 summarizes the application of the model in a spatially-explicit, deterministic approach. This procedure enables mapping of the distribution of the disposition classes in the catchment of the lakes, which allowed for identification of critical locations. In a second analysis, the model was applied in a probabilistic approach, which enabled accounting for uncertainties. A ranking of the lakes according to their impact index was established. The ranking allows for identification of hotspots of current and future RAIS in the Swiss Alps. In a third step, an uncertainty analysis and a sensitivity analysis were carried out to assess the reliability and the robustness of the model results. This knowledge enabled assessment of the relevance of a potential lake-outburst event in Switzerland triggered by an impact wave, which is discussed in Chapter 9.

CHAPTER 6

SPATIALLY-EXPLICIT, DETERMINISTIC ASSESSMENT OF THE ROCK-AVALANCHE IMPACT DISPOSITION

This chapter aims at identifying locations of enhanced RAID in the catchments of Swiss high-mountain lakes, which is an important requirement for risk management as outlined in Chapter 3. The RAIS model was implemented in a GIS, which was an optimal precondition for a spatially-explicit analysis of the distribution of disposition classes in the catchment of high-alpine lakes. For this purpose, a deterministic RAID-assessment approach was developed, which is presented in the following.

6.1 Procedure

The spatially explicit distribution of the disposition classes was evaluated by means of a GIS-based multi-criterion evaluation (MCE), based on the datasets and categories presented in the previous chapter. A MCE consists of six steps (Castellanos Abella and Van Westen, 2007), which were as described below for the RAID-assessment. The procedure is also represented in Figure 6.1 by means of an exemplary catchment.

Firstly, the problem had to be defined. In line with purpose of the RAID model and the aim of present study (see previous chapter), the MCE was developed with regard to the following leading question (which is in line with the research question 2). "Which potential detachment zones, from which mass movements that might reach a lake, are the most susceptible to rock-slope failure?"

Secondly, the criteria that were going to be evaluated with regard to the defined problem had to be determined. The choice of the disposition parameters considered in the present assessment had already been made within the development of the RAID model explained in the previous chapter. The first row in Figure 6.1 illustrates the categorized datasets of the five disposition

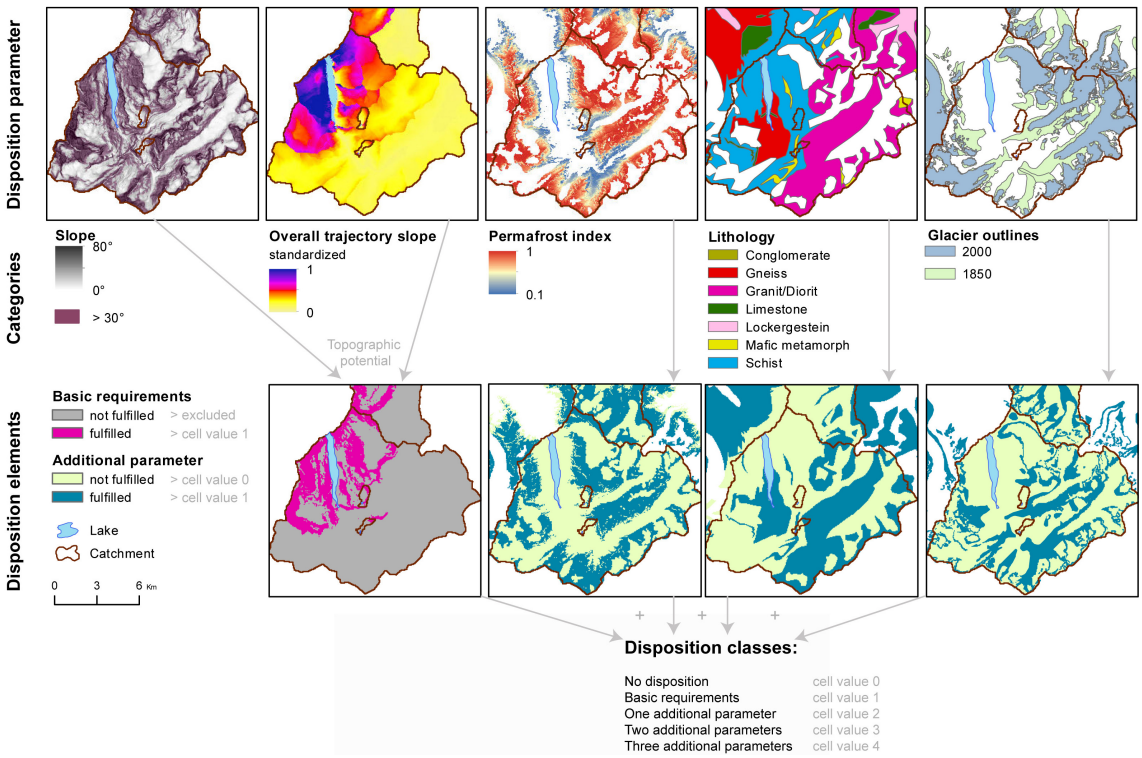

Figure 6.1: Implementation of the RAID model into a GIS-based MCE: categorization of the disposition parameters (above) and their classification into disposition elements (below) with the example of present conditions in the Mauvoisin region by means of the rules outlined in Table 5.1. The model results in a disposition class per cell.

parameters slope, overall trajectory slope, permafrost, lithology and deglaciation.

Thirdly, the data had to be standardized. This assessment was carried out on pixel-scale, which featured a resolution of 25 m according to the DEM. The pixels of the topographic potential (consisting of slope and overall trajectory slope) adopted from Serraino (2011) were allocated the standardized values of the corresponding overall trajectory slope. The areas not fulfilling the basic requirements were in the same step excluded from further analysis in the assessment and allocated the value 0. The pixels of the additional parameters were quantified with 1 or 0 for categories potentially contributing or not, respectively, to slope instability according to the classification in Table 5.1. The resulting layers (representing the disposition elements) are illustrated in the second row of Figure 6.1.

The fourth step in a MCE would consist of weighting of the disposition parameters according to their importance (Castellanos Abella and Van Westen, 2007). A certain weighting was already introduced into the model by distinguishing between decisive and non-decisive disposition parameters. No further weighting factors were introduced, as the data and knowledge for justification is currently too scarce.

The criteria are aggregated in a fifth step of a MCE. Here the values of the additional parameters (assigned in the third step) were aggregated to the area fulfilling the basic requirements per pixel in a non-weighted linear combination using a GIS raster calculator. Correspondingly, each pixel resulted in a value between 0 and 4, which were assigned the previously defined disposition

classes: No disposition (cell value = 0), Basic requirements (cell value = 1), One additional parameter (cell value = 2), Two additional parameters (cell value = 3) and Three additional parameters (cell value = 4). Only larger and connected areas could be considered to cope with the aim of mapping large-volume rock-avalanche disposition areas. Small-scale features had to be reduced. This was achieved by revising the cell's value with the help of the "Spatial Analyst's" tool "Majority Filter". This tool assesses the spatial connectivity of cells. The pixel's values were adapted to the surrounding ones, if at least half of the four corner neighbour cells featured the same value.
A MCE is completed only with a validation or a sensitivity analysis. This sixth step was carried out within the reliability and robustness assessment of the RAID model presented in the upcoming Chapter 7. Correspondingly, the results presented in the next section refer to the basic MCE only.

This procedure was carried out for both time steps, the present situation and for the strongly deglaciated Alps. The MCE resulted in the direct attribution of disposition class per pixel, which was the smallest unit according to Figure 5.1b in Chapter 5. The results on catchment scale (i.e. the disposition indicators) were generated as follows. The disposition area was calculated considering the area fulfilling at least the basic requirements. The disposition intensity was generated through summing up the pixel values over the entire catchment. The aggregated disposition area and the aggregated disposition intensity were calculated as elaborated in Section 5.1.3.

6.2 Results

RAID maps
The spatially explicit representation of the disposition classes derived from the GIS-based MCE resulted in two maps for the entire Swiss Alps, illustrating the distribution of the disposition parameters in the catchments of present and potential future lakes. Figure 6.2 illustrates the allocation of the disposition classes in lake catchments of the Mauvoisin region for present (Fig. 6.2a) and potential future conditions (Fig. 6.2b). The uncoloured area does not fulfil the basic requirements and correspondingly does not exhibit any RAID. The map feature a quadripartite colour scale for the area fulfilling the basic requirements: orange indicates areas only fulfilling the basic requirements whereas the darker colours denote the modelled or mapped presence of one to three additional parameters.
These maps were the basis for evaluation of the RAID on catchment and regional scale, presented in the following.

Analysis of the disposition class distribution
A semi-quantitative analysis of the distribution of the disposition classes in these maps depicted several interesting aspects about the current RAID in catchments of high-mountain lakes in the Swiss Alps and their assumed changes.
From the 538 currently existing lakes analysed and from the 1056 lakes assumed in periods of

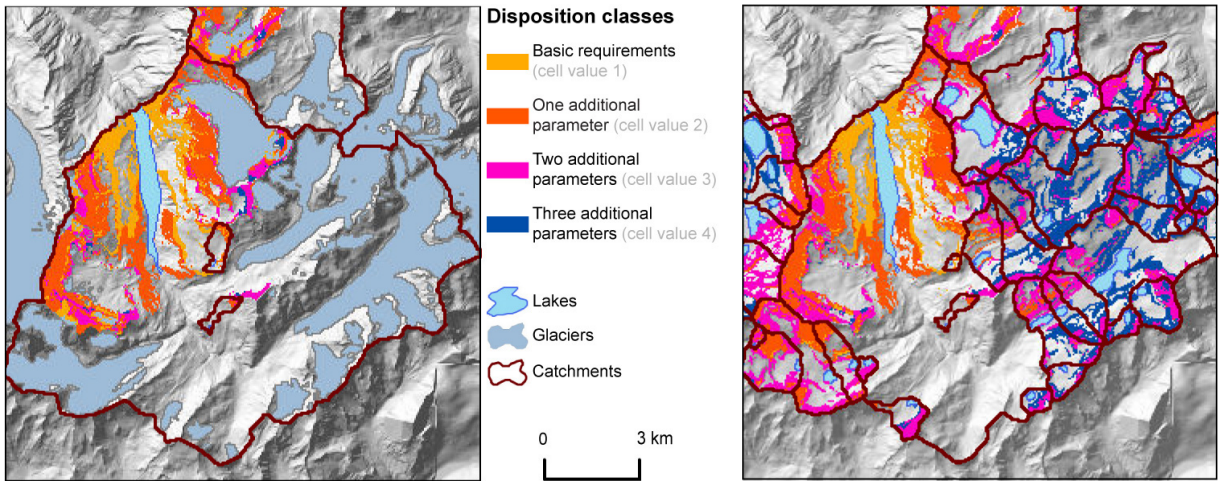

(a) Present conditions (b) Future conditions

Figure 6.2: Spatial distribution of the rock-avalanche impact disposition classes in the catchments of present (a) and future (b) lakes in the Mauvoisin region.

strongly deglaciated Alps, only 36 and 37, respectively, do not feature any rock-avalanche impact disposition at all. This equalled a sample of 6.7% and 3.5% respectively.
The maps of the disposition class distribution illustrate further important evolutions in high-mountain areas, which can also be observed with the example of the Mauvoisin region (Fig. 6.2). The majority of present lakes do not feature many other lakes further uphill, as today often one or only a few lakes exist in a valley. Currently only two lakes exist above the lake Mauvoisin (Fig. 6.2a). Once the Alps are strongly deglaciated, this situation is modelled to have changed in many cases. For the Mauvoisin region, the number of additional lakes is modelled to raise to 27.
Together with the increase in the number of lakes, a decrease in the extent of the catchments can be observed. This is true as much for already existing as for potential future lakes. For currently existing lakes, this is due to the modelled formation of new lakes further uphill. For potential future lakes, the catchment size is often limited by topographic conditions.
The absolute size of the catchments is not assumed to be an indicator for RAID, in contrast to the disposition area. In most of the potential future lakes, the disposition areas represent higher percentages of the catchment areas, which at the same time feature rather dark colours, indicating the assumed presence of several additional disposition parameters. These developments indicate a shift from large catchments featuring relatively small disposition areas to more lakes with smaller catchments featuring a higher percentage of disposition area and more higher than lower disposition classes.
The changes in disposition area and disposition intensity could also be expressed qualitatively (Section 5.1.3). But it is not feasible to discuss the changes in RAID for each catchment because of the large number of lakes analysed. To nevertheless analyse the developments in RAID from current to future conditions, the aggregated disposition indicators are discussed.

Analysis of the aggregated disposition indicators
The aggregated disposition area derived from this deterministic MCE is modelled to increase

to 223% from current 397,5 km^2 to 889,5 km^2 under the future conditions of deglaciated Alps. The aggregated disposition intensity is in the same time period modelled to increase to 291% from the current dimensionless number of 1,861,786 to 5,419,761 under the future conditions of the deglaciated Alps.
The quantitative disposition area and intensity results conform with the qualitatively observed changes in the RAID-maps. The meaning of these developments could further be assessed by means of the impact index. This will be done in the next chapter, taking also into account the parameter uncertainties.

CHAPTER 7

PROBABILISTIC ROCK-AVALANCHE IMPACT DISPOSITION ASSESSMENT CONSIDERING PARAMETER UNCERTAINTIES

The main aim of the RAID-model is to enable prioritization in risk management of high-mountain lakes in the Swiss Alps by identifying the hotspots of RAIS. Reliable and robust results are required for this purpose, but a model is always a simplified construct of the real world. The uncertainties with regard to the mapped and modelled input data and the correctness of the categorization are obvious, especially with regard to future conditions (see Section 5.1.2). The model was implemented as a probabilistic approach into a Bayesian network (BN), to analyse present and future RAID under consideration of the inherent parameter uncertainties.

7.1 Development of a Bayesian network

The development of a BN for RAID-assessment is presented. Firstly, the principles of BNs are explained (Section 7.1.1) to guarantee the understanding of the implementation of the RAID-model (Section 7.1.2) and the inherent parameter uncertainties (Section 7.1.3).

7.1.1 Background on Bayesian networks

A BN is a graphical probabilistic model for interpreting certainty of factors (Kim and Pearl, 1983), which facilitates the explicit modelling of uncertainties involved in an event-oriented model (Grêt-Regamey et al., 2013). BNs belong to the most consistent frameworks for decision-making under uncertainty (Faber and Maes, 2005), thanks to their capacity to include as much

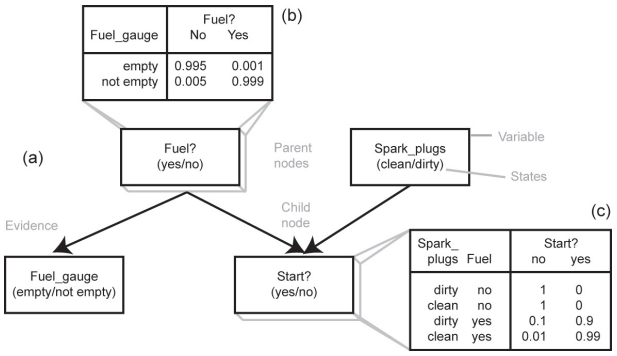

Figure 7.1: A simple example of a BN (Kjærulff and Madsen, 2013). The illustrated car ignition problem is a consequence either of missing fuel or of dirty spark plugs (a). A BN consists of variables (parent nodes, child nodes, evidences), which exhibit a set of mutually exclusive states. Dependencies between the variables are represented with arcs and the probability of variables conditional on parent nodes is specified in CPTs (b and c).

quantitative data as expert knowledge. They further offer the advantage of representing the relationships between the variables explicitly, which enables traceability of the modelling process. Finally, new evidence can be included in a BN at any point, as they are capable of learning.

The design and the operation mode of a BN is summarized with the help of an example given by Kjærulff and Madsen (2013), illustrated in Figure 7.1. In this simple – thematically different – example, the reasons for ignition problems in a car are assessed, assuming them to be a consequence either of missing fuel or of dirty spark plugs. The BN is composed of a set of variables which are implemented as nodes in the model (Fig. 7.1a: Fuel, Spark_plugs, Fuel_gauge, Start) and which are specified a set of mutually exclusive states (e.g. Fuel? (yes/no)). Arcs connect the variables following child-parent relationships and determine the causal dependency among these. The conditional probabilities of child nodes on their parent nodes are specified in conditional probability tables (CPTs) (Figs. 7.1b and c). E.g., the car will only start with a probability of 0.99 if spark plugs are clean and if fuel is available. The only observable variables (evidences) are the ignition problems and the fuel gauge.
BNs derive the joint probability distribution of a target node x_i (e.g. *Start?*) in the form of Equation 7.1 (or of Equation 7.2 for more complex networks), with $pa(x_i)$ being the value distribution of the parent nodes (i.e. Fuel? and Spark_plugs) (Grêt-Regamey et al., 2013). This calculation is based on the first Bayesian Theorem (Jensen and Nielsen, 2007).

$$P(x_i,x_2,x_3) = P(x_i) * P(x_i|x_2) * P(x_i|x_3) \tag{7.1}$$

$$P(x) = P(x_1,...,x_n) = \Pi_{i=1}^{n} P(x_i|pa(x_i)) \tag{7.2}$$

Once the status of another variable - the evidence e - is known (e.g. the status of the fuel gauge), the conditional probabilities for a subset of variables are inferred by means of the second Bayesian Theorem in Equation 7.3 (Jensen and Nielsen, 2007; Pearl, 1988). The probable cause of an effect cant thereby be concluded.

$$P(x|e) = P(x) * P(e|x)/P(e) \tag{7.3}$$

BNs are applied to a number of environmental modelling issues (Aguilera et al., 2011), also to natural hazards (e.g. Blaser et al., 2011; Grêt-Regamey and Straub, 2006; Medina-Cetina and Nadim, 2008; Straub, 2005; Wang et al., 2013). They further suggest an evolution of event trees

applied to assessing cascading multi-hazards, because they allow for inclusion of probability-density functions (to account for the inherent uncertainties) instead of one single probability value at each node (Marzocchi et al., 2012; Nadim and Liu, 2013). A BN is therefore assumed to be a suitable tool for probabilistic assessment of the RAIS of high-alpine lakes in Switzerland.

7.1.2 Implementation of the RAID model into a Bayesian network

The RAID model was implemented into a BN as illustrated in Figure 7.2, with the help of the licence-free (limited) version of Netica (Norsys, 2013). As outlined in the previous section, one outcome of the BN is a joint probability distribution of the aspired result. The probability distribution of the disposition classes per pixel would have hardly been possible to evaluate (e.g. Kunz, 2011). Therefore the catchment was defined as the smallest assessable unit (Fig. 5.1b). The disposition parameters were implemented as input nodes (first row). The mutually exclusive states of these nodes consisted to the categories of the disposition parameters. The probability of the categories were assigned for each catchment separately, corresponding to the percentage each category was modelled/mapped in the respective catchment. These percentages were de-

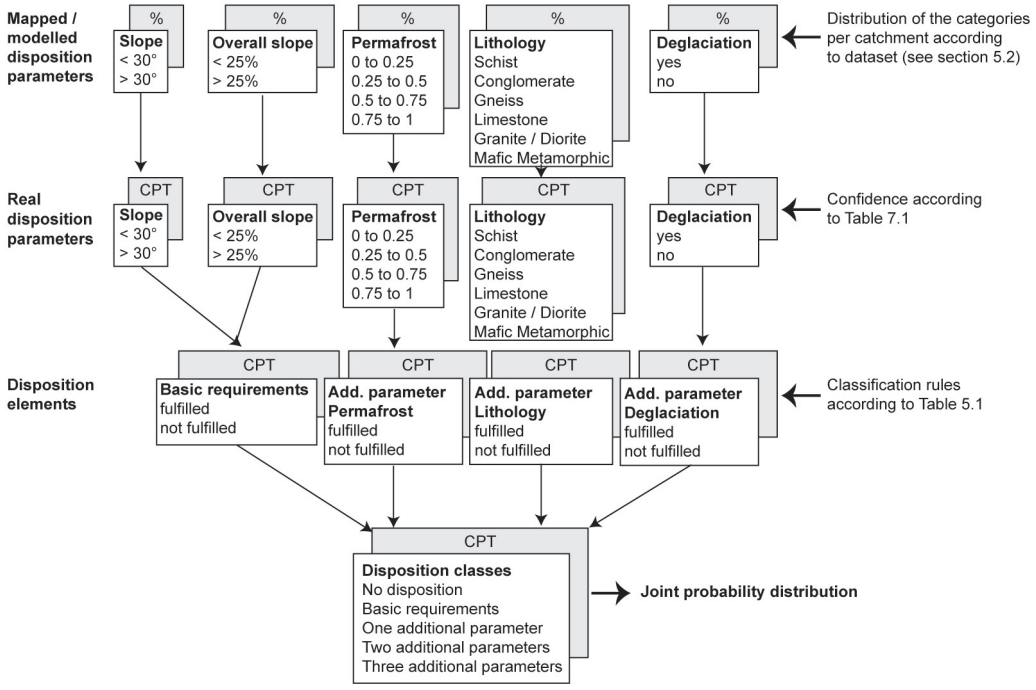

Figure 7.2: Implementation of the RAID-model into a BN. The percentage (%) each category was modelled or mapped in the catchment, serving as input data. The conditional probability tables (CPT) in the second row indicate the probability of the characteristics of a modelled or mapped disposition parameter being in accordance with the real occurrence (according to Table 7.1). The CPT's in the third row contain the deterministic decision rules (0 for "not fulfilled" or 1 "fulfilled") as defined in Section 5.1.2 in Table 5.1. The BN results in a probability distribution of the disposition classes per catchment according to Equation 7.2.

rived from the GIS-based datasets introduced in Section 5.2.2. These nodes were the parents of a second set of nodes, indicating the probability of the characteristics of a modelled/mapped disposition parameter being in accordance with the real occurrence (second row). These nodes were connected with CPT, including the confidence into the mapping or modelling. This confidence accounts for the parameter uncertainty introduced in both working steps, in the choice of the datasets and in the categorization process, which is defined in Section 7.1.3. This calculation according to Equation 7.1 resulted in conditional probabilities, indicating the probable percentage of a parameter category in the catchment, given the mapped or modelled distribution and the related confidence. In a third step, these conditional probabilities per disposition parameter were summed up for the categories fulfilling or not fulfilling the basic requirements or the criteria to be classified as additional parameters respectively (see Table 5.1, disposition elements), according to Equation 7.2. This joint probability distribution calculation resulted in the percentage of the catchment area contributing, or not, to rock-slope stability and lake impact disposition for each disposition element (last node).
The probability of the characteristics of a modelled or mapped disposition parameter being in accordance with the real occurrence is referred to as the parameter uncertainties. These uncertainties, implemented in the CPT of the nodes in the second row (Fig. 7.2) are explained in the next section.

7.1.3 Definition of parameter uncertainties

The basic source of uncertainty is the accuracy of the datasets, which were introduced by generalization and the mapping or modelling as a function of the available process understanding. Further uncertainty was introduced by the process of categorization. In the following these confidences will be expressed as percentages, indicating the feasibility of the characteristics of a disposition parameter at a certain location being in accordance with the mapped or modelled value. If not indicated differently, e.g. by precision indications of the corresponding data providers, these confidences were composed by expert assessment of the reliability, as described below. A summary is compiled in Table 7.1.

Slope
The mapping of the disposition parameter slope was assumed to be reliable for present conditions. In Switzerland, a Lidar-DEM with 2-meter resolution is available for areas below 2200 m a.s.l. A 25m-resolution DEM covering the entire study was applied for the present study, in accordance with the other dataset's resolution. This level of generalization was considered adequate for the assessment of large rock avalanches. Therefore, the confidence of a slope angle being appropriately mapped for present conditions was set to 95 %. The uncertainty in the modelled glacier thickness, which served as the basis for DEM-estimation of the future deglaciated Alps, were estimated by Linsbauer et al. (2012) to be around 30%. Therefore the confidence of a slope angle being appropriately modelled for future conditions was set to 70 %.

Overall trajectory slope
The mapping of the parameter overall trajectory slope was considered to be mostly appropriate

Disposition Parameter	Categories	**Confidence** P.C.	Source	D.A.	Source
Slope	$< 30°$	95%	e.a.	70%	Linsbauer et al. (2012)
	$> 30°$	95%	e.a.	70%	Linsbauer et al. (2012)
Overall trajectory slope	$< 25\%$	85%	e.a.	60%	e.a.
	$> 25\%$	85%	e.a.	60%	e.a.
Permafrost	0.00-0.25	80%	e.a.	70%	e.a.
	0.25-0.50	65%	e.a.	65%	e.a.
	0.50-0.75	65%	e.a.	50%	e.a.
	0.75-1.00	80%	e.a.	65%	e.a.
Lithology	all categories	95%	BWG and SGTK (2000)	85%	e.a.
Deglaciation	yes	90%	e.a.	90%	e.a.
	no	95%	e.a.	95%	e.a.

Table 7.1: Confidences into the parameters representing the uncertainties inherent in dataset and categorization of the disposition parameters. P.C. = present conditions, D.A. = deglaciated Alps, e.a. = expert assessment.

for today's conditions. But small-scale features were likely lost, because of the generalisation to 25 m resolution. The confidence was set to 85%. For future conditions, the reliability of the overall trajectory slope was assumed to be rather low, as it is based mostly on assumptions – as much for the DEM as for the position and shape of the future lakes. This reasoning resulted in a confidence value of 60% only.

Permafrost

Areas featuring permafrost index-values smaller than 0.25 or higher than 0.75 were assumed to be reliably classified. The confidence was set to 80%. Rather low confidence (65%) was allocated to the categories around the threshold value of 0.5. For future conditions, no baseline for permafrost assessment exists. Setting the confidences was therefore fully based on expert assessment. The confidence in values classified lower than 0.25 was set slightly lower than for present conditions (70%). The confidence in the class between 0.25 and 0.5 remained 65%. The confidence of the class of 0.5-0.75 however was reduced to 50%, as it includes the unknown evolution of permafrost in today's glacier beds, which is why the confidence in assumptions on future development of permafrost in deglaciated areas is very weak. The areas classified as 0.75-1 were allocated a reliability of 65%, as future evolution of permafrost in this area is not known.

Lithology

The lithology dataset was elaborated for scales up to 1:300,000 (BWG and SGTK, 2000). The confidence was set to 95% for the investigation on present conditions, as a scale of 1:25,000 was applied in this study. For future conditions, the lithology below the currently-ice-covered area had to be estimated. The confidence was fixed as 85%.

Deglaciation

The area mapped as not deglaciated since the LIA was assumed to be very reliably assessed, whereas there was a slightly lower confidence in the mapping of glacier outlines of the LIA.

The corresponding reliabilities were set 95% and 90% respectively. The same confidence values were applied for the study of future conditions, as complete deglaciation of the area covered by glaciers since the LIA was assumed.

7.2 Procedure of the probabilistic RAID-assessment

The probabilistic evaluation of the RAID was carried out by means of the BN elaborated on a catchment scale. The input information on the categorized disposition parameters were exported from the datasets outlined in Section 5.2.2, in the form of a percentage distribution of the categories per catchment for both time steps separately. These datasets were then imported into Matlab, where the BN established with Netica was implemented to allow for automatized handling of the large number of lakes.

Contrary to the deterministic approach, the results were not mapped in a spatially explicit way, for the reasons explained in Section 7.1.2. The probabilistic procedure resulted in several spatially inexplicit products describing the RAIS of the lakes on a catchment scale. The principle outcome was the probability distribution of the disposition classes per catchment, from which the disposition indicators were derived. The disposition area was generated by multiplication of the entire catchment area with the percentages taken up by the disposition classes' basic requirements, one, two and three additional parameters. The disposition intensity was constructed analogous to the quantification of the disposition intensity in the deterministic approach (Section 6.1): the number of pixels equivalent to the area covered by the individual disposition classes were multiplied by a factor of one to four for the disposition classes' basic requirements, one, two and three additional parameters, respectively.
The probabilistically-derived disposition indicators were assumed more suitable for ranking of the Swiss high-mountain lakes according to their impact index than the deterministically-derived. The lakes were therefore ranked for both time situations separately regarding their impact index.

7.3 Results

The results of the probabilistically derived disposition classes and indicators are presented and also compared to the deterministically-derived results and qualitative observations of the disposition maps. Further the ranking of the impact indices of the lakes is presented.

Aggregated disposition areas
The disposition area aggregated over the current catchments in the Swiss Alps covered roughly 264 km^2. This equals 12.6% of the total catchment areas in the entire Swiss Alps. At the moment of the strongly deglaciated Alps, the aggregated disposition area will have increased to 288% or 763 km^2. Not only the aggregated disposition area is modelled to rise but also the percentage of the disposition areas per catchment is modelled to grow to 26.3% in average.

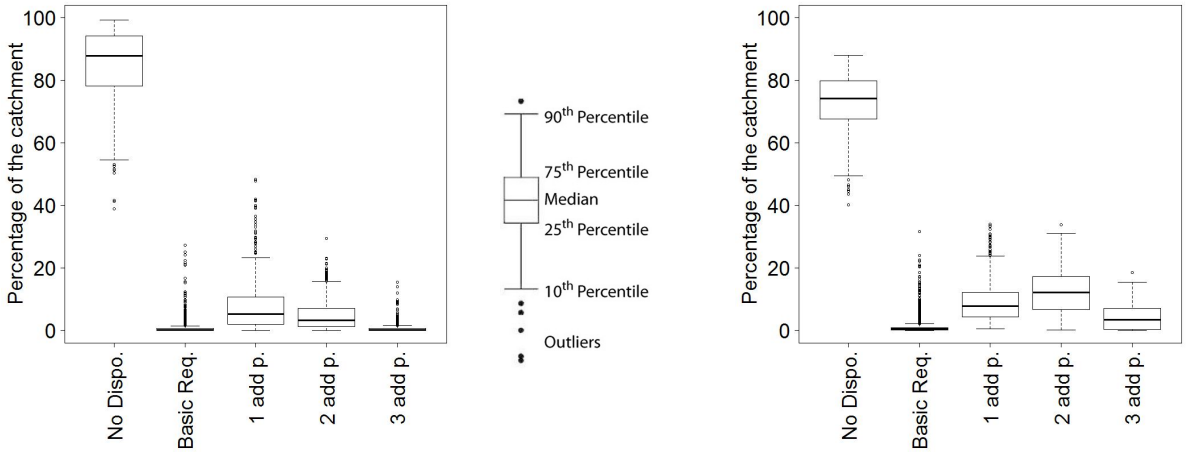

(a) Current conditions (b) Deglaciated Alps

Figure 7.3: Disposition class distributions in the catchments of the Swiss Alps for (a) current conditions (538 lakes) and for (b) the deglaciated Alps (1056 lakes). Each entry represents one catchment. The results illustrate a raise in both indices, disposition area and intensity.

These results confirmed the visual impression from the disposition class maps (compare with Section 6.2).

Disposition class distributions

The distribution of the disposition classes is illustrated in the boxplots (Fig. 7.3) for the two time steps separately, considering all respective catchments. This illustration indicates a decrease of the area featuring no disposition from a median of 88% to 74% in the future. Instead, the median of the disposition classes two and three additional parameters rose from 3% to 12% and from 0.2% to 3.5%. The distribution of the areas exhibiting basic requirements only remained almost unchanged, but the median of the class one additional parameter rose slightly from 5.3% to 7.9%. It can further be observed that none of the catchments, not even outliers, exhibited a disposition area larger than 38% (not in present nor in future condition).

The aggregated disposition intensities increased between the two time steps to 328%, which is 40% more than the increase of the aggregated disposition area. These results confirm the deterministic evaluation of the disposition intensity, with the result that future catchments will feature higher disposition intensities than lower ones.

Ranking of the lakes according to their impact index

The impact index was built as a product of the disposition intensity and area per catchment. The twenty lakes ranked highest according to their impact index are presented in Table 7.2. As mentioned in Chapter 2, all lakes above 1,500 m a.s.l. were included in the analysis, artificially dammed as much as natural lakes. The highest impact indices for current conditions resulted for the largest lakes, measured by their surface area. These are mostly artificially dammed for hydropower-generation purposes. But also small lakes are prone to large RAIS, especially in future conditions. Remarkably, also the natural Lake Trift (rank 18), which recently formed as a consequence of glacier recession, is within the 20 lakes currently featuring the highest RAID. 15 of the lakes currently ranked within the 20 highest impact dispositions are also listed in the rank-

ing for future conditions. Apart from two exceptions (Lake di Luzzone and Lake Limmeren), the 18 lakes ranked highest are currently located in the cantons Valais, Bern and Grisons, whereas in future they are expected to be concentrated in the cantons Valais and Grisons.

7.4 Discussion

These results are very important for risk management, because they allow first-order prioritization of hazards, also for future conditions. The Bernese lakes, for example, were not assumed to disappear. But potential future lakes take hold of some of the disposition area, as illustrated by the example of Mauvoisin region in Figure 6.2. In such locations, the possibility of an impact through an outburst flow from another lake situated higher up the valley would have to be assessed.
This assessment shows that the RAIS of potential future lakes can be in the range of the RAIS of current artificially dammed lakes. In the case of artificially dammed lakes, powerplant operations are in charge of safety aspects. Natural lakes, in contrary, are not necessarily under observation and often feature relatively low or unstable freeboards, two signs of enhanced outburst hazard (see Section 4.3.3 for more explanations). This constellation shows again the importance of future-oriented hazard analyses.
The research question "Which of the present and potential future high-mountain lakes in the Swiss Alps are most susceptible to rock-avalanche impacts?" could be answered based on the ranking of the lakes according to their impact index. But the RAID model and -assessment were built on assumptions and on a small database (Fischer et al., 2012) in addition to the uncertainties inherent in the datasets and the categorization. It is therefore indispensable to know about the reliability and the robustness of the RAID-model and the results just presented. These aspects are treated in the following Chapter 8, before the research question is concluded in Chapter 9.

Rank	Current conditions				Rank	Deglaciated Alps				Rank
	Lake name	Location		L.T.	L.A.	Lake name	Location		L.T.	L.A.
1	Lac de Mauvoisin	Val de Bagnes	VS	ad	6	Lai da Ova Spin	Ofenpass	GR	ad	81
2	Grimselsee	Grimsel	BE	ad	5	Lac de Mauvoisin	Mauvoisin	VS	ad	7
3	Lago di Luzzone	Vale di blenio	TI	ad	19	Marmorera	Bivio	GR	ad	15
4	Göscheneralpsee	Göschenen	UR	ad	18	Zervreilasee	Vals	GR	ad	11
5	Zervreilasee	Vals	GR	ad	9	Lej da Silvaplauna	Oberengadin	GR	natural	4
6	Lai da Ova Spin	Ofenpass	GR	ad	44	Göscheneralpsee	Göschenen	UR	ad	20
7	Lej da Silvaplauna	Oberengadin	GR	natural	4	Lago di Luzzone	Vale di Blenio	TI	ad	21
8	Lac des Dix	Val d'Hérémes	VS	ad	1	Lej da Segl	Oberengadin	GR	ad	2
9	Oeschinensee	Kandersteg	BE	natural	20	no name	Gornergletscher	VS	modelled	25
10	no name	Férpecle	VS	ad	409	Lac des Toules	Val d'Entremont	VS	ad	46
11	Lac d'Emosson	Forclaz	VS	ad	3	Lac des Dix	Val d'Hérémes	VS	ad	1
12	Gelmersee	Grimsel	BE	ad	27	Lej da S. Murezzan	Oberengadin	GR	natural	37
13	Limmerensee	Glarus	GL	ad	14	Lago d'Isola	Mesoocco	GR	ad	94
14	Lai da Nalps	Sedrun	GR	ad	21	no name	Aletschgletscher	VS	modelled	6
15	Lej da Segl	Oberengadin	GR	natural	2	Lai da Curnera	Sedrun	GR	ad	28
16	Lai da Curnera	Sedrun	GR	ad	22	Arosastausee	Arosa	GR	ad	280
17	Marmorera	Bivio	GR	ad	13	Lai da Nalps	Sedrun	GR	ad	23
18	Triftsee	Susten	BE	natural	37	Lei da Vadret	Rosegtal	GR	natural	206
19	Turtmannsee	Turtmanntal	VS	ad	340	no name	Férpecle	VS	ad	874
20	Lac des Toules	Val d'Entremont	VS	ad	32	Limmerensee	Glarus	GL	ad	411

Table 7.2: Ranking of the lakes featuring the 20 highest impact indexes (first row) for the two time step, under current conditions and for the deglaciated Alps. The lakes are further ranked according to their size, indicated by the lake area (L.A.), rows six and 11. The lake type (L.T.) indicates whether the lake is naturally dammed (natural) or artificially dammed (ad). Potential future lakes (modelled) base on Linsbauer et al. (2012). The lakes are named in the language predominant in the respective cantons. The cantons are: BE = Bern, GL = Glarus, GR = Grisons, TI = Ticino, UR = Uri and VS = Valais. An illustration of the location of these lakes can be found in Figure 9.2.

CHAPTER 8

RELIABILITY AND ROBUSTNESS ASSESSMENT OF THE ROCK-AVALANCHE IMPACT DISPOSITION MODEL

A range of results and conclusions on RAID in catchments of current and future high-mountain lakes in Switzerland were generated in the previous analyses. These outcomes are relevant for risk management. To ensure the quality of the results, the limits of the RAID model are in this chapter tested regarding their influence on reliability and robustness of the RAID results.

8.1 Limits of the model

Parameter uncertainties, accounting for accuracy of the databases and the categorization, have already been included in the BN. General model uncertainties consisting of all deviations between the real world and its simplified representation in the RAID model, however, were not yet treated. Model uncertainties may arise either from the limited knowledge of the analyst about the phenomena or from the simplifications introduced by the analyst and can result (a) in incorrect probability distribution class, (b) in inaccurate distribution parameters, (c) in omission of dependency effects or (d) in discretisation of continuous quantities or representations in terms of expected values (Nilsen and Aven, 2003). In the context of the RAID assessment, these uncertainties can be linked to the following sources of errors:

i The choice of the non-decisive disposition parameters might contain dependency effects or the parameters might simply have been chosen inaccurately (Fig. 8.1a).

ii In the process of the definition of the parameter uncertainties (confidence definition), wrong probability distribution classes might have been assigned to the categories (Fig. 8.1b).

iii And the conducted discretisation into disposition elements by classification of the disposition parameters might have been inappropriate (Fig. 8.1c).

The effects of these uncertainties were analysed as follows.

8.2 Procedure of the reliability and robustness assessment

Exact quantification of these effects is rarely possible due to the lack of process understanding or reference data. Nevertheless, to estimate the importance of the model uncertainties and to assess the relative confidence in the model under such conditions, Apostolakis (1990) suggests introducing weighting probabilities into the model. Based on this methodology, a two-step reliability and robustness assessment approach was developed, following the example of Grêt-Regamey and Straub (2006). The reliability and the robustness of the RAID model were assessed by means of an uncertainty and a sensitivity analysis, where the uncertainty analysis defined the reliability and the sensitivity analysis the robustness of the RAID analysis.
A detailed description of the weighting procedures is given for each potential source of errors (i)-(iii) individually (Section 8.2.1) before the evaluation procedure for both analyses – on uncertainty and on sensitivity – is explained (Section 8.2.2).

8.2.1 Weighting procedure

After the presentation of the principles of the uncertainty and sensitivity analyses, the detailed procedure that was applied with regard to the weightings introduced for the different sources of errors (i)-(iii) is presented in this section.

(i) Effect of the choice of the non-decisive disposition parameters
The first potential source of error was the choice of the non-decisive disposition parameters. There, the incomplete choice of considered disposition parameters and the resulting uncertainty were due to missing information and knowledge. Therefore, the corresponding effect could not be tested, and conclusions requiring confidence in thorough selection of disposition parameters was not possible. It was, however, possible to assess dependency and importance of the chosen parameters to justify their inclusion in the model, which is also one aspect of accuracy. The effects on uncertainty and on sensitivity of the model results were tested by varying the weighting of the non-decisive disposition parameters according to Apostolakis (1990). These effects were tested by means of the simplified deterministic model outlined in Section 6.1, as the BN accounts for uncertainties rather than for weightings. This equals the sixth step of the MCE not yet carried out. In this deterministic MCE, the weighting factor had been set to 1 by default, not stressing any of the parameters (see Section 6.1). In the robustness and reliability analysis, the weighting factor was changed for each parameter one by one consecutively to zero (not considering the parameter) and two (duplicating the importance of the parameter), respectively. This confidence interval was defined based on own estimations. This analysis resulted in six runs, called C-H, whose affiliation to the weightings is outlined in Table 8.1 and in Figure 8.1a. Ndet

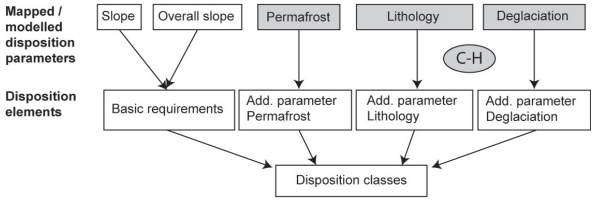

(a) Analysis of the effect of the non-decisive disposition parameters (i). The weighting was varied for each parameter individually according to the runs C-H in Table 8.1.

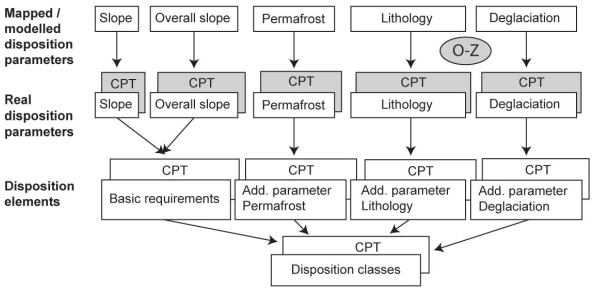

(b) Analysis of the effect of the parameter uncertainties (ii). The weighting was varied for each parameter individually according to the runs O-Z in Table 8.1.

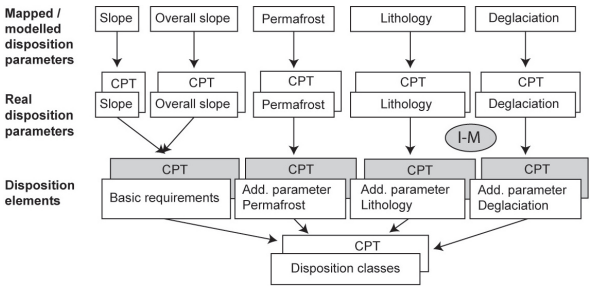

(c) Analysis of the effect of the classification of the disposition parameters into disposition elements (iii). The weighting was varied for each parameter individually according to the runs J-M in Table 8.1.

Figure 8.1: Illustration of the weighting procedure for the different sources of errors assessed (i-iii). The effect of the non-decisive disposition parameters were assessed within the deterministic RAID (a). The effect of the parameter uncertainties and of the classification rules were assessed within the probabilistic RAID-model (b and c). For full illustration of the model refer to Figure 7.2.

corresponds to the default run. For the purpose of this robustness and reliability analysis, the spatial connectivity was not considered decisive, therefore generalization was not included any more and the analysis was run on the raw disposition calculations.

(ii) Effects of the parameter uncertainty definition

An outlining for the definition of the parameter uncertainty, also defined as confidence definition, has been given in Section 7.1.3. Due to a lack of quantitative evidence, most of these probabilities were based on estimations or knowledge of the analyst. To test the influence of the confidences implemented in the CPT's, these values were altered by +/- 30%, which equals weighting factors of 0.67 and 1.33 respectively for each parameter, alternatively resulting in 10 runs, called O-X (Table 8.1 and Fig. 8.1b). The maximum value a CPT could accept was one. Two more runs (Y-Z) were carried out, varying the CPTs of all parameters at once. This assessment was carried out by means of the probabilistic approach implemented in the BN. Therefore the default run is indicated as Np and results were evaluated with regard to this run's results.

(iii) Effects of the classification of the disposition parameters

The third potential source of uncertainties assessed was the classification of the disposition parameters into disposition elements. The applied decision rules are based on the evaluation of the rock-avalanche dataset of 69 events in the Swiss Alps by Fischer et al. (2012) (Section 5.1). In

a first step, these rules were validated by means of an analogue dataset of 23 rock-avalanches in the region of Mount Cook in New Zealand's Southern Alps (Allen et al., 2009a, 2011) to check the feasibility of the derived classification. The disposition parameters present in the detachment zones of New Zealand's rock-avalanches (Fig. 8.2a), were categorized (see table in Fig. 8.2b; row "Categories") according to the categorization applied for the Swiss Alps (Table 5.1) to compare the accordance between the two datasets. The percentage of New Zealand events (table in Fig. 8.2b; row "R.A.") attributable to categories fulfilling the classification rules in Table 5.1 defined the confidence into the corresponding classification rule. However, no confirmation of the assumptions taken regarding the overall trajectory slope values could be gained, as the analyses of Allen et al. (2011) were independent of lake presence. Therefore the confidence value was manually adapted to 90% for classification of the topographic potential fulfilling the basic requirements.

The robustness and reliability assessment of the RAID assessment was then carried out within the probabilistic model (Fig. 8.1c). The agreements between the datasets were implied into the CPTs of the disposition elements, which, in the default run, had been implemented as deterministic rules. Each classification rule was then altered alternatively resulting in four runs (J-L). In a fifth run (M) all rules were varied at once (Table 8.1). The results were evaluated with regard to the default probabilistic run's results (Np).

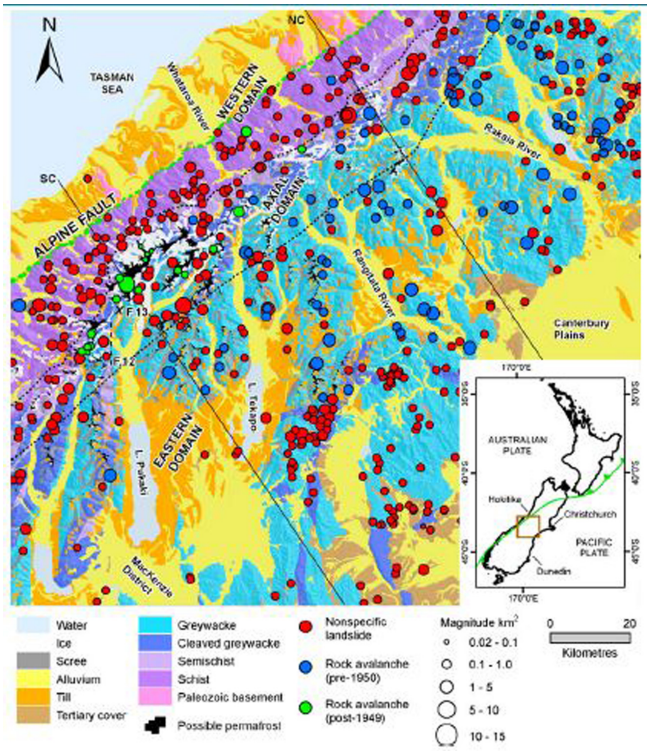

(a) Simplified geological classification of the central Southern Alps (after Cox and Barrell (2007)), showing landslide distribution in relation to the three main geomorphic domains described by Whitehouse (1988). Permafrost distribution is after Allen et al. (2008). Landslide magnitude describes the total affected area (source and deposit areas combined).

Disposition parameters	Categories	R.A.
Slope	< 30°	1
	> 30°	22
Permafrost	not probable	15
	probable/possible	8
Lithology	Schist, Semischist	6
	(fraq) Greywacke	17
Deglaciation	outside 300m buffer of present glaciers	5
	within 300m buffer of present glaciers	17

(b) Characteristics of the release zones of rock avalanches in New Zealand (based on Allen et al. (2009a, 2011)). R.A. = number of observed rock avalanches.

Figure 8.2: Rock avalanches in New Zealand. Figure (a) and caption from Allen et al. (2011). Table (b) contains an evaluation of a dataset of 23 rock-avalanches in the region of Mount Cook in New Zealand's Southern Alps (Allen et al., 2009a, 2011).

8.2.2 Evaluation of the uncertainty and the sensitivity

The results of the three assessments (i)-(iii) were next analysed with regard to the uncertainty and the sensitivity introduced into the results.

Evaluation of the uncertainty
In a first step, the uncertainty in any model result was quantified. This implied the assessment of the effective changes in the dependent values and their significance. Dependent variables chosen for this assessment were the disposition intensity and the disposition area per catchment and the percentage of the disposition classes per catchment. These results were generated for all analyses (i)-(iii), considering different weightings of the assessed parameters in different runs (Table 8.1). These aggregated disposition areas and intensities were then compared to the default run's values for each analysis (i)-(iii) by means of barplots. The significance of the deviation was calculated with the help of the Wilcoxon-test. A Wilcoxon test for dependent groups is a non-parametric test for checking whether the central tendency of two related samples is significantly different (Bortz and Döring, 2006).

Evaluation of the sensitivity
In a second step, the contribution of each parameter to the model prediction and the sensitivity of the reaction of the main results were evaluated in a sensitivity analysis. The main result in the probability assessment was the ranking of the lakes according to their impact index, which was assumed to be the model prediction. The sensitivity analysis was carried out per assessment step (i)-(iii).
Several methods for evaluation of rankings exist. It is not recommended to apply statistical tests on rankings of ordinal data, such as the Cappa-coefficient (Cohen, 1960), to continuous data, as

Varied parameter / element	**Labelling of the runs and weighting factors**												
(i) Weighting of the non-decisive disposition parameters													
	Nd	C	D	E	F	G	H						
Permafrost	1	0	2	1	1	1	1						
Lithology	1	1	1	0	2	1	1						
Deglaciation	1	1	1	1	1	0	2						
(ii) Weighting of the parameter uncertainties. (CPT of the real disposition parameter)													
	Np	O	P	Q	R	S	T	U	V	W	X	Y	Z
Slope	1	0.67	1.33	1	1	1	1	1	1	1	1	0.67	1.33
Overall trajectory slope	1	1	1	0.67	1.33	1	1	1	1	1	1	0.67	1.33
Permafrost	1	1	1	1	1	0.67	1.33	1	1	1	1	0.67	1.33
Lithology	1	1	1	1	1	1	1	0.67	1.33	1	1	0.67	1.33
Deglaciation	1	1	1	1	1	1	1	1	1	0.67	1.33	0.67	1.33
(iii) Weighting of the classification rules. (CPT of the disposition elements)													
	Np	I	J	K	L	M							
Basic Requirement	1	0.9	1	1	1	0.9							
Additional parameter Permafrost	1	1	0.5	1	1	0.5							
Additional parameter Lithology	1	1	1	0.74	1	0.74							
Additional parameter Deglaciation	1	1	1	1	0.78	0.78							

Table 8.1: Weighting factors implemented into the three robustness and reliability analyses (i)-(iii), illustrated in Figures 8.1a, 8.1b and 8.1c. Np indicates the default probabilistic run, Nd the corresponding deterministic run. The capital letters name the single model runs. Note for the analyses (ii) and (iii), that the upper limit of CPT-entries is always 1.

a loss of accuracy would be inevitable through the required process of categorization (Sim and Wright, 2005). Instead Sim and Wright (2005) suggest analysis by means of the bias and limits of agreements between two rankings as described by Bland and Altmann (1986).

More detailed explanations of the evaluations are given in the sections presenting the respective results by means of a precise example.

8.3 Results

The robustness of the dependent values' disposition intensity and area were analysed in the uncertainty analysis, whereas the reliability of the ranking of the lakes by their impact index was assessed in the sensitivity analysis. The results are presented for each weighting procedure (i-iii) per analysis.

8.3.1 Uncertainty analysis - robustness of results

The uncertainty introduced into the model was evaluated through barplots of the aggregated disposition area and intensity for each run per time step of current and future conditions (Fig. 8.3). The uncertainty was defined as the difference between the runs resulting in the lowest and the highest results. These numbers were then transferred to the second part of Table 8.2 and compared to the default results in the first part of the table. Furthermore all parameters causing significant deviations from the default result according to the Wilcoxon test were listed in the table.

(i) Effect of the choice of non-decisive disposition parameters
The uncertainty introduced by different weighting factors of the non-decisive disposition parameters was only analysed for the disposition intensity, as the topographic potential defining the disposition area was not varied due to its decisive character. The results from the aggregated runs summarized in Table 8.2 show that the choice of non-decisive parameters introduces a range of uncertainty which accounts for 74% and 75% of the default deterministic aggregated disposition intensity for present and potential future conditions, respectively. For both time steps, the minimum values were achieved by weighting the deglaciation with zero and the maximum values were caused by doubling the weight of deglaciation. The differences introduced by varying the weighting factor of deglaciation were strongly significant for both time steps. Permafrost has an effect, which is, however, not significant at the 0.05-level. Lithology variations also caused significant effects.

(ii) Effects of the parameter uncertainty (confidence) definition
The uncertainty inherent in the defined confidences in the mapped/modelled disposition parameters measured 115% and 46% of the default probabilistic run for present and potential future disposition areas, respectively. The uncertainties are in the same range (128% for present and 42% for future conditions) for the disposition intensity. All extreme values were caused by

varying all weighting factors at once. The parameters causing a strongly significant deviation for present and, a bit less strong, for future conditions, were weighting of overall trajectory slope and of all factors together. Reducing the confidence in the gradient also had a significant influence, but only for present conditions. This was true as much for disposition intensity as for the disposition area.

(iii) Effects of the classification of the disposition parameters

The feasibility of the classification of the disposition parameters into disposition elements had in a first step been evaluated by means of an analogue dataset of rock avalanches in New Zealand (Table in Fig. 8.2b). This assessment showed very good agreement between the elaborated classification and the presence of the corresponding disposition parameters in New Zealand's detachment zones for slope (agreement in 100% of the cases), deglaciation (78% agreement) and lithology (74% agreement). Only for permafrost is the agreement of the classifications rather weak with 34%.

The influence of these uncertainties in the aggregated disposition intensity amounted for 68% for present and 26% for future conditions. The maximum and the minimum values were caused by variation of basic requirements and the additional parameter permafrost for present and by variation of basic requirements and additional parameter deglaciation for future conditions, respectively. Contrary to the other three variations, the influence of the additional parameter deglaciation was not statistically significant. The uncertainty of the disposition area amounts for 59% for present and 18% for future conditions. In both time steps the significant variations were caused to be equally strong by basic requirements and all classifications at once.

Summary

To summarize, the additional disposition parameters lithology and deglaciation caused significant deviations of the aggregated disposition intensity. The absolute uncertainties were, however, smaller than the ones inherent in the parameter confidence definitions of slope, overall trajectory slope and all parameters together. The smallest (but still significant) uncertainties were caused by the classification of the basic requirements and correspondingly also of all classification rules together.

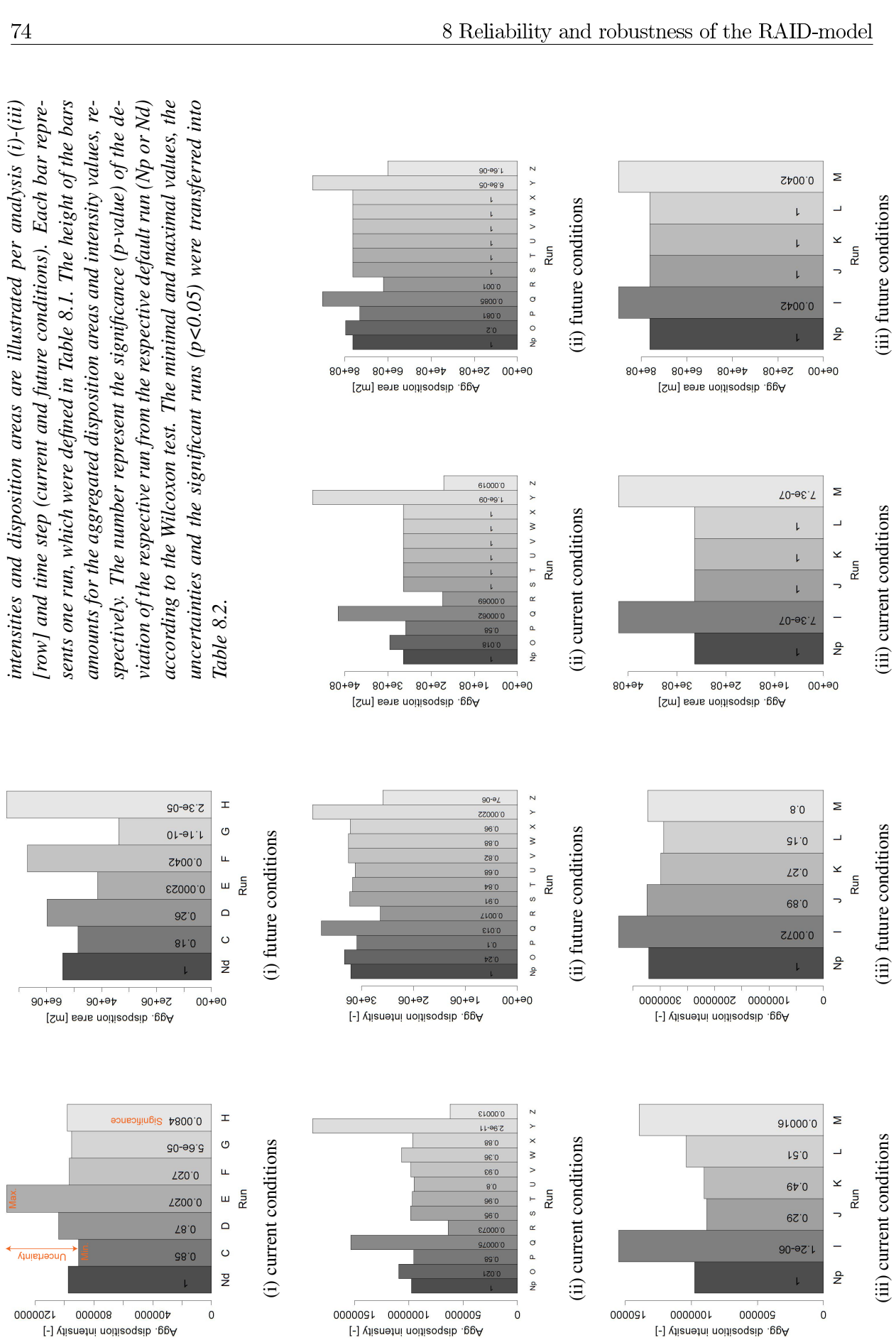

Figure 8.3: Results of the uncertainty analysis. The aggregated disposition intensities and disposition areas are illustrated per analysis (i)-(iii) [row] and time step (current and future conditions). Each bar represents one run, which were defined in Table 8.1. The height of the bars amounts for the aggregated disposition areas and intensity values, respectively. The number represent the significance (p-value) of the deviation of the respective run from the respective default run (Np or Nd) according to the Wilcoxon test. The minimal and maximal values, the uncertainties and the significant runs (p<0.05) were transferred into Table 8.2.

Results						
Coefficient	**Aggregated disposition intensity [-]**			**Aggregate disposition area [m^2]**		
Time step	Current conditions	Deglaciated Alps	Increase	Current conditions	Deglaciated Alps	Increase
Probabilistic approach (Np)	975'243	3'208'278	= + 328%	264'356'163	762'682'948	= + 288%
Deterministic approach (Nd)	1'861'786	5'419'761	= + 291%	397'481'249	889'533'125	= + 223%
Difference Nd-Np	886'543 = 91%	2'221'483 = 69%		133'125'086 = 50%	126'850'177 = 17%	

Uncertainty analysis - robustness of the dependent values								
Coefficient	**Aggregated disposition intensity [-]**				**Aggregate disposition area [m^2]**			
Time step	Current conditions		Deglaciated Alps		current conditions		Deglaciated Alps	
(i) Effects of choice of non-decisive disposition parameters								
min	1'175'372	G	3'381'374	G				
max	2'548'201	H	7'458'148	H				
Uncertainty	1'372'829	=74%	4'076'774	=75%				
Significant runs	E (**), F (*), G (***), H (**)		E (***), F (**), G (***), H(***)					
(ii) Range of uncertainties introduced through parameter uncertainty definition								
min	620'900	Z	2'589'189	Z	170'805'055	Z	601'021'466	Z
max	1'885'633	Y	3'942'491	Y	474'267'142	Y	948'800'077	Y
Uncertainty	1'246'733	=128%	1'353'302	=42%	303'462'087	=115%	347'778'611	=46%
Significant runs	O(*), Q(***), R(***), Y(***), Z(***)		Q(*), R(**), Y(***), Z(***)		O(*), Q(***), R(***), Y(***), Z(***)		Q(**), R(**), Y(***), Z(***)	
(iii) Range of uncertainties introduced through classification								
min	884'227	J	2'932'629	L	264'356'163	-	762'682'948	
max	1'551'160	I	3'763'558	I	420'079'676	I/M	899'878'483	I/M
Uncertainty	666'933	=68%	830'929	=26%	155'723'513	=59%	137'195'535	=18%
Significanct runs		I(***), M (***)		I(**)		(I(***), M(***)		I(**), M(**)

Table 8.2: Results and uncertainties of the aggregated disposition intensities and areas are transferred from Figure 8.3. The significant runs are classified according to the significance levels of the Wilcoxon test in p<0.001(***), p<0.01(**), p<0.05(*). The uncertainty is also expressed in percentage of the corresponding default run (Nd or Np).

8.3.2 Sensitivity analysis - reliability of ranking

Independent of the range of uncertainties included in the results of the sums and areas, the model prediction does not necessarily have to depend on a weighting factor. Therefore in this chapter, the sensitivity of the ranking against the uncertainties will be discussed. For this purpose, the varied ranking was always put in agreement with the default run, to get the agreement between the two runs, according to the methodology described by Bland and Altmann (1986). In this approach, the agreement between two runs is described by plotting the differences of one run against the mean of both runs. The confidence interval, defined as the value differing by two times the standard deviation from the mean, was determined as the descriptive dimension of agreement. The resulting plots are illustrated in Figure 8.4 for the variation of the non-decisive disposition parameters (i). The plots of the other analyses are available in Appendix A. These results are summarized in Table 8.3.

(i) Effects of the choice of the non-decisive disposition parameters
The variation of the weighting of the non-decisive disposition parameters did not imply strong changes in the ranking. For present conditions, the variations measured between 0.7% (4 ranks) and 4.1% (22 ranks), while the deviation for future conditions ranged from 1.2% (13 ranks) to 3.0% (32 ranks). For both time steps permafrost caused the least and deglaciation the most changes in the ranking. In the case of lithology and deglaciation, ignoring the parameter causes roughly twice the deviation than if the parameter was weighted double. The deviations caused by variation of the weighting of the non-decisive disposition parameters on behalf of the deterministic MCE lie in the range of the confidence interval between the two methods of 10.4% (56 ranks) and 18.5% (195 ranks) for present and for future conditions, respectively.

(ii) Effects of the parameter uncertainty (confidence) definition
The confidence intervals gained by taking into account the confidence of the parameter uncertainty definition ranges from 0.4% (2 and 4 ranks) to 17.7% (95 ranks) for present and to 10.7% (113 ranks) for future conditions. The non-decisive disposition parameters featured narrow confidence intervals between 0.4% and 1.8% for both time steps.

(iii) Effects of the classification of the disposition parameters
The confidence intervals range from 0.7% (4 ranks) and 1% (12 ranks) to 14% (75 ranks) and 4.4% (49 ranks) for present and future conditions, respectively. The widest confidence intervals resulted for both time steps equally through variation of the classification confidences of the basic requirements or all elements at once. The effect was thereby approximately three times stronger for present than for future conditions. The additional parameters featured narrow confidence intervals around 1% for both time steps.

Qualitative evaluation of the plots (Fig. 8.4 and Appendix A) suggested that – if distinguishable – for all analyses (i)-(iii) only the first approximately 50 and the last approximately 80-100 ranked lakes featured fewest variations for both time steps. For present conditions this means that for the 9% of the lakes ranked highest and for the 17% of the lakes ranked lowest for impact disposition, the ranking is more reliable than for the remaining 74% of the lakes. For

future conditions this is true for only 5% at the beginning and for the 9% at the end of the ranking.

Summary
The sensitivity of the ranks was hardly significant, contrary to the uncertainties of the aggregated disposition intensity and area, especially for those lakes featuring the highest ranks. The ranking can therefore be assumed reliable. Further interpretations are provided in the next section.

8.3.3 Interpretation

Subsequent to the evaluation of each analysis, an overall interpretation of the RAID assessment in the catchments of high-alpine lakes in Switzerland is given in this section.

Interpretation regarding the RAID-model design
The ranking of the lakes was not sensitive to the varied weightings of the non-decisive disposition parameters and can be considered reliable in this regard. This observation should not, however, lead to the conclusion that those parameters might as well have been removed from the RAID model. The uncertainty analysis showed that at least lithology and deglaciation do have a significant influence on the disposition intensity. Also the qualitative map of the disposition classes benefits from the inclusion of the additional disposition parameters, as it illustrates the characteristics as well as the history of a location influencing long-term RAID.
The small influence of the permafrost and deglaciation on the ranking could be explained by their comparatively small area. As for lithology the weak effect might be due to the chosen categorization. Most lithology categories were classified as contributing to RAID, therefore different weighting only influenced disposition intensity but not the ranking.

The uncertainty introduced by parameter confidence definition for current conditions is higher than the other analyses. The ranking for both conditions is, however, the least sensitive or in the same range as the one from the analysis of the classification (iii). Furthermore, the influence of the uncertainties in the confidence definition is significantly higher for present than for future conditions in both the uncertainty and in the sensitivity analysis. Originally the confidences set in the present parameters were relatively high (closer to the upper maximum of 1) in comparison to the ones of the future parameters (Table 7.1). In the ranking this effect was, however, not represented. This shows that a deterministic approach is much more susceptible to uncertainties – even minor ones – than a probabilistic approach, and that parameter uncertainties should be included, even if they were poorly known. The result is still more robust than if they were not taken into account.

The classification introduced the smallest uncertainties from all analyses even though, in the case of permafrost, it featured the highest weighting factor. The confidence intervals for the ranking equalled, however, the ones from the parameter uncertainty analysis (ii). Significant deviations were only reached by variation of the basic requirement and all parameters at once, even though basic requirements classification was assumed to be the most reliable rule. Classification rules are less crucial than the parameter uncertainty definition.

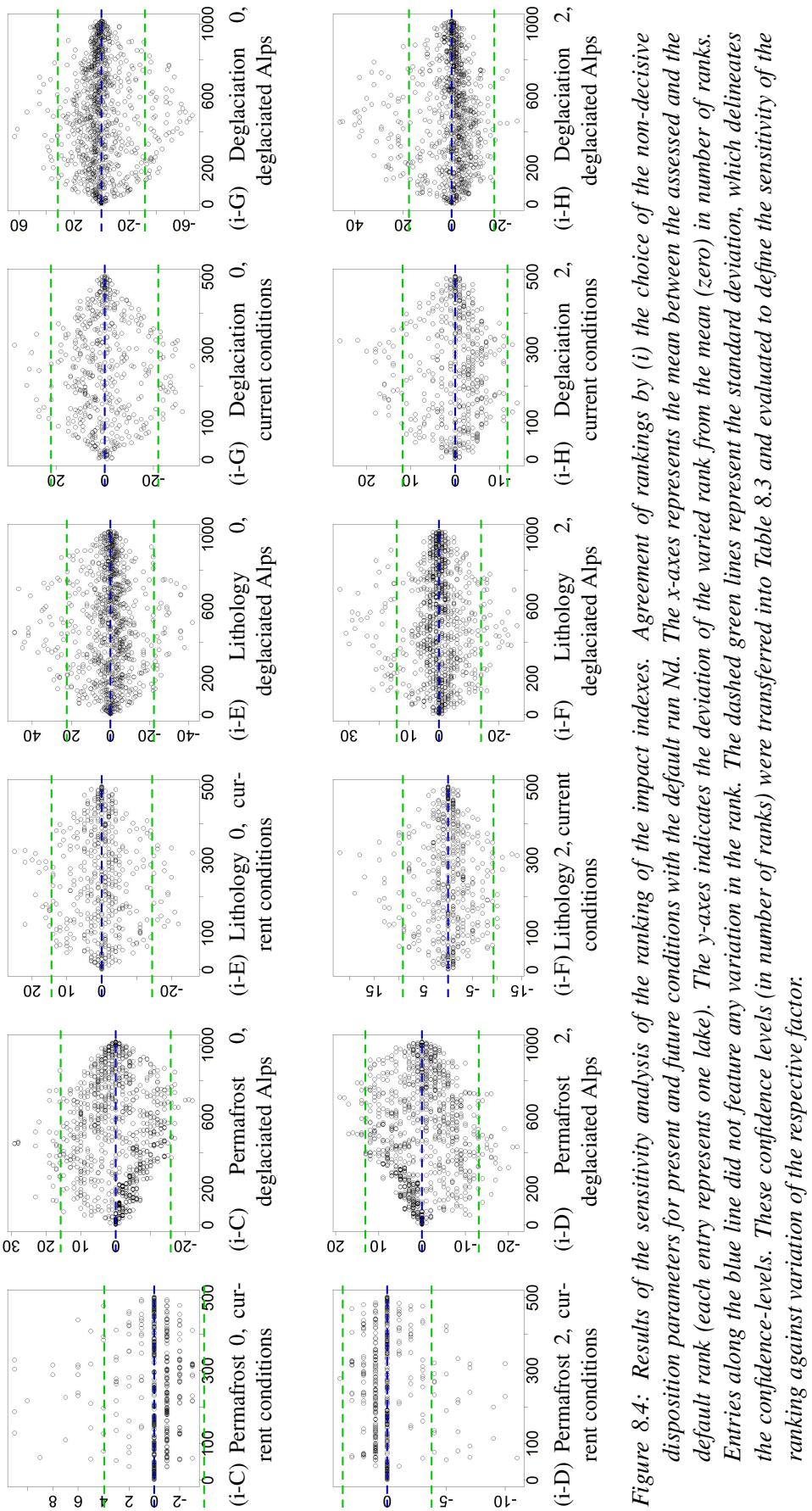

Figure 8.4: Results of the sensitivity analysis of the ranking of the impact indexes. Agreement of rankings by (i) the choice of the non-decisive disposition parameters for present and future conditions with the default run Nd. The x-axes represents the mean between the assessed and the default rank (each entry represents one lake). The y-axes indicates the deviation of the varied rank from the mean (zero) in number of ranks. Entries along the blue line did not feature any variation in the rank. The dashed green lines represent the standard deviation, which delineates the confidence-levels. These confidence levels (in number of ranks) were transferred into Table 8.3 and evaluated to define the sensitivity of the ranking against variation of the respective factor.

Weight	Varied disposition parameter or element									
	(i) Confidence intervals resulting from variation of non-decisive disposition parameters weighting									
	Permafrost		Lithology		Deglaciation					
	C	D	C	D	C	D				
0:	4 =0.7%	16 =1.5%	14 =2.6%	22 =2.1%	22 =4.1%	32 =3.0%				
2:	4 =0.7%	13 =1.2%	9 =1.7%	14 =1.3%	12 =2.2%	18 =1.7%				
	(ii) Confidence intervals resulting from variation of parameter confidences									
	Slope		Overall slope		Permafrost		Lithology		Deglaciation	
	C	D	C	D	C	D	C	D	C	D
0.67:	52 =9.7% *	68 =6.4% *	40 =7.4% *	42 =4.0%	2 =0.4%	5 =0.5%	5 =0.9%	9 =0.9%	2 =0.4%	4 =0.4%
1.33:	13 =2.4%	80 =7.6% *	62 =11.5% *	58 =5.5% *	2 =0.4%	5 =0.5%	2 =0.4%	5 =0.5%	5 =0.9%	19 =1.8%
	All Parameters									
	C	D								
0.67:	66 =12.3% *	113 =10.7% *								
1.33:	95 =17.7% *	105 =9.9% *								
	(iii) Confidence intervals resulting from variation of classification confidences									
	Basic requirements		Permafrost		Lithology		Deglaciation		All elements	
	C	D	C	D	C	D	C	D	C	D
individual:	74 =13.8% *	47 =4.0%	7 =1.3%	14 =1.3%	7 =1.3%	11 =1.0%	4 =0.7%	12 =1.0%	75 =14.0% *	49 =4.4%
	Agreement of rankings of Ndet and Nprob									
	C	D								
	56 =10.4% *	195 =18.5% *								

*Table 8.3: Sensitivity of the ranking with regard to the weighting factors derived from Figure 8.4 and from figures in Appendix A. The entries are explained as follows [example 4=0.7%]: The first numbers [4] represent the deviation in number of ranks of the varied ranking from the mean with the default ranking (green lines in Figure 8.4 and in Appendix A). This deviation was put into relation to the total number of lakes assessed (current conditions: 538 lakes; future conditions: 1056 lakes) [(100/538)*4=0.7%]. The deviation was marked significant (*), if it exceeded 5% of the total number of lakes assessed. C. = current conditions, D = deglaciated Alps*

Comparison of the deterministically versus the probabilistic RAID
The direct comparison of the default deterministic and the default probabilistic rankings shows that the agreement for present conditions (10.4%) is better than the one of the probabilistic approach in comparison to the variation of all its parameter confidences (16.7% and 13%). For future conditions the agreement is, however, clearly weaker (18.5% vs. 10.4% and 11.4%). The plot shows that the deterministic approach tends to overestimate the rank of the lakes in comparison to the default probabilistic run. This is due to the effect observable in Table 8.2. The deterministically derived disposition intensity is strongly higher (present +91%, future +69%) than the disposition area (present +50%, future +17%). This leads to different indexes.
The probabilistic approach influences disposition intensity rather than area. The relative changes between the time steps for both methods are nevertheless in a comparable range (size: probabilistic +328%, deterministic +291%. Area: probabilistic +288%, deterministic +223%).
Therefore the map is important and considered generally reliable, even though it ignores critical gaps in process understanding or missing data.

8.4 Discussion

In this part an approach for assessing the RAIS of present and future high-alpine lakes in Switzerland was proposed. A RAID-model was developed and implemented into a deterministic and into a probabilistic framework by means of a BN. Present and modelled overdeepenings (assumed locations of potential lakes formation) were ranked regarding their RAIS, and the spatial distribution of the disposition classes in the catchments was illustrated in two maps for both time steps, with the help of disposition parameters derived from literature (slope, overall trajectory slope, permafrost, lithology, deglaciation). The results and the main conclusions have already been outlined and will now be critically discussed.

Data
The assessment was carried out on a basis of 25m-resolution datasets. This seems a rather coarse resolution; however, not all datasets were available in more detail. Moreover it is not reasonable to expect a high level of detail if the processes and the conditions are in reality poorly known. This is especially true for future conditions. The assessment endeavoured to detect large-scale slope instability disposition, as the aim of the study was to make statements regarding potential rock avalanches and not rock falls. Therefore the chosen scale is considered adequate.
The number of the non-decisive disposition parameters is certainly not complete, nevertheless it is probably at the maximum possible considering current knowledge and available datasets over all of Switzerland. As for lithology the chosen categorization might not have been the most adequate. Regarding classification of the lithologies, perhaps geotechnical or geomechanical aspects might have been more adequate (see the explanation in Section 4.3.4). This information is nonetheless difficult to achieve at the assessed regional scale. Permafrost is a recent research field and process understanding is relatively limited. The basis for definition of the classification threshold was consequently weak. This should not, however, be a reason to ignore the effect of permafrost, as revealed by the uncertainty and sensitivity analysis. Deglaciation contained

several processes that can alter geomechanical rock properties, as outlined in Section 4.3.4. As most of these processes can hardly be directly observed, the consideration in this general is assumed appropriate.

Method

The RAID model was applied by means of two approaches which aimed at different purposes. The simple, deterministic approach benefited from the advantages provided by the spatial presentability of the datasets, allowing for the mapping of the disposition classes. The probabilistic approach was more complex, but it resulted in more robust and reliable results, thanks to the consideration of parameter uncertainties. The probabilistic assessment was carried out by means of a BN, which also allowed a well-grounded discussion on different kind of uncertainties inherent in the RAID model.

BNs are frameworks for considering relations and interrelations between processes (explained in Section 5.1), which is crucial for multi-hazard analyses (Kappes et al., 2010). In the present study, the probability distribution of the disposition classes per catchment was only derived by means of Equation 7.2. Inference according to Equation 7.3 was not required within the treated research question. The BN allowed a detailed analysis of the model uncertainties. A BN also features the advantages of being able to learn and to be extended at any point. As such, the elaborated RAID model could now be extended in any direction. It is also feasible to include the trigger parameters and their probability of occurrence into the model. Further, the entire situation of a lake hazard assessment as illustrated in Figure 4.2 could be implemented in a BN, taking the RAID model as a starting point. An even larger advance would be to include consequences of a lake-outburst event, a prime example of which can be found in Straub (2005).

Results and their relevance for integrated risk management

The RAID model is a simple reproduction of reality, based on little case-study data and correspondingly on many assumptions. A detailed uncertainty and sensitivity analysis revealed the influences of these effects. Especially the main outcome of the model, the ranking of the lakes according to their impact index, had reliable and robust results. The model can therewith be assumed valid.

The RAID model delivered results on different scales, from the disposition classes per pixel, up to the ranking of the lakes according to their impact index on the regional scale of the Swiss Alps. These results enable the identification of hotspots of RAID and localization in the catchments, also for future conditions. These are two crucial points in risk management.

The RAID model is also a contribution to systematic event analyses in specific cases, as much for rock-avalanche assessment as for lake-outburst assessments. It allows a certain approximation to probability of occurrence by means of the disposition. Existing lake-outburst assessment schemes, as presented in Section 4.3.3, could be specified. Reynolds (2003) for, example, considers "ice-/rock-avalanche risk" as a trigger parameter of a lake-outburst event. The qualitative probability description (none, low, medium, large) could be derived by means of the RAID elaborated in this thesis, at least for Switzerland.

The RAID is only one aspect of the lake hazard assessment, as outlined in Figure 4.2. Therefore it would be inadequate to prioritize the lakes only regarding their impact index. However these assessments show several things that should be adequately considered when assessing a

particular lake. Generally the area fulfilling the basic requirements can also act as a basis for assessment of other mass movements potentially impacting a lake, such as ice avalanches, snow avalanches or collapse of moraines. In this case, adaptations of the overall trajectory might be necessary; further explanations in this regard are given in Section 10.3.1. Furthermore, the possibility of a lake being impacted by the outburst flood of a lake situated uphill and being triggered by a rock-avalanche impact can be qualitatively assessed for a region. As illustrated in Figure 6.2, the catchments of currently existing lakes might decrease due to the formation of new lakes further up valley. If the disposition area also decreases, the impact index will also decrease. The new index, however, does not account for the increasing possibility of a chain of lake outbursts.

The RAID model elaborated in this thesis had meaningful and robust results. The RAIS of high-alpine lakes in Switzerland is increasing as a consequence of ongoing changes in the environment. The following chapter closes the study by putting the RAID in context of settlement and utilization of the Alpine Region to illustrate the relevance of the subject to Swiss society.

CHAPTER 9

RELEVANCE OF ROCK-AVALANCHE IMPACT SUSCEPTIBILITY OF HIGH-ALPINE LAKES IN SWITZERLAND

The rock-avalanche impact disposition for high-alpine lakes in Switzerland was assessed in the previous chapters. Such an impact can trigger far-reaching outburst flows, which might heavily affect down-valley areas. The consequences can be devastating in densely populated areas, as illustrated in the beginning (Section 2.1). The present chapter contains an outline of the damage potential opposed to potential lake-outburst events, with the aim of illustrating the relevance of the scenarios of high-mountain lake-outburst events triggered by rock avalanche-induced impact waves in Switzerland.
For this purpose, the highest RAIS are localized and compared with the damage potential to identify areas that might be prone to larger risks, as much for current as for future conditions. This comparison also provides the answer to the research question "Which of the present and potential future high-mountain lakes in the Swiss Alps are most susceptible to rock-avalanche impacts?"

9.1 Method

This qualitative assessment is carried out by visually comparing hazard and damage potential in a very general manner at the regional scale of the Swiss Alps. The hazard is represented by the RAIS and the damage potential by the (assumed) distribution of the infrastructure. For this purpose, the ranking of the lakes according to their probabilistically-derived impact index is illustrated in Figure 9.2a for current and in Figure 9.2b for future conditions. This RAIS is then confronted qualitatively with the damage potential.

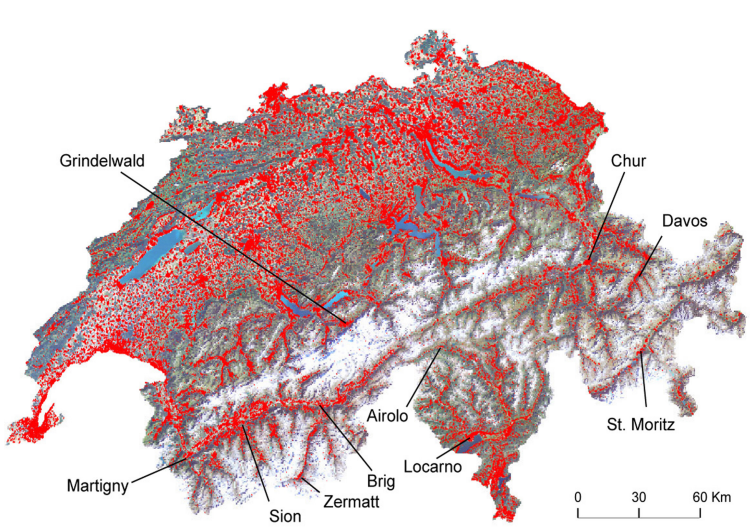

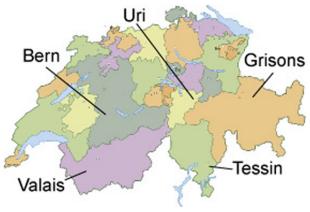

Figure 9.1: Current distribution of buildings (in red) in Switzerland and some cities indicating the damage potential in the mountain cantons. Upper figure: cantons' names.

For current conditions, the distribution of buildings and cities was exemplarily illustrated. For sustainable risk management and long-term planning, these conditions had to be assumed to be different in the future. Many thematic scenarios of developments in Switzerland exist, such as scenarios of population development for 2060 (BFS, 2010), long-term BIP scenarios for 2040 (SECO, 2005) or scenarios for energy perspectives for 2050 (BFE, 2011a,b). Here, the long-term relevance of RAIS of high-alpine lakes in Switzerland was established through confrontation with future land use estimated by means of scenarios of spatial development for 2030 (Perlik et al., 2008). These scenarios are based on four sustainable development paths, three of which were considered realistic by the authors. The corresponding three scenarios of spatial distribution of settlement and infrastructure were compared to the RAIS, to account for different possible developments.

9.2 Results

Current relevance

Lakes exhibiting high impact indexes (Fig. 9.2a) predominate in the Bernese Alps (e.g. the Lakes Grimsel, Oeschinen and Trift), in the Valais (e.g. Lakes de Dix, Mauvoisin and de Emosson), in the western parts of Grisons, especially in the upper Engadin, and in the adjacent areas of Central Switzerland in Uri (Lake Göschenen) and in the Northern Tessin (Lake di Luzzone). Large uncertainties in the ranking of the RAIS predominate for less hazardous lakes only, according to the sensitivity analysis (Section 8.3.2).

The Bernese Alps are densely populated by cities, towns and tourist centers (Fig. 9.1). Some critical situations have already been identified and required risk-reduction activities. Examples are the ice-avalanche impact hazard at Lake Trift, which formed in the last 18 years (Dalban Cannassy et al., 2011) and the collapse of the rock-snout next to the lower lake of Grindelwald, which had formed since 2005 (Haeberli et al. (2012) and Chapter 14 of this thesis). Some of the largest cities of the Valais (e.g. Martigny and Sion) are located at the mouth of valleys

that feature lakes with high impact indexes. But smaller villages are also located in the potentially affected side valleys. The lakes in Grisons are located in less densely populated areas. But especially in the upper Engadin, the impact on tourism could be considerable (NELAK, 2013). The valley bottoms of canton Uri are not characterized by large settlements but exhibit some of Europe's main north-south transport and traffic routes.
Critical situations related to rapid mass movements impacting lakes are currently a problem in some parts of Switzerland. They mainly emerge from lakes recently forming, rather than from the large lakes artificially dammed for hydro-power purposes.

Future relevance
The number of high-mountain lakes for the deglaciated Alps is simulated to at least double. This development on its own doubles the probability of a rock-avalanche impact in Switzerland. The lakes ranked highest assuming deglaciated Alps are mostly located in Valais and in Grisons (Fig. 9.2b). Most of them are artificially dammed lakes, which already exist. The disposition intensity in these catchments is nevertheless assumed to rise for future conditions, mostly as a consequence of glacier recession. The probability of a rock-avalanche impact therefore rises also for these lakes. But a considerable number of lakes featuring intermediate to high ranks are also located in the Bernese Alps and Central Switzerland. Moreover, some of the largest new lakes are modelled for areas whose valley bottoms are already today densely populated. The most impressive example in this regard is the lake simulated in bed of the Aletsch Glacier above the city of Brig (see Chapter 15 for more details).

The future RAID should be compared to future damage potential rather than to the current settlements. The final results of the spatial scenarios A, B and D from Perlik et al. (2008) are in the following qualitatively outlined, to enable this comparison.
Scenario A assumes development under ongoing scepticism, where people act cautious and individualistic, aspiring to autonomy instead of growth. The resulting spatial scenario represents spatial dispersion. It considers the alpine region mostly as reserve area, where the maintaining of the broad and cost-intensive infrastructure is nevertheless assumed. Further tourist centres are noted in the regions of Zermatt, Grindelwald, Davos and St. Moritz. Areas of agglomeration are indicated in the regions of Brig, Martigny, St. Moritz, Davos, Chur, and Locarno/Airolo. Coincidence of dense land-use with especially high RAIS of lakes can therewith roughly be derived at least for the regions of Brig, Martigny and St. Moritz.
Scenario B assumes development through survival of the fittest, where people act dynamic and individualistic to achieve personal success. The resulting spatial scenario contains metropolitan expansion, which acts on the assumption of generations of metropolitan expansion attended by withdrawal from the alpine region: the broad infrastructure will be abandoned and especially southern valleys are only inhabited seasonally. This does not, however, imply an emptying of the alpine area. Tourist centres will still be distributed over the entire Swiss Alps, and the spheres of interest and influence of the metropolitan areas are assumed to reach far into the valleys (especially in the lower Valais) and contain agglomerations. Again, concurrence of damage potential and high RAIS of lakes can be assumed for the Valais and the upper Engadin.

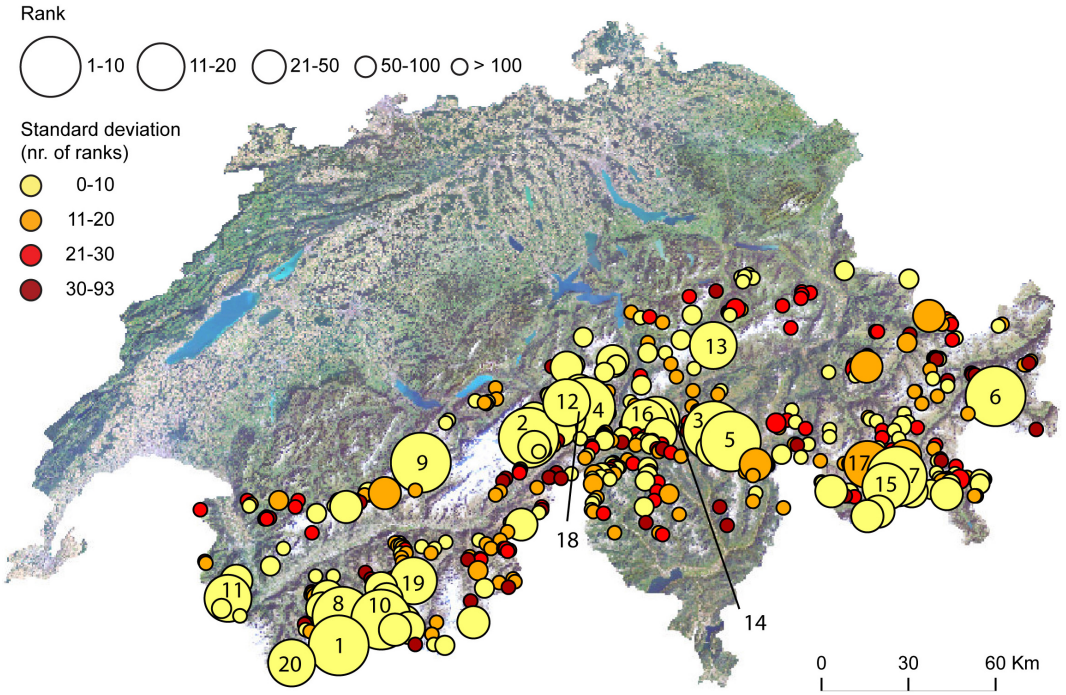

(a) Current RAID.

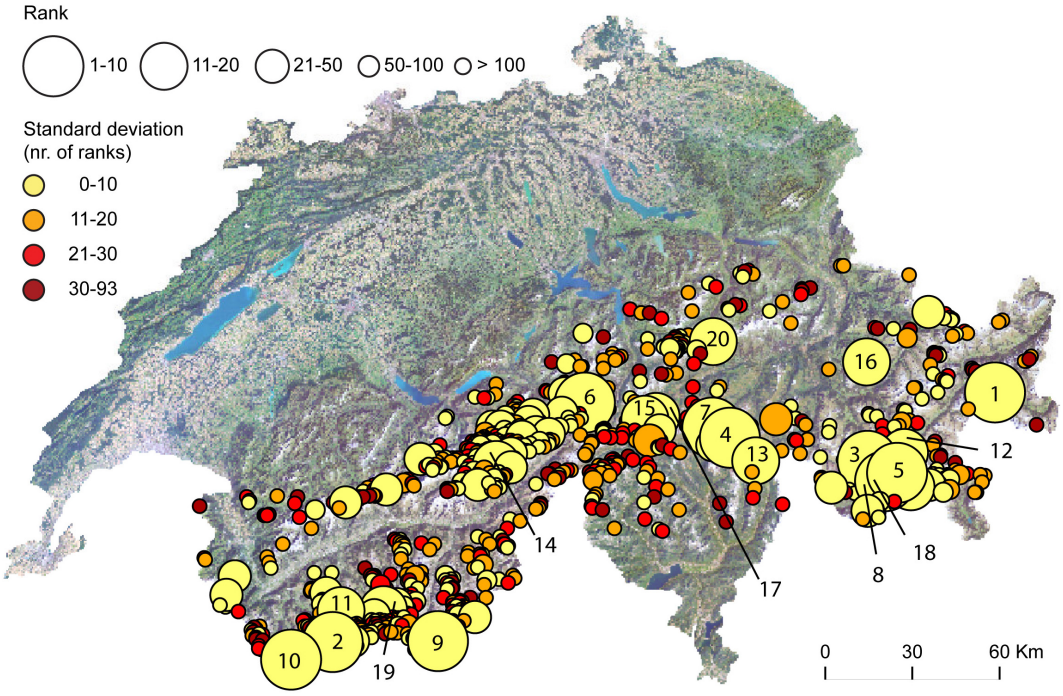

(b) Future RAID.

Figure 9.2: RAID. The size of the point indicates the rank of the lake according to its impact index, while the colour indicates the robustness of the rank. The lakes exhibiting the 20 highest impact indices are located for both time steps (they were introduced in Table 7.2).

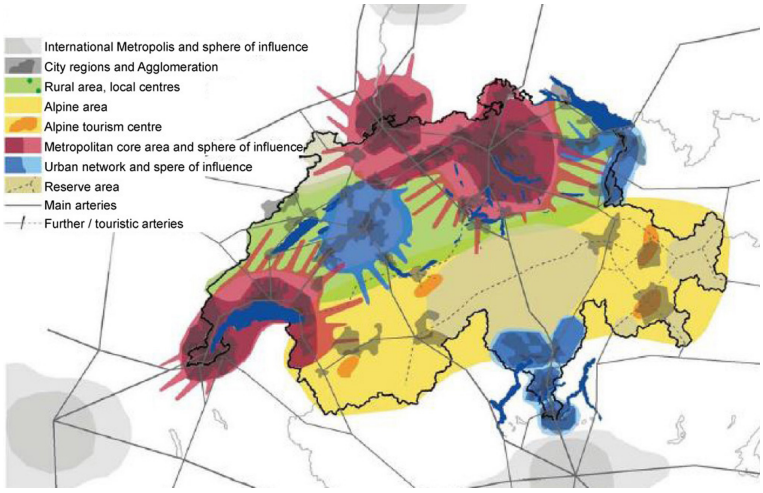

(a) Spatial scenario A: Spatial dispersion

Figure 9.3: Scenarios of spatial development in Switzerland for 2030 after Perlik et al. (2008).

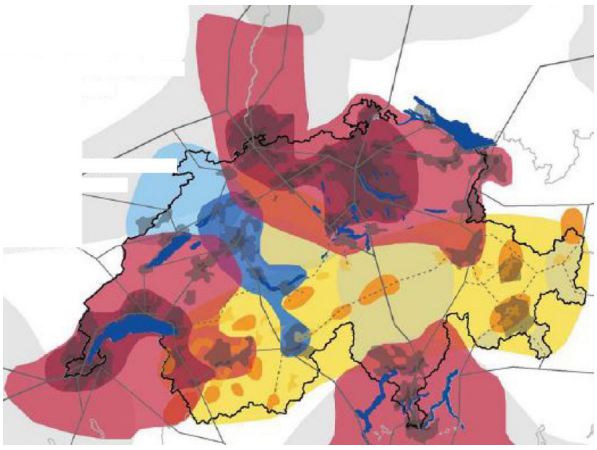

(a) Spatial scenario B: Metropolitan expansion

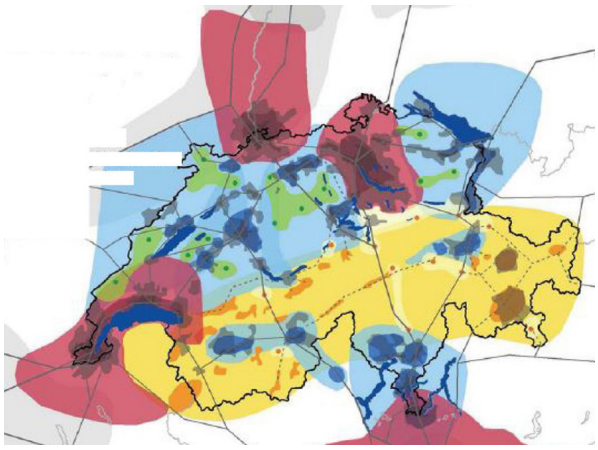

(b) Spatial scenario D: Spatial equity

Scenario D assumes development in rediscovered harmony, where dynamic and social behaviour leads to solidary growth. The resulting spatial scenario represents spatial equity, which assumes a productive use of alpine regions. It will be characterized by productive agriculture, alpine cities and tourist centres directly in the Alps as well as by spheres of interest and agglomeration of cities like Chur, Brig, Martigny or others. This development would lead to a dispersed distribution of damage potential also within the reach of regions other than the already-mentioned Valais or the upper Engadin.

Spatial developments of Switzerland in the near future indicate ongoing settlement and utilization of the Alpine regions in all scenarios, also in areas prone to potential lake-outburst events. A lake-outburst event due to a rock-avalanche induced impact wave is thereby a relevant hazard scenario for the Swiss Alps today and in the future.

9.3 Discussion

The RAID assessed in this part of the thesis is a step further in the direction of hazard assessment and risk management of high-alpine lakes in Switzerland. Comparisons of hazards and damage potentials on a regional scale allows us to point out hotspots, also of potential future risks. The following restrictions must, however, be considered in interpreting this comparison of hazard and damage potential.
The different time frames aspired to must be taken into account. The spatial scenarios only range up to the year 2030, while the lake-formation and RAID scenarios consider longer-term developments in the Alps. The RAID scenario further assumes complete deglaciation of the Alps and accounts for modelled overdeepenings (Linsbauer et al., 2012) only , which are assumed sites of lake formation. Other lake types (introduced in Section 2.2), which may form in other locations, are not considered. The RAID was assessed in this thesis, because this hazard is very likely to persist for a long time period, since climate change also affects slope stability in the long term. Transient hazard situations, e.g. caused by ice avalanches, can provoke equally dangerous consequences and should be incorporated into risk analyses.
But detailed risk analyses can anyway not be carried out on this regional scale. The RAID model is an advancement in the field of event analysis; it also allows for certain approximations on the probability of occurrence by means of the disposition intensity. Informations or estimations on the effect of a rock avalanche impacting a lake cannot, however, be derived from the approaches presented in this part. For more information on hazard assessments refer to Section 3.2.1. The composition of the avalanche would have to be assessed in more detail, because pure rock avalanches are rare in glacial environments; they are more likely to transform into mixed rock/ice avalanches, which feature different flow behaviour (more in this regard in Section 10.1). But even more importantly, parameters of spatial dispersion of both hazard and damage potential are missing in this regional-scale assessment. The following parameters would at least be required, in order to derive risk estimates rather than merely illustrating potential hotspots of hazard and damage potentials: the probability of a lake-outburst event as a consequence of a rock-avalanche impact, and the spatial probability and the intensity of the triggered outburst flow as well as the spatial allocation of the different land-use classes would have to be known at least for the vicinity of the potential outburst path.

The presented study nevertheless expanded the knowledge basis and process understanding and shows potential hotspots, which is a first step towards risk management of low-probability and high-magnitude events. Detailed hazard and risk assessment, however, have to be carried out for every lake individually. Methods applying to an event analysis were already introduced in Chapter 4, to which the subsequent Part III ties up. The subject of this part is effect analysis of the process chain triggered by a mass movement impacting a high-mountain lake. A method for conducting future-oriented risk estimations considering future hazards and land-use changes is presented with the help of a case study in the Aletsch region in Switzerland in Chapter 15 in the consecutive Part IV.

Part III

Hazard analysis of outburst flows triggered by impact waves on local-scale

Once a hazardous situation or a risk hotspot is detected, a detailed hazard analysis might be required. This part deals with local-scale hazard assessment of individual lakes with regard to an outburst flow triggered by avalanche-induced impact-waves under current conditions. The currently available knowledge for identification and assessment of hazards in an event analysis was already summarized in Chapter 4.

The first chapter in the present part enhances this compilation of the state-of-the-art with regard to methods and tools available for estimating the effect of a slope failure by assessing the triggered process chain.One of the first case studies (Lake 513), where numerical simulations of the different processes involved in the process chain were assembled for hazard assessment, will be presented in the subsequent Chapter 11. The influence of uncertainties and their propagation throughout this process chain are assessed by means of this case study in the proximate Chapter 12. The knowledge gained in these analyses is then applied in Chapter 13 to a complete hazard analysis of ice avalanches at Mount Hualcán, combining techniques for event and effect analysis.

CHAPTER 10

EFFECT ANALYSIS OF RAPID MASS MOVEMENTS TRIGGERING IMPACT WAVES

The present chapter enhances the state-of-the-art compilation (summarized with regard to an event analysis in Chapter 4) with an overview on methods and tools available for estimating and analysing the effect of a slope failure by assessing the processes involved in the outburst flow triggered by the impact wave. The aim of the present chapter is to provide answers to the research question three, "How can the process chain of a lake-outburst flow due to an impact wave triggered by a rapid mass movement be analysed for the purpose of a risk analysis?"

Different perspectives for looking at the process chain of a glacier lake-outburst flow triggered by an avalanche-introduced impact wave exist (Carrivick, 2010). This problem was already given attention when defining the term of "high-mountain lake-outburst flows" in Section 2.2. One position is taken up by geomorphologists, who describe the single processes on basis of observations, e.g. by means of their origin. They distinguish, e.g. between mass movements of glacial ice, ice avalanches, rock/ice avalanches, glacial debris flows and outburst-generated debris flows (Evans and Delaney, 2015). Natural hazards specialists, in contrast, would classify the impacts of the processes. Evans and Delaney (2015) summarize the aforementioned examples as catastrophic mass flows, as they all consist of a mixture of earth materials, water, snow and ice, which are characterized by sudden release, high mean velocities (>5 m/s) and large runout distances in comparison to the volume. Another point of view is from the physical modellers, who try to simulate the physical behaviour of the process. Of course, it would be desirable to model all processes and their interactions physically correctly. Up to today, this is, however, not possible. Therefore, the key issues of every individual setting have to be identified and their effects on the process chain have to be estimated in the best way possible.
To overcome these communication difficulties, a geophysical classification of gravitational mass flows is elaborated in Section 10.1. Based on these terminologies, the components involved and their behaviours and interactions are explained in detail in the subsequent Section 10.2, for the

purpose of identification of key information for risk management. Different assessment methods for the single components are then presented in detail in Section 10.3. The methods are also evaluated regarding their application to assessment of the process chain. Depending on the setting and the data availability, different approaches can be chosen.

10.1 Geophysical classification of gravitational mass flows

The processes that can trigger an impact wave and the processes that are triggered by a lake-outburst event (presented in Chapter 4 or indicated by Evans and Delaney (2015) as catastrophic mass flows) belong to gravitational mass flows. In this section, a process- and rheology-based geophysical definition of the involved movements is given, to account for their behaviour.

Gravitational mass flows belong to the group of hillside denudation processes, which differ regarding movement velocity and water content, classified by Carson and Kirkby (1972) in a triangle among the mass movement types "wet and rapid fluvial flow", "dry, spontaneous and rapid landslides", and "slow, permanent landslides" (Fig. 10.1a). The behaviour of a gravitational mass movement further depends on the composition of the flowing material (water-solid fraction content) and the solid fraction type (Coussot and Meunier, 1996), as illustrated in Figure 10.1b. Suspension transports fine and cohesive materials, while bed load consists of coarse, cohesion-less and granular material.

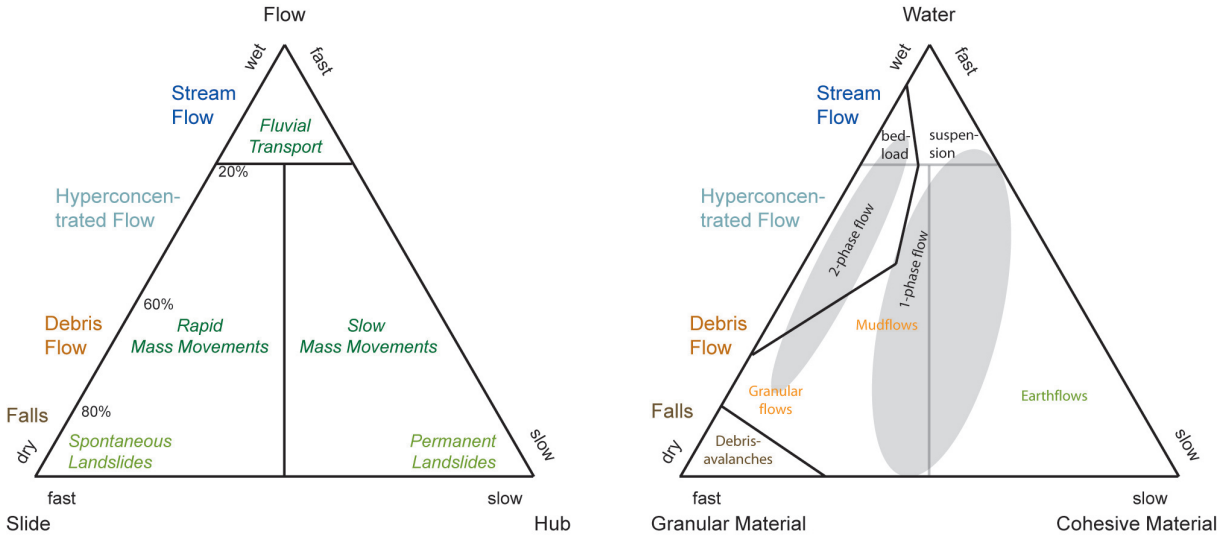

(a) adapted from Carson and Kirkby (1972)

(b) including material type (Coussot and Meunier, 1996).

Figure 10.1: Classification of hillside denudation processes and gravitational mass movements. The processes differ in sediment concentration (wet-dry) (Lavigne and Suwa, 2004; Lavigne and Thouret, 2003) in the velocity (fast-slow) (Carson and Kirkby, 1972) and in material type (granular - cohesive) (Coussot and Meunier, 1996).

All mass flows involved in an impact wave-triggered lake-outburst flow can therefore be assigned to any process on the axes of rapid mass movements between stream flows and debris avalanches, depending on their respective compositions. A short characterization of the most important processes is given here, even though strict distinctions of the phenomena is hardly possible.
Both stream and hyperconcentrated flows vary slowly in time and space regarding their local flow intensities (discharge and flow depth). Hyperconcentrated flows, contrary to the stream flows, contain a larger amount of bed load (Coussot and Meunier, 1996). Stream flows were defined up to a maximum sediment concentration of 20% by volume, followed by hyperconcentrated flows, which carry between 20 and 60% by volume of bed load (Lavigne and Suwa, 2004). As the mean velocity of the coarsest solid particles, the bed load, differs from the velocity of the suspension and the water in the same flow, a two-phase flow should be applied for approximation. Debris flows reach velocities in the range of 0.5-10 m/s and are transient phenomena, which often feature almost periodic surges and completely break and change the initial structure of the material during the flow. A debris flow's deposition is characterized by the stop of the entire mass including the water, as the mixture can be approximated as a one-phase flow of a viscous fluid. A debris flow containing a high part of cohesive particles is called mudflow, as the grain motion is imposed by the behaviour of the entire mass by an interstitial fluid. If the fine fraction in a debris flow is small enough (less than 20% of water by volume (Lavigne and Thouret, 2003)), the direct grain contact defines the mass behaviour, which is called a granular debris flow (Coussot and Meunier, 1996).
Granular mass movements start in rocky or granular mass ruptures and are amongst the fastest landslides, reaching velocities greater than 10 m/s. Again, different classifications exist (e.g Clague and Roberts, 2012; Cruden and Varnes, 1996; Hungr et al., 2005; Varnes, 1978). For the present study, differentiations on basis of the volume will be applied (Fort et al., 2009). Rockfalls, mostly detaching from discontinuities, comprise small volumes (<10'000m^3) of blocks falling or often jumping freely through the air. These movements feature little potential for triggering lake outbursts (as already argued in Section 4.2.2), contrary to rock-slope failures along rather planar surfaces, which can result in large (often >10^6 m^3) and extremely rapid (>25 m/s) rock avalanches (Hungr et al., 2001).

Not included in this classification are ice avalanches as they do not directly contribute to hillside denudation. Similarly to rock avalanches, ice avalanches detach into granular flows. Contrary to rock avalanches, ice avalanches feature smaller densities, can reach longer runout distances (up to 30% more than rock avalanches (Bottino et al., 2002)) due to the reduced friction and can more easily liquidize. In a glacial environment, pure rock avalanches are rare they are also more likely to contain a variable amount of ice, either as part of the initial detaching mass or due to entrainment. The same applies to ice avalanches. For assessment of the flow behaviour (contrary to the event analysis (Section 4.3.4)), most cases must be assumed to be combined rock/ice avalanches, which combine the respective characteristics (Schneider et al., 2011).
Process transformation during movement as a consequence of melting, of entrainment or of deposition of (additional) material along the flow path (Evans and Delaney, 2015) is a general feature of these rapid mass movements. Correspondingly, they have to be classified as complex

motions, as they can modify flow rheology and behaviour several times along the way and cannot explicitly be allocated to one specific flow type (Hungr et al., 2005; Clague and Roberts, 2012). This classification of the mass flows is the basis for the assessment of the effect of a slope failure on a high-mountain lake, which is treated in the following section. To ease understanding, "avalanche" is applied throughout this chapter for all kinds of mass flows emerging from slope failures (rock, ice and rock/ice avalanches).

10.2 Cascading processes of slope failures: components, their behaviour and interactions

The process chain of an outburst flow triggered by an avalanche-induced impact wave is composed of the steps illustrated in Figure 10.2. After the detachment of the slide mass, the *avalanche* behaves as a gravitationally-driven rapid mass movement. Its behaviour (reach, intensity, volume, geometry/shape) is governed by the parameters slope geometry, slope material, avalanche geometry and avalanche material properties (Pfeiffer and Bowen, 1989). If a lake is located within the avalanche runout, an impact is the consequence.
During the immersion of the avalanche into the lake in the so-called *splash zone*, the momentum is transferred from the sliding mass to the water (Di Risio et al., 2011). Different types of avalanches can cause different effects. Rock avalanches are dense mass movements, which have the potential to transfer large impulses into the water. Ice avalanches dampen their own impact wave, because the ice floats on the surface of the lake. Rock/ice avalanches combine these effects.
The wave enters the *near field stadium* soon after its generation, where it assumes its shape in dependence of the characteristics of the slide. Decisive features are slide velocity, volume, depth, width, density, porosity, front shape, underwater travel time and slope angle (Panizzo et al., 2005a). The wave can either take a Stokes-like, a conoidal-like, a solitary-like or a bore-like form (Heller and Hager, 2011) (Fig. 10.3), which is a function of the sliding mass volume velocity and the reservoir size, volume and depth (Fritz et al., 2003b; Zweifel and Minor, 2004; Panizzo et al., 2005a). The degree of the impact further depends on the impact width and the

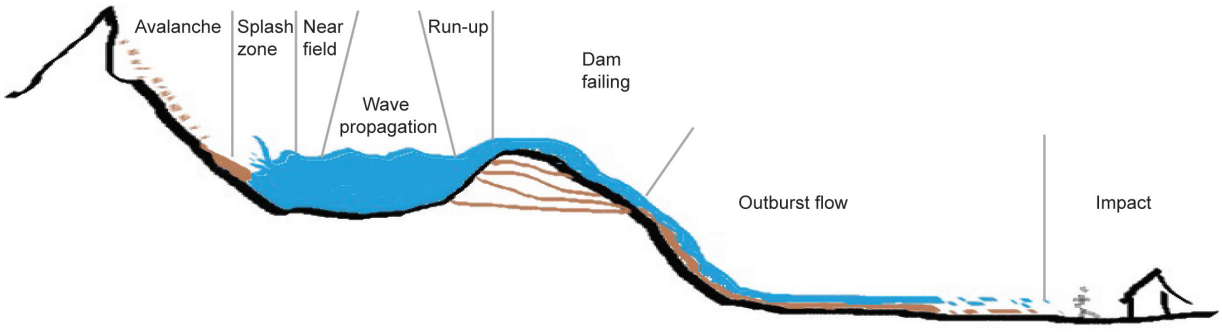

Figure 10.2: Delineation of the processes involved in a lake-outburst flow triggered by an impact wave (after Heller and Hager (2011) and Worni et al. (2014)).

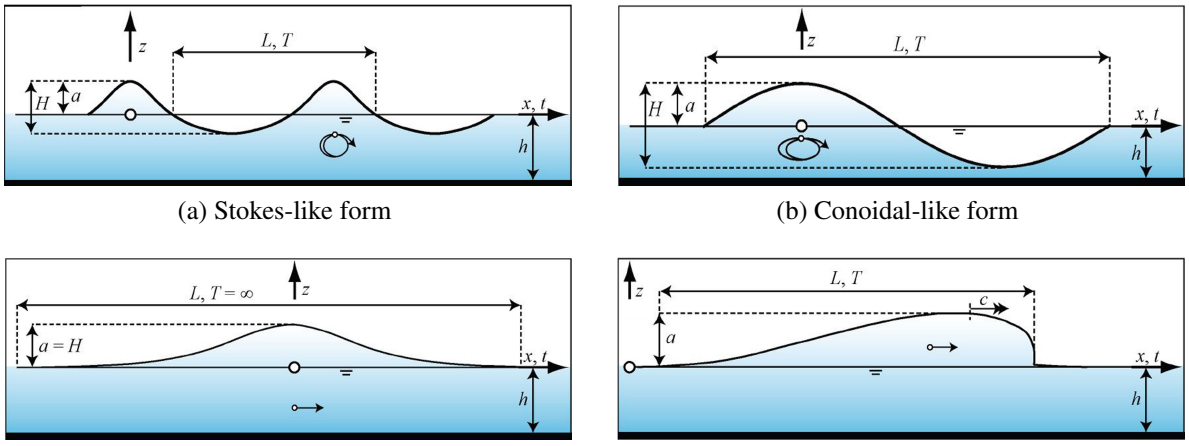

(a) Stokes-like form

(b) Conoidal-like form

(c) Solitary-like form

(d) Bore-like form

Figure 10.3: Wave forms according to Heller and Hager (2011)

disaggregation of the sliding mass (Antunes do Carmo and Carvalho, 2011). In this listing, the first wave-type corresponds to the smallest and the last one to the largest in terms of volume transportation (Di Risio et al., 2011). Subsequently, this *wave propagates* through the lake until it *runs up* and eventually overtops the dam. These motions are a function of the lake basin and the surrounding topography. The runup further depends on the wave height and length and is very sensitive to the impact velocity (Heller et al., 2008).
If the runup exceeds the freeboard, overtopping is the consequence of an impact wave. As explained in Chapter 4, overtopping can further lead to *dam failure*; the respective relationships are illustrated in Figure 4.2. The specific failure mechanism and the exact motion of failure depend mainly on the dam type (ice, earthen, rock) and are therefore very diverse; the processes involved were explained in Section 4.2.1. For hazard assessment, the breach initiation, the time to peak discharge and the discharge are crucial to know (Morris, 2000). The breach initiation lasts from the moment the overtopping flow starts the process of retrogressive erosion of material from the downstream dam face and crests and stops as soon as erosion continues in the upstream face of the dam (Morris et al., 2008). The duration of this action is referred to as breach-initiation time, while the moment of breaching up the dam is the failure time (Wahl, 1998). Once the upstream face is breached up, breach formation takes place until the breach has formed fully; this duration is called breach-formation time. Breach growth takes place during breach formation and indicates erosion of the lateral sides of the breach. The type of outflow hydrograph used depends on the rate of breach formation and the final breach size (Fread, 1991).
The process finalizing the chain is another rapid mass movement, the *outburst flow*, which directly affects the damage potential. The outburst flow can occur in a variety of forms, mainly characterized by the outflow hydrograph and its bed load, the channel gradient as well as the vegetation cover, the sediment type and availability along the flow path (Hürlimann et al., 2008; O'Connor et al., 2013). Consequently, *flow impacts* on infrastructure and settlements are also diverse and are a function of the spatial dispersion (reach and inundation) and the intensity of the flow.

In this section, the process chain of a lake-outburst flow triggered by an avalanche induced impact wave was presented. The components involved, their behaviour and interactions were exposed, roughly. To more precisely delineate the interactions between the processes and the corresponding effects, the process chain has to be assessed, e.g. through modelling, for each case specifically. The available methods and their compatibility to represent parts of the process chain are discussed in the following section.

10.3 Assessing and modelling the components of the process chain

A wide range of different approaches is available to assess the processes outlined above. At least as wide is the range of respective literature, some of which is summarized in Table 10.1. Gaining an overview of the assessment approaches and the simulation softwares currently in use for the different geomorphologic processes involved in the process chain is not an easy task, as every modelling community uses different terms or classification systematics and because a trade-off between geomorphological descriptions of processes and computational simulations exists (Carrivick, 2010). The approaches also differ regarding the purpose for which they were established (e.g. physical description of motion to enhance process understanding vs. implementation of geomorphological observations vs. objective-oriented setups (e.g. for hazard assessment)). Correspondingly, the outputs of the models differ. In this section, an outline on different assessment approaches and their outputs (as far as they can be conceived from literature) for the components of the process chain will be given with an appreciation of their application to hazard assessment of the entire process chain. The aim of the effect analysis is to derive conclusions on the lake-

Review	Content
Rapid mass movements	
Volkwein et al. (2011)	Give an overview on rockfall hazard assessment. The process of rockfall is, as outlined in Section 10.1 not of much relevance for the present study, as the energy included in a fall is too small.
Hungr et al. (2005); Dai et al. (2002); Worni et al. (2013)	Reviews on simulation of rapid mass movements
Manville et al. (2013)	Review of debris flows assessment focusing on lahars
Malet et al. (2007); Hürlimann et al. (2008)	Reviews on assessment of landslides (runout calculation methods), especially of rapid mass movements
Impact waves	
Heller et al. (2008)	Summary on models suitable for the assessment of impact waves
Di Risio et al. (2011)	Review on forecasting of landslide generated impact waves by empirical equations
Ataie-Ashtiani and Najafi Jilani (2006)	Overview on numerical and experimental studies on landslide generated waves
Dam breach	
Singh (1996)	One of the most cited review on dam breach assessment and subsequent outburst flow assessment
Morris (2000); Worni et al. (2012b)	Reviews on dam breach assessment
Carrivick (2010)	Comparison of dam break modelling point of views from hazard managers and from numerical modellers.
Westoby et al. (2014)	Review on processes and modelling approaches involved in outburst flows from moraine-dammed lakes

Table 10.1: A compilation of reviews with regard to hazard assessment of rapid mass movements, impact waves and dam breach.

outburst flow reach, inundation and intensity from the knowledge on the initial slope failure location, volume and mass composition.

A first difficulty in elaborating this compilation consists in finding a universal nomination of the assessment types. The terminology applied in the following is based on Heller et al. (2008), although with minor adaptations to make it compatible to the entire body of literature.
The most simple type of assessment approaches rely on *empirical equations*. According to Heller et al. (2008), universal equations derived from either model experiments or from real cases are implied in this category. The resulting estimations act in the first place as a support decision on whether more detailed analyses are required. The second category of assessment approaches are *analytical methods*. Some authors (Hungr et al., 2005) compile all models, which are based on physical rules of solid or fluid dynamics in this category. In the present study, the more narrow understanding of Heller et al. (2008) will be applied, defining analytical methods as improvement of process understanding via mathematical reasoning only. The third category contains *physically-based numerical simulations* of conservation equations of mass, momentum and energy that describe the dynamic motion of the process together with a rheological model simulating the material behaviour. These categories aim at direct application to hazard assessment and are hence important for the present study.
Heller et al. (2008) distinguish two more assessment types. Specific situations can also be evaluated by means of *precise model experiments*, for which a specific case is recreated in the laboratory. This was, for example done for an impact wave in a water reservoir as a consequence of a snow avalanche (Fuchs et al., 2011). This method is, however, extremely extensive in many aspects (Heller et al., 2008) and will be considered no further in the present analysis. *Experimental simulations* based on physical laboratory experiments can help researchers understand behaviour of a process and therefore act, for example, as a basis for (numerical) modeling (Carrivick, 2010). Ataie-Ashtiani and Nik-Khah (2008) for example, conducted a range of experiments with sliding masses into reservoir, which helped to determine the slide and its impact characteristics, which served as an extension to the LS3D-model for subaerial landslides. A direct application for hazard assessment is, however, not the main purpose of these assessment approaches; therefore they will also not further be treated in this study.

In the following, approaches describing the motions contained in the process chain of a lake-outburst flow triggered by an avalanche-induced impact-wave will be described for the first three categories. Also their suitability for integration into the model chain will be discussed. The focus will be put onto description of the effects of slope failure.

10.3.1 Empirical equations

Empirical equations are usually applied as first-order estimations and are either derived from model experiments or from observations of real cases. An overview of the general scope of application is provided here.

Rapid mass movements
Empirical equations describe in a general mode the runout distance and the distribution of the

	Rock avalanches	Ice avalanches	Debris flows	Stream flows
Value	30°	17°	11°	3°
Reference	Kaibori et al. (1988)	Alean (1985)	Huggel et al. (2003)	Allen et al. (2009b)

Table 10.2: A summary of commonly applied angles of reach from Bolch et al. (2012).

debris independent of the exact movement type (Dai et al., 2002). All kinds of avalanches impacting a lake as well as all kinds of outburst flows from a lake are considered rapid mass movements (see Section 10.1 for the argumentation).

Empirical methods can only provide an estimate of the profile of the travel path (Hürlimann et al., 2008). These empirical relationships require, however, little input information, which are the event location and volume, and the longitudinal profile along the flow path. Dai et al. (2002) summarize two basic concept of empirical mass movement models.
The most basic concept of runout calculation was introduced by Heim (1932) as the "Fahrböschung", also called angle of reach or energy-line method (Worni et al., 2013), which is the ratio between the vertical drop and the horizontal projection of the maximum runout distance. In the rock-avalanche impact disposition model elaborated in this thesis (Chapter 5), it is referred to as the overall slope trajectory. Commonly applied values are listed in Table 10.2. An advancement of this concept (Corominas, 1996; Rickenmann, 1999) considered the dependency of runout distances with the magnitude of the initial volume (Scheidegger, 1973). These approaches do not deliver information on intensity, which is crucial for hazard mapping.
The second type of mass movement equations also accounts for the mass loss of a debris flow along its flow path (Cannon and Savage, 1988) and contain a volume-change rate through including morphological features in the form of a stepwise multivariate regression-analysis. These models require a profile of the flow path, knowledge of the failure zone and the initial failure mass, as well as of slope gradient, vegetation types and channel morphology (optional).
Intensity information can only be indirectly incorporated into these empirical equations via other empirical relationships. Relationships between flow volume and the maximum area of inundation are suggested for different flow types by Iverson et al. (1998); Jakob (2005); McKillop and Clague (2007a). First-order estimations of the flow intensity can be derived with the help of equations for peak discharge as a function of the flow composition (Jakob, 2005).

Impact wave
Di Risio et al. (2011) give an extended review on empirical estimations on impact waves generated by subaerial slides. Typical results are estimations of the initial wave height, period, length and amplitude. Equations based on indoor experiments for wave generation by means of parameters from a granular slide impact and equations for wave propagation in 2D and 3D as well as estimates of runup and overtopping are, for example, provided by Heller et al. (2008). But these overtopping parameters (discharge, overtopping time, etc,) refer to a dam without freeboard. This information is therefore of little use in most safety assessments of high-mountain lakes.
Further, forces of a wave impacting a dam can be estimated empirically (e.g Heller et al., 2008). Necessary input information are slide characteristics (such as impact velocity, slide width, vol-

Dam type	Equation	Reference
Moraine dam	$Qmax = 0.0048V^{0.896}$	Popov (1991)
	$Qmax = 0.72V^{0.53}$	Evans (1986)
	$Qmax = 0.045V^{0.66}$	Walder and O'Connor (1997)
	$Qmax = 0.00077V^{1.017}$	Huggel et al. (2002b)
	$Qmax = 0.00013P_E^{0.60}$	Costa and Schuster (1988)
	$Qmax = 0.063P_E^{0.42}$	Clague and Evans (2000)
Ice dam	$Qmax = 75(V/10^6)^{0.67}$	Clague and Mathews (1973)
(drainage)	$Qmax = 46(V/10^6)^{0.66}$	Walder and Costa (1996)
(sudden break)	$Qmax = 2 * V/t_w$	Haeberli (1983)
	$Qmax = 1100(V/10^6)^{0.44}$	Walder and Costa (1996)
Earth- and rock-filled dams	$Qmax = 0.72V^{0.53}$	Evans (1986)

Table 10.3: Empirical peak-discharge equations for dam-breach assessment (Table from Huggel et al. (2002b), extended with equations from Wang et al. (2008)). V = lake volume; P_E = the potential energy of the reservoir, defined as the product of dam height [m], lake volume [m^3] and the specific weight of water [9,800 N/m^2]. t_w = time constant of 1,000 s.

ume, height, density and porosity) as well as information on the lake shape and the subwater topography.

Dam Breach

Empirical equations for predicting breach parameters of earthen dams have been developed based on case-study data. The formulas allow for prediction of breach parameters, like the breach-formation time or the breach geometry (Atallah, 2002), by means of regression equations (Morris et al., 2009). Some equations further calculate the outflow hydrograph with the help of the breach form (Wahl, 1998). Input parameters depend on the formula, but they often involve overtopping height, discharge volume, dam height and width. Results usually refer to the process of dam failure rather than to the outflow. An extensive overview on equations for breach-width, failure-time and peak-flow equations including uncertainty ranges is given by Wahl (2004); Pierce et al. (2010). These estimations mostly apply to artificial embankment dams.

Investigations specifically regarding high-mountain earth dams also exist, and they mainly focus on estimation of peak discharges. A compilation of peak discharge equations for different dam types is summarized in Table 10.3. For hazard assessment, it has to be considered that most equations referring to moraine-dam peak-discharges orientate themselves on average-discharge measurements. Maximum peak-discharges can be derived by equations provided (e.g. Clague and Mathews, 1973; Evans, 1986; Haeberli, 1983). Kershaw et al. (2005) further provide an overview on equations for velocity estimation, which are mainly based on observations of past events, and hence will not be expressed here, as they are not suitable for predictive lake-outburst flow assessment

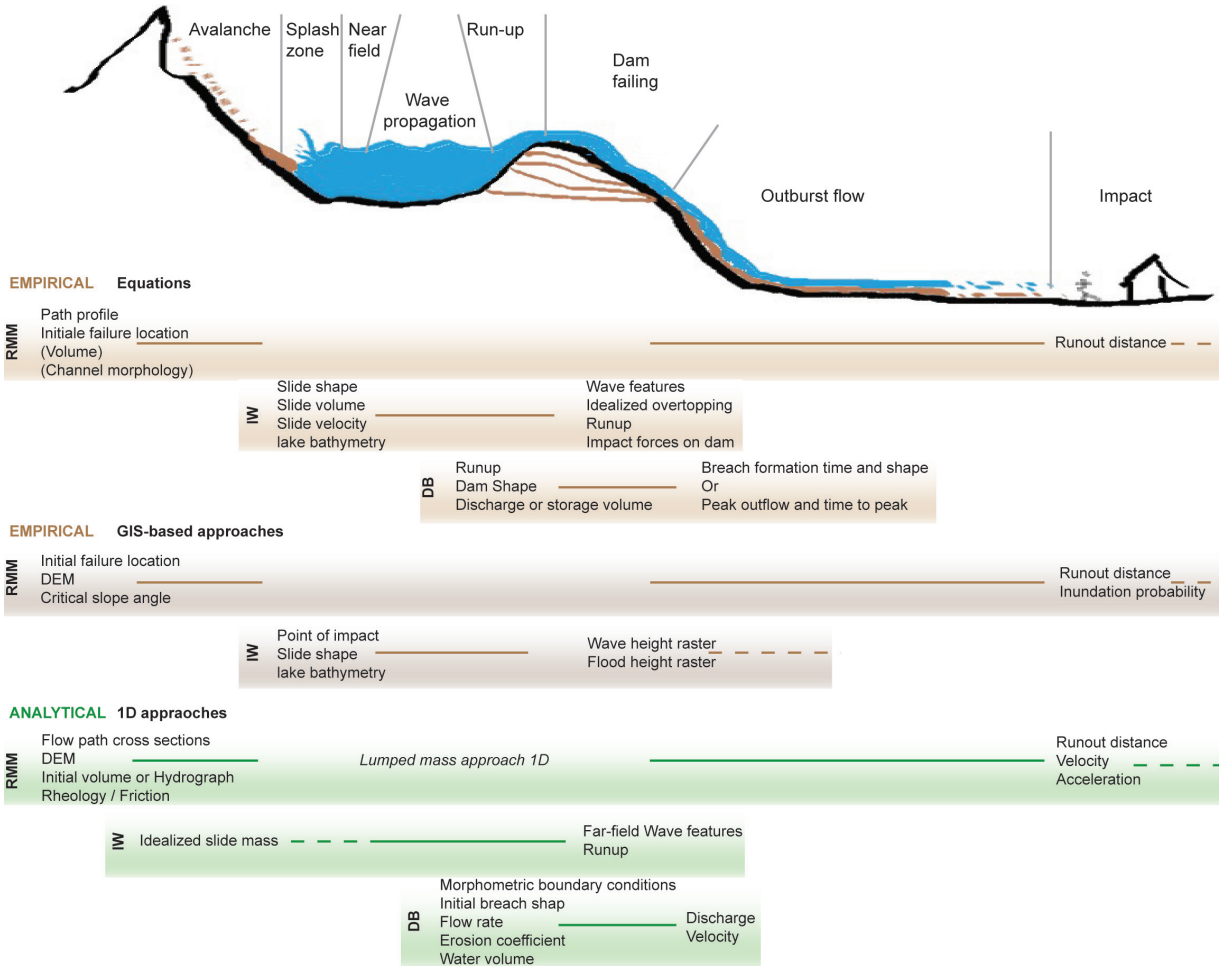

Figure 10.4: General overview of applications of empirical and analytical methods for the processes involved in the cascade. The input data (left columns) and the output data (right columns) indicate the suitability of the models for coupling. RMM = Rapid mass movements, IW = Impact wave, DB = Dam breach.

10.3.2 Analytical methods

Analytical models describe the behaviour of a process by means of mathematical reasoning.

Rapid mass movements

Analytical models for rapid mass movement describe the physical behaviour of the movement in a lumped-mass approach, where the debris mass is assumed to be a single point (Dai et al., 2002). The dynamic of the flow is calculated along a previously selected flow path. The runout distance, velocity and acceleration can be calculated assuming the movement being controlled by a single force resultant, which represents the gravity as well as all movement resistance.

The thereby derived velocities often had unrealistically high results (Hungr et al., 2005). To achieve more realistic flow velocities, adaptations were carried out, e.g. by implementing the Voellmy two-parameter rheological relationship for frictional-turbulent resistance into the model (Körner, 1976).

Analytical models require a DEM, the cross-section's shape, initial volume or input hydrographs and rheological or friction parameters. These kinds of models are only applicable for slides of limited displacement that do not disintegrate during motion. Furthermore, the calculations only work in one dimension, and spreading effects on the fan cannot be represented (Hürlimann et al., 2008). Therefore these approaches are not very suitable for representing complex motions such as avalanches or lake-outburst flows.

Impact wave
The process of wave generation is generally too complex to be described analytically (Heller et al., 2008). Reasonable results for the far-field can nevertheless be generated with the help of strong simplifications in wave theory and idealized slides (Di Risio and Sammarco, 2008). These analytical solutions are in satisfactory agreement with experiments performed in a two-dimensional flume, and can nevertheless be applied to validation of numerical models and to estimation of the order of magnitude of impact waves.

Dam Breach
The breaching of earthen dams is in one-dimensional, analytical solutions described as a two-phase, water-sediment interaction process (Singh, 1996). The process is calculated in three parts: the reservoir water-mass depletion, the broad-crest weir hydraulics and the breach-erosion relation, which is based on an initially defined (rectangular, triangular, trapezoidal) breach cross-shape. The analytical solutions are governed by the equation of reservoir water balance and a relationship between the rate of erosion and the flow characteristics. The enlargement of the breach is continued until the reservoir is empty or until the dam resists the erosion, which requires empirical determination of an erosion coefficient. Depletion of the reservoir also affects the rate of discharge.
The analytical solutions of an earthen dam-breach are mostly implemented as simulations software; an appraisal of their suitability for assessment of the process chain will be given in the next section, which deals with numerical simulations.

10.3.3 Numerical simulations

Numerical simulations are computer-based reproductions of the reality (e.g. of a behaviour, a process or other complex systems) in a simplified way. Numerical simulations consist of a quantity-oriented computer model, which contains the equations and algorithm applied to describe mathematically the behaviour of a process or a system. The computational simulation refers then to the actual running of the software or program that contains the model on a simplified topography. A simulation software program therefore models a real phenomenon with a set of mathematical formulas on a computer.
Many ways of classifying numerical simulations exist, and they depend on the processes they are applied to (for mass flows see (e.g. Hungr et al., 2005; Manville et al., 2013; Westoby et al., 2014)). To deal with the variety of origins of the simulation applications gathered here, only a very general classification will be applied. More detailed descriptions of fundamental principles and differences in the simulation software will be treated in the sections dealing with the applica-

tion fields according to the geophysical processes: (i) non-physically based simulations, which build on parametrical or analytical computer model and (ii) physically-based simulations.

10.3.3.1 Non-physically based simulations

Non-physical simulations contain all numerical simulations whose computer models consist of the parametrical or analytical description of the process as described before.

Rapid mass movements
An enhancement of the empirical equations is the implementation of empirical knowledge into GIS-based flow routing algorithms. These approaches allow to simulate a flow in a DEM, which has an empirically-derived stopping-criteria implemented (Hürlimann et al., 2008). A summary on different algorithms and their discussion can be found in Huggel et al. (2003) or in Westoby et al. (2014). Hürlimann et al. (2008) distinguish between two algorithm types (single and multiple flow-direction model) which are relevant for runout prediction. Single flow-direction models (such as the D8-algorithm) calculate the flow direction as the line of dips between two neighbouring pixels with the highest gradient. Multiple flow-direction models allows the flow to invade several neighbouring cells (Huggel et al., 2003). This approach generates inundation probabilities and maximum runout distances given a flow-dependent average slope angle as a stopping criterion. A more complex GIS-routing model connects empirical relationships between flow volume, cross-sectional area and planimetric inundation-area in software which was originally created with regard to volcanic lahars (LAHARZ). Necessary input parameters are a DEM and the initial flow volume (Iverson et al., 1998; Schilling, 1998).
None of the methods generate volume, energy or velocity information, which are required for risk-oriented hazard assessment.

Impact Wave
Analogous to the numerical simulation of rapid mass movements, non-physically based impact-wave simulations consist of the empirical equations implemented into a GIS-environment.
Cannata et al. (2012) implemented the empirical equations derived by Heller et al. (2008) into a GRASS-GIS environment. This approach requires an elevation raster accounting for the bathymetry and a lakewater depth raster and, on the sliding mass: bulk-slide density, porosity, volume, width, thickness, coordinates of the impact point on the lake, water depth in the area of impact, impact velocity, impact inclination angle and the impact azimuth angle. According to the equations from Heller et al. (2008) a wave height and a flood height raster map are given as outputs; the process of impact-wave generation is, however, not described.

Dam breach
Parametrical or analytical dam-breach models cannot be separated from semi-physically-based models without ambiguity, as a dam-breach simulation software can consist of up to five components, each of which is based on specific parametrical, analytical or physical assumptions. Singh (1996) identified these five components of dam breach simulations as (1) upstream channel routing, (2) reservoir hydraulics, (3) hydraulics of flow over the dam, (4) breach morphology and (5) downstream flow routing. The assignment of the abilities of the most known simulation

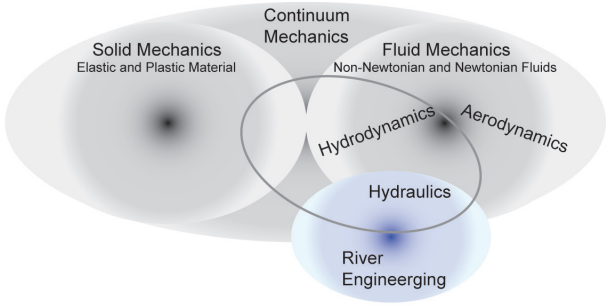

(a) Physical classification of branches in Continuum Mechanics. The circle indicates the disciplines relevant for the present thesis.

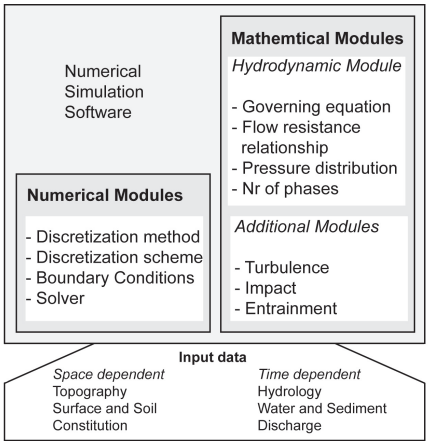

(b) Composition of simulation softwares for CFD, after Feah et al. (2011).

Figure 10.5: Introduction into physically-based simulation.

programs can be found in Singh (1996). Dam-breach models further differ regarding treatment of (a) the breach morphology, (b) the flow over the dam, (c) the sediment transport and (d) the mechanics of the breach side slopes (Morris et al., 2009). Semi-physical solutions use case study information to estimate the failure time and the ultimate breach geometry, to then simulate breach growth as a time-dependent linear process, and to compute breach outflows using principles of hydraulics (Wahl, 1998). Most non- or semi-physical simulations represent the flow over the dam with a weir equation, assume critical flow-conditions on the dam crest and treat the breach growth as a function of time. These models usually require initial empirically-derived information on the shape of the initial breach cross-section and assume immediate breach (Morris et al., 2009). Further knowledge on the erosion coefficient is needed, which is often based on assumption, as the knowledge of physiochemical soil characteristics is rare. For these reasons, non- or semi-physical dam-breach approaches are judged to be useful for reconstructive dam-breach modelling. For predictive outburst modelling, however, none of these simulation softwares are applicable, as they do not take into account the variable material properties and boundary conditions (Westoby et al., 2014).

10.3.3.2 Physically-based simulations

To understand the mechanism and the differences between the (non-)physically-based simulations, an introduction into the underlying physical principles and the setup of numerical simulation softwares will be given first. As also outlined in the introduction to this Section 10.1, the use of different terms and classifications is an obstacle in coupling models. Therefore this knowledge on the basics of physically-based numerical simulations is also crucial for understanding the advantages, the disadvantages and the applicability of the model to complex high-mountain terrains and to the corresponding geophysical processes.

Introduction into Continuum Mechanics

The geophysical description of rapid mass movements according to their flow velocity, material type or sediment concentration has already been given in Section 10.1 in Figure 10.1. In a more general physics, all these movements are described assuming the theory of the continuum mechanics (Fig. 10.5a), which is the study of physics of continuous material, either of the motion of solid mechanics or of the motion of fluid mechanics. In the fluid mechanics, fluid dynamics describes the movement of fluid flows in pipes or on external surfaces and can be applied to aerodynamics, which is the study of air and other gases in motion or to hydrodynamics, which is the study of liquid in motion. If the theoretical foundation of fluid mechanics (especially of hydrodynamics) is applied to the engineering use of fluid properties, the topic is called hydraulics. The principle of motion is the basis of the continuum mechanics. The behaviour of all kinds of materials is numerically described with an equation of motion. Motion is defined as the change in position of an object with respect to time and its reference point. It is described by displacement, direction, velocity, acceleration and time. Motion follows the conservation laws for mass, linear momentum and energy. These laws state that the total momentum of all objects in a closed system remains unchanged over time. The momentum of an object is directly related to its mass and velocity. Motion is observed by attaching a frame of reference to a body.

To summarize, all flows (independent of the geophysical classification according to water-sediment ratio, material type or velocity) are physically described on a basis of the equation of motion. In fluid mechanics, computational fluid dynamics (CFD) is the solution or analysis of problems regarding liquid and gases with surfaces defined by boundary conditions by means of numerical methods or algorithms.

Introduction into Computational Fluid Dynamics (CFD)

Simulation softwares for CFD contain two integral parts (Faeh, 2007; Manville et al., 2013) whose functioning has to be understood in order to choose an adequate model combination to represent impact-wave triggered outburst flows, and will therefore be introduced in the following discussion. The components indicated in Figure 10.5b are indicated in italic in the text.

Numerical module

Firstly, a CFD software contains numerical modules with methods for solving the equations within given boundary conditions. The *boundary conditions* define the surfaces of a flow, such as the permeability of channel walls or the inlet/outlet regime definitions of open boundaries.

To be solved numerically, the continuous equations of motion have to be discretized, which is the process of transferring the continuous hydrodynamic equations and the additional modules into discrete counterparts. *Schemes for discretization* (Table 10.4) can base on an Eulerian (a) or a Lagrangrian (b) reference frame and consist of a structured (c), unstructured (d) or of a meshless (e) grid. Structured grids allow fast calculations and can be mapped in Cartesian domains; they are not, though, very suitable for complex terrain (Feah et al., 2011). Unstructured grids mostly appear in form of triangles, which are highly flexible and suitable for complex geometries. They can, however, not be mapped in Cartesian domains. For flows in the topographically complex high-alpine setting, the choice of a moving Lagrangrian instead over an Eulerian reference frame is preferable, as it accounts better for the unsteady nature of the landslide motion (Potter, 1973).

Numerical Element	Description
Discretization schemes	(Feah et al., 2011; Keiser, 2006; McDougall, 2006) 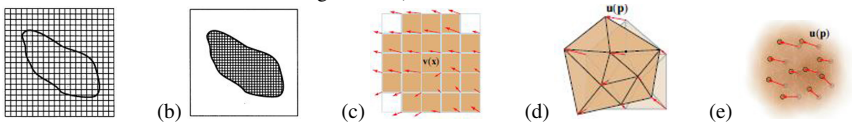 (a) (b) (c) (d) (e)
Eulerian reference frame	The grid is fixed in space and the flowing mass moves upon it (a)
Lagrangian reference frame	The grid is located within the flowing mass and correspondingly moves together with the slide (b). It provides higher resolution within the flow given the same computational effort, but is nonetheless more delicately suited to numerical problems.
Grid types	structured (c), unstructured (d), meshless (e)
Discretization methods	
FVM	is a cell-average value solution, which guarantees the conservation of fluxes through a particular control volume. It is fast, especially for large problems, due to advantages in memory usage and solution speed. (Eymard et al., 1998)
FEM	discretizes over the entire volume or area of a given element. It is usually applied to solids but also feasible for fluids. FEM is much more stable than the FVM, but requires, however, more memory and is slower than the FVM. The Boundary Element Method (BEM) considers the same principles. Discretization, however, only takes place on boundaries and surfaces. The values are then interpolated upon the width of the element. (Keiser, 2006)
FDM	works on point-value solutions, which are simple to program. It is mostly used in complex geometry with need for high accuracy and efficiency. (Keiser, 2006)
VOF	Describes the interface of meshbased multi-phase approaches. It is a eulerian solution of Navier Stokes equations, mostly discretized by FVM, which tracks the free surface locations by calculating the proportion of each 3D-mesh element being filled with water. (Abadie et al., 2010; Hirt and Nichols, 1981; Kothe et al., 1999; Woodhead et al., 2007)
SPH	The advantages of SPH over finite difference schemes are many; most relevant for modelling of geophysical flows Monaghan (2005) are the following: the resolution can be made to depend on position and time; complex physics can easily be implemented, because of the close similarity between SPH and molecular dynamics; interface problems among several materials can be easily solved, which is crucial for interconnection of geophysical processes or for simulation software describing multi-phase flows. (Benz, 1990; Monaghan, 2012; Vignjevic and Campbell, 2009)

Table 10.4: An overview of a set of components of numerical modules in CFD, relevant for the choice of an adequate software for a specific assessment.

Different *discretization methods* can be applied (summarized in Table 10.4). In meshbased approaches, the continuous topography is therefore divided into discrete elements related together by a topological map, upon which the interpolations functions of the equation of motion can be carried out (Keiser, 2006). The most common methods are the finite volume method (FVM), the finite element method (FEM) and the finite difference method (FDM). Meshbased approaches feature the disadvantage of not being capable of adapting to changes in the physics of the continuum (Keiser, 2006). Large deformations can lead to severe stability and accuracy problems and to complex re-meshing operations required through changes in topology-introduced numerical errors. These problems can be overcome by meshless discretization methods. These methods approximate the flow based on interpolation points, which represent particles that move with the material. A wide range of meshless techniques exist; one of the oldest and most often-applied ones are the meshless Smooth Particles Hydrodynamics (SPH), which differ from the meshbased methods in the manner of depth integration (Hungr et al., 2005). SPH solves the equation of fluid dynamics by replacing the fluid with a set of particles (Monaghan, 1992). Therefore no grid is used and the complicated description of free surfaces becomes easier (Monaghan, 2012).

Equation of motion	Description
Navier-Stokes equations(NS)	
3D NS	Perfect 3D description of the Newtonian motion of fluid, which account for rather short water waves (compared to the wave depth). The direct solution of the full NS equations is only possible numerically for local problems due to their complexity (DNS = Direct Numerical Solutions).
RANS	The Reynolds-averaged NS equations (RANS) are a simplified, time-averaged form of the NS equations. They do not numerically integrate small-scale turbulence, but rather account for them with the help of a turbulence module, which connects the flow velocity and the shear stress by means of a friction factor.
LES	Large eddy simulations (LES) is a mathematical model for turbulence used in NS equations. These numerical solutions are an alternative to RANS. Their solution is attainable with supercomputers.
St. Venants equations (SV)	
2D SW	2D SV equations are also called Shallow Water (SW) equations. They represent a simplification of the RANS equations under the following assumptions: (a) the length of the flow is clearly larger than its depth, and the vertical flow characteristics are neglectable, which results in (b) neglectable vertical flow velocities and (c) static vertical pressure distribution.
1D SV	Further simplification of the 2D SW-equations into one dimension.
Boussinesq-approximation	
3D	Approximation to water waves, which account for non-linear, long water waves (compared to wave depth) and, contrary to the NS equations, incorporate frequency dispersion, which considers the dependence of the wave propagation velocity from the wave's length.
Potential flow	
3D	Representation of an ideal fluid motion assumed for homogeneous stream flows without whirls or friction forces.

Table 10.5: A selection of relevant of motion of Newtonian fluids implemented as governing equations in the hydrodynamic module of CFD-software (Feah et al., 2011).

Physical and mathematical modules

The second part of numerical simulations consists of the mathematical models describing the processes. In any given case, every simulation software contains at least a *hydrodynamic module*, which describes the fluid flow and its pressure distribution and viscosity in space under consideration of the before mentioned conservation laws (Teman, 1984). Integral components of the hydrodynamic module are the governing physical equation of motion (the most common ones are explained in Table 10.5), a flow-resistance relationship, definition of the fluid type and the number of phases, which are described in more detail in the next paragraph. Further empirical, analytical or physical modules can be added, which will be presented in the respective process-oriented sections.

Different *governing equations* exist to describe the motion of fluid, which are delineated in Table 10.5. The choice of the respective representation of the equation of motion hence also defines the number of dimensions in which the flow is represented. There nonetheless exist several interpolation techniques for simulation of a 3D- or a 2D-behaviour on basis of the 1D- or 2D-equations, e.g. by modelling a non-hydrostatic *pressure distribution* (Hungr et al., 2005). These solutions will in the following be called quasi-3D or -2D approaches. The results, which can be achieved by applying a certain dimension, will be outlined when presenting the process-oriented software. A comprehensive review on required input and output parameters, as well as on implications for computational time, can be found in Woodhead et al. (2007).

All presented governing equations describe water waves, which are defined as Newtonian fluids, in which the viscous stresses are proportional to the strain rate in Newtonian fluids. Vis-

Relationship	Definition
Laminar flow	Describes liquefied flows containing granular or clayey materials.
Turbulent flow	Refer to water or granular mixtures with low-solids concentration and widely applied in engineering using the Manning equation. This equation relates the velocity of an open flow to the surface roughness, plant cover, cross-section shape and flow depth. It assumes that all flows are driven by gravity. A table of empirical values of the Manning coefficient is given by Chow (1959). Other equations exist (e.g. Chézy-term).
Plastic flow	Is often applied to liquefied soil, under the assumption of the basal shear resistance being equal to a constant yield strength.
Bingham resistance	This model combines plastic and viscous behaviour. A Bingham fluid is described as a rigid material below a threshold-yield strength, which behaves as a viscous material above.
Herschel-Bulkley	Enhancement of Bingham-model, accounting also for shear-thinning behaviour of mud (mixtures of water, clay and grains)
Frictional basal resistance	Is proportional to the effective bed-normal stress at the base, which is the difference between the total stress and the pore-fluid pressure at the base. It is also called Coulomb relation for viscous fluids.
Voellmy resistance	This model combines frictional (Coulomb) and turbulent behaviour. Specializations exist, e.g. the Voellmy-Salm model for snow avalanches.

Table 10.6: Empirical rheological relationships for (single-phase) Non-Newtonian fluids (Coussot and Meunier, 1996; Hungr and McDougall, 2009; Naef et al., 2006).

cosity measures the resistance of a fluid to deformation due to shear stress caused by the friction between neighbouring particles. All fluids featuring different flow properties (compare with Figure 10.1) are summarized as Non-Newtonian fluids. Their behaviour can be included into the hydrodynamic model with the help of empirical rheological relationships (also referred to in literature as rheological material-parameters or flow-resistance parameters) (Naef et al., 2006). *Flow-resistance relationships* can therefore account for different fluid types (depending on geological material), by describing the basal shear-resistance governed by the basal rheology, which may differ from the internal rheology (Hungr and McDougall, 2009). An overview over the most common relationships is given in Table 10.6, a detailed review is available in Ancey (2007).

Most numerical representations of flows consist of one continuous body. This assumption is especially oversimplified, when rapid mass movements exhibit multiple components or when processes interact. Examples are a water flow with sediment transport at the bottom or a granular flow impacting a fluid (Feah et al., 2011). More sophisticated softwares attempt to simulate *multi-phase fluids*, mostly by theoretical formulations describing multiphase mixtures, which apply different motions of flow for the different components (Manville et al., 2013). In mesh-based multi-phase simulations, the interface between the components has to be descriped, what VOF is often used (Table 10.4).

Finally, every simulation software requires two types of user-defined input data (Faeh, 2007): space-dependent topographic information and time-dependent hydrology input-data. In the following discussion, a more detailed description and evaluation of the single software types and additional modules will be given with regard to process description.

Simulation of rapid mass movements

As shown in Figure 10.1, the transition between the different rapid mass movements from stream flow over more bed loaded flows to rock avalanches is floating. Correspondingly, a clear attribution of the softwares to a certain flow behaviour is difficult, especially as landslides tend to

Formula	Definition
Meyer-Peter&Mueller	Was developed for rather coarse sand. It does not consider slope effects (Meyer-Peter and Müller, 1948).
Bagnold-Visser	Is more suitable for suspended load of fine sand (Visser, 1988).
Smart	Based on the Meyer-Peter&Mueller formula but is developed for bed load transport over a range of steep slopes 0.04-20% (Smart, 1984).
Rickenmann	Is also developed for bed load transport over steep slopes (0.1-20%) of hyperconcentrated flows (Rickenmann, 1991).
Takahashi	Is developed for debris flows over steep slopes (Takahashi, 1991).
VanRijn	Simulates suspended transport (Carrivick, 2007).

Table 10.7: A selection of sediment transport equations.

change their behaviour along the flow path due to entrainment and/or deposition (Manville et al., 2013).
Up to a debris content of 20%, hydraulic models assuming Newtonian flow are appropriate. A fully physical approach describes the flowing mass as an open-surface hydraulic flow (overland flow), for which only a DEM, the surface roughness, and the boundary conditions have to be specified (Hungr and McDougall, 2009). A Non-Newtonian flow has to be simulated for a flow containing larger sediment concentrations (Worni et al., 2012a). Simulation softwares designed for rapid mass movements might additionally account for suspended or bed load sediment transport as well as entrainment or deposition of material along the flow path. The most common sediment transport equations (Aksoy and Kavvas, 2005; Merritt et al., 2003; Tingsanchali and Chinnarasri, 2001) are summarised in Table 10.7.

Sediment transport equations are, however, not able to simulate the behaviour of debris flow or even of granular flow. Therefore software that allows a flexible treatment of the flow (e.g. by choice of different rheologies) might be preferable to overland-flows simulations.

Another approach for simulation of rapid mass movements can be applied, to more appropriately simulate different flow regimes (McDougall, 2006; Worni et al., 2012a). This second type of model acts after a principle named by Hungr (1995), the principle of equivalent fluid, which defines the flow as a homogeneous block of hypothetical material, whose form and behaviour is governed by rheological relationships based on experimental or empirical knowledge. It features the disadvantage of the need for calibration of the parameters (Mazzanti and Bozzano, 2009) and therefore does not represent a fully physical approach (e.g. Hungr and McDougall, 2009). In the present study, the term equivalent fluid will be applied. It is nevertheless a very important tool for hazard assessment, as it permits assessment on basis of observations where a lack of process understanding predominates (Carrivick, 2010), e.g. for ice avalanche simulation. Space-dependent input (topographic data) data for equivalent fluid simulations are usually DEM- and rheology-specific via back-calibrated friction values. The optional additional modules might require further information, e.g. information on the depth and the coefficient of the erodible layer. As time-dependent data, the information on release area (location, height, width) or the inflow hydrograph have to be specified; description of boundary conditions is not required. Direct outputs then are flow velocities, heights, pressure or stress distribution and momentum. All models deliver the information as static, animated or isometric views. The exact format, then, depends on the software. RAMMS, for example, delivers line or time plots as well as

ASCII-files (Christen et al., 2007), while other softwares establish contour maps (Denlinger and Iverson, 2004; McDougall and Hungr, 2004; Pitman et al., 2013).

To summarize, equivalent-fluid approaches are suited for simulating avalanches. Application examples are given by Margreth et al. (2011); Preuth et al. (2010); Schneider et al. (2014). To simulate a lake-outburst flow, a wider range of simulation software is available, ranging from equivalent-fluid approaches to hydraulic overland-flow routings. Examples of simulations of outburst flows with overland flow models are given for Jökulhlaups with Delft3D or with SOBEK by Carrivick (2006, 2007). It is not yet clear which of the approaches is more suitable for application to large-scale flows that change their rheological behaviour along the flow path. Both approaches feature considerable sources of uncertainty: the equivalent fluids by rheology calibration and the hydraulic simulations by definition of the boundary condition (Worni et al., 2012a). Corresponding comparisons were undertaken, e.g. by Mergili and Schneider (2011), by comparing a hydraulic (FlO-2D) and an equivalent fluid (RAMMS) simulation for a potential lake outburst flow in Tajikistan. Depending on the (observed/expected) characteristics of the flow, the most appropriate software should be chosen.

Programm	**Numerical Module** *Discretization*			**Mathematical Modules** *Hydrodynamics*					*Additional Modules*		**Source**
	Mesh	Reference frame	Scheme	Equations	Integration	Dimension	Rheology	Phases	Sediment Transport	Additional	
IBER	unstructured	Eulerian	FVM	2D SW	depth	quasi 3D	Manning	1	Sediment	Turbulence	IBER (2010a,b)
Hec-Ras	structured	Eulerian	FDM	1D SV	cross section	quasi 2D	Manning	1	Sediment	Water quality	Brunner (2010)
SOBEK	structured	Eulerian	-	1D SV and 2D SW	-	1D or 2D	Manning	1	Van Rijn, Frijnk	Rainfall-Runoff Water Quality	Deltares (2013) Carrivick (2006)
Delft3D	structured	Eulerian	FDM	2D SW	depth	quasi 3D	Manning	1	Meyer-Peter & Mueller, VanRjin	Wind stresses Water quality Turbulence	Deltares (2011) Carrivick (2007)
BASEMENT	unstructured	Eulearian	FVM	2D SW and 1D SV	depth	quasi 3D and 1D	Manning/ Equivalen Sand roughness	2	modified Meyer-Peter & Müller	Dambreach	Feah et al. (2011); Volz et al. (2010); Worni et al. (2012b)
FLO-2D	structured	Eulearian	FDM	2D SW and 1D	depth	quasi 3D and 1D	Manning / Bingham	1	Meyer-Peter & Müller	Dambreach	FLO-2D (2014); O'Brien et al. (1993); O'Brien (2003)

Table 10.8: Numerical and mathematical details of a selection of software simulating overland flows.

Programm	**Numerical module** *Discretization*			**Mathematical modules** *Hydrodynamics*					*Additional Modules*	**Source**
	Mesh	Reference frame	Scheme	Equations	Integration	Dimension	Rheology	Phases		
RAMMS	unstructured	Lagrangian	FVM	2D SW	depth	quasi 3D	Voellmy-Salm	1	Entrainment Random Kinetic Energy	Christen et al. (2007) Sovilla et al. (2006)
DAN	meshless	Lagrangian		1D SV	depth	quasi 2D	Laminar, Turbulent, Plastic, Bingham, Frictional, Voellmy	1	Entrainment	Hungr (1995, 2008); Hungr and McDougall (2009)
DAN3D	meshless	Lagrangian	SPH	2D SW	depth	quasi 3D	Frictional Voellmy		Internal strain Internal stresses Entrainment	Hungr (2008) Hungr and McDougall (2009) McDougall (2006)
-	structured / rectangular	Eulerian	FEM / FVM	2D SW	depth	quasi 3D	Coulomb	2	-	Denlinger and Iverson (2001, 2004); Iverson et al. (2004)
TITAN2D	structured / rectangular	Eulerian	FEM / FVM	2D SW	depth	quasi 3D	Coulomb	2	Entrainment	Pitman and Le (2005); Pitman et al. (2013); Sheridan et al. (2005)

Table 10.9: Numerical and mathematical details of a selection of software simulating equivalent fluids.

Simulation of impact waves

According to the geophysical description of impact-wave generation, the corresponding numerical simulation has to be able to represent computational domains that change over time and locations in the impact zone. The respective moving areas are the dry coastal area, the dry portion of the slide and the wet portion of the slide corresponding to the submarine part of the slide and the water (Bornhold and Thomson, 2012). This is the reason why softwares simulating submarine landslides by displacement of the floor, even though they are accurate and well studied, should not be applied for a full physical description of the motion of subaerial impacts (Ataie-Ashtiani and Najafi Jilani, 2006). As described above, one approach to simulating subaerial impacts is by rigid slides. The rigid slide approach is experimentally well validated for rigid slides of idealized shapes. The water-slide interactions in subaerial tsunamis, however, are more complex than the physics in Newton's law and in inviscid-flow theory. A lack of relevant experimental results is the main reason why no realistic simulations of deformable slides, such as rock avalanches, can be carried out for impact-wave-generation assessment (Abadie et al., 2010), though a corresponding experiment was recently started (Fritz et al., 2003b,a).

In numerical modeling of tsunamis, the main concern in various approaches is the accuracy of approximate equations for describing the nonlinearity effects and frequency dispersion of waves. Regarding this, the Boussinesq-type models are more efficient than models based on Navier Stokes or potential flow equations (Ataie-Ashtiani and Yavari-Ramshe, 2011). The potential flow has been proven applicable to underwater slides (Abadie et al., 2010) but not to subaerial slides, as it cannot be applied to cases where strong vorticity is created by flow separation or interface reconnection, which both occur in subaerial slide cases.

A study on the impact of the mesh onto landslide impact waves in cases of flows limited by vertical walls showed that the results were not sensitive to the type of mesh (Serrano-Pacheco et al., 2009). Therefore, the choice of the type of grid can be left to the modeller or can be guided by the interest to fit irregular boundaries.

Tsunami-simulation software does usually not contain flow resistance relations or sediment transport equations – they are not suited for outburst flow modelling. This is different with dam breach models.

Programm	**Numerical Module** *Discretization*				**Mathematical Modules** *Hydrodynamics*					*Impact*		**Source**
	Mesh	Reference frame	Scheme	Interface	Equations	Integration	Dimension	Slide rheology	Phases	Impact slide	Wave simulation	
THETIS	mixed	mixed	FVM	VOF	NS	DNS	3D	Newtonian	3	rigid sliding	ge, pr	Abadie et al. (2010)
-	unstructured	Eulerian	FVM	VOF	NS	LES	3D		3		ge, pr, ru	Liu et al. (2005)
FUNWAVE	structured	Eulerian	FDM	-	Bousinessq	depth	quasi 3D		1		pr, ru, in	Ataie-Ashtiani and Malek-Mohammadi (2008); Kirby et al. (1998)
LS3D	structures	Lagrangrian	FDM	-	Bousinessq	depth	quasi 3D	-	1	rigid sliding, truncated hyperbolic secant func.	ge, pr, ru	Ataie-Ashtiani and Najafi Jilani (2007); Ataie-Ashtiani and Yavari-Ramshe (2011)
Geris	structured	Eulerian	FVM	VOF	Tree-based	-	3D		1			Popinet (2003, 2009)
SPHysics	meshless	Lagrangrian	SPH	SPH	variable	-	2D or 3D	variable	1	rigid, wedged		Gomez-Gesteira et al. (2012b,a)
-	unstructures	Eulerian	FVM	time dependent of bathymetry deformation	2D SW	depth	quasi 3D					Delis and Kazolea (2011)
	mixed	Eulerian	FVM		2D SW	depth	quasi 3D	-	1		ge, pr, ru	Serrano-Pacheco et al. (2009)
-	unstructured	Lagrangrian	FEM	Particle finite element method	2D SW	depth	quasi 3D	Bingham	1	rigid submarine slides or granular aerial slides	ls, ge, pr, ru	Cremonesi et al. (2011)
I-SPH	meshless	Lagrangrian	SPH	SPH	NS	DNS	3D	Bingham and Generall cross	2	submerged rigid or deformable slide	ls, ge, pr, ru	Ataie-Ashtiani and Shobeyri (2008)
FLUENT 6	unstructured	Eulerian	-	VOF	RANS	-	3D		2	rigid slide or multi-block	ge, pr	Biscarini (2010)
GeoClaw	structured	Eulerian	FVM	-	2D SW	depth	quasi 3D	-	1 (2)	-	pr,ru,in	George (2011); Berger et al. (2011)

Table 10.10: Numerical and mathematical details of a selection of hydraulic simulation software with impact modules applied to impact wave generation modeling. ls = landslide, ge = generation, pr = propagation, ru = runup, in = inundation.

Simulation of earthen dam breaching
Physically-based simulations provide accurate results of the behaviour of water level and velocities in a plane and are recommended for dam breaks or curved-flow simulations, because they simulate basic erosion processes and breach mechanics with a minimum of simplifying assumptions (Feah et al., 2011). Furthermore, there is distinction between two types of physically-based dam breach models. (a) Physically-based, empirical models include parametrical descriptions of, e.g. the erodibility coefficient, while (b) physically-based, theoretical models describe the entire process physically by including physical description of erosion process. These models require a large amount of parameters to be calibrated, such as soil properties (Morris et al., 2009). For hazard analysis, the simulation of different dam-breaching aspects is, however, more crucial than the type of model applied. The term breaching is usually applied to the entire process without reflecting on the different steps involved, which are breach initiation, breach formation and breach growth. While non- or semi-physically based breach-models assume instantaneous breach by simulating breach formation and breach growth only (Zhu et al., 2004), physically-based simulations take into account retrogressive erosion and therefore also allow estimations on the breach initiation time (Morris et al., 2008). This is crucial to know, for example, with regard to planning of early warning systems. An overview on dam-breach simulation software can be found in Singh (1996) and a more extended review, also including the newer physically-based models, is given by Morris et al. (2009).

10.3.4 Model application to process chain

The previous three sections provided an overview on empirical, analytical and physically-based methods available for assessing the processes involved in the cascade of a lake-outburst flow triggered by an avalanche-induced impact wave. This fourth section summarizes the findings with regard to the application of the models, to assess the process chain. These explanations hence also answer the research question phrased at the beginning of the chapter.

Numerical simulations of coupled processes
Even though no approach yet exists for reproducing the entire process chain of an outburst flow generated through an avalanche-induced impact-wave, several efforts to connect at least some elements in the chain were made, thanks to the application of fully physical-based softwares.
Actually, the new generation of physically based dam-breach simulations (e.g. Basement) can be put into this category, as they can be applied for wave propagation, runup, dam-breaching, and outburst flow routing. This is a reasonable approach if little bed load transport with the outburst flow is assumed, e.g. in hyperconcentrated flows. Even less sophisticated dam-breach simulation softwares, which account for inflow routing, could be used for impact generation. In DAMBRK, for example, a slide input-module (considering landslide volume, porosity and impact time) is included (Fread, 1982). As physically based models mostly work with the same physics, some successful attempts to apply them to different processes were carried out, which makes the classification into "overland flow", "tsunami" and "dam-breach" models ambiguous. GeoClaw, which was originally established for submarine-generated tsunamis, was proved suitable for simulation of lake-outburst flows in mountainous terrain (George, 2011) and is currently

extended to a 2-phase model, in order to better account sediment transport. Overland-flow models based on the equations of shallow water can contrariwise be applied to wave propagation and runup simulation in a lake (e.g. IBER) (Schneider et al., 2014).
Coupling of different processes is, of course, easier for processes exhibiting similar physical behaviours, such as water-related processes. Nevertheless, attempts to couple simulations of more different physics are attempted. Pastor et al. (2009) present innovative approaches to coupling complex numerical simulations of landslides impacting a reservoir and the thereby generated impulse wave in 3D. Other approaches of directly coupling simulations of granular flows (Domnik et al., 2013) with impact wave models are in development (Pudasaini et al., 2014), but not yet implemented into a software, which could eventually be applied by hazard-assessment experts. Therefore other approaches have to be found for current hazard assessment of the entire process chain of an outburst flow triggered by an landslide-induced impact wave.

Coupling of models for hazard assessment
The data required for hazard-map generation (the runout distance, the spatial distribution and the intensity of the outburst flow (Hürlimann et al., 2008)) can only be generated by physically-based (pseudo)3D-simulations (Westoby et al., 2014; Woodhead et al., 2007). The outburst flow has therefore to be estimated as physically based. The choice between an overland-flow or an equivalent-fluid simulation, however, has to be made with regard to the expected rheological behaviour of the flow. In most cases, a model is preferable, which allows flexible treatment of flow rheology, as the flow behaviour is likely to change along the flow path due to entrainment and/or deposition.
The dam breach model has to be chosen with regard to the assessment purpose (Wahl, 2004). If early warning is desired, then the newest generation of physically based simulations has to be applied to get the initiation time. If only an outburst hydrograph for downstream routing of the flow is required, e.g. in combination with an equivalent fluid simulation, breaching time and peak outflows can also be gained by simpler semi-physical simulations, which assume instant breach (Zhu et al., 2004). For a realistic reproduction of the breaching process, lateral erosion and head cutting should be physically represented also, because softwares implementing empirical breach parameters (e.g. DAMBRK) tend to overestimate peak breach flow (Chauhan et al., 2004). All these dam-breach models would, nevertheless, deliver the input hydrograph that is required for equivalent flow simulations of the outburst flow.
For impact generation, things get more difficult. The impact is so complicated, that either empirical equations derived from experiments only are implemented into GIS-based softwares, or a correct simulation of the impact is only possible via physically-based simulation softwares. Empirical equations and the respective GIS-based implementations are a feasible approach for first-order assessments on whether overtopping has to be expected or not. The necessary input parameters can be generated by any numerical mass-movement simulation. They are, however, not suitable as an integral part of the assessment chain, as the most important results for dam-breach and outflow modelling, the overtopping discharge and time, only refer to an idealized dam without freeboard. Current numerical impact-wave simulations are based on three assumptions: (1) the surface wave and landslide satisfy the SW approximation. (2) In case of rigid-body landslides, the material moves as a non-deformable body with specified bottom fric-

tion. For viscous landslides, the moving mass is treated as an incompressible, isotropic laminar fluid that rapidly reaches a steady state. (3) Seawater is treated as an incompressible inviscid fluid (Bornhold and Thomson, 2012). These assumptions, especially those regarding the impacting slide, are strongly simplified and do not meet the motion description of a real avalanche; they therefore cannot replace a more process-specific simulation of a rapid mass movement. An approximation of the impact could be achieved by deriving avalanche velocities, impact location and width from an equivalent fluid simulation, which would act as a basis of definition of the moving mass module in impact-wave models. For preliminary analyses, approximation of the avalanche velocities by means of analytical models are also feasible.
Experimental analyses indicate (Panizzo et al., 2005b), however, that reasonable runup estimates can also be achieved without representing the splash- and near-field zones of an impact wave. This consideration contains the principle of continuum conservation during the impact, which justifies a direct integration of the avalanche hydrograph at the moment of impact into an inflow hydrograph of physically-based overland- or dam-breach simulation software, applying a mass- or momentum-correction. Again, physically-based simulations of only the landslide deliver this information. Non-physically based or analytical solutions can, nevertheless, be applied as first-order assessments of whether an impact is feasible or not.

To sum up, a wide range of assessment techniques are available, which are more or less developed, depending on the process concerned. As hazard assessment of the process chain with physically based, fully-coupled simulations is not yet possible, other combinations have to be applied. The most appropriate combination of models or simulations has to be chosen with regard to the respective situation. Generally speaking, the more parameters a model features, the more process-specific are the physics, but the more difficult the calibration (Singh, 1996). The fewer parameters a model features, the more general is its outcome and the easier its application. Regardless of any model constraints, the most appropriate model combination also depends on the respective topographic situation, data-availability, scale of the study area, computational power available, and purpose of the study (e.g. first-order assessment vs. detailed hazard analysis).

10.4 Discussion

This chapter contains an overview on methods suitable for effect analysis of rapid mass movements triggering impact waves and the thereby-caused lake-outburst flow. The research question treated was, "How can the process chain of a lake-outburst flow due to an impact wave triggered by a rapid mass movement be analysed for the purpose of a risk analysis?".
An extensive answer was formulated in the final part of the previous section with regard to empirical, analytical and physically-based assessment methods. This reprocessing showed that the process understanding and representation is unequally advanced for the different processes. Advantages are produced, however, also for the critical motions such as the momentum transfer during impact wave generation as well as moraine-dam failure. The need for coupled analysis of the system instead of only single processes has been widely recognized by modellers as

well as by hazard specialists. At present, strong efforts are being made in this direction, mostly within the communities of impact wave modellers and outburst flow modellers. This is possible because in CFD, all models are based on the same physical principles. The terminologies currently applied (e.g. according to geophysical processes) are, to a certain point, arbitrary. Often the additional modules only define the gemorphological field of application of the simulation software.

There is broad potential in numerical modelling and advances in physical understanding of the interface between processes as well as in relatively new approaches, such as SPH, which are promising to one day be suitable for integrating all processes included in the process chain into numerical modelling. At present, this is not yet the case.

Despite this ongoing development, approaches for assessing the effect of a landslide impacting a reservoir based on currently available and easy-to-calibrate models have to be found. Feasible combinations have been presented in the previous section. The assessment of a process chain by means of a model chain inevitably comprises assumptions and manual adjustments at the cutting points. In the following, a coupling of two softwares for simulating landslide and the thereby triggered impact wave propagation and runup will be presented and tested regarding propagation of uncertainties with the help of the case study of the 2010 outburst event of Lake 513, Peru.

CHAPTER 11

2010 OUTBURST EVENT OF LAKE 513: CASE-STUDY AND EVENT DESCRIPTIONS

First steps towards full representation of lake-outburst flows triggered by rock/ice avalanche-induced impact waves were carried out in the Cordillera Blanca for the Lake 513 (Schneider et al., 2014) and for the Lake Palcacocha (Somos-Valenzuela et al., 2013; Chisolm et al., 2013). The example of Lake 513 was chosen as a cause study, because a good documentation of the outburst event is available, which is required to back-calibrate the numerical simulations. No equally well reported event has recently happened in the European Alps. Further reasons for the choice of this example were the synergies to larger projects in Peru of our institution, which provided data, support and a platform to exchange knowledge and experiences with Peruvian and other international colleagues.
The outburst event of Lake 513 serves as a case study for the following chapters and will therefore be introduced in detail in this chapter. In a first section, a general description of the setting and the hazard situation is given, followed by a detailed description of the 2010 outburst event. The second section outlines the composition of the numerical reproduction of this event, which formed the basis of the uncertainty-propagation analysis presented in the next chapter.

11.1 Case study

Lake 513 is a high-mountain lake in the Cordillera Blanca, a mountain range in the centre of Peru, north of the capital Lima. A well-arranged and comprehensive description of the area, as well as an integral compilation of the socioenvironmental factors forming the history of hazard and management evolution at Lake 513 is given in Carey et al. (2012) and has recently also been resumed by other authors (e.g. Klimeš et al., 2014; Schneider et al., 2014). Therefore only a compact description of the case study site with regard to the 2010 outburst event will be given here.

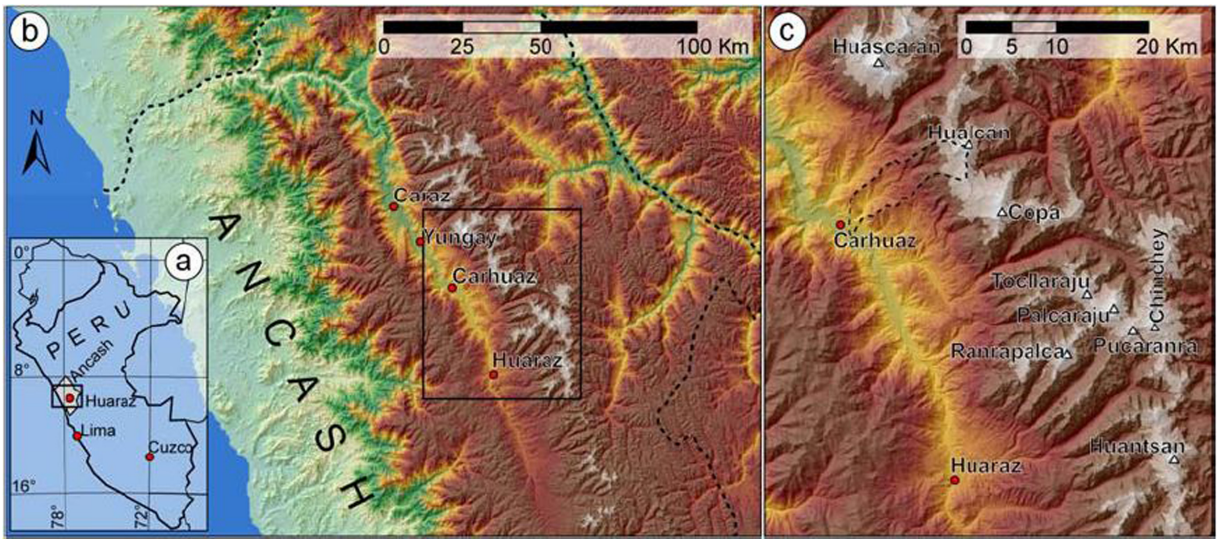

Figure 11.1: Location of Lake 513. (a) Location of province of Ancash (gray) in Peru. (b) Overview of the Cordillera Blanca (gray) within Ancash (dashed line). (c) Detail of the Cordillera Blanca with the cities of Huaraz and Carhuaz and the Chucchun river catchment as the main study site (dashed line). Gray areas indicate the glaciers in the year 2003 and the triangles show peaks >6,000 m a.s.l. and the corresponding names. Rectangles correspond to the extents of the sub-images and background image is a colored hillshade relief derived from ASTER GDEM2 data. Figure and caption from Schneider et al. (2014).

Lake 513 is located above the city of Carhuaz (14,000 inhabitants) at the foot of Glacier 513 on Mount Hualcán at 9°12'50"N and 77°33'10"W. This lake formed in the early 1980s and was first reported by the Unidad de Glaciología (Reynolds et al., 1998). As floods from Mount Hualcán had been reported from early days (Lliboutry et al., 1977), the situation had already been under observation; a detailed description on hazard recognitions at that mountain can be found in Carey et al. (2012). To summarize, the south face of Mount Hualcán is glaciated beginning at an altitude of 4,600 m a.s.l. Over large parts, this face features a steep topography, and a cliff located at 5,450 m a.s.l. runs across the entire face. These locations are potential detachment zones, where continuous ice- and snow-avalanche activity can be observed. The lake was therefore considered extremely dangerous, and water was pumped out in 1988 to prevent immediate damage. After the refilling of the lake in the subsequent rain season, a syphoning system was installed, to maintain a low lake level. This installation allowed for the lowering of the lake level by about 5 m, which prevented major damage; but ice pieces slipped into the lake in 1991, which caused a small but alarming outburst flow. Thereafter the water table was lowered to a permanent level at 4,428 m a.s.l., also leaving a freeboard of 19 m, by means of drainage tunnels through the bedrock dam, which were constructed in 1993/94 (Portocarrero, 2013b; Reynolds et al., 1998). Since then, the situation was assumed adequately safe by residents, authorities and engineers (Carey et al., 2012); therefore recommendations requiring complete protection of the inhabitants of Carhuaz by means of hazard zones (INAGGA, 1997) were not implemented (Carey et al., 2012).

11.1.1 Reports from the 2010 outburst event

On 11 April 2010 around 08.00, a combined rock/ice avalanche detached from the southwestern slope of Mount Hualcán at about 5,400 m a.s.l. and impacted Lake 513. Avalanche volume estimates differ considerable. Carey et al. (2012) estimated a volume between 200,000 m^3 and 400,000 m^3, while Valderrama and Vilca (2012) suggested higher volumes of about 1,500,000 m^3 and even suggested the impact of a second (smaller) avalanche a few hours later. For the purpose of this study, the following description and modelling will concentrate only on the first event description, to reduce complexity.
Field evidence showed that the impact wave overtopped the bedrock dam by 5 m at a width of 20-25 m and thereby triggered an outburst flow that reached 13 km, all the way to Río Santa in the valley bottom. Schneider et al. (2014) divided the process chain of the outburst flow caused by a rock/ice avalanche-triggered impact wave into five parts:

- Combined rock/ice avalanche flowing from Mount Hualcán into Lake 513
- Impact wave triggered by the rock/ice avalanche, which overtopped the dam
- Formation of a debris flow by lateral erosion and sediment entrainment, with subsequent deposition in the fan above Pampa Shonquil
- Continuation of the flow over the Pampa Shonquil as a hyperconcentrated flow
- Initiation of a secondary debris flow below Pampa Shonquil due to increase in flow-channel gradient, flow velocity and erodibility of the material

Three out of these five parts of the process chain refer to the outburst flow, which indicates the complex nature of the process. For better understanding of the flow behaviour, the traces were mapped.

11.1.2 Mapping of the outburst flow traces

Method
The flow traces were assessed by means of field observations in October 2010 and based on a DigitalGlobe-image, which was created shortly after the event in June 2010. The observations were recorded on an 8-m DEM derived from WorldView satellite-images generated in spring of 2012. The flow traces were mapped according to the manual "Symbolbaukasten zur Kartierung der Phänomene" (BUWAL and BWG, 1995). In doing so, five processes were recognized and considered for mapping. Differentiation was made among downwards erosion (degradation), lateral erosion, generation of zones for relocation of material, inundation and deposition.

Results
The flow traces are shown in Figure 11.2. After overtopping the rock dam, the flow eroded deeply to immediately deposit the material on the flat Pampa Shonquil, which was then mainly inundated and where some lateral erosion took place. After the water intake at the outflow of the Pampa, stronger erosion took place again in the steeper and narrower parts of the channel,

alternating also with the formation of relocation zones in flatter parts of the stream bed. In the last kilometres, inundation and deposition together with lateral erosion were the predominant processes. The key characteristics of this mapping are mostly in line with the detailed analysis of 120 cross-sections by Klimeš et al. (2014), carried out chronologically closer to the event. This knowledge was the basis for numerical reproduction of the event by Schneider et al. (2014), which is summarized in the next section.

11.2 Numerical reproduction of the 2010 outburst event

Schneider et al. (2014) reproduced this event with the help of two physically-based numerical simulation softwares. The rock/ice avalanche and the outburst flow were represented with RAMMS, a simulation tool which is based on the principle of equivalent fluid (Section 10.3.3.2). The impact wave was simulated with the help of IBER, a basic hydrodynamic simulation software applicable to overland flows. This software will be introduced in more detail in the following paragraphs.

11.2.1 Description of applied software

Description of RAMMS

RAMMS is a single phase, equivalent fluid simulation software for rapid mass movement systems (see Table 10.9). With information on the DEM, on the release area and the model friction parameters, it computes time-dependent flow height, velocity, kinetic energy, momentum, frictional work rate, flow pressure, final deposition heights and maximum values of mass movements. RAMMS considers the mass and momentum conservation principle and assumes the flows to exhibit a shallow geometry. The motion is considered unsteady and non-uniform with varying height and velocity, the depth velocity profile, however, is uniform. The numerical scheme applied in RAMMS to solve the corresponding second-order depth-integrated equations of the flow motion in a 2D-Cartesian coordinate system was described by Savage and Hutter (1989). It is extended by a Coulomb friction law according to the Voellmy-Salm (VS) model (Salm, 1993), a random kinetic energy model and an entrainment module.

In the following, only a comprehensive summary of the principles and of the applied composition of RAMMS is given, which refers to Christen et al. (2010a), if not indicated otherwise. Further reading, however, is available. The governing equations were amongst others described by Schneider et al. (2010) and discussed by Kowalski (2008). The description of their implementation and their application to case studies was given by Christen et al. (2010a,b). Discussions on the schemes and the modules included in RAMMS can be found in several publications. Hutter et al. (2005) discussed the limits and possibilities of the Savage-Hutter model. Bartelt et al. (1999) reflected on the VS model, while Naef et al. (2006) more generally compared several resistance relations. The importance of entrainment was discussed with the example of snow avalanches by Sovilla et al. (2006, 2007).

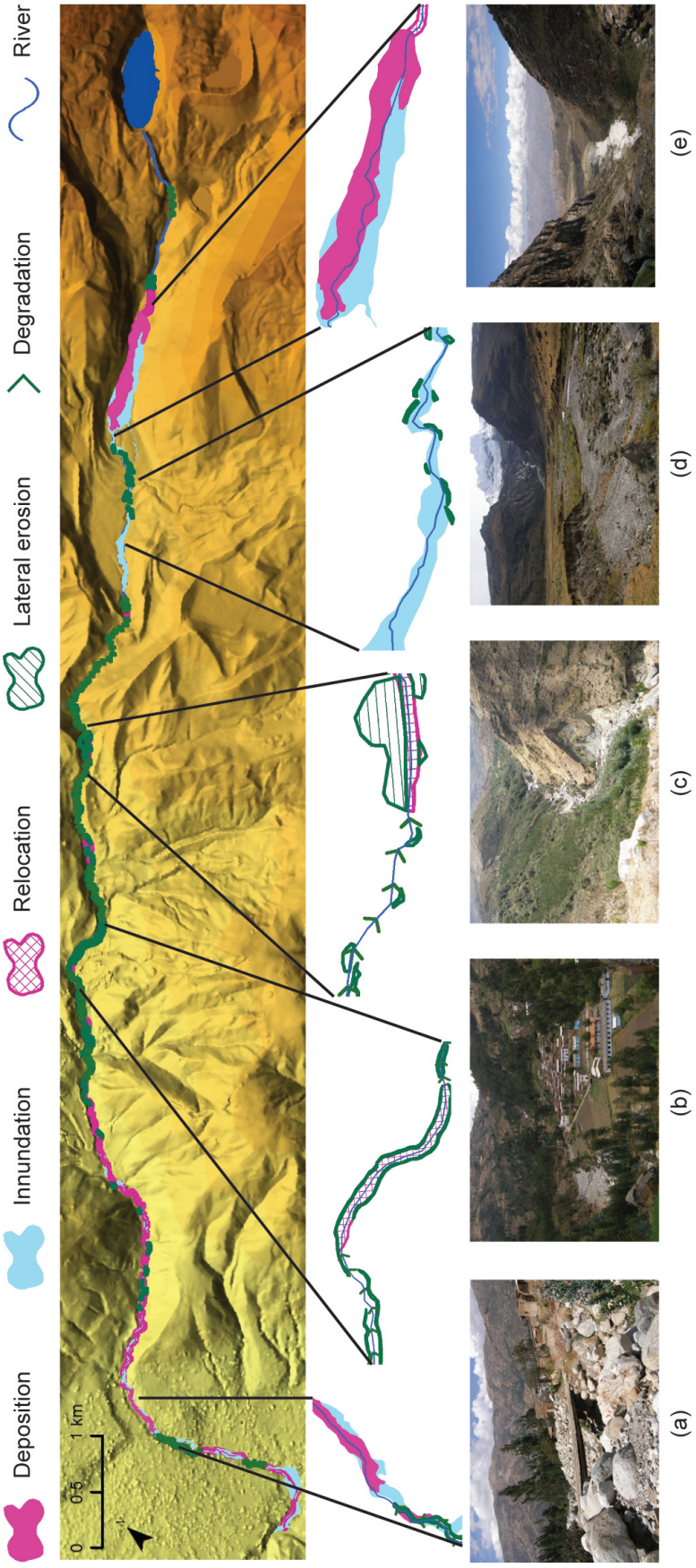

Figure 11.2: Traces of the 2010 outburst flow in the Río Chucchún. (a) Bridge at the entrance of Carhuaz, which was destroyed, (b) Pariacaca, (c) erosion below Pampa Sonquil, (d) view over Pampa Shonquil towards Mount Hualcán from the water intake, (e) Pampa Shonquil as seen from near Lake 513

The basic setup of RAMMS consists of the VS friction model, which was already implemented in the code AVAL-1D serving for avalanche runout estimations according to the corresponding Swiss guidelines (Salm, 1993). Acceleration of the flow is, as a basic principle, a function of the gravity and the flow height, which is, however, slowed down by friction. The VS model consists of only two calibration parameters, which relate the mean flow velocity and the flow height to the shear stress at the flow's base (Preuth et al., 2010). The velocity-independent dry Coulomb term μ had been initially stated by Voellmy (1955). It consists of the ratio of the shear stress and the basal normal stress (Bartelt et al., 2007) and is therefore proportional to the normal stress at the bottom. μ is multiplied in the model with gravity and flow height, and it is thereby connected to the mass's properties and defines the runout distance. The second friction term is the velocity-dependent ξ, which represents the viscous and turbulent friction and also depends on terrain geometry and the gravity. The VS model can simulate the maximal velocity and flow height at the head of an avalanche and therefore the runout. However, it works poorly with deposition and entrainment, which define the flow's width and size, as it cannot model the evolution of the flow body.
RAMMS therefore offers the option of implementing the additional model of random kinetic energy (RKE) into the VS model, which tracks the evolution of the velocity within an avalanche and hence permits a more realistic modelling of entrainment and deposition. This energy equation describes how the random fluctuations of individual grains, which possibly reduce the shear resistance, are created from the mean flow, and how the fluctuations decay in time, as they are a function of the frictional work rate. The kinetic energy model was not applied in the present study; therefore it will not be presented in more detail. General evaluations of the random kinetic energy model can, however, be found in Bartelt et al. (2007, 2012) and in Preuth et al. (2010) for rock-avalanches especially.
In RAMMS, entrainment is implemented as a rate-controlled, history-dependent approach, which regulates the uptake and the time delay necessary for accelerating the mass to the flow velocity. This effective entrainment rate is parametrized by a dimensionless entrainment coefficient that defines the volumetric entrainment rate per unit avalanche velocity. The entrainment rate is identical to the mean flow velocity when the dimensionless coefficient equals 1. Ploughing can be modelled with a coefficient around 0.8 and basal entrainment with smaller values (Bartelt et al., 2012; Christen et al., 2010b). The entrainment rate further is scaled with the density ratio of the eroded layer and the eroding flow. Sovilla et al. (2006, 2007) stated that an increase in the flow mass leads to greater runout disctances and flow heights, but not necessarily higher velocities. In the first part, during entrainment, the velocity of the avalanche is lower, but it is higher in the second part due to higher depth. Entrainment consideration is further crucial, as flows that entrain more mass along the track exhibit higher kinetic energies than avalanches starting with the same mass in the release zone (Sovilla et al., 2007).

Description of IBER

IBER is a hydrodynamic model for simulating turbulent-free surface unsteady flow and environmental processes in river hydraulics (see Table 10.8). The range of applications of IBER covers river hydrodynamics, dam-break simulation, flood-zone evaluation, sediment-transport calculation, and wave flow in estuaries. The latest version of IBER consists of three main computational

modules: a hydrodynamic module, a turbulence module and a sediment transport module. All of them work over a non-structured finite volume mesh made up of triangular and/or quadrilateral elements. In the hydrodynamic module, the depth-averaged 2D SW-equations are solved by an explicit upwind first-order scheme, which performs well with irregular geometries such as high-mountain topography (IBER, 2010a,b).
The hydrodynamic module contains the basic 2D SW-equations and principles of mass and momentum conservation. These standard equations can be extended, including further components: roughness, hydrological processes (rainfall, losses) and wind. For the present study, most of these features were considered negligible, as they account for river rather than lake systems. Roughness only was included. The roughness is characterized by bed friction, which has a double effect on the flow equations. On one side it produces a friction force that opposes the mean velocity, and on the other side, it produces turbulence. The turbulence production was neglected here. The bed stress, released by the opposing velocities, depends on a friction coefficient, which can be evaluated with the help of the Manning formula explained in Table 10.6.
The turbulence module accounts for small-scale fluctuations, which can numerically not be disintegrated in space and time (closer explained in Table 10.5). The sediment transport module solves the non-cohesive sediment non-stationary transport equations. The equations include the bed load transport equations and the suspended sediment transport equations, coupling the bed load and the suspended load through a sedimentation-rise term. The sediment transport module uses the velocity, depth and turbulence fields from the hydrodynamic and turbulence modules. The bed load is calculated using an empirical formula chosen from the Meyer-Peter&Muller or the Van Rijn Methods (explained in Table 10.7). The suspended load transport is modelled from a depth-averaged turbulent transport equation. Neither of these two modules were considered important in the present study and will therefore not being introduced any further.

These two models had been applied by Schneider et al. (2014) to generate hazard maps for the town of Carhuaz based on back-calibration of the models by means of the 2010 event.

11.2.2 Composition of the simulations

The simulations by Schneider et al. (2014) were run on the basis of the 8-m DEM derived from 2012 WorldView satellite images, and bathymetric data was derived from field campaigns in July 2007 and June 2011 (Cochachin, 2011). Schneider et al. (2014) ran three scenarios considering different initial volumes. Here is presented a scenario to which they allocated a return period of 30 years.
This retrospective setup considered the calibration best fitting to the 2010 event, as it allowed for generation of the assumed 5-m height of the overtopping wave on the dam crest. The initial rock/ice avalanche was simulated with RAMMS, applying μ and ξ values of 0.12 and 1000 and accounting for basal entrainment along the flow path (depth of erodible layer = 0.1m, density of erodible layer =1,000 kg/m^3 and entrainment factor 0.09). The initial avalanche volume was assumed at 350,000 m^3, and the avalanche density was set to 1,000 kg/m^3. Schneider et al. (2014) then entered an inflow hydrograph into IBER that resembled the rock/ice avalanche flow and that produced an overtopping wave height of 5m. IBER was calibrated with a Manning's

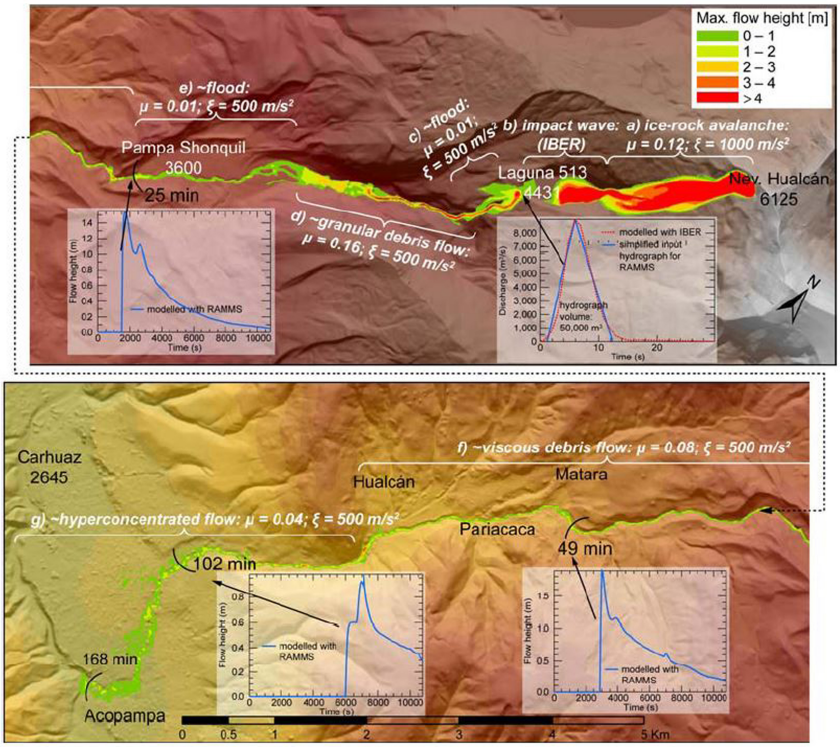

Figure 11.3: Process chain of the 11 April 2010 event, modelled as follows: (a) rock/ice avalanche using RAMMS; (b) impact wave using IBER; and (c) to (g) flood to debris flow using RAMMS. The process cascade was initiated with an estimated rock/ice avalanche volume of 450,000 m^3. Parameters μ and xi correspond to the applied dry Coulomb and "turbulent"/viscous friction coefficient of the Voellmy model, respectively (Christen et al., 2010b). Background: color-shaded relief of WorldView 8m-DEM. Figure and caption from Schneider et al. (2014).

n of 0.25. The overtopping hydrograph was, in the next step, entered as the input hydrograph into the RAMMS outburst-flow simulation. According to the flow behaviour described in the previous section, different friction parameter calibration was applied, as summarized in Figure 11.3. Basal entrainment was also considered in along the flow path, where recognized (compare with Figure 11.2). Further information on model setup is attached in Appendix B.

Synthesis

The 2010 event at Lake 513 is well documented, and served as one of the first case studies for physically-based numerical representation of the process chain of a lake-outburst flow triggered by a rock/ice avalanche-induced impact wave. The generated results served as a basis for risk management. Nevertheless, the need still remains to investigate the effect of assumptions taken in the simulation of the chain and the propagation of the corresponding uncertainties on the simulation results (Schneider et al., 2014). A corresponding assessment is presented in the next chapter.

CHAPTER 12

UNCERTAINTY PROPAGATION IN COUPLED IMPACT-WAVE SIMULATIONS

Schneider et al. (2014) prove the simulation chain to derive feasible results for hazard mapping. However, they also point out the need for systematic analysis of uncertainty propagation and its influence on hazard parameters. This gap will be addressed in the present chapter, which tackles the research question 5, "How do uncertainties propagate in the numerical simulation of the process chain of a lake-outburst flow due to an impact wave triggered by a rapid mass movement?" with the help of the 2010 event at Lake 513 presented in the previous chapter.

12.1 Coupling avalanche and impact-wave simulations

For the purpose of the uncertainty-propagation analysis, the focus will be put on the coupling of the rock/ice avalanche with the impact-wave simulation, as the overtopping height is the only feature of the 2010 event known reliably at the lake. As previously mentioned, the event of the lake outburst through overtopping is a function of the impulse introduced by the impacting rock/ice avalanche. As in the present case, the dam breach process is not of importance, the uncertainties in the outburst flow simulation are rather due to missing process understanding or knowledge. In exchange for this reduction, the process of transforming the RAMMS-results into the IBER input-hydrograph will be elaborated further. The transformation of the RAMMS-output (flow height and flow velocities on the shoreline of the lake) into an inflow-hydrograph for IBER is assumed to be a considerable source of uncertainties. Even though the digital information on the flow characteristics would be available at any point on any time point, RAMMS is not laid out to generate an output defining the topo-evolution along a line profile, which could represent the impact at the lake shoreline. Therefore the RAMMS results had to be transmitted manually into the impact hydrograph required by IBER.
The flow height and velocity of the rock/ice avalanche along the lake shoreline were hence read out per time step and multiplied by the impacting avalanche width to get the inflow discharge

over the impact time in m^3/s. Two transformation methods were established and tested: (i - *mean*) flow height and velocity values were considered at the location of mean values along the shoreline and multiplied by the entire avalanche width or (ii - *max*). Flow height and velocity values were considered at the location of maximum values along the shoreline and multiplied by a proportion of the avalanche width. In this procedure it must be considered that IBER simulates water flows only, while RAMMS can simulate flows of different densities, which has implications on the impulse which is transferred during impact. Schneider et al. (2014) aspired correct momentum transfer by assimilating the rock/ice-avalanche density to the one of water and, in exchange, augmenting the initial avalanche volume to 450,000 m^3 (Fig. 11.3), which accounts for the differences in density between the two flows.
In the following, the uncertainty analysis will be explained further.

12.2 Procedure of the uncertainty-propagation analysis

The uncertainty propagation was analysed based on this scenario as implemented, by evaluating the sensitivity of the overtopping wave against scenario and model parameter definition. This was done with the help of an analysis of variance (ANOVA). In the following paragraphs, the mode of operations of an ANOVA will be explained; then the procedure of application to the simulation chain is illustrated.

12.2.1 Background on analyses of variance

ANOVA is a statistical method for measuring the influence of independent input factors on dependent response variables by calculating the absolute amount of variance caused by the independent factors and by comparing the means of two or more groups of samples. Depending on the number of independent factors and dependent variables, several setups are possible (Kabacoff, 2011; Mickey et al., 2004).
In the simplest case, a one-way between-groups ANOVA, the influence of the groups of one factor on the one response variable is assessed. If two or more independent factors and their interactions with the dependent variables are considered, the setup is called a multiple-way ANOVA. If two or more factors are crossed, then it is a factorial ANOVA.
The ANOVA generates three sample variances: (a) the observed total variance, which is based on the variances of all measured values from the total mean value; (b) the treatment variance, which defines the proportion of the total variance which is composed by the factor only; and (c) the error variance, which consists of the discrepancy between the total and the treatment variances. The ANOVA tests whether the variance of one dependent variable between the groups of one independent factor is bigger than the variance within these groups. For this purpose, the ratio between the mean square of the treatment variance and the mean square of the error variance is calculated, based on which the significance of the result is derived by means of the test statistics F. The null hypothesis is that there is no difference in the dependent variable between

the groups. If the result is significant at a certain significance level α, the null hypothesis can be rejected. Rejection of the null hypothesis means that the deviations are not within natural fluctuations and that the means of the groups differ significantly from each other. Distinction is made between main effects and interactions. Main effects identify the effects of a single factor on the dependent variable. In other words, the main effect indicates the variations in the dependent variable, which is caused by the groups of the independent factor. Interactions, on the other hand, disclose where a variation of the dependent variable is caused by interplay of different independent factors rather than only by alteration of an individual independent factor. A post-hoc test then allows for allocation of the variations for significant main effects. It carries out a pairwise comparison of the groups' means in the dependent variables per independent factor, to detect the (significant) differences.

If the analysis features more than one response variable, the setup can be changed into a multivariate analysis of variance (MANOVA) for the purpose of simultaneously testing more than one dependent outcome. MANOVAs and ANOVAs differ mainly in two points. Firstly, a MANOVA is able to take into account multiple independent and multiple dependent variables within the same model, permitting greater complexity and more powerful statistical tests, while ANOVA ignores the inter-correlations between the independent factors. Secondly, MANOVA applies a number of multivariate measures (Wilks' lambda, Pillai's trace, Hotelling's trace and Roy's largest root) to test the null hypothesis, rather than using the F-value as the indicator of significance. The MANOVA null hypothesis assumes that the mean on the composite variable is the same across groups. The four multivariate measures differ in how they combine the dependent variables in order to examine the amount of variance in the data. Pillai's trace test is considered the most reliable of the multivariate measures and offers the greatest protection against the incorrect rejection of a true null hypothesis. It is the sum of the variance, which can be explained by the calculation of discriminant variables. It calculates the amount of variance in the dependent variable that is accounted for by the greatest separation of the independent variables.

The analysis of variance in the overtopping wave generated by the simulation of the rock/ice avalanche-induced impact wave will be explained in the following.

12.2.2 Analysing the variance in the overtopping waves against uncertainties in the simulation

Composition of the analysis of variance

To fit the simulation into the frame of an ANOVA, terminologies must first be defined. The terms of independent factors and dependent variables are assigned in Figure 12.1. Independent factors refer to the possible sources of uncertainties considered in the present study, which were introduced during initial volume assumption, calibration or coupling of the simulations. These are (1) assumptions on the initial rock/ice avalanche volume, (2) calibration of the friction parameters μ and ξ in RAMMS and (3) assumptions about entrainment considered in RAMMS. Further, the (4) transformation of the RAMMS-output (flow height and flow velocities on the shoreline of the lake) into an inflow-hydrograph for IBER by means of the above-described

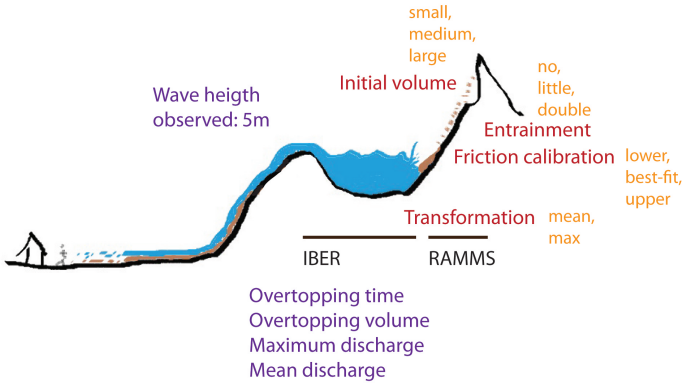

Figure 12.1: Independent factors (red) with groups (orange) and dependent variables (purple) of the simulation of the rock/ice avalanche-triggered impact wave in Lake 513 with the help of the software RAMMS and IBER.

methods (i - *mean*, ii - *max*) was also considered a possible source of uncertainties.
These parameters were tested regarding their influence on overtopping parameters that are crucial for outburst-flow modelling, which were named dependent variables in the present study. These were overtopping time, volume, and wave height as much as mean and maximum discharge.

The initial model adjustments were adapted from the 30-year scenario for Lake 513 from Schneider et al. (2014), as described in the previous chapter. This retrospective simulation composition was considered the calibration best fitted to the 2010 event, as it permitted generation of the assumed 5m height of the overtopping wave on the dam crest. Schneider et al. (2014) considered an initial rock/ice-avalanche volume of 350,000 m^3 and applied moderate friction and entrainment assumptions. Emanating from these assumptions, possible upper and lower values were established based on further literature and personal expertise (Table 12.1). These ranges accounted for the uncertainties in calibration/establishment of the independent factors. To gain the data basis for evaluation, 54 simulations were run, applying all possible adjustment combinations from Table 12.1 once. The effect of the independent factors on the dependent variables was then defined by means of an analysis of the variance based on the 54 simulations.

Analysis of the variance in the overtopping waves characteristics
The present study featured four independent factors and five dependent variables. In statistical terms, this composition is called a four-way, between-groups, factorial MANOVA. The evaluation procedure will be explained in more detail in the following paragraphs.

In a first step, a MANOVA was carried out, testing the significance of the variations caused in all dependent variables (Fig. 12.1) by the main effects and the first-order interactions between the independent factors. First-order interactions indicate the interplay between two factors at the same time. A full MANOVA, which would have considered all possible interactions between all independent factors (up to third-order interactions in this case), was abstained from. The corresponding results would have been practically impossible to interpret. The importance of the main effects and the interactions was tested with the help of the Pillai's trace test.
In a second step, the univariate results of the independent factors were tested with the help of multiple ANOVAs for each dependent variable. The importance of the variances of the groups'

Independent factors Groups	Values			**Source and notes**	**Abbr.**
Initial Volume of the rock/ice avalanche					*Vol*
lower	200,000 m^3			lowest feasible value (after Carey et al. (2012))	small
2010-event	350,000 m^3			most feasible value (after Carey et al. (2012))	medium
upper	500,000 m^3			highest feasible value (after Carey et al. (2012))	large
Calibration of friction parameters in RAMMS					*Cal*
		μ	ξ		
lower		0.26	1000	μ for snow/ice avalanches (Margreth et al., 2011)	lower
2010-event		0.12	1000	best-fit (Schneider et al., 2014)	best-fit
upper		0.03	3000	for rock/ice avalanches (ξ (Stricker, 2010), μ (Sosio et al., 2012))	upper
Entrainment along the rock/ice avalanche flow path					*Er*
	D	Rho	k		
lower	0	0	0	no erosion assumed	no
2010-event	0.1	1000	0.09	best-fit (Schneider et al. 2014)	little
upper	0.2	1000	0.18	double erosion assumed	double
Transformation of the rock/ice avalanche characteristics into impact hydrograph					*Trans*
mean				expert assessment	mean
max				expert assessment	max

Table 12.1: Grouping of the independent factors for the analysis of variance in the dependent variable. μ = coulomb-friction, ξ = viscous friction, D = erodible layer depth, Rho = density of erodible layer, k = entrainment factor. The abbreviations (Abbr.) will be applied to the results of the ANOVA.

means were tested by means of the Wilcoxon-test. For the important main effects, a pairwise comparison of the groups' means by a TukeyHSD post-hoc test helped to locate the variations. This procedure would also have been possible for the interactions; the results, however, would have been hardly interpretable. Therefore the significant interactions were detected by means of visual interpretation of the interaction plots in Appendix E.

Evaluation of the results

This analysis was carried out for two data sets. One contained all model runs, while the second data set incorporated the results of the simulations only, which resulted in an overtopping wave. The sum of the squares of the treatment variance was applied as an indicator of the absolute variance introduced by each independent factor on each dependent variable. Thereby the study distinguished between main effects and interactions. Furthermore, the statistical tests (Pillai's, Wilcoxon and TukeyHSD) allow for derivation of the significance of the variances in the dependent factors groups' means. The number of data underlying the present analyses is, however, too small to generate enough statistical power. The significance levels were therewith applied to qualitative description of the variances between the groups' means. The importance levels applied were "strong" ($p<0.001$; ***), "considerable" ($p<0.01$; **) and "noticeable" ($p<0.05$; *), indicating whether the results of the different groups ranged within natural fluctuation or whether their influence was important.

12.3 Results regarding the influence of uncertainties on the overtopping wave

The presentation of the results is divided into three parts. Firstly, the outcomes of the simulations are presented without further quantitative evaluation (Section 12.3.1). Secondly, the raw results of the quantitative (M)ANOVA in the dependent variables are presented for each individual variable (overtopping time, volume, maximum discharge, mean discharge and overtopping height) (Section 12.3.2). Thirdly, these outcomes are summarized per independent factor (inital volume, calibration, entrainment and transformation), with regard to their influence on the dependent variables (Section 12.3.3). These findings are put into context with the model physics and the impact-wave theory (Section 12.3.4).

12.3.1 Qualitative description of the simulation results

The results of the RAMMS-avalanche and the IBER-impact wave simulation are summarized in this section based on Figure 12.2 and Table 12.2.

RAMMS-Output

The rock/ice avalanche was modelled to reach the lake after 41 s on average. The fastest and the slowest movements lasted 25 s and 60 s, respectively. 40 out of the 54 rock/ice avalanches were modelled to impact the lake on a width between 100 m and 160 m. Only fourteen rock/ice avalanches were assumed to be between 200 m and 350 m wide. The impact time lasted 60 s on average, but ranged, however, from 25 s to 90 s. The median volume impacting the lakes was modelled at 459,169 m^3, ranging from 115,424 m^3 to 906,152 m^3. Two outliers reached up to 1,053,833 m^3 and 1,198,166 m^3.

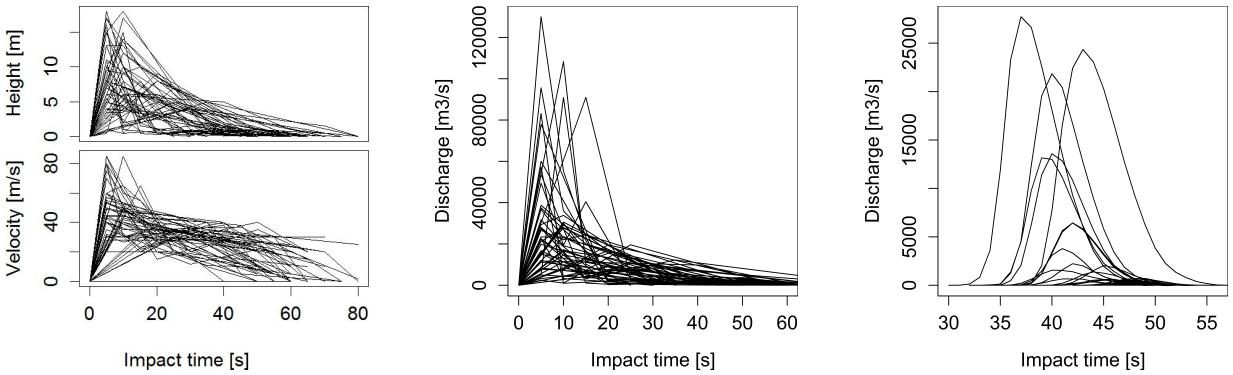

(a) RAMMS output (b) Impact hydrographs (IBER input) (c) Overtopping hydrographs (IBER Output)

Figure 12.2: Results of th 54 simulation runs. The (a) RAMMS avalanche-simulation results on the lake shoreline were converted into the (b) impacting hydrographs (the transformation methods are described in Section 12.1), which leaded to overtopping simulations by IBER (c). The attribution of the curves to the groups of the independent factors is illustrated in Appendix C.

Three flow regimes could be distinguished, indicating different impact histories. Type 1 featured short impact times (30 s to 40 s) with high flow peaks after 10 s to 15 s. These peaks featured velocities of up to 80 m/s, whereas the flow heights reached up to 17 m. Type 2 reached the highest flow characteristics somewhere in the middle (approximately after 20 s) of the rather long-lasting impact of approximately 60 s. Type-2 rock/ice avalanches featured velocities around 40 m/s and flow heights between 3 m and 10 m. The impact of type-3 rock/ice avalanches was characterized by two peaks or a constant flow value in the impact period of about 20 s to 40 s. This impact type was characterized by velocity peaks between 20 m/s and 40 m/s and flow heights around 5 m.

A first qualitative analysis of the influence of the input parameters on flow characteristics did not allow for identifying many patterns. Nevertheless, it can be observed that velocity peaks higher than 55 m/s were only caused by runs with calibration *upper*. While calibration *lower* reached maximum velocities of 45 m/s only, calibration *best-fit* was able to cause slightly higher velocities up to 55 m/s. Furthermore, the time plots suggest that the higher calibration (*upper*) tends to lead to shorter impact times than the other calibrations. For the other input parameters, no clear pattern can be distinguished. The flow characteristics picked according to the two transformation methods can be distinguished as follows: the mean velocity and height values assumed over the entire flow were not assumed to be higher than 60 m/s or 10 m, respectively. Higher values were only derived by picking the maximum values. The avalanche volumes rose with rising initial volume as well as with rising entrainment. No influence of calibration or transformation could be derived from qualitative analysis of the impact volumes.

IBER-Input

From these rock/ice avalanche results, the input hydrographs for IBER were constructed. The maximum discharge of the impacting rock/ice avalanche at the lake outline is, on average, 32,490 m^3/s, ranging from 5,000 m^3/s to 130,000 m^3/s. Qualitative analysis of the discharges shows an increase with rising initial volumes, calibration and entrainment. Moreover the transformation method *max* leads to slightly higher maximum discharges.

IBER-Output

Of the total 54 impacts generated, 26 waves were modelled to overtop the dam and 7 of these

Hydrograph Characteristics		**minimum**	**median**	**average**	**maximum**
Impact hydrographs					
Impact time	[s]	25	60	60	90
Avalanche volume	[m^3]	115,400	459,200	479,600	1,198,000
Max. Discharge	[m^3/s]	5,000	22,990	32,490	130,000
Overtopping hydrographs					
Overtoping time	[s]	5	13	13	21
Overtopping volume	[m^3]	63	3,527	29,946	171,368
Maximum discharge	[m^3/s]	19	682	4,997	27,731
Mean discharge	[m^3/s]	10	278	1,569	8,160
Overtopping height	[m]	0.2	3.1	3.7	9.2

Table 12.2: Statistics of the 54 impact hydrographs, which were applied as Input for IBER (upper part of the table) and of the 26 overtopping hydrographs, resulting from IBER simulations (lower part of the table).

26 impacts caused even a second overtopping wave roughly 100 s after the first one. In the following, only the first overtopping wave will be described. These overtoppings lasted between 5 to 21 s and caused outflows between 63 m^3 and 171,368 m^3. The mean and the median outflow volume, however, amounted to only 29,946 m^3 and 3,527 m^3. An analogous distribution was modelled for the maximum and the average discharges. Maximum discharge values ranged from 19 m^3/s to 27,731 m^3/s, with a mean of 4,997 m^3/s and the median at 682 m^3/s. The average discharge was modelled from 10 m^3/s to 8,160 m^3/s, with average and median values of 1,569 m^3/s and 278 m^3/s, respectively. The overtopping waves reached heights between 0.2 m and 9.2 m above the dam crest, mean and median both being around 3 m. In the following, the variance in the IBER results will be analysed.

12.3.2 Quantitative analysis of variance in dependent variables

In this section, the influence of the independent factors on the dependent variables that characterize the overtopping waves is presented. In a first step, the influence of the independent factors on the dependent overtopping wave's variables (Table 12.2), whose variance was quantified above, was tested by means of a MANOVA (Table 12.3). The null hypothesis tested by the Pillai's trace test was that for all dependent variables the means of the groups per factor do not differ from one another. This hypothesis had to be rejected for the main effects of all runs (and interactions between calibration with volume and transformation); it could, however, be accepted for the overtopping runs. Further information on the composition of the variances could hardly be gained from this result, as it is too complex. Therefore the variance in the dependent variables was examined in univariate analyses in the next step.
In a second step, the univariate results of the independent factors were tested with the help of multiple ANOVAs per dependent variable (overtopping time, volume, height, mean and maximal discharge). The range of results and the means were plotted in boxplots (e.g. Fig. 12.3a.) The sum of the square of the treatment variance was represented in barplots as an indicator of the absolute variance introduced by each independent factor on each dependent variable (e.g.

Main effects / Interactions	**All runs** Importance		**Overtopping runs** Importance
Main effects			
Volume	1.20E-03	**	0.487
Calibration	8.38E-04	***	0.608
Erosion	0.048	*	0.169
Transformation	1.66E-04	***	0.341
Interactions			
Vol:Er	0.671		0.232
Vol:Cal	0.013	*	0.479
Vol:Trans	0.174		0.459
Er:Trans	0.829		0.085
Cal:Trans	0.124		0.373
Cal:Er	0.568		

*Table 12.3: MANOVA results: Importance of the main effects and interactions of the independent factors on all dependent variables after the Pillai's trace test. The importance was classified in "strong" ($p<0.001$; ***), "considerable" ($p<0.01$; **) and "noticeable" ($p<0.05$; *). For abbreviations see Table 12.1.*

Figs. 12.3b and 12.3c). The corresponding importance analyses on the groups' means after the TukeyHSD test were summarized in tables (e.g. Table 12.3d), to distinguish between main effects (Vol, Cal, Er, Trans) and interactions (e.g Vol:Er, Vol:Cal,...). The main effects referred to the effect of a single factor (variance in dependent variable can be explained through differences in the means caused by the groups of independent factors). These effects (respective the differences between the groups' means) were either "noticeable" (*), "considerable"(**) or "strong"(***). If no main effect was noticeable, this meant that the variance introduced in the dependent variable ranged within the natural fluctuation.
These analyses were again carried out for all 54 runs as well as for the overtopping 26 runs. The results of the univariate analyses of variance are fully presented in Appendix D and the interactions are plotted in Appendix E. A summary of the results is presented in the following for each dependent variable.

Variance in overtopping time
27.2%, and hence the largest component of the total variance in all runs, and 32.5% of the variance in the overtopping runs - which constitutes its largest component - were caused by calibration only (Figs. 12.3b and 12.3c). These main effects were strong and noticeable, respectively. *Upper* resulted in the only calibration group, whose means differed strongly from both other groups' means (Table 12.3d). It was also the only group that caused overtopping times up to 21 s, while maximal values for both calibrations *lower* and *best-fit* reached up to only 14 s (see Fig. 12.3a).
The main effect introduced by the initial volume amounted to 24.6% and 20.6% of the variances of all and of the overtopping runs and therefore constituted the second largest components of both variances (Figs. 12.3b and 12.3c). In the case of all runs, the groups' means all differed strongly from one another, while in the case of the overtopping runs only the means of the groups *small* and *large* volumes differed noticeably (Table 12.3d). From Figure 12.3a, a continuous rise of the median overtopping times as a function of the initial volume can nevertheless be distinguished. Maximal values reached up to 14 s, 17 s and 21 s for the initial volumes *small*, *medium* and *lower*, respectively.
The input-variable entrainment answered with 7.4% and 8.3%, the fourth largest components of both the variances of all and of the overtopping runs (Figs. 12.3b and 12.3c). This main effect was considerable for all runs only where the means of *double* entrainment differed considerably and noticeably from *no* and *little* entrainment, respectively (Table 12.3d). It can also be observed in Figure 12.3a that the boxplots extend over comparable ranges of overtopping times per analysis.
The main effect of the transformation methods on the variance in all runs was strong and answered with 13.7%, the third largest component (Fig. 12.3b). In the variance of the overtopping runs, its influence of 2.2% was, contrary to expectations, amongst the smallest (Fig. 12.3c). The groups almost did not differ in the range of the overtopping times they caused. For *mean*, contrary to *max*, the four highest values were considered outliers (Fig. 12.3a).

Interactions between two of the four independent variables answered with 13.7% and 34.1% of the variance of the overtopping time in all and in the overtopping runs, respectively. 6.5% and hence the largest component of the variance in all runs was explained by interactions between

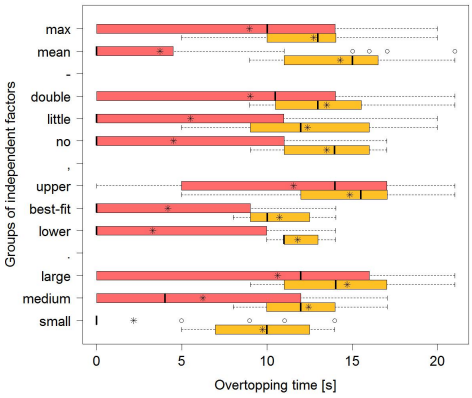

(a) Range of results per factors group. Red = all runs, yellow = overtopping runs only, * = means.

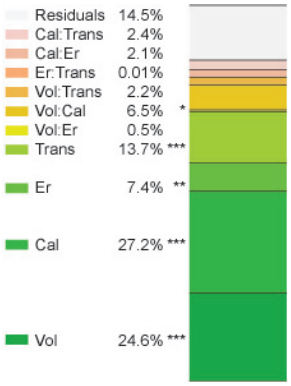

(b) Total variance in all runs

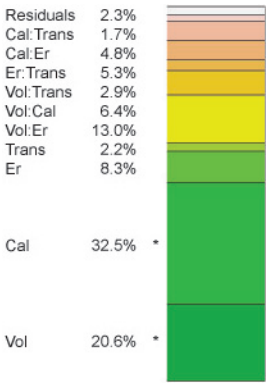

(c) Total variance in the overtopping runs

Groups		A. runs	O. runs
Trans	mean-max	***	
Er	little-no		
	double-no	**	
	double-little	*	
Cal	lower-best fit		
	upper -best fit	***	*
	upper-lower	***	*
Vol	medium-small	***	
	large-small	***	*
	large-medium	***	

(d) Importance of the differences between the groups means in (a). A. runs = all runs, O. runs = overtopping runs.

Figure 12.3: Variance in the overtopping time. For abbreviations see Table 12.1. For explanation of boxplots (a) see Figure 7.3. The percentages in (b,c) refer to the sum of square, indicating the absolute variance introduced by the factor/interaction. The importance (b,c,d) was classified in "strong" (***), "considerable" (**), "noticeable" (*), after the Wilcoxon-test (b,c) and after the TukeyHSD-test (d), respectively, whose results are summarized in Appendix D.

calibration and initial volume (Figs. 12.3b and 12.3c). The overtopping time rose noticeably as a function of the initial volume where the *upper* calibration was applied (Appendix E). In the case of the overtopping runs, no interactions were important. Initial volume and entrainment nevertheless accounted for 13%, volume and calibration for 6.4%, and entrainment and transformation for 5.3% (Figs. 12.3b and 12.3c).
14.5% and 2.3% of the entire variance in all and in the overtopping runs remained unexplained by the main effect and the interactions among the four independent variables (Figs. 12.3b and 12.3c).

To summarize, the initial volume, calibration, and their interactions amounted for 58.3% and for 59.5% of the entire variance in all runs and in the overtopping runs. Strong differences were shown between all groups of the initial volume and between the *upper* and the other calibration groups. The main effects of other independent variables were also important, while the interactions ranged within natural fluctuations.

Variance in overtopping volume

24.3% and hence the second largest component of the total variance in all runs and 33% of the variance in the overtopping runs, constituting their largest components, were caused by calibration only. These main effects were strong and noticeable, respectively (Figs. 12.4b and

12.4c). *Upper* calibration resulted in the only group whose means differed strongly from both other groups' means (Table 12.4d). This is also clearly visible in the boxplots in Figure 12.4a, which indicate the highest overtopping volumes achieved by outliers of the calibrations *lower* and *best-fit* at 10,215 m^3 and at 7,007 m^3 only for both analyses.
The main effect of the initial volume amounted to 14.4% and 13% of the variances of all and of the overtopping runs and hence constituted the third largest and second largest components of the respective variance. This effect was strong on the variance in all runs' results only (Figs. 12.4b and 12.4c). The means of the groups differed noticeably and strongly in the analysis of all model runs only, in comparison of the *large* volume to *medium* and to *small* volumes, respectively (Table 12.4d). A clear difference between the groups was visible (Fig. 12.4a), however, in the entire range of overtopping volumes. Maximal values, which were mostly considered (far) outliers of 10,272 m^3, 79,572 m^3 and 171,369 m^3, were generated by the initial volumes *small*, *medium* and *large*, respectively.
The input variable entrainment answered with 4% and 10.1%, the sixth and the fifth largest components of the variances in all runs or in the overtopping runs (Figs. 12.4b and 12.4c). A noticeable difference between the groups' means was present only for all runs between *no* and *double* entrainment (Table 12.4d). Differences in the ranges of overtopping volumes can be

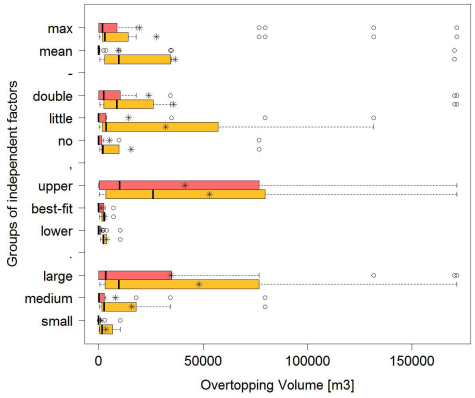

(a) Range of results per factors group. Red = all runs, yellow = overtopping runs only, * = means.

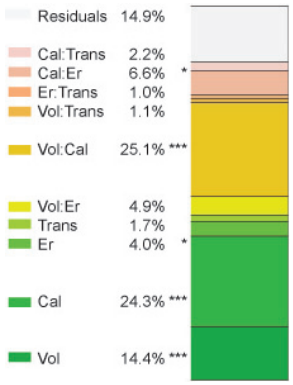

(b) Total variance in all runs

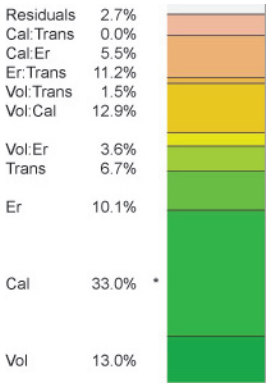

(c) Total variance in the overtopping runs

Groups		A. runs	O. runs
Trans	mean-max		
Er	little-no		
	double-no	*	
	double-little		
Cal	lower-best fit		
	upper -best fit	***	*
	upper-lower	***	*
Vol	medium-small	***	
	large-small	***	
	large-medium	***	

(d) Importance of the differences between the groups means in (a). A.runs = all runs, O. runs = overtopping runs.

Figure 12.4: Variance in the overtopping volume. For abbreviations see Table 12.1. For explanation of boxplots (a) see Figure 7.3. The percentages in (b,c) refer to the sum of square, indicating the absolute variance introduced by the factor/interaction. The importance (b,c,d) was classified in "strong" (***), "considerable" (**), "noticeable" (*), after the Wilcoxon-test (b,c) and after the TukeyHSD-test (d), respectively, whose results are summarized in Appendix D.

derived qualitatively from Figure 12.4a. Maximal values, which were considered far outliers in the analysis of all runs, reached up to 76,747 m^3, 131,549 m^3 and 171,368 m^3 for *no*, *little* and *double* entrainment, respectively.
1.7% of the variance in all runs and 6.7% of the variance in the overtopping runs were caused by the transformation. No important main effect was noted in any analysis (Figs. 12.4b and 12.4c). Both transformation methods led median overtopping volumes between 0 m^3 and 9,626 m^3, whereas maximal values reached up to 171,368 m^3, which were considered far outliers (Fig. 12.4a).

Interactions between two of the four independent variables answered with 40.9% and 32.1% of the variance of the overtopping volume in all runs and in the overtopping runs, respectively. 25.1% and thus the largest component of the variance in all runs was explained by interactions between calibration and initial volume (Figs. 12.4b and 12.4c). The overtopping volume rose strongly if the *upper* calibration was applied in combination with *medium* and *large* initial volumes. Further 6.6%, of the variance in all runs was answered by interactions between calibration and entrainment. The overtopping volume rose noticeably as a function of the entrainment, where the *upper* calibration was applied (Appendix E). Analysing the overtopping runs only, interactions between volume and calibration, as much as between entrainment and transformation, accounted for 12.9% and 11.2% of the variance in the overtopping volume. As for all other interactions, they were, however, not considered important (Figs. 12.4b and 12.4c). 14.9% and 2.7% of the entire variance in all runs and in the overtopping runs remained unexplained by the main effect and the interactions among the four independent variables (Figs. 12.4b and 12.4c).

To summarize, the initial volume, calibration and their interactions amounted for 63.8% and for 58.9% of the entire variance in all runs and in the overtopping runs. Especially the means of the group's *large* initial volume and *upper* calibration differed from that of the other groups. The main effects of other independent variables were hardly noticeable, and also most interactions ranged within natural fluctuations, with the exception of interactions between the initial volume and calibration.

Variance in the maximum discharge
26% and 35% of the variances in all runs and in the overtopping runs constituted their largest components and were caused by the main effects of calibration. These main effects were strong and noticeable, respectively (Figs. 12.5b and 12.5c). *Upper* calibration resulted in the only group whose means differed from both other groups' means (Table 12.5d). This is also clearly visible in the boxplots in Figure 12.5a, which indicate the highest overtopping maximum discharges achieved by outliers of the *lower* and *best-fit* calibration at 2,094 m^3/s and at 1,377 m^3/s, only for both analyses.
The main effect introduced by the initial volume amounted to 14.6% and 12.7% of the variances of all runs and of the overtopping runs and thus constituted the third largest and the second largest components of the respective variance. This main effect was strong for the variance in all runs only (Figs. 12.5b and 12.5c). The *large* initial volume resulted in the only group whose mean differed strongly from both other groups' means (Table 12.5d). A clear difference between the groups was visible (Fig. 12.5a), however, in the entire range of overtopping maximum dis-

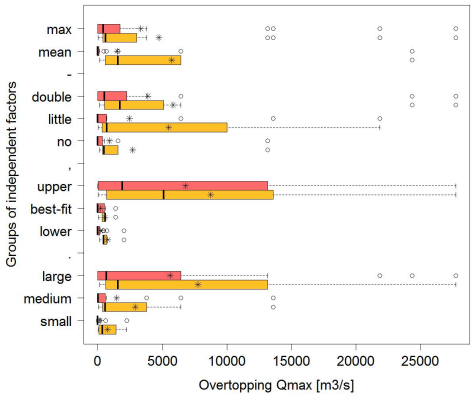

(a) Range of results per factors group. Red = all runs, yellow = overtopping runs only, * = means.

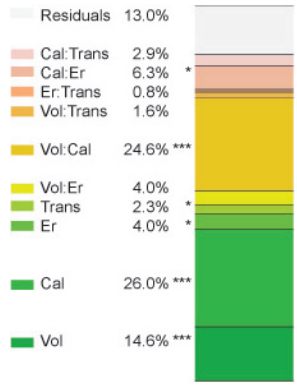

(b) Total variance in all runs

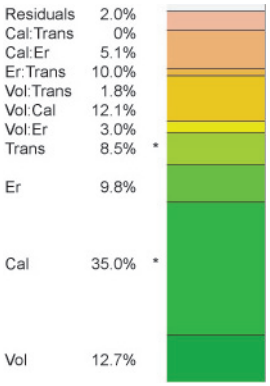

(c) Total variance in the overtopping runs

Groups		A. runs	O. runs
Trans	mean-max	*	*
Er	little-no		
	double-no	*	
	double-little		
Cal	lower-best fit		
	upper -best fit	***	*
	upper-lower	***	*
Vol	medium-small		
	large-small	***	
	large-medium	***	

(d) Importance of the differences between the groups means in (a). A.runs = all runs, O. runs = overtopping runs.

Figure 12.5: Variance in the maximal discharge. For abbreviations see Table 12.1. For explanation of boxplots (a) see Figure 7.3. The percentages in (b,c) refer to the sum of square, indicating the absolute variance introduced by the factor/interaction. The importance (b,c,d) was classified in "strong" (***), "considerable" (**), "noticeable" (*), after the Wilcoxon-test (b,c) and after the TukeyHSD-test (d), respectively, whose results are summarized in Appendix D.

charges. Maximal values, which were mostly considered (far) outliers of 2,229 m^3/s, 13,582 m^3/s and 27,731 m^3/s, were generated by *small*, *medium* and *large* initial volumes, respectively. The input variable entrainment answered with 4% and 9.8%, the fifth biggest components of the variances in all and in the overtopping runs (Figs. 12.5b and 12.5c). A noticeable difference between the groups' means was present only for all runs between *no* and *double* entrainment (Table 12.5d). Differences in the ranges of overtopping maximum discharges can be derived qualitatively from Figure 12.5a. Maximal values, which were mostly considered far outliers, reached up to 13,156 m^3/s, 21,842 m^3/s and 27,731 m^3/s for *no*, *little* and *double* entrainment, respectively.
2.3% of the variance in all runs and 8.4% of the variance in the overtopping runs were caused by the transformation. This main effect was noticeable in both analyses (Figs. 12.5b and 12.5c). While *mean* led to only one value higher than 6,447 m^3/s at 24,351 m^3/s, *max* caused several far outliers up to 27,732 m^3/s (Fig. 12.5a).

Interactions between two of the four independent variables answered with 40.2% and 32% of the variance of the overtopping volume in all runs and in the overtopping runs, respectively. 24.6% and hence the largest component of the variance in all runs was explained by interactions between calibration and initial volume (Figs. 12.5b and 12.5c). The overtopping maximal dis-

charge rose strongly if the *upper* calibration was applied in combination with *medium* and *large* initial volumes. Furthermore, 6.3% of the variance in all runs was answered by interactions between calibration and entrainment. The overtopping maximal discharge rose noticeably as a function of the entrainment, where the *upper* calibration was applied (Appendix E). Analysing the overtopping runs only, interactions between volume and calibration as much as between entrainment and transformation accounted for 12.1% and 10% of the variance in the overtopping maximal discharges. Alike for all other interactions, they were, however, not considered important (Figs. 12.5b and 12.5c).
13% and 2% of the entire variance in all and in the overtopping runs remained unexplained by the main effect and the interactions between the four independent variables (Figs. 12.5b and 12.5c).

To summarize, the initial volume, calibration and their interactions amounted for 65.2% and for 59.8% of the entire variance in all runs and in the overtopping runs. Especially the means of the groups *large* initial volume and *upper* calibration differed from the other groups for all runs. The main effects of other independent variables were also noticeable in all runs. Most interactions ranged within natural fluctuations, with exception of interactions between the initial volume and calibration.

Variance in the mean discharge
26.8% and 35.9% of the variances in all runs and in the overtopping runs constituted their largest components and were caused by the main effects of calibration. These main effects were strong and noticeable, respectively (Figs. 12.6b and 12.6c). *Upper* calibration resulted in the only group, whose means differed from both other groups' means (Table 12.6d). This is also clearly visible in the boxplots in Figure 12.6a, which indicate the highest overtopping mean discharges achieved by outliers of the *lower* and *best-fit* calibrations at 730 m^3/s and at 467 m^3/s only for both analyses.
The main effect introduced by the initial volume amounted to 15% and 12.9% of the variances of all runs and of the overtopping runs and thus constituted the third largest and the second largest components of the respective variance. This main effect was strong for the variance in all runs only (Figs. 12.6b and 12.6c). The *large* initial volume resulted in the only group, whose mean differed strongly from both other groups' means (Table 12.6d). A clear difference between the groups was visible (Fig. 12.6a), however, in the entire range of overtopping mean discharges. Maximal values, which were mostly considered (far) outliers of 685 m^3/s, 4,421 m^3/s and 8,160 m^3/s were generated by the *small*, *medium* and *large* initial volumes, respectively.
The initial variable entrainment answered with 4.1% and 9.9%, the fifth largest components of the variances in all runs and in the overtopping runs (Figs. 12.6b and 12.6c). A noticeable difference between the groups' means was present only for all runs between *no* and *double* entrainment (Table 12.6d). Differences in the ranges of overtopping mean discharges can be derived qualitatively from Figure 12.6a. Maximal values, which were mostly considered far outliers, reached up to 4,263 m^3/s, 6,264 m^3/s and 8,160 m^3/s for *no*, *little* and *double* entrainment, respectively.
2.3% of the variance in all runs and 7.8% of the variance in the overtopping runs were caused by the transformation. These main effects were noticeable in both analyses (Figs. 12.6b and

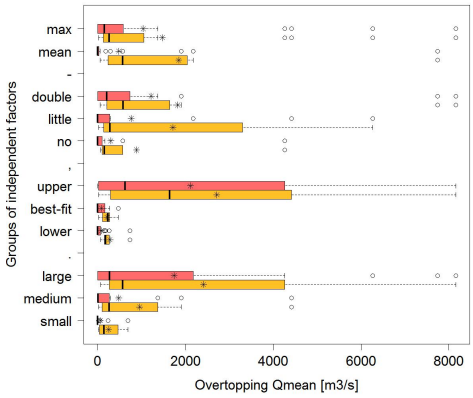

(a) Range of results per factors group. Red = all runs, yellow = overtopping runs only, * = means.

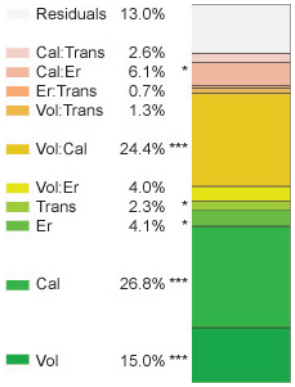

(b) Total variance in all runs

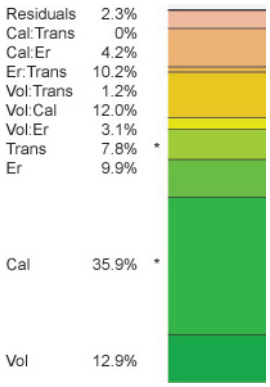

(c) Total variance in the overtopping runs

Groups		A. runs	O. runs
Trans	mean-max	*	*
Er	little-no		
	double-no	*	
	double-little		
Cal	lower-best fit		
	upper -best fit	***	*
	upper-lower	***	*
Vol	medium-small		
	large-small	***	
	large-medium	***	

(d) Importance of the differences between the groups means in (a). A.runs = all runs, O. runs = overtopping runs.

Figure 12.6: Variance in the mean discharge. For abbreviations see Table 12.1. For explanation of boxplots (a) see Figure 7.3. The percentages in (b,c) refer to the sum of square, indicating the absolute variance introduced by the factor/interaction. The importance (b,c,d) was classified in "strong" (***), "considerable" (**), "noticeable" (*), after the Wilcoxon-test (b,c) and after the TukeyHSD-test (d), respectively, whose results are summarized in Appendix D.

12.6c). While *mean* led to only one value higher than 2,000 m^3/s at 7,743 m^3/s, *max* caused several far outliers up to 8,160 m^3/s (Fig. 12.6a).

Interactions between two of the four independent variables answered with 39.1% and 30.7% of the variance of the overtopping volume in all runs and in the overtopping runs, respectively. 24.4% and hence the largest component of the variance in all runs was explained by interactions between calibration and initial volume (Figs. 12.6b and 12.6c). The overtopping mean discharge rose strongly if the *upper* calibration was applied in combination with *medium* and *large* initial volumes. Furthermore, 6.1% of the variance in all runs was answered by interactions between calibration and entrainment. The overtopping mean discharge rose noticeably as a function of the entrainment, where the *upper* calibration was applied (Appendix E). Analysing the overtopping runs only, interactions between volume and calibration as much as between entrainment and transformation accounted for 12% and 10.2% of the variance in the overtopping mean discharges. As for all other interactions, they were, however, not considered important (Fig. 12.6b and 12.6c).

12.8% and 2.3% of the entire variance in all and in the overtopping runs remained unexplained by the main effect and the interactions between the four independent variables (Figs. 12.6b and 12.6c).

To summarize, the initial volume, calibration and their interactions accounted for 66.2% and for 60.8% of the entire variance in all runs and in the overtopping runs. Especially the means of the groups *large* initial volume and *upper* calibration differed from the other groups for all runs. The main effects of other independent variables were also noticeable in all runs. Most interactions ranged within natural fluctuations, with the exception of interactions between the initial volume and calibration.

Variance in overtopping height

29.2% and 31.1% of the variances in all runs and in the overtopping runs constituted their largest components and were caused by the main effect of calibration. These main effects were strong and noticeable, respectively (Figs. 12.7b and 12.7c). In the case of the overtopping runs, the main effect was, however, not attributable to one specific group. In the case of all runs, *upper* calibration resulted in the only group, whose means differed strongly from both other groups' means (Table 12.7d). It was also the only group that caused overtopping heights up to 9.2 m, while maximal values for *lower* and *best-fit* calibration reached up to 4.6 m and 3.6 m only (see Fig. 12.7a).

The main effect introduced by the initial volume amounted to 22.3% and 16.2% of the variances of all and of the overtopping runs and hence constituted the second and third largest components of the respective variance. This effect was strong for all runs only where the means of the *large*

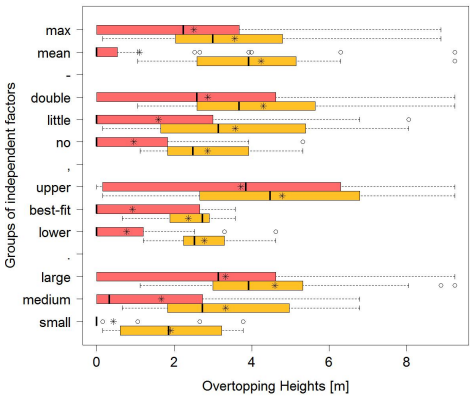

(a) Range of results per factors group. Red = all runs, yellow = overtopping runs only, * = means.

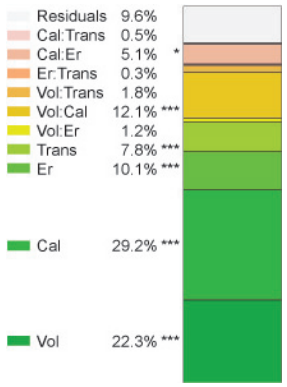

(b) Total variance in all runs

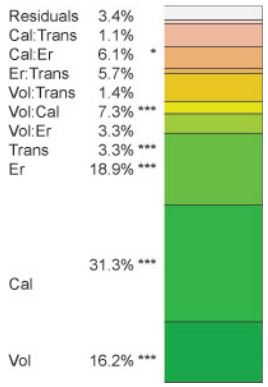

(c) Total variance in the overtopping runs

Groups		A. runs	O. runs
Trans	mean-max	***	
Er	little-no		
	double-no	***	
	double-little	**	
Cal	lower-best fit		
	upper -best fit	***	
	upper-lower	***	
Vol	medium-small	**	
	large-small	***	
	large-medium	***	

(d) Importance of the differences in the groups means in (a). A.runs = all runs, O. runs = overtopping runs.

Figure 12.7: Variance in the overtopping heights. For abbreviations see Table 12.1. For explanation of boxplots (a) see Figure 7.3. The percentages in (b,c) refer to the sum of square, indicating the absolute variance introduced by the factor/interaction. The importance (b,c,d) was classified in "strong" (***), "considerable" (**), "noticeable" (*), after the Wilcoxon-test (b,c) and after the TukeyHSD-test (d), respectively, whose results are summarized in Appendix D.

initial volume differed strongly from the other groups' means (Figs. 12.7b and 12.7c). The difference between the mean of *small* and *medium* volume was considerable (Table 12.7d). A continuous rise of the median overtopping height as a function of the initial volume can nevertheless be distinguished from Figure 12.7a. Maximal values reached up to 3.8 m, 6.8 m and 9.2 m for *small*, *medium* and *large* initial volumes, respectively.
The input variable entrainment answered with 10.1% and 18.9%, the fourth and the second largest components in the variances of all runs and of the overtopping runs, respectively (Figs. 12.7b and 12.7c). This effect was strong for all runs only where the means of *double* entrainment differed strongly and considerably from *no* and *little* entrainment, respectively (Table 12.7d). A continuous rise of the median overtopping height as a function of the entrainment can nevertheless be distinguished from Figure 12.7a. Maximal values reached up to 5.3 m, 8.1 m and 9.2 m for *no*, *little* and *double* entrainment, respectively.
The main effect of the transformation methods was strong and answered with 7.8%, the fifth largest component of the variance in all runs (Fig. 12.7b). In the variance of the overtopping runs its influence of 3.3% was, to the contrary, amongst the smallest (Fig. 12.7c). The groups almost did not differ in the range of the overtopping times they caused. For *mean*, contrary to *max*, the six highest values were considered outliers (Fig. 12.7a).

Interactions between two of the four independent variables answered 21% and 24.9% of the variance of the overtopping time in all and in the overtopping runs, respectively. 12.1% and thus the largest component of the variance in all runs was explained by interactions between calibration and initial volume (Appendix E). The interaction between calibration and entrainment was noticeable and accounted for 5.1% of the variance in all runs. Both interactions caused a strong rise in the overtopping heights as a function of the initial volume as well as of entrainment, where the *upper* calibration was applied. In case of the overtopping runs, no interactions were considered important. Initial volume and calibration nevertheless accounted for 7.3% and entrainment and calibration for 6.1% (Figs. 12.7b and 12.7c).
9.6% and 3.4% of the entire variance in all and in the overtopping runs remained unexplained by the main effect and the interactions among the four independent variables (Figs. 12.7b and 12.7c).

To summarize, the initial volume, calibration and their interactions amounted for 63.3% and for 54.6% of the entire variance in all runs and in the overtopping runs. Strong differences were shown among all groups of the initial volume and between the *upper* and the other calibration groups. The main effects of other independent variables were also important, while the interactions ranged within natural fluctuations, with the exception of the interaction between the initial volume and calibration.

Synthesis
All main effects were noticeable, considerable or strong, considering all runs. The largest contributions to the variance in all dependent variables were caused through the initial volume, calibration of RAMMS and interactions between them. The attribution of the variance in the dependent variables to the independent variables, only considering the overtopping runs, was similar to the one in all runs, without, however noticeable differences between the groups' means. The variations in the dependent variables thus ranged within natural fluctuations. These results

indicate that variations in the independent variables were decisive regarding whether a wave overtops or not; the values of the overtopping waves, however, ranged within natural fluctuations.

12.3.3 Analysis of the influence of the independent factors

The univariate analyses of the variance in the dependent variables (in quotation marks) are compiled for the independent factors (in italic) in this section. These compilations are presented in detail in Appendix D with Table D.2 referring to all runs and Table D.3 referring to the overtopping runs.

Initial volume
The main effects caused by the *initial avalanche volume* explained the second highest part of the variance for all dependent variables (except for the "overtopping wave's height"), which was 14-24% and 13-20% for all runs, and for the overtopping runs, respectively. For all runs, results in "overtopping volume", "maximum" and "average discharge", the interaction between *initial volume* and *calibration* explained twice as much of the variance than did the main effect of the *initial volume*. In the case of the overtopping runs, the main effect of the *initial volume* was in the same range as the interaction of *initial volume* and *calibration*. For all model runs, the influence of the *initial volume* was always strong. These differences were always caused by *large initial volumes*. Only in the case of the "overtopping height" and "time" did all three categories differ strongly from each other. In case of the overtopping runs, the differences are for all dependent values located between *small* and *large initial volumes*. The variance introduced by the *initial volume* was noticeable for the "overtopping time". Four overtopping runs were caused by *small*, nine by *medium* and 13 by *large initial volumes*. The *initial volume* was involved in interactions with *calibration*, which is described in the next paragraph. The *initial volume* was involved in explanation of 32-45% of all runs' variance, and of 28-43% of the overtopping waves' variance.

Calibration
Calibration explained for all dependent variables the largest variance of the main effects. For all model runs it explained between 24-29% of variance, whereas *calibration* was responsible for 31-36% of the variation in the overtopping runs. The variation caused by *calibration* was always strong in the case of all model runs. Considering only the overtopping waves, *calibration* was the only independent factor, which caused a variance that differed strongly from the other independent factors. The main variance was always caused by the *upper calibration*. For all model runs, *upper calibration* differed strongly from the other *calibration groups*, whereas for the overtopping runs, the variation was noticeable (except in case of the "overtopping height"). The *lower calibration* caused five, *best-fit* seven and *upper calibration* 14 overtopping waves. *Calibration* was also involved in interactions with the *initial volume*, which were strong for all runs where the interactions explained 12-25% of the variance. This interaction also explained 6-13% of the variance in the overtopping runs, the differences within the groups' means were, however, not noticeable. The interaction between *initial volume* and *calibration* was usually located

in a rise of the dependent value for all *initial volumes* when *upper calibration* was assumed. Therefore, main effects and interactions of *calibration* were involved in explaining 38-60% and 45-53% of the variances for all runs and for the overtopping model runs, respectively.

Entrainment
Entrainment explained the third largest variance of the main effects for the dependent values, with exception of the "overtopping time" for all runs and the "overtopping volume" for the overtopping runs. The variance explained by the main effects of *entrainment* was, however, smaller than the interaction between *initial volume* and *calibration*. For all model runs, the main effects of *entrainment* were strong for the "overtopping height", considerable for the "overtopping time" and noticeable for the "overtopping volume", "average" and "maximal discharge". *No* and *little entrainment* did not differ noticeably from each other for any dependent value. *Double entrainment*, however, differed from *no* for all dependent values and also from *little entrainment* for the "overtopping time" and "height". Differences for all dependent values were located between the categories *no* and *double entrainment*. *No entrainment* caused six, *little* 8 and *double* entrainment 12 overtopping waves. For all runs, the interactions in which *entrainment* was involved were negligible. *Entrainment* was involved in explaining 10-17% and 28-34% of the variance of all runs and of the overtopping model runs, respectively.

Transformation
Transformation explained the least of the main effects, with exception of the "overtopping time" in all model runs, where *transformation* explained more of the variance than *entrainment*. For all model runs, *transformation* explained 11-8% and 2-8% for the overtopping model runs. For all model runs, this was less than the percentage explained by the noticeable interactions. For the overtopping model runs, this was less than the percentage explained by interactions between the *initial volume* and *calibration*, or between *entrainment* and *transformation*. The main effect of *transformation* in all model runs was strong for the "overtopping time" and "height", considerable for the "maximal" and the "average discharge". For the overtopping model runs, the main effect was only noticable for the "maximal" and the "average discharge". *Transformation max* caused 19 and *mean* seven overtopping waves. In all model runs, none of the interactions involving *transformation* were noticeable. For the overtopping waves, the interaction between *entrainment* and *transformation* explained 10-11% of the variances in the results of "overtopping volume", "average" and "maximal discharge". The effect was that the results for *max* (which lead to higher results than *mean* in case of *no* and *little entrainment*) lead to lower results than the *mean*, if *entrainment* was *double*. *Transformation* was involved in explanation of 6-18% and of 12-20% of all variations for all and for the overtopping model runs, respectively.

Synthesis
Roughly summarizing, *calibration* of the RAMMS friction parameters introduced the highest variances in the overtopping waves, followed by the *initial volume*, *entrainment* and *transformation*. Often the interactions between two factors explained as much of the variance as the corresponding main effects, especially in the case of the *initial volume* and *calibration*. The sum of the square is an indicator for the absolute variance, and the respective percentages are distributed comparably between the factors for both all runs and the overtopping model runs. The importance from the groups' means in this case resulted mainly from these groups, which

were able to cause overtopping waves. This explanation only does not apply to *transformation*. The two methods mainly changed the character of the impacting slide. The variances of dependent values within the overtopping waves were in the range of the natural exceptions, with only a few exceptions.
Another overall observation regarding the dependent variables' variance was that the "overtopping time" and "height" directly characterized the overtopping wave, while the "overtopping volume" and the "discharge", describe the overtopping hydrograph as a consequence of the runup rather than the wave. I.e., a long-lasting, flat wave can cause the same overtopping volume as a short but high wave.

12.3.4 Interpretation of the influence of the independent factors

The influence of the independent factors presented in the previous section is interpreted here in consideration of the physics implemented in RAMMS and IBER, as outlined in Section 11.2 and compared with analytical and empirical knowledge on impact waves (Section 10.2, with the goal of answering the research question. The momentum transfer during the impact is described by means of literature on wave generation only (Heller et al., 2008). As IBER only models wave propagation and runup by conserving the mass and the impulse, the momentum transfer has to be discussed with literature on wave generation.

Initial volume
As Panizzo et al. (2005b) stated, the wave type and the energy of the wave are mostly a function of the landslide volume, but also of the impact velocity. A higher slide volume leads to rather solitary waves and influences as much the wave height as the wave period or length. Di Risio et al. (2011) confirm that the wave height depends on the impact energy. From this theory, a rise in overtopping wave height and time, as much as a rise in the volume and discharges as a function of the initial volume, could be expected. The ANOVA-analysis runs of the overtopping wave height and time confirmed this theory, where the differences among the groups' means were significant considering all runs. The absolute variance in the overtopping volume and discharges were also strongly influenced by the initial volume, however as much in interaction, mostly with calibration, than as a main effect. Not only the absolute variance in the overtopping waves, but also the fact of whether an avalanche leads to an overtopping wave, were significantly a function of the initial volume.

Calibration
Calibration concerned the friction parameters implemented in RAMMS. The Coulomb term μ influences the runout distance as a function of the flow height. In the present study, this effect did not seem to be crucial, as all avalanches reached the lake and no systematic influence on the flow heights could be distinguished. The viscous term ξ is more crucial, as it influences the flow velocity. The effect of the calibration on the flow velocity was so strong that it was clearly distinguishable in the manually read-out results, even independent of the transformation methods. Correspondingly, the impacting hydrographs differed strongly as a function of the calibration; especially for the calibration u, a tendency towards shorter but high-volume and clearly higher

maximum discharges could be identified. These facts suggest that the faster the landslide, the steeper the impact front.
As stated above, empirical descriptions on the transfer of the impulse (Di Risio et al., 2011; Heller et al., 2008; Panizzo et al., 2005b), agree that this raise in velocity caused by the calibration creates higher wave heights and longer wave periods. This effect was again transferred into the overtopping wave by IBER, causing an equally strong variance in all five dependent variables. The effect of the calibration is reinforced in interactions with the initial volume, the main effect of the calibration is nonetheless stronger than the one of the initial volume. This suggests that for a scenario of this magnitude the overtopping wave is more sensitive to variations in velocity than in the initial volume.

Entrainment
In this study, basal entrainment was modelled by all chosen settings, which leads to changes in the flow height and mass, which again influences the runout distance by means of reduction in the Coulomb-friction term μ. It does not, however, necessarily influence the flow velocity, as speed is reduced during entrainment and only rose in a second part thanks to the higher flow volume (Sovilla et al., 2006, 2007). Even thought the entrainment rate depends, on the other hand, on the avalanche speed, it is mostly defined by the entrainment coefficient. These effects were, however, rarely distinguishable in the absolute avalanche flow heights and velocities at the impact. The impact hydrographs also did not differ systematically or significantly; nevertheless a tendency towards higher volumes and maximum discharges as a function of entrainment was distinguishable, while no differences in variation of the impacting time were recorded.
The effect of entrainment on the wave height thereof was mostly via the avalanche volume, which resulted in a picture of variances in the dependent values that was comparable to the factor initial volume. The effect was, however, weaker, as much regarding the absolute variances as regarding the significance of the groups' differences. Entrainment introduced considerable variance into the overtopping waves' height and time, but was, however, not crucial in the variance of the overtopping hydrographs (overtopping volume and discharges).

Transformation
Transformation determined how the rock/ice avalanche flow height and velocity were assessed at the moment of impact into the lake. In the method *mean*, flow height and velocity values were considered at the location of mean values along the shoreline and multiplied by the entire avalanche width, while in *max* flow height and velocity values were considered at the location of maximum values along the shoreline and multiplied by a proportion of the avalanche width. It thereby defined the shape of the impacting mass and the impact time, but not the impact volume or discharge. Transformation *mean* caused lower impact velocities, lower impact heights and showed a tendency towards longer-lasting impacts. Transformation *max*, on the other hand, caused higher impact velocities, higher impact heights and a tendency towards lower impacting times.
According to Heller et al. (2008) the impulse was higher for *max* than for *mean*. As the wave type is a function of the impact volume and the impact velocity (Panizzo et al., 2005b) it can be suggested, that transformation *max* lead to rather solitary than to stokes-kind waves. This lead to variances in the overtopping wave's height and time, the overtopping volume or discharge

was, however, little affected by the transformation method. The transformation was further not decisive for whether a rock/ice avalanche leads to overtopping or not. This means that reading out the RAMMS-results manually is not a critical factor for the wave modelling. It remains unclear whether manual methods are accurate at all, or how the results would differ, if the modelled impacting hydrograph could be numerically integrated into the wave model.

Summary of the main outcomes
Even though the interpretation of the simulation results was not always straightforward, the variance in the dependent variables could reasonably be explained with numerical implementation of mass and flow movements and with the wave-impact theory. The momentum transfer between slide and water is a complex coupling of all independent factors; therefore it is difficult to determine which factor is most important. This complexity was confirmed by the large and sometimes significant effects of the interactions, which could explain larger parts of the variance than the main effects only. From the dependent variables, the overtopping wave height and time reacted more sensitively to all independent factors, as they represent the impact waves characteristics. The overtopping volume and discharge stand for the overtopping hydrograph, which depends on the composition of the wave characteristics. Regarding subsequent outburst-flow modelling, it can be carefully stated that the hydrograph is mostly dependent on the initial volume and thereby on the impacting volume, the calibration of the RAMMS-friction parameters (which mostly alters flow velocity), and the interactions of these two independent factors rather than of entrainment or transformation method. From this analysis it can be concluded that back-calibrating the simulation chain by means of only the overtopping height is feasible. It is not, however, complete, as uncertainties regarding the overtopping time and thus also regarding the overtopping volume and maximum and mean discharges remain.

12.4 Discussion

This chapter dealt with the effect analysis of an avalanche-induced impact wave. The research question treated was, "How do uncertainties propagate in the numerical simulation of the process chain of a lake-outburst flow due to an impact wave triggered by a rapid mass movement?". This effect was investigated with the help of the 2010 event at Lake 513 presented in the previous chapter, applying an analysis of variance in the overtopping wave's characteristics (overtopping height, time, volume, mean and maximal discharge) with regard to the independent factors. A compilation of the main outcomes was given in the previous section; the rough summary thereof is as follows. In this example (of a relatively small avalanche), the uncertainty in initial volume, calibration of RAMMS, entrainment, and transformation are decisive regarding whether a wave overtops or not. The variance in the overtopping waves, however, ranges within natural fluctuations. Further, it is noticeable that the overtopping time and height reacted very similarly to variations in the independent factors, and that the results with regard to overtopping volume, mean, and maximum discharge are also alike.
The interaction between a rapid mass movement and a lake is, of course, more complex and uncertainties can be introduced by more sources than the four investigated ones. Statistical

analysis is, however, always a trade-off between completeness and interpretability, which requires focus on the most important factors. In the following paragraphs, the chosen approach is discussed.

Further sources of uncertainties

The influence of the RKE-model implemented in RAMMS (see Section 11.2) was assumed negligible, as it was described by Sovilla et al. (2007) to mostly influence runout distances rather than flow velocities. It must nevertheless be stated that the RKE might have supported the effect of entrainment (Sovilla et al., 2006). These characteristics, however, showed results that were not crucial to the present study, as the results of the rock/ice avalanche simulation were comparable to similar simulations (e.g. Dalban Cannassy et al., 2011).
IBER simulated the wave progapation and runup, while turbulence and sediment transport were supposed to be insignificant in the present case. Sediment transport was not assumed to take place at all during wave propagation and runup in the lake, and the effect of vertical turbulence was assumed to be smaller compared to the effect of bottom friction (Dao and Tkalich, 2007). The effect of friction on wave propagation and run-up, is implemented in IBER by means of the Manning coefficient. This friction value is more investigated than the one for rock-/ice avalanches. The present study therefore made use of established recommendations (Chow, 1959), to keep the analysis simpler. Still, a certain influence of the Manning value has to be assumed for waters shallower than 50 m (Dao and Tkalich, 2007), which is even stronger for waters shallower than 10 m (Myers and Baptista, 2001). These conclusions should not be mixed with results from Worni et al. (2012b), who qualified the Manning-n as critical regarding the robustness of the model output. Their statement refers to the simulation of an overland flow, which was in the present study carried out with the equivalent fluid software RAMMS.

The avalanche width is also described as influencing the impulse transfer (Lynett and Liu, 2005). This factor was considered insignificant for the present case study, as the slide widths were barely influenced by flow parameters. They were quite consistent at the moment of impact due to topographical conditions. The density of the impacting slide, another important factor defining the runup because of the momentum transfer (Lynett and Liu, 2005), is described as causing an effect comparable to the one of the slide width (Heller et al., 2008). To reduce complexity, density was assumed to be a constant factor, as it is easier to estimate than the four chosen independent factors and because it was altered to enable correct momentum transfer. The influence of the DEM, the bathymetry or the calculation grid resolution on simulation accuracy are other considerable sources of uncertainty whose inclusion would have gone beyond the scope of the present study. Discussions in this regard can be found in Myers and Baptista (2001) for hydrodynamic tsunami simulations or in Scheuner et al. (2009); Stolz and Huggel (2008) for RAMMS.

For these reasons, the analysis of the variance in the dependent overtopping variables was limited to the influence of the four chosen independent factors. This setup was already at the limit of interpretability and also of expressiveness of the results. 54 simulations is a respectable base of data for modellers. From a statistical point of view, however, the number of simulation runs available for testing the effect per dependent variable and independent factor is still small. Even though the method for analysis of variance is still assumed to be appropriate for answering the

research question regarding the uncertainty propagation in coupled simulations, the resulting numbers have to be treated carefully, especially with regard to significance. Further fundamental limits of the validity of the results emerge from the experimental setup.

Validity of the study and the results

Friction calibration of RAMMS was stated to have a slightly stronger influence on the overtopping wave than the initial volume. This statement is valid only for volume variation within a certain rock/ice avalanche scenario. In the present study, the small scenario, as defined by Schneider et al. (2014), and the corresponding uncertainty range was assessed. The findings of this study are infeasible for a comparison of this scenario to a larger rock/ice avalanche scenario.

Further, the findings regarding the influence of the transformation methods have to be interpreted, considering that they apply to manual transformation only. Manual interpretation will always introduce uncertainty. Unfortunately, the current setups of RAMMS and IBER neither prepare nor allow, respectively, direct transfer of the numerical avalanche results in the inflow hydrograph for wave propagation simulation. Therefore no general statement regarding the reliability of the manual approach as such can be made. Preliminary assessments of Guillén Ludeña et al. (2014), suggest, however, that the manual method underestimates the impacting volume, but changes the form of the slide in such a way that the overtopping results were nevertheless overestimated. The shape of the slide is known to have an influence on the runup (e.g. Lynett and Liu, 2005).

The findings regarding entrainments are valid for the process of basal entrainment only. The influence of entrainment might also differ if values represented ploughing instead of basal entrainment. Ploughing takes place at the front of the flow and alters the impacting flow, generating different wave forms. This was not assumed in the present study.

Despite all these restrictions, the analysis of variance allowed for drawing of conclusions on the influence of the simulation-input factors on the resulting overtopping variables, even though they were not always straightforward or simple. Some open questions for further research still remain.

Open questions

It would, for example, be highly interesting to compare this simulation setup to a simulation that also simulates the process of impact. If IBER were replaced with a designated impact wave model (as compiled in Table 10.10 in Section 10.3.3.2), RAMMS results could be applied, to define the velocity and shape of the sliding block. This setup would permit checking the assumption that adequate runup simulation is possible without numerical representation of the impact generation. Furthermore, the effect of the manual transformation of the RAMMS results into impact hydrographs could also be verified. This second point would ideally be tested by means of a fully physically-based multiphase simulation (e.g. on the basis of the SPH technique), which is, though, still very challenging.

In this study, the uncertainty propagation was tracked. This assessment was pursued with a goal of establishing a qualitative categorization of the parameter uncertainties and parameter sensitivity according to the example of Worni et al. (2012b). Thereby more generally valid conclusions might be generated.

Another open question, which was explicitly omitted in the presented analysis of variance, is the importance of the location of the release area, which also influences the runup according to Lynett and Liu (2005). This crucial issue will be extensively treated within the evaluation of different (in location and size) rock/ice avalanche scenarios in the next chapter.

Relevance for risk management

Hazard assessment by means of numerical simulation of process chains such as impact-triggered lake-outburst events is a young research field (Schneider et al., 2014; Worni et al., 2014). The main contribution of the present study was to show, that coupling of simulations (even including manual transfer) delivers reasonable results of an overtopping wave. The present study showed, that IBER conserves the mass or momentum; so overtopping results are rather a consequence of assumptions taken in the avalanche simulation. The importance of these initial parameters was already known for avalanche simulations; the present study showed their significance for coupled simulations.

Coupling of numerical simulations is a requirement for intensity maps generation, and the advantages of the combination of the models therein outweigh the disadvantages introduced by blurring. To reduce this effect, scenario simulation is recommended. A corresponding example is presented in the next chapter.

CHAPTER 13

HAZARD ANALYSIS OF POTENTIAL ICE AVALANCHES AT MOUNT HUALCÁN

This chapter aims to bring together the methods presented and the advances elaborated in local-scale hazard analysis of the process chain of a lake-outburst flow triggered by an avalanche-induced impact wave. The research question treated is, "How can ice-avalanche scenarios be developed and their effects on a lake be simulated and evaluated?". Ice-avalanche scenarios emerging from Mount Hualcán above Lake 513 will again serve as an example.
Firstly, ice-avalanche scenarios are defined in an event analysis. The effect analysis is then carried out by simulating the ice avalanche with RAMMS, the impact wave with IBER and the outburst flow with RAMMS again. The conclusions and findings from the analysis of variance will also be taken into account when interpreting the results.

13.1 Data and method

Fur the purpose of the present study, the detachment of an ice avalanche in the south face of Mount Hualcán was assumed to be the initial event. Little experience with hazard analysis of ice avalanches is available, and no standard procedures exist. According to the general procedure of a hazard analysis (presented in Section 3.2.1), the proceeding is divided into an event and an effect analysis. Difficulties for the event analysis arose from the remote and dangerous location of potential detachment zones. The south face of Mount Hualcán is glaciated beginning at an altitude of 4,600 m a.s.l, where continuous ice- and snow-avalanche activity can be observed. This setting makes a local investigation practically impossible and an assessment on a basis of remote sensing observations is also hardly feasible due to the extremely steep topography. Therefore, innovative approaches combining different methods were elaborated to define potential release scenarios.

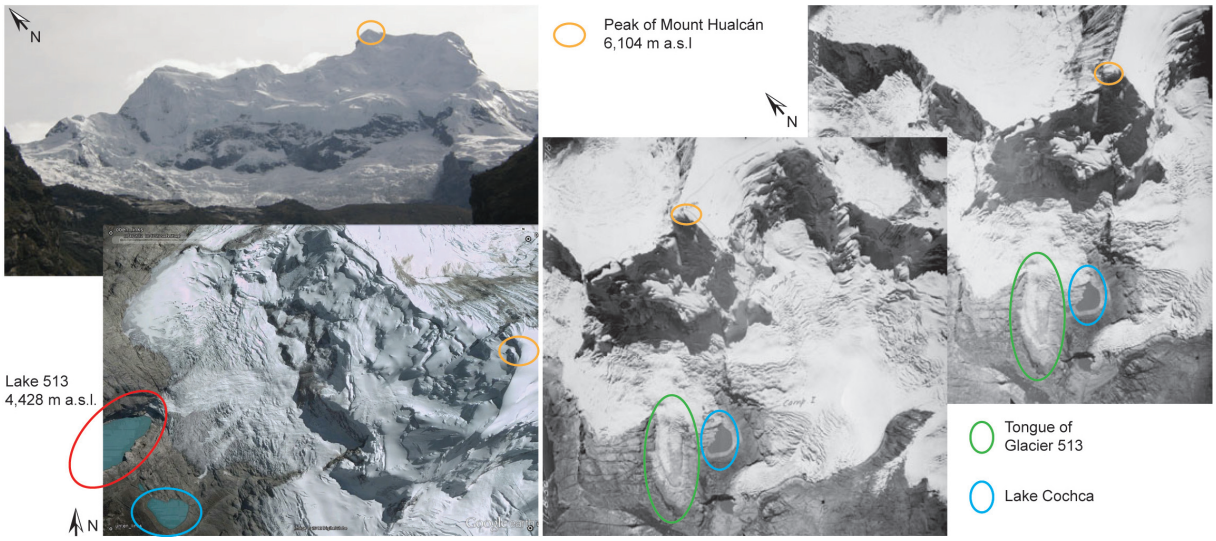

Figure 13.1: Basis for the ice-avalanche scenario elaboration. Field observations in autumn 2012 (upperleft image), Google Earth 2003 image (lowerleft image) and aerial images from 1950 (images to the right).

13.1.1 Elaboration of ice-avalanche scenarios

Here an approach was developed which is based on the analysis of the evolution and dynamics of the glacier and understanding of the mountain's characteristics. This procedure represents a mixture of analysis of the terrain and of geomorphologic features in the terrain attesting to, e.g. past ice-avalanche paths as described in the theoretical background on hazard analyses in Section 3.2.1. The analysis is based on on-site observations and optical examination of a Google Earth image from 2003, as well as on stereoscopic analysis of two analogue aerial photographs of Mount Hualcán from 1950, provided by the Peruvian Unidad de Glaciología y Recursos Hydricos (illustrated in Figure 13.1).

In a first step, the glacier was observed on-site in autumn 2012 and compared to the Google Earth image. This allowed location of zones of detached ice, of moving ice (i.e., creeping steep parts or hanging glaciers), or of newly formed objects; it also permitted recording of changes in glaciation. Further, ice thicknesses were estimated based on the on-site observations and estimations of experts. In a second step, the two analogue aerial photographs from 1950 were analyzed with the help of a stereoscope. The glaciation was also compared manually with the 2003 Google Earth image and the corresponding changes were documented. This two-step approach allowed for an inventory of the glacier conditions at Mount Hualcán over the last 60 years, but more importantly, it allowed for recognition and location of the dynamic and more stable parts of the glacier.

These results were in a next step used to determine potential detachment zones. Areas that showed movements in the past, steep areas, new hanging glaciers, cliff-type situations or potential evolving hanging glaciers were assumed areas prone to ice-detachment. Topographic characteristics, ice crevasses and ice thicknesses supported in delineating area and volume of potential ice avalanches. It was distinguished between small-, medium- and large-size events.

Often, ice avalanches also sweep along rocky parts during detachments (more explanations are given in Section 4.2.2), resulting in combined rock/ice avalanches. The corresponding volumes are hardly assessable. This is why ice avalanches only were considered in the present study. The role of combined rock/ice avalanches is nevertheless included in the discussion of the results.

The effects of nine of these potential ice avalanches were assessed in a following step. In addition, an extreme scenario was assumed, representing much larger extents of ice detachments, which could for example be triggered by earthquakes.

13.1.2 Application of the model chain to ice-avalanche scenarios

The effects of three potential ice avalanches per event size from the enumerated detachment zones in Figure 13.3 were next simulated with RAMMS and IBER. The initial volumes were approximated to the upper estimates illustrated in Figures 13.3b-d. The extreme scenario was implemented as simultaneous release of the large release zones 7 and 9.
The simulations were run based on the 8-m DEM derived from 2012 WorldView satellite images, and bathymetric data was derived from field campaigns in July 2007 and June 2011 (Cochachin, 2011). Parameters for friction calibration (μ=0.12/ξ=1000) and entrainment (depth of erodible layer = 0.1m, density of erodible layer =1000kg/m^3 and entrainment factor 0.09) in RAMMS were determined according to the variables, which were back-calibrated by Schneider et al. (2014) to best fit the 2010 event (Table 12.1). RAMMS results were transformed into the IBER hydrograph with the help of the *mean* method (see Section 12.1 for closer explanation). IBER was run with a Manning value of 0.25. The simulation of the outburst flows was carried out with RAMMS, taking into account different flow behaviours along the path according to Schneider et al. (2014) (see Figure 11.3 in Section 11.2).

The hazard scenarios resulting from the event analysis and from the numerical process-chain simulations are presented in the next section.

13.2 Results

13.2.1 Dynamics in glaciation, potential ice-avalanche detachment zones and volumes

A first step toward understanding of the mountain's characteristics and the glacier's evolution was attempted through comparison of field observations with Google Earth images and aerial images. The thereby-detected dynamics are illustrated in Figure 13.2 and served as a basis for locating potential ice avalanche-detachment zones and volume estimations.
Many serac zones were observed in the moderately steep part below the cliff, which is characteristic of ice loss. It was assumed that the seracs would collapse successively rather than detach

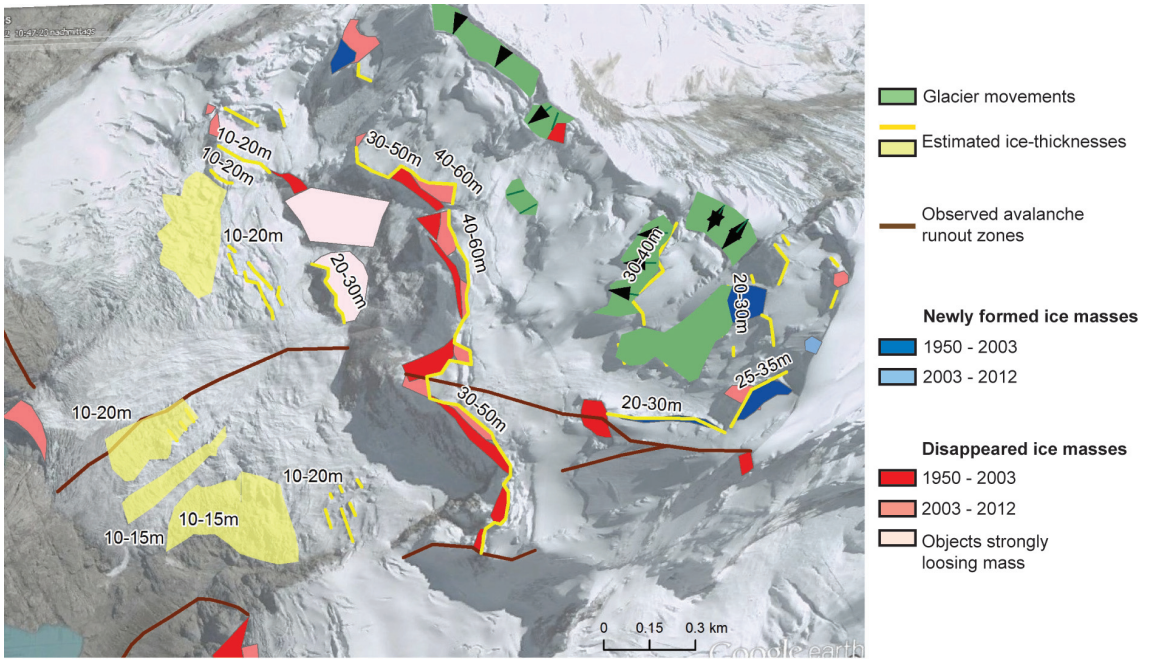

Figure 13.2: Glacier dynamics of Mount Hualcán south face. Mapped changes and dynamics in glaciation, observed changes in the last 60 years at Mount Hualcán south face. The Google Earth 2003 image serves as background.

as a large ice mass. Therefore, these areas were assumed to be zones of continuous erosion (Fig. 13.3a). Considerable ice masses were mapped to have disappeared along the cliff at 5,450 m a.s.l. During the field observation period, continuous breaking off of small ice avalanches was observed. It was noted that ice avalanches flow as much towards Lake 513 as in the direction of Lake Cochca. Therefore the cliff was also considered to be a zone of ongoing erosion. Nevertheless, impressive crevasses were detected near this ice front of approximately 40-60 m in height, therefore several medium- to large-scale detachments from this location are also conceivable. Behind the cliff, a rather flat and stable area is located before the ascent to the peak. Here, large ice masses were observed to deform into ductile, partly formed, hanging glaciers. Further patches of ice were observed to have disappeared, while new hanging glaciers have formed since 1950. In summary, the uppermost 1,000 vertical metres of the Hualcán south face is a very active zone with estimated ice thicknesses between 10 to 40 m, where several potential detachment zones were located.

Volume estimates were gained considering the area within crevasses and the corresponding ice-depth approximations. Related small-size scenarios include release volumes around 40,000-100,000 m^3 (Fig. 13.3b), release volumes of medium-size scenarios are considered to be around 200,000-900,000 m^3 (Fig. 13.3c), and large scenarios are expected to involve initial volumes around 1,000,000-2,000,000 m^3 (Fig. 13.3d). Extreme scenarios, assuming simultaneous triggering of two large ice avalanches simultaneously, e.g. by an earthquake, can involve initial volumes up to 4,000,000 m^3 of ice.

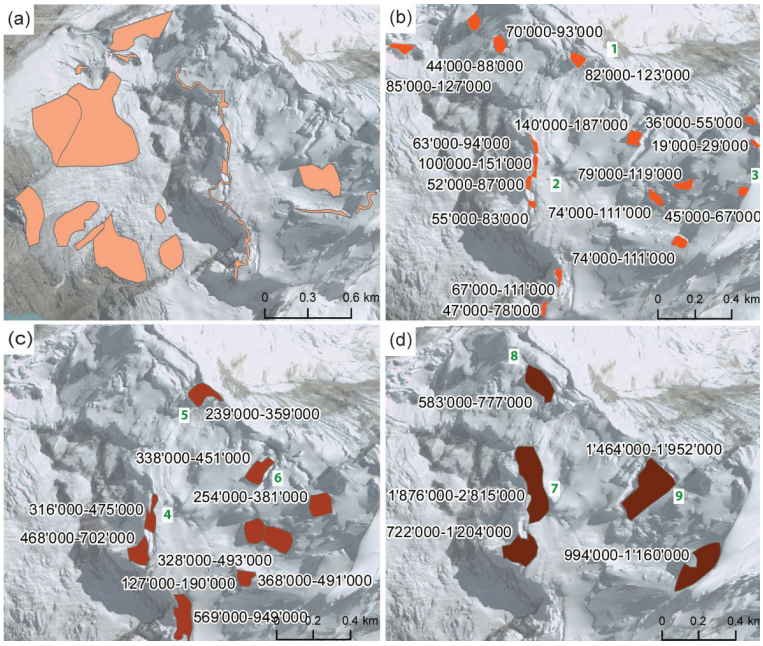

Figure 13.3: Potential ice-avalanche detachment zones and ranges of estimated volumes (m^3) at Mount Hualcán south face include; (a) zones of continuous erosion; detachment zones of potential (b) small ice-avalanche events, (c) medium ice-avalanche events, (d) large ice-avalanche events. Effect analyses were carried out for the potential detachment zones numbered in red.

13.2.2 Modelling the effects as a process chain

The effect of selected, potential ice avalanches was then assessed by means of numerical simulations applying RAMMS and IBER. The RAMMS ice-avalanche simulations suggested that all potential ice avalanches might reach Lake 513, independent of their detachment locations or initial volumes (Fig. 13.4). The simulation further indicated that with one exception only (simulation 1), all avalanches might split and also flow towards Lake Cochca. Six out of these nine avalanches were even modelled to impact Lake Cochca (scenarios 2, 3, 4, 6, 7, 9 and extreme). Therefore, another hazard is located in Lake Cochca, which will necessitate further assessment not included in the present study. In most cases, however, the main flow was simulated to tend towards Lake 513. This splitting of the flows nevertheless implied a decrease in the mass impacting Lake 513. This mass loss might be the reason why finally only two large scenarios (7 and 9) and the extreme scenario contained an overtopping of the Lake 513. In the large scenarios, overtopping volumes of 66,000 m^3 (scenario 7) and 75,000 m^3 (scenario 9) were simulated. The overtopping volume triggered in the extreme scenario differed in the order of one magnitude of about 325,000 m^3.

The routings of these three outburst flows were again simulated with RAMMS. The resulting inundation scenarios are illustrated by means of hydrographs along the course in Figure 13.5b. The effect of the outburst event is simulated perceptibly until the confluence with the Río Santa in all three scenarios. Analogous to the overtopping volumes, the flow characteristics of the two large scenarios were comparable, and only the extreme scenario indicated a larger discharge. According to this simulation, parts of the centre of Carhuaz would be affected by the outburst flow, even though middle to strong inundation heights (>2 m) would only be expected in or directly adjacent to the river bed.

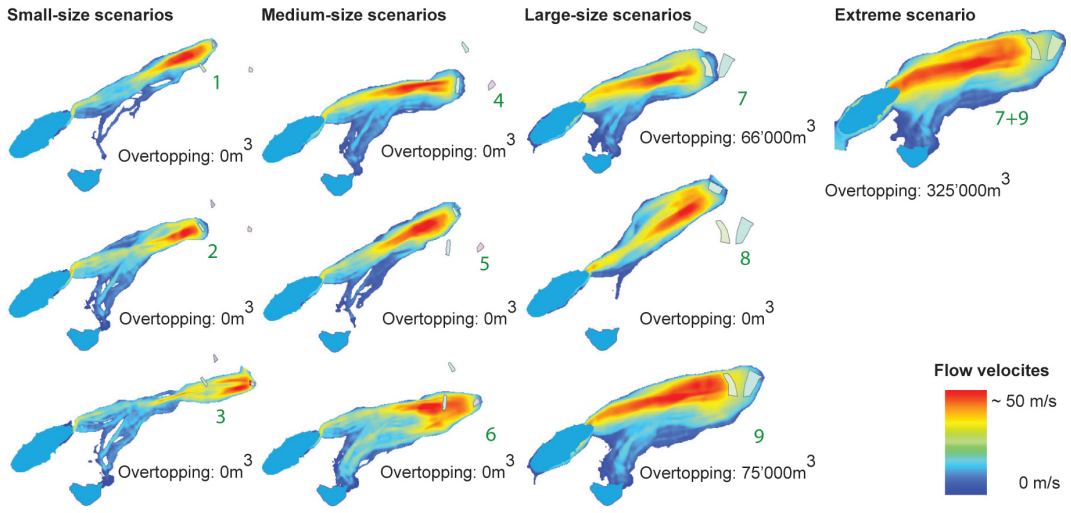

Figure 13.4: Simulated flow traces of potential ice avalanches at Mount Hualcán south face (maximal flow velocities generated by RAMMS are illustrated). The effects on the Lake 513, here the overtopping volumes, were generated with IBER. The scenario numbers are defined in Figure 13.3.

13.3 Discussion

Currently available hazard assessments of ice avalanches are applicable to already-identified problematic zones only (e.g. Margreth and Funk, 1999; Margreth et al., 2011; Pralong et al., 2005). In the present study, however, a more future-oriented approach was established, based on understanding of the glacier's dynamics. Correspondingly, little reference work is available for direct comparison of the methods or results. To compensate, findings from the analysis of variance presented in the previous chapter are considered in the discussion.

Data, method and results

The ice-avalanche volumes elaborated in the present study fit into the range of empirical values gathered by Schneider et al. (2011), which were also applied as a reference for scenario definition by Schneider et al. (2014). The rating of the scenarios however, was not in line with Schneider et al. (2014), whose ice-avalanche volume assumptions per scenario (small, medium, large) were one magnitude higher than the ones from the present study. Their medium scenario already contained ice-avalanche volumes up to 1 million m^3 and initial volume of their large scenario corresponds to the extreme scenario of the present study. These differences are justified in different assumptions regarding the nature of the avalanches. While only ice avalanches were assumed in the present study, Schneider et al. (2014) adapted the volume estimations to combined rock/ice avalanches.

The main effects of initial volume and calibration together with their interactions resulted in the analysis of variance (Chapter 12) to explain roughly between 60% and 70% of the variances in the overtopping wave's characteristics. The definition of these two factors is thus highly responsible for whether a wave overtops or not in Lake 513.

The applied friction and entrainment calibration fit to the 2010 event (Schneider et al., 2014), whose initial volume was assumed to be between 200,000 m^3 and 450,000 m^3 (Table 12.1). The

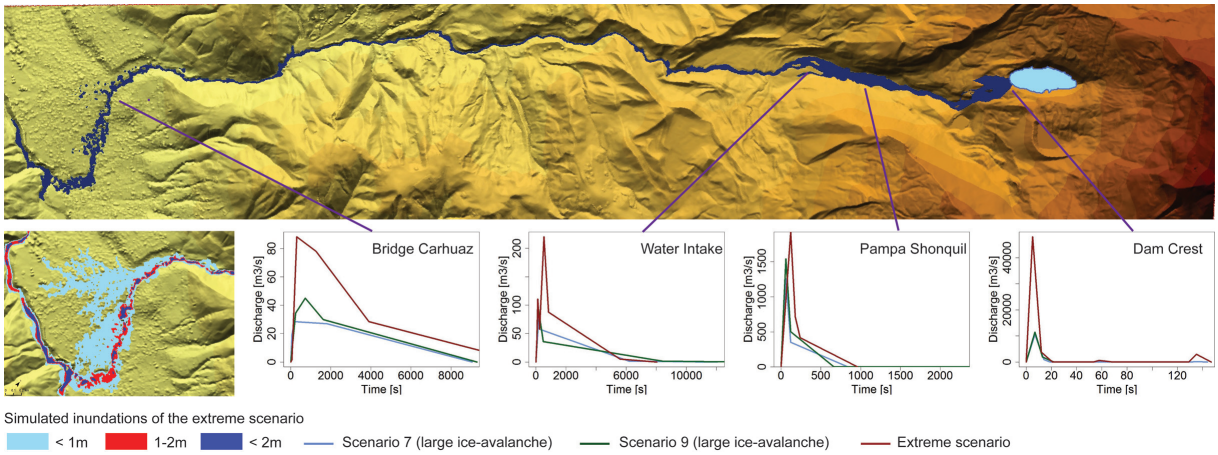

Figure 13.5: Modelled hydrographs of the lake-outburst flows and the inundation simulated in Carhuaz for the extreme scenario. For the scenario number refer to Figure 13.3.

volumes of the small and medium scenarios of the present study were mostly in this range. The corresponding simulation results at the impact in the lake can therefore be assumed to be reliable with regard to the friction values chosen. For the large and the extreme scenarios, however, lower friction could have been assumed (e.g Margreth et al., 2011; Preuth et al., 2010; Schneider et al., 2010; Sosio et al., 2012). This would have been even more justified, as the initial volumes of the ice avalanches corresponded to the upper estimations and it would have been feasible to define lower friction values for the large/extreme ice avalanches. A reduction in friction would have implied even higher impact momentum and larger impact waves (Section 12.3.4). From the calibration point of view, the impacts and the overtopping waves are possibly underestimated, also with regard to the number of scenarios including overtopping.
Higher entrainment rates of the ice avalanches would also have been legitimate, especially as basal entrainment only was assumed. Comparisons of the effects can, for example, be found in Margreth et al. (2011), who tested different entrainment parameters in relation to the snowpack stability. But comparison to the analysis of variance might be more informative for the present simulation. The results of the previous chapter indicate that the overtopping volume of large and extreme scenarios might have risen by approximately 10% through changes in entrainment. Entrainment was, however, not considered to raise the number of overtopping waves.
The simulations of the overtopping waves can also be regarded as robust with regard to the transformation of the RAMMS results into IBER input-hydrographs, according to the analysis of variance. Other preliminary assessments, however, doubt the reliability of the mass-conservation principle implemented in the manual method, as it leads to conservative overtopping results (Guillén Ludeña et al., 2014).

For simulation of debris flows, fine DEM in the range of 1-4 m are recommended for detailed hazard analysis (Bühler et al., 2011; Stolz and Huggel, 2008). The present simulation on basis of an 8-m resolution DEM is nevertheless considered adequate for the narrow channel of the Río Chucchun, where topography basically prohibits much spread of the flow. Simulation of the potential affected area on the fan, however, should be interpreted more carefully. This resolution is, though, a rather good basis for such little monitored and investigated areas. More crucial

regarding the accuracy of the outburst-flow simulation might have been the RAMMS calibration, which was discussed by Schneider et al. (2014).

Implications for risk management in Carhuaz

Several conclusions regarding risk management in Carhuaz can be drawn from this ice avalanche hazard analysis. Only large or very large ice avalanches (featuring at least 1 million m^3) are considered capable of triggering an overtopping of the rock dam of Lake 513. A considerable amount of an ice avalanche is assumed to split off and flow towards the smaller, moraine-dammed Lake Cochca. Therefore a detailed hazard assessment of this lake is recommended, first efforts were presented by Schneider et al. (2013).

Considering uncertainties and their propagation through the simulation, especially regarding friction calibration, more than the three overtopping scenarios modelled here are could feasibly affect Carhuaz. This is even more likely if combined rock/ice avalanches are assumed (see the results of Schneider et al. (2014)). But small ice avalanches are unlikely to trigger an outburst event. Due to the topography along the channel of the Río Chucchun, the outburst flow varies in discharge rather than in inundation area. Differences have to be expected for the fan, where only very large ice-avalanche scenarios are assumed to affect large areas outside the river channel.

In the present study it was abstained from transformation of the outburst-flow simulations into hazard maps and from finalizing the risk analysis, because the main features of hazard maps, damage potential and risk in Carhuaz were already presented (Portocarrero, 2013a; Schneider et al., 2014).

Synthesis

Coupling simulations is afflicted with large uncertainties which do have considerable effects on the results, as assessed in the previous chapter. Hazard analysis based on a single simulation run is therefore highly difficult. The application of a simulation chain to a set of scenarios nevertheless allows this study to draw valuable conclusions on the overall hazard situation, as demonstrated in this chapter.

This chapter concluded the part on local-scale hazard assessment of impact wave-triggered lake-outburst flows by combining innovative ice avalanche-scenario development with numerical simulations of the triggered process chain and interpretation of the results under consideration of the uncertainty propagation.

But a hazard analysis is not an ending point. It is the base and input for a risk analysis, which is the topic addressed in the next part.

Part IV

Advancing and expanding consequence analyses and risk estimations for high-mountain lake-outburst events

The Parts II and III addressed specific gaps with regard to the first objective of the thesis. The first objective was to improve systematic analysis and anticipation of hazard potentials emerging from high-mountain lakes within the framework of integrated risk management.
The second objective of the thesis is to improve and expand consequence analyses and risk calculation approaches with regard to high-mountain outburst flows, also considering future conditions. This objective is treated in the present section, in which selected issues of damage potential and risk estimations regarding high-mountain lake-outburst events will be treated.
Firstly, quantification of all costs caused by the 2008 lake-outburst event in Grindelwald, Switzerland, is presented (Chapter 14). Secondly, a method for conducting future-oriented risk estimations considering future hazards and land-use changes will be presented, with the help of a modelled overdeepening (which is assumed to be a potential location of a future lake) above the town of Naters, Switzerland (Chapter 15).

CHAPTER 14

COST ASSESSMENT OF A LAKE-OUTBURST FLOW IN GRINDELWALD WITH REGARD TO TOURISTIC INFRASTRUCTURE

Lake-outburst events can cause disasters with consequences reaching farther than the directly affected area, as illustrated with some examples in Section 2.1. Correspondingly, inclusion of the direct costs only into risk analyses is not always adequate. In Switzerland, for example, the loss is defined as the value of exposed objects and the number of persons exposed. A complete cost assessment considers, along with the direct costs, the indirect, intangible, business-interruption and risk-reduction costs (see Section 3.2.2).
The present chapter treats the research question, "Can a complete costs assessment be carried out as part of a practical application to a lake-outburst event?". For this purpose, the damage potential estimations, loss and costs caused by a lake-outburst flow in Grindelwald in 2008 will be reprocessed with special focus on the touristic infrastructure.

The main text and some illustrations reproduced here were originally published by Lehmann Friedli and Schaub (2013) in German, which will not explicitly be referenced any more. The publication of Lehmann Friedli and Schaub (2013) (and the present chapter) constitutes a summary of the study carried out by Lehmann Friedli (2013), where the methodology and the results are described in more detail. The present chapter picks up and reflects upon some of the main outcomes with regard to the present study. That is why they might, in places, differ from conclusions drawn in Lehmann Friedli (2013).
Based on a collaboration with Therese Lehmann Friedli I (Yvonne Schaub) provided a risk managers expertise to complete the tourism-oriented cost assessment. As such, I elaborated the risk management framework for the study in (a) allocation of the costs for loss and risk-reduction measures accordingly (summarized in Table 14.3), in (b) elaboration of the structure of the work

and in (c) the discussion and interpretation of the results. I further actively participated in (d) the paper writing and editing process.

14.1 Grindelwald case-study description

Grindelwald (also known as the Eiger village) is a place in the Swiss Alps at 1,050 m a.s.l. It is a lively community, frequently visited by mountaineers and visitors from all over the world, thanks to its affiliation with the Jungfrau-Aletsch UNESCO World Heritage Site. This makes Grindelwald one of the most important tourism centres in the Bernese Alps (Lehmann Friedli, 2013).

The lower Grindelwald glacier has decreased strongly in mass and length during the last 150 years. As one consequence, a lake formed in 2007 on the flat tongue of the glacier, which featured a volume of 240,000 m^3, and that increased to 2.6 million m^3 in 2009 (Werder et al., 2010). This lake was also partially dammed by deposition of a rock-slope failure which occurred in 2006, when 172,000 m^3 of rock detached from the east flank of the Eiger (Oppikofer et al., 2008). This lake formed in a highly dynamic environment and was affected by further slope failures. Parts of the lateral moraine regularly impacted the lake, but never caused the lake to burst out (NELAK, 2013). However, on 30^{th} May 2008, 800,000 m^3 of water drained progressively and temporary blockages caused four waves with peak discharges up to 110 m^3/s (Fig. 14.2). As a consequence, a tunnel was constructed in 2009/2010 to control the lake level (Gletschersee, 2012).

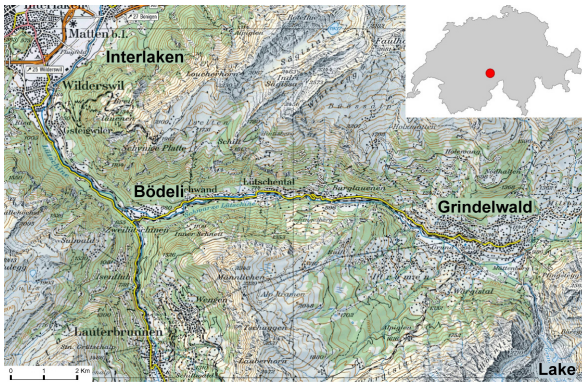

(a) Location of Grindelwald in Switzerland.

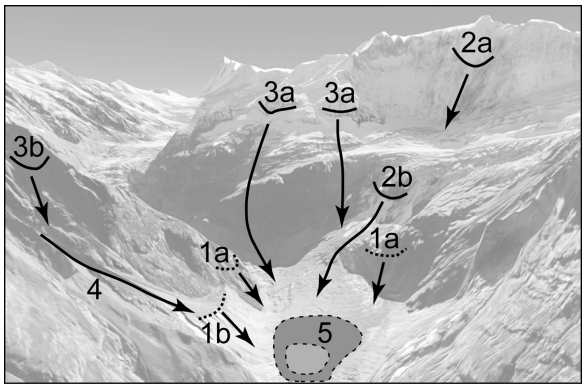

(b) Hazards at the lower Grindelwald glacier (Haeberli et al., 2010a).

Figure 14.1: The case study of Grindelwald. The hazards in Figure b are as follows: (1a) rockslides, (1b) lateral moraine failure, (2ab) ice avalanches, (3a) degradation of permafrost, (3b) rockfall Mättenberg, (4) debris flows and erosion of lateral moraine in warm permafrost, (5) glacier lake.

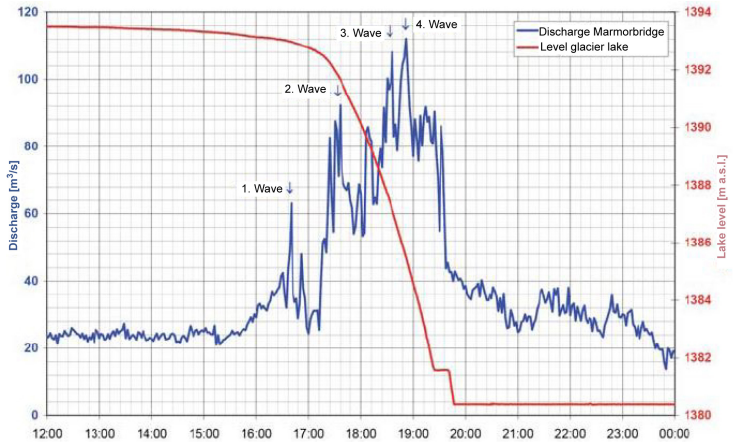

Figure 14.2: Discharge curve of the lake-outburst event of May 30th 2008 at the lower Grindelwald glacier. The progressive enlarging of the channel was combined with several sudden ruptures after channel blockage. Diagramm: Nils Hählen, Oberingenieurkreis I Kanton Bern, 2008. Figure and Caption from Haeberli et al. (2012).

14.2 Method

For the purpose of the present study, the hazard situation before construction of the tunnel was assumed. As a starting point for cost estimation, the appraisal of the potential direct, primary costs in the region of Grindelwald in the case of a lake-outburst flood without the tunnel (Hählen, 2008) was taken. These direct costs only comprised material assets (infrastructure and buildings). A listing of all kinds of costs presented in Section 3.2.2 was established on the basis of these estimations and related to the phases of a lake-outburst event as presented in Figure 3.2. This compilation is illustrated in Table 14.3, which is explained in the following paragraphs.
To merge the points of view of risk managers and tourism professionals, the damage potential was classified according to the chronological incurrence into primary (at the day of the event), secondary (in consequence of an event) and tertiary (after the event) damages (Weber, 2007). Distinction was made between expected costs through loss (combined as damage potential) and costs for risk-reduction measures. The vulnerability of objects and the lethality of persons were not considered, to keep things reasonably simple and because no risk estimation was attempted. The exposure scenario assumed the event occurring during touristic high season in July, and the study area also included the entire catchment of the River Lütschine down to Bödeli and Interlaken, next to the destination Grindelwald (see Fig. 14.1a). The hazard scenario assumed was an inundation along the River Lütschine as a consequence of a lake outburst with peak discharges of 200 m^3/s.
On this basis, the secondary and tertiary costs for tourism were estimated with the help of experiences gained from the strong avalanche activities in 1999 in Switzerland (Nöthiger, 2003) and from the flooding event in Engelberg in 2005 (Weber, 2007). These cost estimates were evaluated in an expert hearing by four persons who work in fields concerned by the 2008-outburst event (see Lehmann Friedli (2013) for more details).

14.3 Resulting costs

The total damage potential resulted from the direct, primary damages analysed by (Hählen, 2008) and from estimates on the secondary and tertiary damages as described in the previous section. The hazard situation before construction of the tunnel was assumed.

14.3.1 Expected costs through loss without the tunnel

Given the above-described situation, 80% of the primary damage caused in the phase during the event (Phase 2, Table 14.3) is located in the area of Bödeli and 6% in the community of Grindelwald. The estimated direct costs in Grindelwald amount to 3.1 million Swiss francs and are mostly composed of damage to buildings and to touristic infrastructure. The latter is composed of:

- Railway station and several railway tracks
- Two camping sites
- Valley station of the cable car (including the carpark)
- Access road to Grindelwald and several local roads
- Hiking trails along the river Lütschine

The direct damage potential resulted in 92 million Swiss francs. Expenses were incurred on buildings (65.7 million Swiss francs) as well as on roads and railway tracks (26.3 million Swiss francs) (Hählen, 2008). The extended primary damage potential on touristic infrastructure is summarized in Table 14.1.

The expected loss with relevance to tourism is higher than what is declared in Table 14.1, because damages to buildings, roads and railways, which were considered in the direct-damage

Damage potential	**Cost unit**	(CHF)	**Total** (CHF)
Car parking and Railway station	apiece:	30,000	6,000
(July: 200 cars, 5 motor coaches)	Coach:	300,000	1,500,000
	Car:	20,000	4,000,000
Camping sites	apiece:	50,000	100,000
(July: full occupancy, 66 residence and 108 touristic places)	Caravan:	30,000	1,980,000
	Tent:	1,000	100,000
Hiking trails along the river Lütschine	per m:	200	2,000,000
Damage to shorelining (several km)		2,500,000	
TOTAL			13,700,000

Table 14.1: Estimation of the extended primary damage potential regarding touristic infrastructure in case of a lake-outburst event. CHF = Swiss francs.

potential, would also strongly affect tourism. In total, four-fifths of the direct damage potential refers directly or indirectly to tourism.

In a next step, the secondary damages involving business interruption and indirect costs during or in direct consequence of the event were estimated (Phase 3a in Table 14.3). The estimation of costs was based on past event analyses, for instance from the flood in Engelberg in 2005 (see Weber (2007)). The following assumptions were made for the analysis:

- 14-day interruption of traffic on the road to Grindelwald in July
- 14-day interruption of the railway tracks to Grindelwald Dorf, simultaneously
- 14 days of strong disturbances on the roads in the areas of Interlaken and Bödeli, resulting in reduced operation of industry and service

For Grindelwald the touristic sales per year were assumed to be 350 million Swiss francs, to calculate the expected loss per day (Table 14.2). The same amount can be applied to Interlaken because of the similar amount of overnight stays. In Interlaken, the sales per day, however, have a smaller result than for Grindelwald, because Interlaken has a longer high season.
The secondary damage potential amounts to at least 36 million Swiss francs. This estimation constitutes probably the lower limit, because the assumption on the duration of interruption would have to be extended for certain businesses (Hählen, 2008). The railway station and the adjacent tracks would, for instance, be completely destroyed in case of such an event. This could lead to a complete interruption for up to three months.

Overall the tertiary damage (Phase 3b in Table 14.3) can only be assessed descriptively. Analyses of the strong avalanche activities in winter 1999 (Nöthiger et al., 2002) showed that the number of day trippers immediately and precipitously reduced in the month of occurrence. Some of the month's overnight visitors were already on location, but their number decreases continuously as a consequence of the event, upon which the inland tourists leave before the foreign ones. Furthermore, some tour operators might temporally remove the destination from their range. The short-term low-point in overnight stays, however, is only reached after disarming of the situation. After recovering from the event, domestic overnight tourism recovers faster than international tourism: foreign visitors generally hesitate longer in booking. The number of day trippers can, however, rise immediately upon re-opening of the transportation routes, because of gawkers.
As a consequence of such an event, the image of a tourist destination is likely to change, which

Damage potential	**Assumptions / Unit**	**Total (CHF)**
Business interruptions Destination Grindelwald	CHF 350 million sales per year and 250 days high season in tourism- 1,400,000 CHF/day	19,600,000
Business interruptions Region Bödeli	CHF 350 million sales per year and 300 days high season in tourism - 1,170,000 CHF/day	16,330,000

Table 14.2: Top-down calculations of the secondary damage potential with relevance to tourism through business interruptions. CHF = Swiss francs.

does not necessary implicate loss. The media push the destination into the public interest with shocking news; as a long term-effect, however, the name of the destination tends to stay in memory (Weber, 2007). This leads to a normalization of the overnight stays at some point without effects of compensation. The event of a lake outburst, however, can in this regard not be compared to a normal inundation if the event repeats regularly. Such subsequent events would increase uncertainty and cause a lasting negative image.
The costs for potential, tertiary damages can raise up to several million Swiss francs during high season (Weber, 2007). This effect would be especially strong in the case of Grindelwald, due to the expected decrease of foreign tourism: 2.5 times more international than domestic tourists stay overnight.

14.3.2 Costs of risk-reduction measures

Risk-reduction measures can be divided into several parts, in line with integrated risk management illustrated in Figure 3.2. In the following, the risk-reduction measures applied in Grindelwald with regard to the outburst event in 2008 will be discussed.
Emergency provisions mainly aim at mitigation of fatalities (BABS, 2013). The unclear situation before construction of the tunnel provoked high costs for the corresponding emergency provisions (Phase 1 in Table 14.3). A warning system was set up, which caused high expenses for both public and private stakeholders. The cantonal spendings on technical surveillance, warning- and alarm deployment as well as for expertise amounted to roughly 350,000 francs per year for the entire region. Most of the costs were incurred by Grindelwald. The communities were burdened with personnel costs for the surveillance and emergency planning. In Grindelwald the corresponding expenses amounted to several thousand Swiss francs per year. Assuming a situation of threat for five years, would result in total costs of about 3 million Swiss francs.
Reconditioning and reconstruction costs for clearing and reparation (Phase 3a in Table 14.3) of buildings are, in Switzerland, usually included in the buildings' insurance policies in the amount of 10% of the loss amount (GVB, n.y.). In the case of Grindelwald, reparation costs were also assumed to be 10% of the damage to buildings and thereby amounted to 6.6 million Swiss francs. These costs do not consider missing person-days, because that information was not available for the analysis. Efforts of the army, air force, fire fighters and the road service department are included in the personnel costs of the community, canton and the state and are hence not explicitly shown in this analysis either (Nöthiger, 2000). Also not explicitly shown

	Uncertainty of Tourists		Image transformation	
	Short-term (Following month)	**Short-term** (Two monthes later)	**Mid-term** (one year later) **without** protection constructions	**Mid-term** (one year later) **with** protection constructions
Daytrippers	↗	↗	→	→
National overnighters	↘	↗	↘	→
International overnighters	↓	↘	↘	→

Figure 14.3: Tertiary damages. Possible variations in frequency in the short- and middle-terms.

are workplace absences of volunteers assisting in the disaster zones.
One consequence of inundation scenarios with peak discharges around 200 m^3/s, would be deposition of large amounts of bed load, because the river Lütschine would have to open new tracks. The costs for removal would amount to approximately 2.5 million Swiss francs, assuming a minimal deposition volume of 100,000 m^3 (outburst event in 2008: 600,000 m^3).
After the event in 2008, a tunnel was built to prevent another outburst. It is 2 km long and costs of construction were 15 million Swiss francs. The tunnel allows for control of the lake level during the melting period. Up to now, the tunnel has proven itself, and only minor adaptations are foreseen. The entire area is highly dynamic, and is still intensively monitored (Gletschersee, 2012).
In total, the expenses for risk reduction measures summed up to at least 28 million Swiss francs.

14.3.3 Comparison of all costs

Compared to the annual touristic sales of 700 million Swiss francs in Interlaken-Grindelwald, the secondary damage potential with a height of 36 million Swiss francs amounts to 5% of these sales in the scenario of a lake outburst without tunnel. The reporting of the situation before the construction of the tunnel in Europe certainly caused an advertising effect. The uncertainty caused by the negative reports made tourists hesitatant and produced a negative image change, which had to be compensated by huge efforts in marketing. These efforts can easily lead to sales shortfalls of 10%. The secondary and tertiary damage potential amount in additional costs at the height of two-thirds of the primary damage potential, which is illustrated in Figure 14.4.
Even though the expenses for risk reduction – in total 28 million Swiss francs – seemed high, they only amount to four-fifth of the entire damage potential (Fig. 14.4). From this comparison

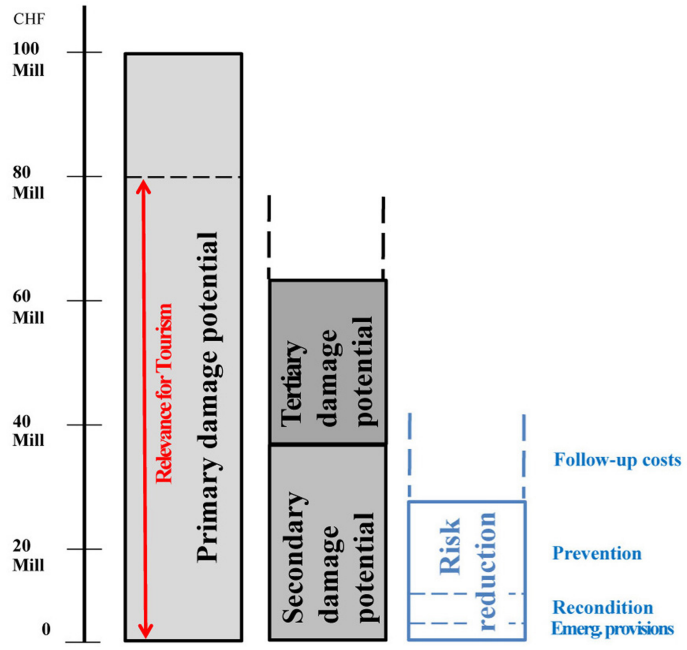

Figure 14.4: Comparison of the primary to the secondary and tertiary damage potential and to the costs for risk reduction measures. CHF = Swiss francs.

it can, however, not yet be concluded that the risk-reduction measures were cost effective, as important elements of risk analyses were not considered, such as vulnerability and lethality.

14.4 Discussion

Method and Results

In this chapter a study was presented which aimed to quantify all kind of costs caused by a lake-outburst flow and to compare them to each other. The research question treated was, "Can a complete costs assessment be carried out as part of a practical application to a lake-outburst event?". The study was carried out with the help of the case study of a lake outburst in Grindelwald, and focused strongly on touristic aspects.

The study results show that it is possible to estimate and quantify costs almost entirely. This assessment was possible thanks to the well-documented analysis of the 2008 event and because of experiences reported from comparable incidents. The available knowledge could also be applied to potential outburst events, at least in a well-documented country like Switzerland. For countries where events are documented to a lesser extent, a complete cost-assessment might be more difficult.

The application of the cost-classification according to Meyer et al. (2013) to risk analyses turned out unfavourable, as costs for risk reduction measures are not meant to flow into the risk analysis but are separately assessed during evaluation of risk-reduction measures. The approach was therefore adapted and the study distinguished among primary, secondary and tertiary damage as well as risk-reduction costs (according to Weber (2007)). The investigated costs for business interruption, indirect and intangible costs were considerable, which supports the critique that including direct costs only into the consequence analysis is not adequate, especially for tourism destinations.

Relevance for integrated risk management

Accounting for the entire range of (potential) cost caused by a lake-outburst flow is further important with regard to integrated lake management. It facilitates a more adequate cost-distribution to the different stakeholders and might thereby bring more parties into the decision-making processes. This shared responsibility might support the elaboration of multi-purpose (risk-reduction) measures, which might further facilitate the better embedding of risk management into a more integrated lake management. This management aspect will be further discussed in the final Part V of this thesis after having taken the future-oriented hazard assessment perspective into account in the next chapter.

P	Moment in time / Duration	**Expected costs through loss** (damage potential)	**Costs for risk-reduction measures**
1	*Threat situation* (without protective structures)		**Emergency provisions** • Expertises • Alert and evacuation strategy
2	*The day of the event*	**Primary damage** *(a)* • Buildings • Transportation routes **Extended primary damage** *(a)* • Car parkings • Camping sites • Valley station of the cable car • Hiking roads • Supply and services • River shorelining	
3a	*During and in direct consequence of the event*	**Secondary damage** • Business interruptions (e.g. through blockage) *(c)* • Follow-up costs (e.g. raising insurance rates) *(b)*	**Intervention** *(e)* • Preparations of personnel and material for intervention (e.g. sandbags, operation schedules) • Evacuation **Recondition and reconstruction** *(b)* • Clearing and reparation (of buildings, man-days of task-forces (army, etc)) • Removal of flood depositions
3b	*After the event* (mid-term effects)	**Tertiary damage** • Business interruptions because of uncertainties (insufficient information, missing accessibility, etc) *(c)* • Image transformation *(d)*	
4	*Improvement and development* (with protective structures)		**Prevention** *(e)* Construction of protective structure • Investment • Operation
1	*New threat situation*		**Follow-up** costs *(e)* • Reparation of structures • Follow-up investments • etc

Table 14.3: Phases (P) of the threat situation (after Figure 3.2 in Section 3.1) caused by the lake-outburst event in Grindelwald and allocation of the corresponding costs for loss and for risk reduction measures according to BABS (2013); Weber (2007). Classification of costs after Meyer et al. (2013): (a) direct costs, (b) indirect costs, (c) business-interruption costs, (d) intangible costs, (e) risk-reduction costs

CHAPTER 15

DAMAGE POTENTIAL AND RISK ESTIMATION FOR FUTURE CONDITIONS WITH THE EXAMPLE OF NATERS

In Chapter 3 the procedure for damage potential and risk estimation was presented. The available assessment methods or guidelines aim at taking the current status, especially with regard to damage potential assessment. One of the challenges of anticipatory risk management is, however, to integrate future physical hazards with future damage potential, given future socioeconomic conditions. To project socioeconomic conditions and exposure into the future, land-use modelling is typically applied, following a number of storylines (e.g. Bouwer et al., 2010). In Switzerland, spatial development scenarios have been generated at national scale (Wissen Hayek et al., 2011), a set thereof was presented in Chapter 9 and discussed with regard to the relevance of the long-term rock-avalanche impact susceptibility of high-alpine lakes in Switzerland. Yet, downscaling of the scenarios to the scale and purpose of local land-use scenarios for risk estimations remains challenging.

This chapter is based on a study published by Nussbaumer et al. (2014), which aims at reduction of important existing gaps with respect to local-scale future risks from lakes in deglaciated areas. If not referenced otherwise, figures are from Nussbaumer et al. (2014). This chapter, however, picks up and reflects some the main outcomes with regard to the present study.
This paper emerged from the Diploma Thesis of Souria Nussbaumer, which I (Yvonne Schaub) accompanied as her direct supervisor. As such I contributed to reflections on research questions, methodology and discussion of the results, mainly with regard to risk management aspects. Within the paper writing process, I provided much of the background on risk estimations, finalized illustrations and incorporated many reviewers comments, such as the comparison of the two risk matrices.

The method presented is concentrating on the case study of the Grosser Aletsch glacier region and therein on the community of Naters. The objective of this study was (1) to develop a feasible

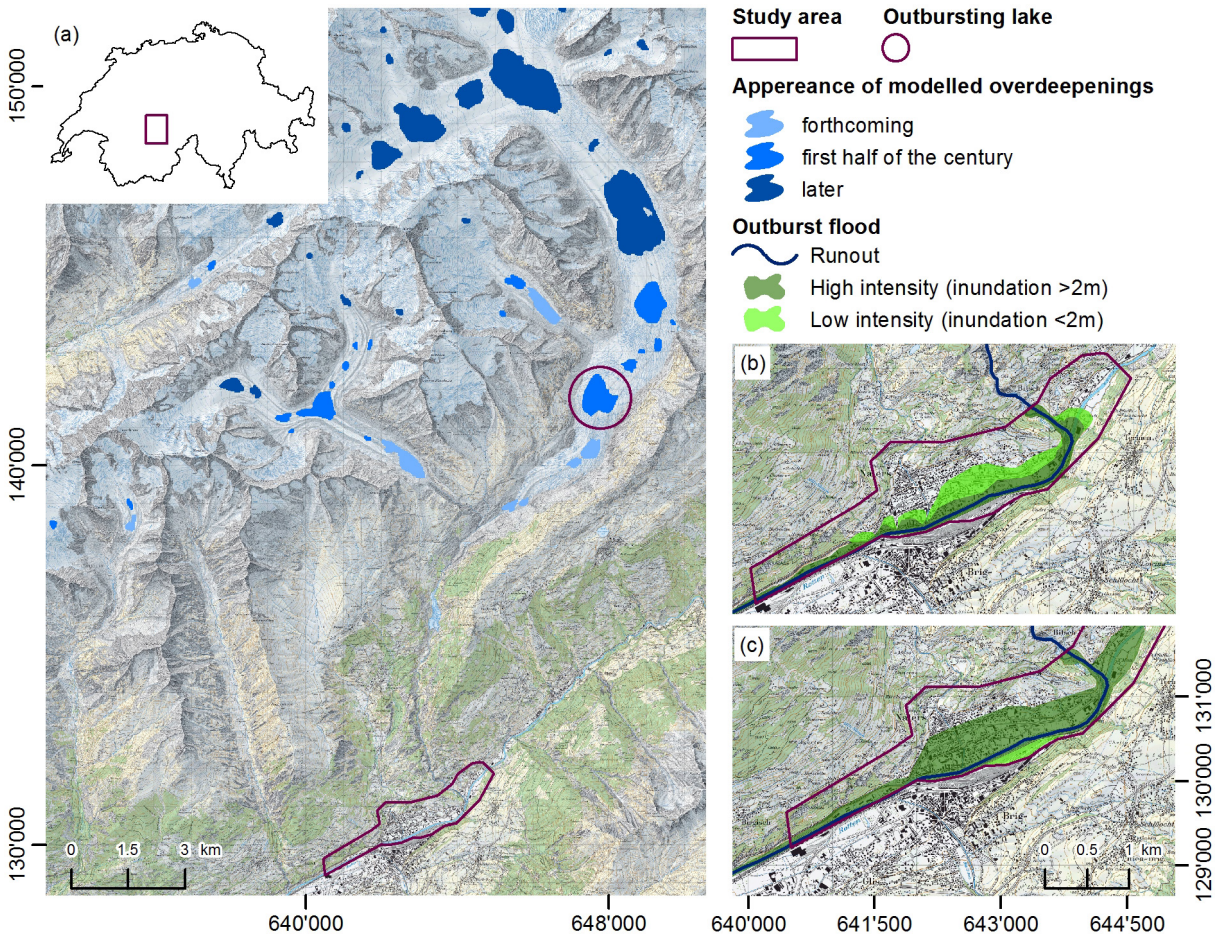

Figure 15.1: (a) Location of the risk study area in Naters, Switzerland and of modelled overdeepenings in the glacier beds in the Aletsch glacier area, which are assumed potential sites of future lake formation (Linsbauer et al., 2013). Integration of the intensity maps elaborated for the outburst scenarios of 4 million m^3 (b) and 20 million m^3 (c). DEM25 reproduced with permission of swisstopo (BA110005).

methodology for the evaluation of future risks related to GLOF hazards for a local Alpine setting by assessing changes in hazards and land-use; and (2) to apply the methodology to the case study of Aletsch/Naters (Valais, Switzerland). Both, the methods and the results should be of use for medium- to long-term planning, and allow anticipating risk reduction. Accordingly, the two time horizon addressed are the years 2021 and 2045.

Naters is a municipality in the canton Valais in Switzerland at an altitude of 673 m a.s.l. It is a typical Swiss dormitory town, most of the people work in bigger towns nearby. In the last decade a considerable increase in population has taken place, as Naters has become a zone of attraction, especially to people from adjacent small villages. About 90% of the Naters' 8,300 inhabitants live in the valley bottom where also extensive agriculture is conducted. The valley is crossed by the rivers Rhône and Massa and surrounded by steep slopes (Swisstopo, 2010) (Fig. 15.1a). The Massa flows to Naters from the reservoir lake Gibidum, which retains the melt water of the Aletsch glacier.

15.1 Data and methodology

In order to estimate the risk of a GLOF in Naters under future conditions, a three-step methodology was developed (Fig. 15.2a). First, socioeconomic scenarios were generated and different driving forces were identified and quantified. This information was implemented in a second step into the land-use scenario modelling. Finally, scenario-based land-use transitions were combined with flood hazard to risk estimations.

Interviews with local authorities were conducted in July 2011 to better understand processes and limitations of land-use changes in the municipality of Naters. Interviewees represented the local planning department and the government of Naters.
Spatially explicit storylines of future land-use changes within the region were modelled on the basis of national survey data from the two survey periods 1979-1985 (BFS, 1986) and 1992-1997 (BFS, 1998). The Swiss land-use statistics differentiate between 45 categories, which were reclassified into nine classes (Table 15.1) identified as most relevant for risk assessment within this study, namely "multi-family house", "single-family house", "mixed-use" (such as business buildings or parks), "industry", "railway", "roads", "agriculture", "forest" and "unproductive area" (such as water bodies or bedrock).
The Swiss land-use statistics were complemented until 2009 through mapping of land-use changes based on a field survey, the interviews with local authorities and the most recent topographic maps (Swisstopo, 2010).
Estimation of economic values of the different land-use classes were adopted from the official Swiss platform for assessment of efficiency of protection measures against natural hazards "EconoMe" (BAFU, 2010). The visualization of the socioeconomic scenarios and the lake-outburst flow modelling rested upon the digital elevation model with 25m accuracy (DEM25), provided by Swisstopo (2010).

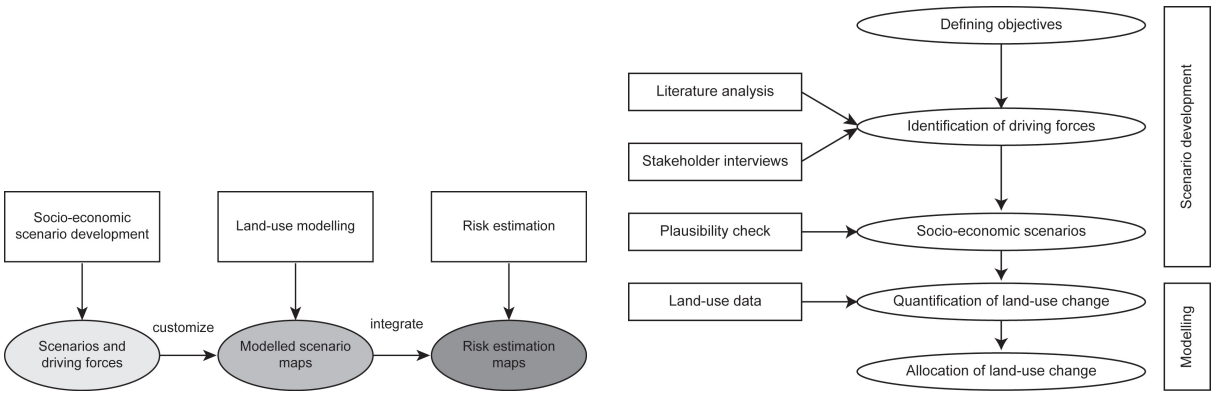

(a) Simplified overview of the methodology. (b) Procedure for generating scenarios.

Figure 15.2: Methodology

15.1.1 Socioeconomic scenario development for land-use changes in Naters

The exploratory scenarios (c.f. Carter et al., 2001) were developed (Fig. 15.2b) following the approach of Wissen Hayek et al. (2011). The goal of the present scenario development was to elaborate plausible land-use storylines for the municipality of Naters until 2045 which cover a wide range of fundamental uncertainties in regional socioeconomic development and associated land-use changes. The extrapolation of the current state of land-use served as a baseline scenario.
The most relevant drivers of regional development, land-use changes and the potential development pathways for Naters were identified based on a literature review (Hiess, 2010; OcCC, 2007; BUWAL, 2003; IPCC, 2012; Voigt et al., 2010), as well as on interviews with representatives of the local planning authority and government (oral statements Holzer (2011); Michlig (2011)). The driving forces and the development pathways were then combined to three land-use scenarios. The scenario storylines could per se not be validated, but plausibility checks were performed by cross-checking the scenarios with other scenarios for Swiss mountain regions (ARE, 2008; Leitungsgruppe des NFP 48, 2007; Walz et al., 2007; Wissen Hayek et al., 2011).

15.1.2 Land-use modelling: quantification and allocation of changes

Similar to other studies (Walz et al., 2007) land-use modelling was performed by first quantifying land-use transition rates and then allocating the changes in space.

Reclassified land-use classes	**Description (original land-use class number)**
Multi-family house (MFH)	Multi-family houses, backyards (27, 47)
Single-family house (SFH)	Single-family houses, agricultural buildings, backyards, allotment gardens (25,28,45,52)
Mixed-use (Mix)	Mixed-use, backyards, sports areas (29,49,51)
Settlements	MFH, SFH, Mix
Industry (Ind)	Industry, industrial railways, repositories, diggings (21,41,64,65)
Railway (Rail)	Train station area, railways, green areas (35,36,67)
Roads (Road)	Roads, Parking lots, green areas (33,34,68)
Agriculture (Agri)	Sparse orchards, gardenings, meadows, pasture lands (77,78,81,82,83,84,85,86,87,88,89)
Forest (For)	Open and closed forests (11,12,13,14,15,16,17,18,19)
Unproductive area (Unprod)	Glaciers, Water, Rocks, open vegetations (90,91,92,95,97,99)

Table 15.1: Reclassification of the land-use classes by (BFS, 2011). The abbreviations will be used further on in the document. To simplify, MFH, SFH and Mix will also be merged to settlements.

Quantification of land-use changes
In the present study, the three socioeconomic scenarios were translated to land-use change rates by a) extrapolation of the observed changes for the trend scenario ["o"] and b) by conditional adaptation of these rates based on the quantification of driving forces in the two further scenarios ["+"] and ["-"]. These scenarios will be explained more in detail in the results in Section 15.2.1. This approach combined the advantages of explorative and rule-based approaches.
Here, land-use transition rates were estimated for two 12-year steps (1997-2009 for validation and 2009-2021) followed by a 24-year step (2021-2045). Because uncertainties increase in future, a 24-year step was chosen instead of two 12-years steps. For this purpose, the observed transition rates from past changes between the two available land-use data sets were first extrapolated for the trend scenarios "o" (BFS, 1986, 1998). These rates were limited to the legal planning constraints in particular relevant for settlement expansion (oral statement Michlig (2011)). For the two further scenarios "+" and "-", rates of land-use change were estimated by quantifying driving forces based on the assumption in the socioeconomic scenarios. Again, these rates were limited to legal constraints. A constant building density was assumed for all cells of the settlement related land-use classes.

Interaction between land-use classes
Land-use classes interacted with each other where expansion of one land-use class happened at the cost of another one. "Agriculture" and "settlements" (including "multi-family houses", "single-family houses" and "mixed-use") as an example interacted strongly with each other. "Forest" interacted with "agriculture" while "industry" and "roads" partly interacted with "settlements". Within "settlements" the increase of "mixed-use" areas was highly dependent on the increase of "multi-family houses" and "single-family houses": An increasing number of inhabitants also requires e.g. more businesses, schools or retreat homes.
The plausibility of the resulting transition rates was tested by comparing the defined rates of change to recent studies of Swiss land-use changes (ARE, 2008; BUWAL, 2003; Hiess, 2010; Leitungsgruppe des NFP 48, 2007; OcCC, 2007; Walz et al., 2007). These studies were also consulted to determine the transformation rates between certain land-use classes (e.g. from "agriculture" to "mixed-use").

Allocation of land-use change
The final step of the land use modelling was to allocate land-use transition across the landscape based on the following

Driving forces	**scenario "o"**	**scenario "+"**	**scenario "-"**
Subsidization agriculture	business as usual	business as usual	cutbacks
Implications for L/U	decreasing agriculture	decreasing agriculture	abandoning agriculture, increasing forest area
Economic situation	stagnation and downturn	stable	downturn
Implications for L/U	moderate increasing construction	strong increasing construction	decreasing construction
Tourism	business as usual	increasing	decreasing
Implications for L/U	moderate increasing businesses	strong increasing businesses	abandoning businesses

Table 15.2: The development pathways of major driving forces and their implications for land-use within the three scenarios "o", "+" and "-".

- Only cells within the current legally defined construction areas could be transformed to any kind of settlement because of legal constraints (ARE, 2008) and because no adaptation of these construction areas was assumed for the future (oral statement (Michlig, 2011)).
- Certain land-use classes were assumed constant (i.e. "unproductive areas", "roads", "railways" or "bridges") due to topography and lifetime restrictions, and certain land-use classes could only be changed into one direction, i.e. "agriculture" to "settlements" and one type of "settlements" into another type of "settlements" (e.g. "multy-family houses" to "single-family houses"). Exception were "roads" and "unproductive areas" within areas with housing settlements, where an aggregation of the buildings provoked a change within the "roads" or "unproductive area" cells transforming them into "settlement".
- The transition into certain land-use classes was determined by the land-use of the neighboring cells to support clustering of same land-use in line with the federal land-use planning guidelines ARE (2008).

For validation the simulated trend scenario between 1997-2009 was compared with the most recent topographical maps based on 2009 aerial photographs (Swisstopo, 2010).

15.1.3 Risk estimation

To finally estimate the risk, the probability of the event and the damage potential are brought into relation with the help of the intensity maps. A qualitative risk calculation approach is not feasible for future conditions due to the many uncertainties involved, therefore a matrix-based risk estimation technique was chosen, as suggested in Section 3.1.

Hazard

Potential locations and approximate volumes of future lakes in the Aletsch glacier area base on recent studies investigating glacier bed topography and simulating glacial retreat over the next several decades. These studies indicate that new lakes with volumes up to 170 million m^3 may form in the area of Grosser Aletsch glacier over the next 100 years (Linsbauer et al., 2013). For the purpose of the present study an outburst of a potential new lake, which is expected to have reached a volume of about 20 million m^3 until 2045, was assumed (Fig. 15.1a). These data were available in GIS format and represented the starting zones for potential lake-outburst flows. The exact lake-outburst mechanisms obviously cannot be predicted but evidence of existing landslides (Strozzi et al., 2010) and an expected further destabilization of slopes, as derived and justified in earlier chapters of the present publication, suggest that impacts from landslides into the lake and therewith produced displacement waves and outburst floods may be a realistic scenario. As outlined in Figure 15.1a, the risk study area concentrates on the Massa river channel and the flat part of Naters, where most people live. It is defined by the intensity maps of potential lake outbursts, including outburst scenarios of 4 million (Fig. 15.1b) and 20 million m^3 (Fig. 15.1c).

Outburst probabilities were not quantified as return periods, for the reasons discussed in Section 3.2.1, but approximated by using outburst scenarios, as suggested by Schneider et al. (2014).

Accordingly, two outburst flood scenarios were defined on the basis of two different outburst volumes for the same lake, 4 and 20 million m^3, representing partial (higher probability) and full drainage (lower probability), respectively. In a first stage a simple flow-routing model was applied (Huggel et al., 2003) to assess the approximate extent of downstream flooding for a lake outburst from the identified lake (Fig. 15.1a). This GIS-based model distributes flow and mass movements downstream according to geometric and topographic criteria, and thus allows to assess areas potentially affected by an outburst flood.
Layers with different flood height intensities were then evaluated in the field and in GIS for each outburst scenario, based on the calculation of the maximum flood runoff after Huggel et al. (2002a) and the flow capacity of open channels and overspill after Henderson (1966). Two different intensity classes were distinguished for each outburst flood scenarios. These classes build on the official Swiss guidelines (Lateltin, 1997), which differentiate between high intensity for an inundation height of <2m and medium intensity for inundation height $\geq$2m (Fig. 15.1b and 15.1c). Eventually, simple flow dynamics were assessed, in particular flow velocities and flow travel times from the initiation of the outburst flow to the impact in Naters. Calculations are based on published lake-outburst flow velocities (Cenderelli and Wohl, 2001; Schneider et al., 2014) considering a flow travel distance of 14 km.

Damage Potential
The four parameters defining the damage potential according to Bründl et al. (2009) have been introduced in Section 3.2.2 as: (1) the exposure probability of an object/person while a scenario is occurring; (2) the spatial probability that an object/person is directly encountered by the scenario; (3) the loss, consisting of the value of the object/number of persons exposed; and (4) the vulnerability of an object/the lethality of a person against the impact of the event. For the here presented future-oriented risk estimation approach, the parameters were treated as follows:
For scenarios in the future a detailed exposure analysis would introduce an unreasonable level of additional uncertainty, and therefore, a constant exposure situation was considered, with all objects and persons expected to be present (e.g. during daytime of a regular working day).
The here considered flood is assumed to appear over the entire area considered in the intensity maps, therefore a spatial probability of 1 is assigned to every object/person and the parameter not further discussed.
The different categories of variable loss (number of objects and persons) were not monetized but classified independent of each other. The values were assigned to each cell of an ArcGIS raster, applying the four-level scale 1="low", 2="medium", 3="high" and 4="very high" (Table 15.3). Scores for the object values were defined according to the EconoMe database (BAFU, 2010). For persons the scores were estimated as a function of the population density per land-use class. Mortality was not considered in this approach, as it is too variable to be adequately implemented for this purpose.
Vulnerability was considered in both aspects, social and physical. To estimate the social vulnerability in Naters the following factors were considered: economic conditions (wealth), age, nationality and insurance cover. The classification into different vulnerability classes was done based on available literature (Nöthiger et al., 2002; Kantonsforstamt, 2011; Burgerschaft, 2011; BFS, 2011; OcCC, 2007) and interviews with community leaders (oral statement (Michlig,

Scale	**Intensity**	**Loss**		**Vulnerability**	
	Inundation	*Object value*	*Persons*	*Physical*	*Social*
1 = low		Agri, For, Unprod	Agri, For, Unprod	Mix, Ind	Agri, For, Unprod
2 = medium	≤2m	Mix, Ind, Road, Rail	Ind, Road, Rail	Road	Road, Rail
3 = high		SFH	SFH, Mix	SFH, MFH, Rail	SFH, Mix, Ind
4 = very high	>2m	MFH	MFH	Agri, For, Unprod	MFH

Table 15.3: Allocation of the assessment variables into a four-level scale. Intensity is defined by the inundation depth. Allocation of the land-use classes differs between object value and number of persons present for loss, and between physical and social vulnerability respectively. For explanation of the abbreviations see Table 15.1.

2011)), which were also used to eventually assign social groups to the land-use categories. According to that, "multi-family houses" are more vulnerable than "single-family houses". Uninhabited land-use categories such as agricultural or forest areas were classified as low social vulnerability (Table 15.3). In addition to the area-wide social vulnerability classification, specific and particularly vulnerable locations were flagged in the final risk map (Fig. 15.6) such as schools, churches or sports ground (Bara, 2010).
Physical vulnerability was defined as the degree of physical impairment an object experiences when affected by a particular hazard process (BAFU, 2010). The values for physical vulnerability are related to the hazard magnitude according to Bründl et al. (2009). The values for physical vulnerability of each land-use class were derived with respect to high-intensity debris flows from EconoMe (BAFU, 2010). In consideration of the unknown development of the physical vulnerabilities in the future (e.g. through variations in construction techniques), a simplified approach was applied using only one set of values independent of the hazard intensity. This definition resulted, for instance, in high physical vulnerability values for land-use categories such as "agriculture", "forest" and "unproductive land-use", even though they are located at the margin of potentially flooded areas. Specifically, the values for "mixed-use", "roads", "industry", "railway" and "unproductive area" were estimated by averaging the EconoMe-values of similar land-use classes (e.g. values for streets (0.7) were represented in EconoMe by values for motorways (0.45), municipal roads (0.65) and rural roads (0.95)). To be consistent with the other semi-quantitative input grids to the final risk assessment, the assigned scores had to be reclassified to a four-level semi-quantitative scale, with EconoMe values of low (zero) to very high (one) vulnerability where zero means no impairment and one means total destruction. The final classification of land-use classes is provided in Table 15.3.

Risk

Risk is a function (product) of hazard and damage potential as outlined above. In this study all variables were classified qualitatively into an ordinal scale ranging from "low" to "very high", which basically inhibits a mathematical multiplication of the values. Instead a matrix-based risk estimation as suggested by Mergili and Schneider (2011) was applied. This method would also allow to compare the outburst hazard to other hazards in the area, as explained in Section 3.2.1. Three matrices according to the first example in Figure 15.3 were composed for vulnerability (axes: social and physical vulnerability), loss (axes: value of objects and number of persons) and damage potential (axes: vulnerability and loss). Each matrix thus spans a space of four by four cells, with each axis ranging from one (low) to four (very high). The allocation of values

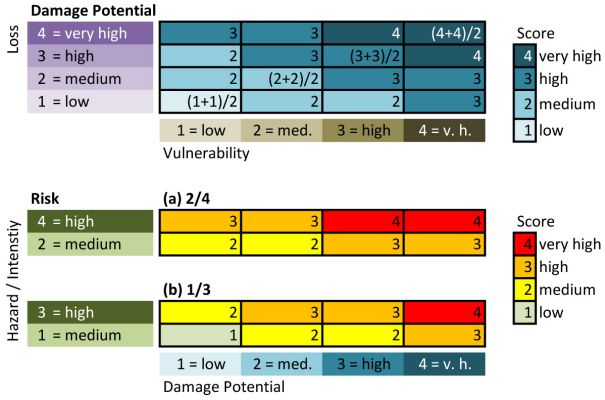

Figure 15.3: Matrix-based definition and weighting of risk classes. The risk parameters loss, vulnerability and the resultant damage potential were assessed according to the first matrix, which illustrates the example of damage potential derivation. Risk was assessed according to the matrices (a) and (b) considering the damage potential and two quantifications of the hazard. The scores are a result of the mean of the value of both axes (rounded), as illustrated by means of four cells in the first matrix.

for each cell in the matrix is based on the average of the corresponding axes values, but actually involves a subjective decision. Therefore, two versions of the final risk matrix (axes: hazard and damage potential) were defined (Fig. 15.3), that should demonstrate the effect of matrix definition on the final risk result.

15.2 Results

15.2.1 Socioeconomic scenarios

The reclassified land-use data set from 1997 showed an increase in "settlements" of +63% or 12 ha and a decrease in the category "agriculture" of -18% or 14 ha as compared to 1985 (Fig. 15.4). These results were confirmed by findings from field surveys, the interviews with the local authorities and recent topographic maps (Swisstopo, 2010), which corroborated the increase of settlements and decrease of agriculture after 1997 in Naters. Based on this, the following factors were identified exerting the strongest influence on land-use changes in settlements and agriculture in Naters and were thus defined as driving forces of the socioeconomic scenarios:

- Agriculture: The steep slopes in Naters with extensive agriculture are currently subsidized by the government. A cutback of the subsidies would lead to abandonment of the agricultural land what would imply growing forest areas as well as an unattractive landscape (Hunziker, 1995), resulting in less tourism in the area.
- Economic situation: Naters has experienced an economic upturn during the last 15 years which, amongst other effects, led to strong and increasing construction works in the area. A possible stagnation of the national economic situation would slow down the construction activities, and a downturn would highly constrain them.
- Tourism: Tourism and economy are closely linked in Naters. An upturn in tourism would imply a strong increase in businesses; a downturn would imply abandoned businesses.

The driving forces and their interactions refer to implications for land-use, which can be consolidated in three scenarios "o", "+" and "-" summarized in the following storylines:

Scenario "o" is a business-as-usual scenario, it represents the continuation of the current trends of land-use until 2045 and is considered the most likely scenarios by stakeholders of Naters. There are no radical changes foreseen in any land-use class. The trend of an increase in the category “settlements” at the expense of "agriculture" in the legally defined zone of construction, which was observed in the past, will continue for the next 10 years. Especially "single-family houses" will rise in numbers, whereas in "mixed-use" a moderate growth is expected. In "multi-family houses" the least increase in settlements is predicted due to compaction of the construction. After 2021 the rate of building construction will correlate with the rate of economic development.
Scenario "+" is marked by a strong increase in building constructions until 2045, particularly within “single-family houses” and “mixed-use”, as a consequence of a stable and prosperous economic situation. The growing tourism sector will benefit from winters with less snow, since parts of the municipality Naters include high-elevation winter tourism areas, which are likely to attract tourists who used to visit skiing destinations located at lower elevations. This development will lead to an increase in business constructions as well as in new public buildings, such as schools or retirement homes. The area within the current construction zone not yet covered with buildings will be developed on a constant rate until 2045.
Scenario "-" is characterized by a decrease in construction activities from 2021 on due to an economic downturn. However, a few settlements will still be built, such as public buildings and “single-family houses” by people not negatively affected by the economic crisis. The tourism sector will decrease, implying abandonment of businesses locations. Furthermore, subsidies to agriculture will no longer be provided by the government. As a consequence, forest areas will increase and landscape may lose attractiveness, which again might result in a decrease in tourism.

15.2.2 Land-use modelling: quantification and allocation of changes

All simulations showed an increase between 3% and 40% in "settlements" (consisting of "multi-family houses", "single-family houses" and "mixed-use") for all scenarios over the entire time span. The increase of these change rates, however, slowed down after 2009 (Table 15.4). In all scenarios "agriculture" was modelled to lose even larger areas in future time spans than during past decreases. Correspondingly, 18% - 37% of the new settlement development took place on formerly agricultural land. "Industry" was projected to decrease in the scenarios "o" and "+" until 2045. "Forest", "unproductive area", "railway" and "roads" did not experience important changes between past and future time spans in any scenario. Generally, the rate of increase in specific land-use classes slowed down with time due to the absolute growth of their respective areas. The scenarios "o" and "+" introduced the same changes in all land-use classes until 2021, afterwards their development started to differ. Scenario "-" developed independent characteristics from the beginning of the modelling (2009) as it is the only scenario including economic downturn.
The results of the allocation of the scenarios for the year 2045 are shown in Figure 15.4 and compared with land-use in 2009. All scenarios implied changes in similar land-use classes, mainly

in "settlements". The changes mainly occurred at the expense of "agriculture". The strong increase in "single-family houses" occurred in the eastern and the northern parts of Naters, where construction was legally approved after 1997. Particularly in the scenario "+" the total number of cells increased about 29% and 33% up to 2021 and 2045, respectively, while "multi-family houses" expanded and aggregated in the area along the river Rhône at the southern border of Naters. This development was similar for all scenarios up to 2021, where the total number of cells increased about 10% - 13%. After 2021 however, this development only continued in the scenarios "o" and "+" (8% and 17%), while multi-family house construction stopped in scenario "-". The same development was also modelled for "mixed-use", where already existing zones expanded along the river in addition to increasing "mixed-use" areas in the center of the village. Change rates amounted least in the scenario "-" (+9% and +3%) and highest (+15% and +16%) in the scenario "+" in both time steps.

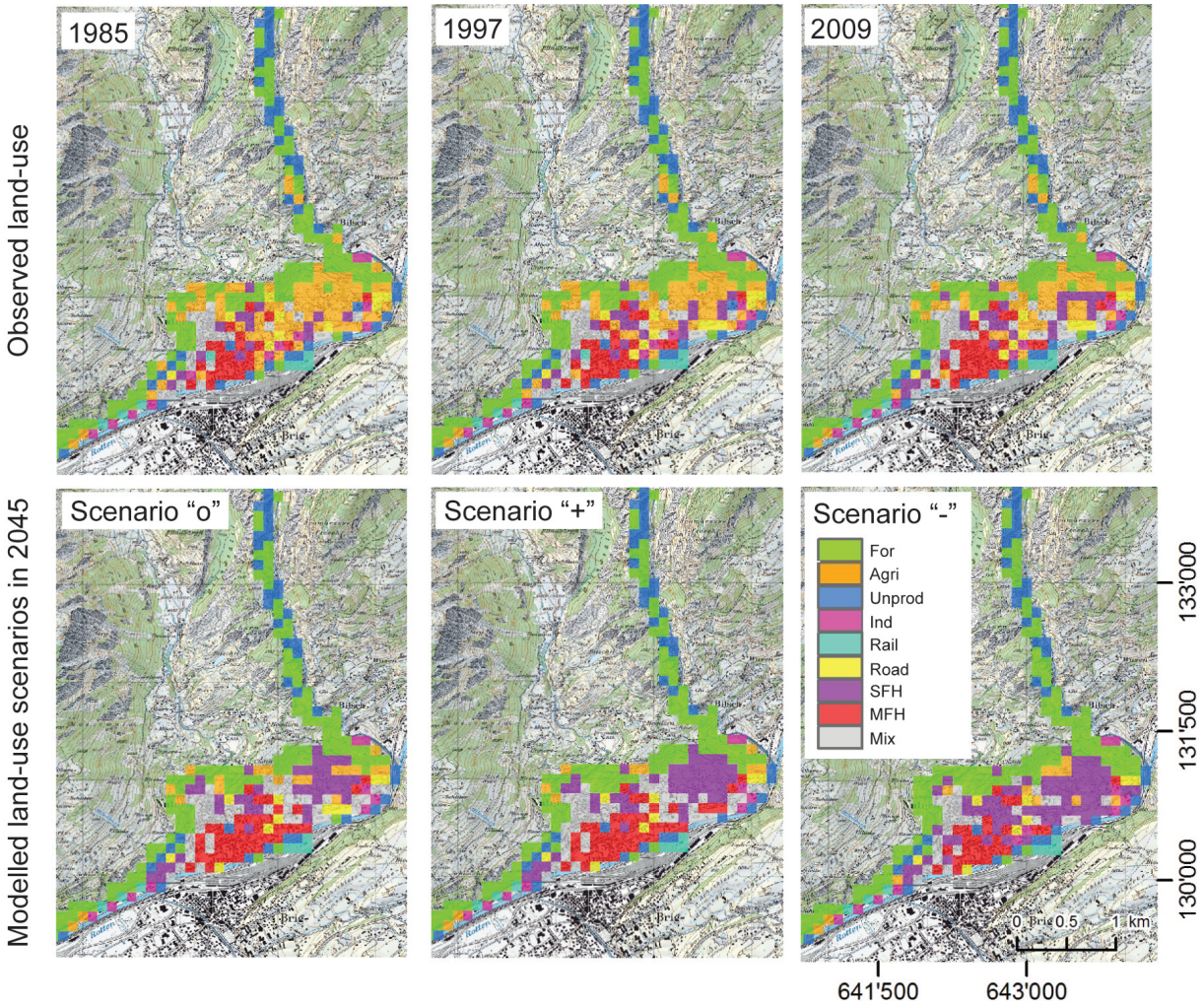

Figure 15.4: Reclassified land-use data sets of 1985, 1997 and 2009 in Naters (upper row). Modelled land-use scenarios for 2045 (lower row). DEM25 reproduced with permission of swisstopo (BA110005) and BFS (1986, 1998). For explanation of the abbreviation see Table 15.1.

Timespan		**1985 - 1997**	**1997 - 2009**	**2009 - 2021**			**2021 - 2045**		
Scenarios		"o" / "+" / "-"	"o" / "+" / "-"	"o"	"+"	"-"	"o"	"+"	"-"
MFH	a	*+13%*	*+19%*	*+13%*	*+13%*	*+10%*	*+8%*	*+17%*	-
	b	*7.1%*	*8.1%*	*9.5%*	*9.5%*	*8.9%*	*10.2%*	*11%*	*8.9%*
SFH	a	*+33%*	*+40%*	*+29%*	*+29%*	*+18%*	*+14%*	*+33%*	*+9%*
	b	*5.3%*	*7.4%*	*9.5%*	*9.5%*	*8.7%*	*10.8%*	*12.6%*	*9.5%*
Mix	a	*+17%*	*+18%*	*+15%*	*+15%*	*+9%*	*+11%*	*+16%*	*+3%*
	b	*7.4%*	*8.7%*	*10%*	*10%*	*9.5%*	*11%*	*11.6%*	*9.7%*
Ind	a	**-8%**	**-8%**	**-18%**	**-18%**	-	**-8%**	**-8%**	-
	b	**3.2%**	**2.9%**	**2.3%**	**2.3%**	2.9%	**2.1%**	**2.1%**	2.9%
Rail	a	-	**-11%**	-	-	-	-	-	-
	b	2%	**2.1%**	2.1%	2.1%	2.1%	2.1%	2.1%	2.1%
Road	a	*+13%*	**-6%**	*+7%*	*+7%*	-	-	**-19%**	-
	b	*3.5%*	**3.2%**	*3.5%*	*3.5%*	3.2%	3.5%	**2.7%**	3.2%
Agri	a	**-18%**	**-20%**	**-33%**	**-33%**	**-24%**	**-37%**	**-37%**	**-36%**
	b	**18.2%**	**14.7%**	**10.2%**	**10.2%**	**11.5%**	**6.9%**	**5%**	**7.9%**
For	a	*+<1%*	*+<1%*	*+<1%*	*+<1%*	*+<1%*	*+2%*	-	*+7%*
	b	*35.2%*	*35.5%*	*35.7%*	*35.7%*	*35.7%*	*36.2%*	35.7%	*38.3%*
Unprod	a	-	**-3%**	**-2%**	**-2%**	-	-	-	-
	b	18.1%	**17.5%**	**17.2%**	**17.2%**	17.5%	17.2%	17.2%	17.5%

Table 15.4: Changes in land-use for each scenario as a result of quantified driving forces, whereby bold indicates an increase and italic a decrease of the area. Each value in every time period relates (a) to the total number of cells of the previous time span and (b) to the percentage of land-use class of the total area per time span. For explanation of the abbreviations see Table 15.1.

15.2.3 Risk estimation

The flood intensity estimations showed (Figs. 15.1b and 15.1c) that the biggest part of the study area will be affected in case of an outburst flow, independent of the outburst scenario (4 or 20 million m^3). The height of the flood varies between 1m and approximately 14m in narrow passages. In both outburst scenarios a maximum estimated retention volume of 2 million m^3 by the barrier lake Gibidum was considered. Thereby, a 1.5 million m^3 flood draining through Gibidum lake would cause high flood intensities (inundation heights >2m) in Naters. Accordingly, high flood intensities were mapped for half, and for most of the area affected in case of an outburst flood of 4 million m^3 and of 20 million m^3 respectively. Outburst flow travel times were calculated based on a range of 3 to 6 m/s average flow velocity (Cenderelli and Wohl, 2001; Schneider et al., 2014), depending on factors such as sediment concentration and flow volume, resulting in 40 to 80 minutes travel time.

In all scenarios, the highest values for the factor loss were mostly modelled in the central part of Naters, where most "settlements" are located (Fig. 15.5). The most striking difference between values for persons and for objects can be seen in "mixed-use", which varied between high (persons) and intermediate (object value) according to the classification presented in Table 15.3.

Only very few areas showed low or intermediate physical vulnerability against an outburst flow in any scenario. Very high physical vulnerability, however, was predominantly present at the marginal areas of the case study area, as it mostly belongs to "forests", "agriculture" and "unproductive areas". The allocation of high vulnerability levels to the above land-use classes is

not made consistently through the international literature but here it was done in the sense of the definition (impairment of an object as affected by a hazard process), and because it is in line with the official government guidelines in Switzerland, i.e. the platform EconoMe (BAFU, 2010). "Multi-family houses" also featured very high physical vulnerability and were located in the areas very close to the river Rhône. Furthermore, virtually the entire centre of Naters showed high physical vulnerability, as it consisted mainly of "single-family houses" and "mixed-use". High and very high social vulnerability clusters in the central part of Naters which was basically due to the high density of "multi-family houses" and "single-family houses" in this area.
According to the approach outlined in Chapter 3 two risk maps were generated, based on the two version of the risk matrices (Fig. 15.3). The first risk map was based on the matrix (a) in Figure 15.3, representing intensity values of two and four, and showed high to very high risk in each socioeconomic and intensity scenario for a large area of Naters. For the larger scenario, i.e. a GLOF of 20 million m^3, the affected area equalled approx. 47% of the total study area (Table 15.5). No low or intermediate risk was modelled, between 16 and 20% of the total study area were assumed affected by high and around 30% by very high risk. In the case of the smaller scenario, i.e. an outburst flow of 4 million m^3, very high risk affected around 11% of the entire study area, whereas the total affected area only equaled around 37% of the entire study area. Some limited areas were found to feature intermediate risk, which was not found for the 20 million m^3 scenario. While for the smaller scenario very high risk areas mostly accumulated along the river, the highest risk class covers substantial areas of the municipality for the larger scenario. The objects of special interest and of particular vulnerability are highlighted in Figure 15.6 and include a church, school and hotel which are found in areas of high to very high risk.
It is interesting to note that for this version of the risk map the socioeconomic scenarios do not exert an important influence on the final risk estimate. This is different for the second version of the risk maps (Fig. 15.7) in which intensity values of one and three according to matrix (b) were implemented. Here, risk maps substantially differ depending on the socioeconomic scenario

(a) risk matrix	**Scenario "o"**				**Scenario "+"**				**Scenario "-"**			
Risk category:	*4Mill. m^3*		*20Mill. m^3*		*4Mill. m^3*		*20Mill. m^3*		*4Mill. m^3*		*20Mill. m^3*	
	%	km^2	%	km^2	%	km^2	%	km^2	%	km^2	%	km^2
1 = low	0	0	0	0	0	0	0	0	0	0	0	0
2 = medium	2.1	0.06	0	0	1.7	0.05	0	0	2.8	0.08	0	0
3 = high	24.0	0.69	18.4	0.53	22.9	0.66	16.7	0.48	23.3	0.67	19.1	0.55
4 = very high	10.4	0.30	28.5	0.82	11.8	0.34	30.2	0.87	10.4	0.30	27.8	0.80
No value	63.5	1.83	53.1	1.53	63.5	1.83	53.1	1.53	63.5	1.83	53.1	1.53

(b) risk matrix	**Scenario "o"**				**Scenario "+"**				**Scenario "-"**			
Risk category:	*4Mill. m^3*		*20Mill. m^3*		*4Mill. m^3*		*20Mill. m^3*		*4Mill. m^3*		*20Mill. m^3*	
	%	km^2	%	km^2	%	km^2	%	km^2	%	km^2	%	km^2
1 = low	0	0	0	0	0	0	0	0	0	0	0	0
2 = medium	9.0	0.26	1.4	0.04	5.9	0.17	1.7	0.05	11.5	0.33	1.4	0.04
3 = high	21.9	0.63	32.3	0.93	24.7	0.71	26.4	0.76	21.2	0.61	37.2	1.07
4 = very high	5.6	0.16	13.2	0.38	5.9	0.17	18.8	0.54	3.8	0.11	8.3	0.24
No value	63.5	1.83	53.1	1.53	63.5	1.83	53.1	1.53	63.5	1.83	53.1	1.53

Table 15.5: Affected area per risk category as well as per land-use and intensity scenario. Total case study area = 2.88 km^2. Values in percent only refer to the affected area. The upper and the lower part of the table refer to the risk matrices (a) and (b) applying the values 2 and 4 and 1 and 3 respectively.

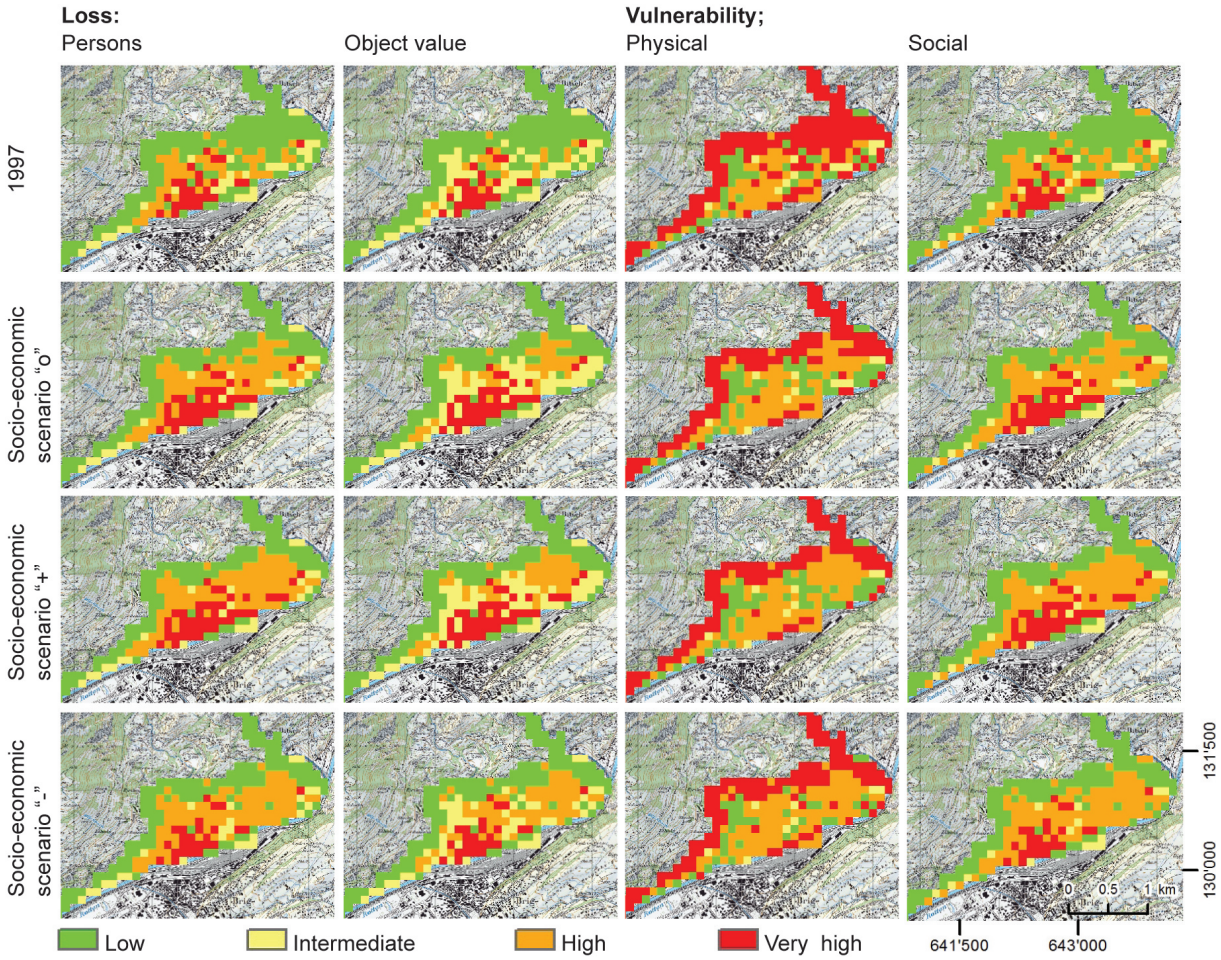

Figure 15.5: Spatial allocation of the assessment variables loss and vulnerability following the four-level scale defined in Table 15.4. DEM25 reproduced with permission of swisstopo (BA110005) and BFS (1986, 1998).

used. For the larger hazard scenario (i.e. an outburst of 4 million m^3) very high risk was only modelled for those parts of the city center which were close to the river, amounting to about 5% of the case study area. Considerable parts of Naters (9%, 6% and 12% for the socioeconomic scenario "o", "+" and "-", respectively) were modelled to be affected by intermediate risk. In case of am outburst of 20 million m^3 only small areas (of around 1.5%) of intermediate risk were distinguished, contrary to the first risk maps (Fig. 15.6) which did not feature any intermediate risk. Across all socioeconomic scenarios in the larger hazard scenario, very high risk was mainly concentrated in the city center and amounted to 13%, 19% and 8% of the study area for the socioeconomic scenarios "o", "+" and "-", respectively.

15.3 Discussion

In this study a method was developed to assess local-scale damage potential as defined by changing land-use conditions, and therewith future risks related to floods from high-mountain lake-

outburst flows. An extensive review of existing methodologies revealed that there was no adequate approach available which could directly be applied for the purpose of this study. An important body of research on land-use modelling including the assessment of driving forces, scenario development and allocation of change in space is available. Existing land-use models explore the possible changes in the future and at a range of scales but rarely with the primary objective of quantifying damage potential related to natural hazards.
Regarding hazard assessment, recent studies on lake-outburst processes and lake-outburst modelling mainly focus on already existing lakes (Osti and Egashira, 2009; Worni et al., 2012a). Studies on the assessment of local-scale hazards from floods from future lakes are currently a research gap. Therefore, one of the main challenges of this study was to develop, adapt and apply methods from two different scientific fields, i.e. land-use change and lake-outburst research, to achieve the assessment of associated future risks.
The assessment of hazards related to outbursts of future high-mountain lakes involves substantial uncertainties. However, results from models of glacier shrinkage and lake formation are relatively robust for a glacier of the size of Grosser Aletsch. As confirmed by multiple model runs the exact location of a future glacier lake (as subject to uncertainty) does not have a critical effect on flood intensities in Naters. Uncertainties related to outburst volume were accommodated by defining different outburst scenarios, an approach that is also applied for present-day lake-outburst flood hazards (Schneider et al., 2014) and that is generally recommended in situations of problematic knowledge on probabilities (Stirling, 2007). Outburst flow travel times can also vary by about a factor of 2 or more. Larger flood scenarios tend to show higher flow velocities, and thus shorter travel times, which translates into shorter lead time for warning (Schneider et al., 2014).

Uncertainties are also substantial with respect to future damage potential, the second component of the risk assessment. Similarly to the hazard assessment, scenarios were defined to cover a range of different land-use trajectories. Definition of scenarios is to some degree arbitrary, therefore an approach that increases consistency was pursued. The most important driving forces of land-use change of this case study were local, regional, national and international economy, and decisions taken by civil society, policy and jurisdiction (oral statements Michlig (2011); Holzer (2011)). Agriculture, economy and tourism were assessed to be related to those drivers, but on the other hand also drive land-use changes in Naters. The socioeconomically driven land-use scenarios were backed by literature-based findings, interviews with local authorities and plausibility tests. Therefore, they were assumed to represent a relatively robust range of possible future outcomes, including the extrapolation of current development. As development in all scenarios remained restricted to the current planning zones, even the scenario "+" has to be considered relatively conservative. More "extreme" scenarios and time horizons beyond 2045 were not considered as the corresponding assumptions would have been more speculative and the respective time horizon less relevant for policy makers. Based on the assessment of driving forces and development of scenarios, land-use transformation rates were quantified and changes in space allocated, using a rule-based model, and considering constraints such as legally defined construction zones.

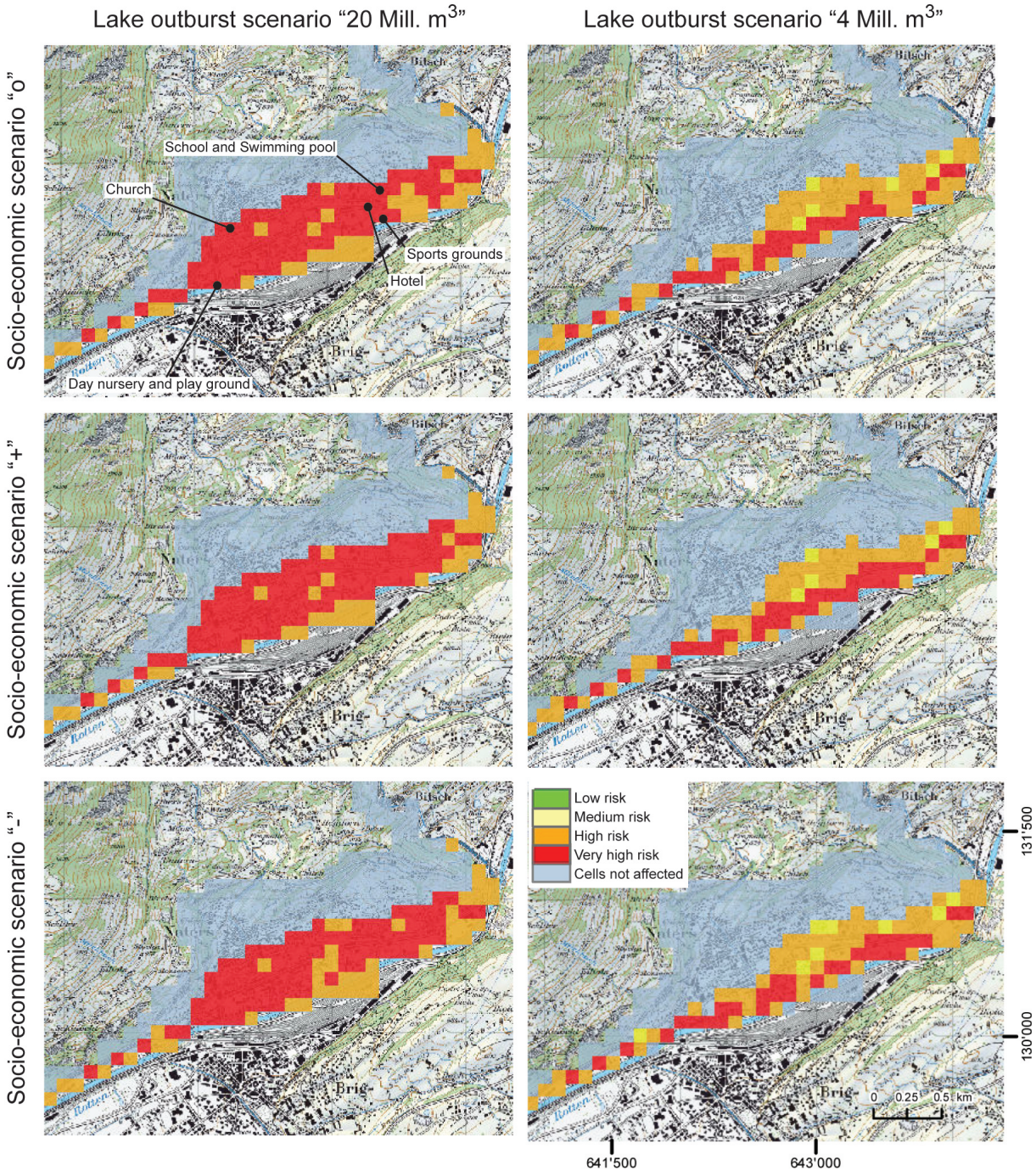

Figure 15.6: Risk for Naters in 2045 for lake outbursts considering the risk matrix (a) in Figure 15.3. The three rows indicate the socioeconomic scenarios "o", "+" and "-", the two columns the lake-outburst scenarios with 20 and 4 million m^3. Arrows indicate hotspot locations of social vulnerability. Reproduced with permission of swisstopo (BA110005) and BFS (1986, 1998).

Land-use scenarios were calculated semi-quantitatively while hazard and risk estimations were based on qualitative matrices. This approach is recommended for studies missing the necessary information on societal or hazardous processes (refer to Section 3.2.3), which is the case for future risk estimations. The resulting risk maps included the spatial distribution and the vari-

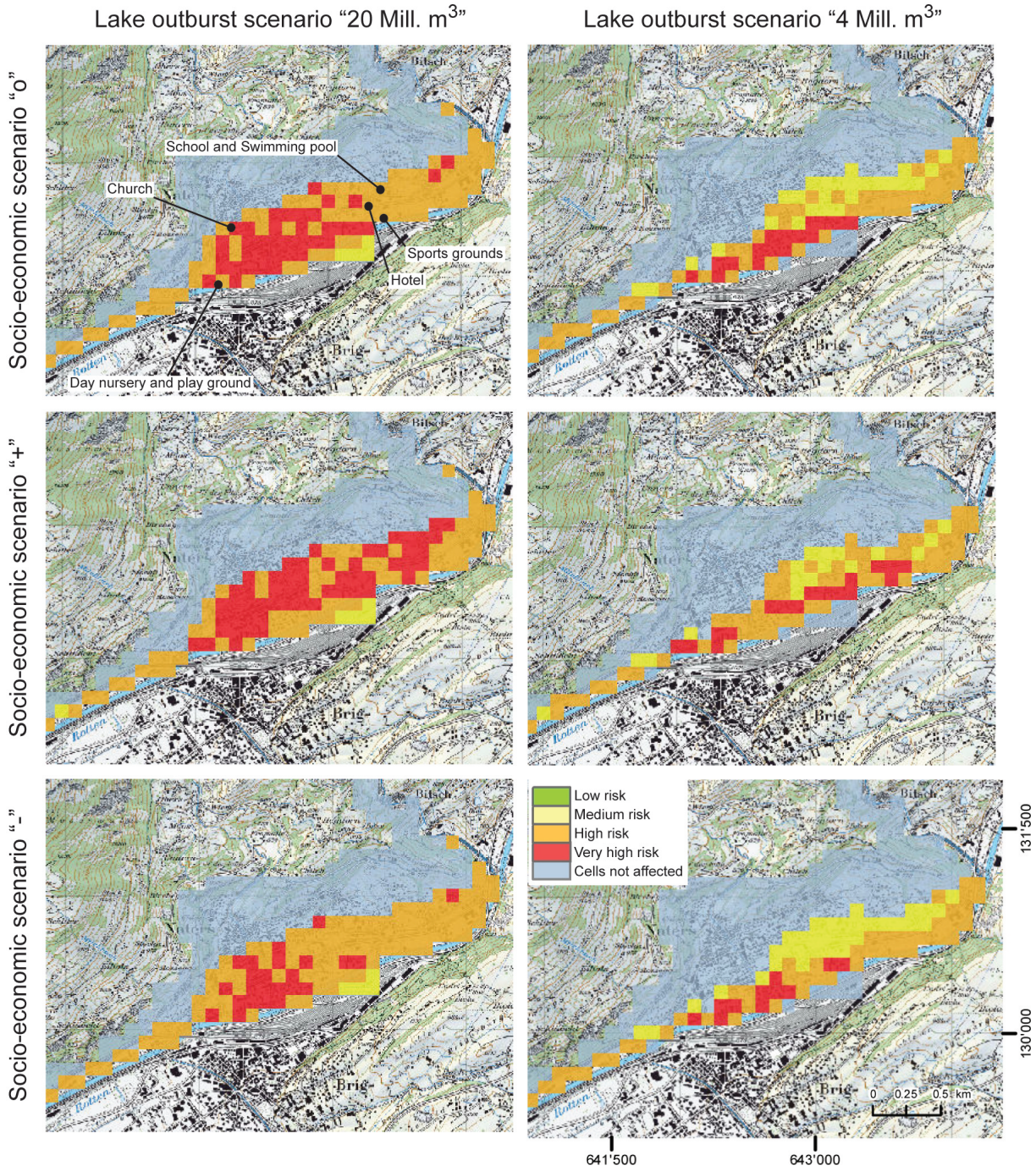

Figure 15.7: Risk for Naters in 2045 for lake outbursts considering the risk matrix (b) Figure 15.3. The three rows indicate the socioeconomic scenarios "o", "+" and "-", the two columns the lake-outburst scenarios with 20 and 4 million m^3. Arrows indicate hotspot locations of social vulnerability. Reproduced with permission of swisstopo (BA110005) and BFS (1986, 1998).

ability of different risk categories. Two risk matrices were applied to demonstrate the effects of (subjective) definition of risk class distribution in the matrix. Results showed that the definition of risk matrices can have a substantial effect on risk results. A risk matrix stronger based towards high risk classes (matrix a) can exert a dominant effect over socioeconomic, while a

more balanced risk matrix (b) quite obviously reduces the proportion of (very) high risk areas and gives higher weight to the effects of socioeconomic development. Based on this analysis, a balanced risk matrix would probably be preferable, however, it should be underlined that the definition and choice of risk weighting is ultimately a task of policy and society and not science (Künzler et al., 2012).

In the context of integrated risk management, a risk analysis is not an endpoint but forms an input for risk reduction measures. The results of this study indicated the important difference between smaller and larger GLOF scenarios in terms of risks encountered in Naters. Accordingly, authorities may also consider investments to prevent large GLOFs reaching the urban areas of Naters, such as by structural measures. However, structural measures might not always be applicable or legally feasible due to various reasons such as costs involved, environmental protection areas or private property. Therefore, strategies to reduce risks of loss of lives by increasing the people's preparedness, once the new glacier lakes will form, may be of relevance (e.g. IPCC, 2012)). Experiences have shown that early warning systems for GLOFs can be effective to achieve risk reduction (e.g Kattelmann, 2003), mainly by decreasing the number of persons exposed. The GLOF travel time estimates indicated warning lead times of about 40 to 80 minutes where smaller and larger flood scenarios again make a difference. This range of warning lead time is considered feasible for an operational early warning system and confirms the potential to reduce risks to future GLOF hazards.

While the value and physical vulnerability of objects possibly affected will typically remain unchanged with an early warning system, the exposure probability of people should be substantially reduced with such risk reduction measures. The exposure probability in case of early warning is related to people's preparedness, and thus could be considered in terms of social vulnerability. Research (e.g. from Hurricane Katrina in 2005) indicates that social aspects such as welfare and social class exert an important effect on response to disasters, including evacuation timing (Elliott and Pais, 2006). For this study an early warning system in place has not been considered in the scenarios but may be integrated in future research. Avoidance of high-loss and high-vulnerability assets in flood prone areas is most important to reduce high and very high risks (e.g. ARE, 2008; Hiess, 2010), especially if structural mitigation measures might not be very feasible. The avoided damage can be estimated from the risk analysis based on the different scenarios.

Overall, this study constitutes one of the first attempts of the integration of spatiotemporal aspects in risk management (Aubrecht et al., 2013; Fuchs et al., 2013), together with other endeavours (Cammerer and Thieken, 2013; Cammerer et al., 2013). It further corroborates the fundamental importance of land-use policies and governance for risk reduction (e.g. BUWAL, 2003; OcCC, 2007). In case of high development trajectories, a main challenge for policy will be to counteract certain driving forces. This study can represent a contribution for local, rural development planning, if additional information on risks related to other natural hazards as well as the coordination with further development plans of the community are considered. More on integrated risk management of high-mountain lakes is elaborated in the next chapter.

Part V

Implications for risk management and conclusions

The principles of risk management were outlined in the beginning of this thesis (Chapter 3). The previous chapters in Part II-IV were concerned with hazard assessment and risk analysis of high-mountain lakes, especially with regard to the process chain of a lake-outburst flow triggered by impact waves.
This part contains a discussion of risk-reduction options as well as risk-management strategies, treating the questions of, "What is allowed to happen?" and "What has to be done?" in Chapter 16. The conclusions then complete the thesis summarizing contributions, achievements and open questions (Chapter 17).

CHAPTER 16

INTEGRATED RISK MANAGEMENT OF HIGH-MOUNTAIN LAKES

The aim of integrated risk management is to regulate the development with the help of risk reduction measures in an anticipatory way (PLANAT, 2013). The most appropriate risk-reduction strategy has to be defined for every individual case, given the variability in topographic settings and societal conditions and preferences. These aspects are considered in the processes of risk evaluation and measurement planning, which follow a risk analysis.
Depending on the temporal and spatial scale of the assessment as well as on the uncertainties involved, risk analyses can either result in quantitative risk calculations (expected annual damage) or qualitative risk estimations, as outlined in Section 3.2.3 and examined on various occasions throughout this thesis. Correspondingly, the present discussion also distinguishes between risk management based on quantitative risk evaluation (Section 16.1) and decision-making under uncertainties (Section 16.2).

16.1 Risk management based on quantitative risk evaluation

Risk can hardly ever be reduced to zero, but attempts can be made to keep it in a tolerable range, which is defined during risk evaluation.

Risk evaluation
As mentioned in Section 3.1, discussions on risk acceptance are lively, as risk perspectives vary with culture, gender or age (Slovic, 2000; Weinstein, 1980). Even within a certain community, not one unique risk acceptance level exists, because individual acceptance might differ from social or expert acceptance, some challenges in this regard are outlined by Bell et al. (2006).
To account for these different points of view, risk managers in Switzerland, for example, distinguish between societal risks and individual risks, as already explained in Section 3.2.3. The individual risk levels are related to the natural mortality rate of a certain societal group. The societal

risk is evaluated by means of frequency-number curves, which are based on probability-density functions of the number of fatalities per year. If the calculated risk exceeds the curve, the risk is assumed unacceptable. The final risk evaluation then adopts these safety goals (PLANAT, 2013). Further relations for defining societally-accepted risk-thresholds are available. A compilation of 25 quantitative methods can be found in Jonkman et al. (2003).

Often, however, the definition of risk as the expected annual damage does not correspond to the perceived risk (Slovic, 2000). Another assumption in risk evaluation regarding risk acceptance is that an event causing, e.g. ten fatalities is perceived as worse by the society than ten events causing one fatality each (BABS and PLANAT, 2008; Wilhelm, 1997). The existence of risk aversion has been investigated within Swiss society, however, without achieving unambiguous conclusions (Plattner, 2006; Rheinberger, 2010). This effect should nevertheless not be completely neglected for low-probability and high-magnitude events, such as lake-outburst flows, especially in Switzerland, where the public awareness for this scenario is still quite low.

Planning of risk-reduction measures

After having found a common understanding of how safe is safe enough, risk managers must in a next step consider the assumption of which protection at what price (Rheinberger, 2011). The advantage of quantitative risk measures is that the expected loss can be directly compared to the cost of risk-reduction measures. A common approach is establishing a cost-benefit relationship to identify the economic efficiency of risk-reduction measures. The simple, underlying evaluation criterion is that the amount of mitigated loss has to exceed the costs of the measure (Fuchs, 2013). In a risk-cost diagram the optimal mitigation strategy can then be graphically derived at the tangent point of the risk-cost curve and the marginal-cost criterion line (according to (Bohnenblust and Slovic, 1998)).

An alternative decision rule is the cost-effectiveness relationship, which only requires monetization of the costs but not of the risks. This approach is also applicable to qualitative risk estimates, e.g. where the probability of occurrence can hardly be quantified.

The variety of measures applicable to risk reduction related to high-mountain lake-outburst events is large and depends strongly on the hazard type and the context of the possible event. A range of possible categories of risk reduction measures was already presented in Figure 3.2 in Section 3.1.

Generally speaking, risk managers can try to improve the preparedness of people potentially affected, which involves avoiding damage through prevention, or through enhancing their preparation in order to cope adequately with the event once it occurs. Another strategy is to minimize the effects and the duration of an event through immediate intervention and consecutive reconditioning. Risk-reduction measures can also be taken in the regeneration phase after an event by reconstructing the damaged infrastructure and then analysing the event in order to enable sustainable long-term planning.

A range of measures was already introduced in this thesis, which is briefly compiled and enhanced with further examples from the literature in Table 16.1 and in Figure 16.2. The engineering solutions reported almost exclusively aimed at controlling the water level of the lakes (Portocarrero, 2013b; Richardson and Reynolds, 2000). This is also the case where impact waves were assumed to be the main trigger mechanism (e.g. Lake 513 and Lake Llaca in Peru

or Lake Trift in Switzerland), because prevention of large slope failure is hardly feasible. But as already mentioned with the example of Naters (Section 15.3), structural measures might not always be applicable or legally feasible due to various reasons such as costs involved, environmental protection areas or private property. Therefore, strategies for reducing risk of loss of human lives by increasing the preparedness of the population may be of relevance (e.g. IPCC, 2012). Avoidance of high-loss and high-vulnerability assets in flood-prone areas is most important for reducing high and very high risks (e.g. ARE, 2008; Hiess, 2010), especially if structural mitigation measures might not be feasible. Experiences have shown that early warning systems for GLOFs can be effective in achieving risk reduction (e.g Kattelmann, 2003). While the value and physical vulnerability of objects possibly affected will typically remain unchanged with an early warning system, the exposure probability of people should be substantially reduced with such risk reduction measures. When installing early warning systems, it must nonetheless be considered that social aspects such as welfare and social class exert an important effect on evacuation timing, amongst other (Elliott and Pais, 2006).

16.2 Decision-making under uncertainties

"Good" decisions are, however, not exclusively taken on basis of full quantitative risk assessment. "Good" decisions are the ones to which no other choice is clearly preferable, given the information available at the time they are made (Cox, 2012). This refers as much to risk-reduction-measure planning as to integrated management of different risks (related to natural hazards). Stirling (2007) contributed to this debate on constructive risk policy by classifying different types of incomplete knowledge. This framework will be presented before elaborating on decision strategies under uncertainties.

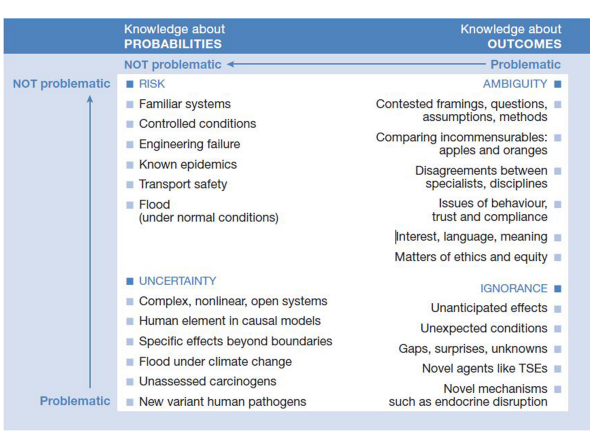

(a) Contrasting states of incomplete knowledge, with schematic examples. Risk" in the present thesis is equal to quantitative risk calculation.

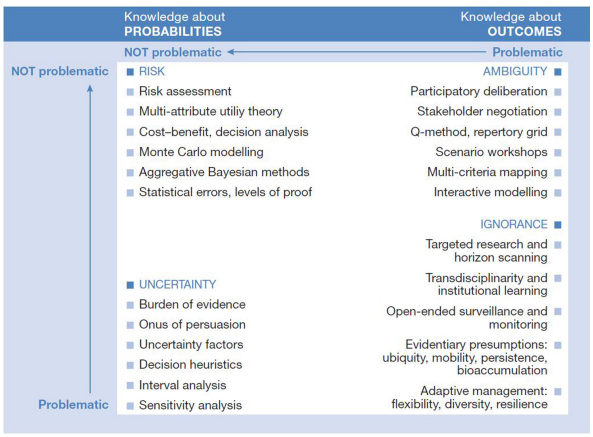

(b) Methodological responses to different forms of incomplete knowledge.

Figure 16.1: Types of incomplete knowledge in risk assessment. Figures and captions (adapted) from (Stirling, 2007).

Risk-reduction category	measure	Example	Source
Preparedness			
Prevention	Siphoning (temp. Water level control)	Palcacocha	Lliboutry et al. (1977)
		Longbasaba and Pida Lake, China	Wang et al. (2008)
		Ghulkin Glacier, Hindukush	Ashraf et al. (2012)
	Tunneling (perm. Water level control)	Lake 513, Peru	Chapter 11
		Tsho Rolpa Lake, Nepal	Bajracharya (2009); Matambo and Shrestha (2011)
	Excavation of spillways (perm. Water level control)	Longbasaba and Pida Lake, China	Wang et al. (2008)
	Reinforcing of outlet structure	Several lakes in the Cordillera Blanca	Lliboutry et al. (1977)
		Grubengletscher, CH	Haeberli et al. (2001)
	Artificial dam	Lake Llaca, Peru	Emmer et al. (2014)
	Barrier constructions below the lake	Lake Llaca (temp.), Peru	Portocarrero (2013b)
	Reduce number of exposed people/assets	Nepal	Bajracharya (2009); Kattelmann and Watanabe (1998)
Emergency provision	Expertises	Grindelwald	Chapter 14
	Alert and evacuation strategy		
	(near) real-time monitoring	Nepal	Bajracharya (2009)
	Create global and local awareness	Nepal	Bajracharya (2009)
	Early warning system (EWS)	Trift	Dalban Cannassy et al. (2011)
		Lake 513, Peru	Schneider et al. (2014)
		Tsho Rolpa Lake, Nepal	Bajracharya (2009); Matambo and Shrestha (2011)
Response			
Intervention	Preparations of personnel and material for intervention	Grindelwald	Chapter 14
	Evacuation		Matambo and Shrestha (2011)
Recondition	see reconstruction		
Recovery			
Analysis of event	Cost analysis / Review of measurements	Grindelwald	Chapter 14
	Elaboration of future hazard scenarios allowing installation of EWS	Lake 513	Chapter 13, Schneider et al. (2014)
Reconstruction	Clearing and reparation buildings	Grindelwald	Chapter 14
	Clearing and reparation of bridges	Lake 513	Carey et al. (2012)
	Removal of flood depositions	Grindelwald, Lake 513	Chapter 14, Carey et al. (2012)

Table 16.1: A compilation of possible risk-reduction measures for high-mountain lake-outburst events and examples of application. Reconstruction activities ideally increase the resisting power in contrast to reconditioning activities, which re-establish the initial conditions (see Section 3.1). A large number of technical prevention measures implemented in Peruvian lakes was recently compiled by Portocarrero (2013b).

(a)

(b)

(c)

(d)

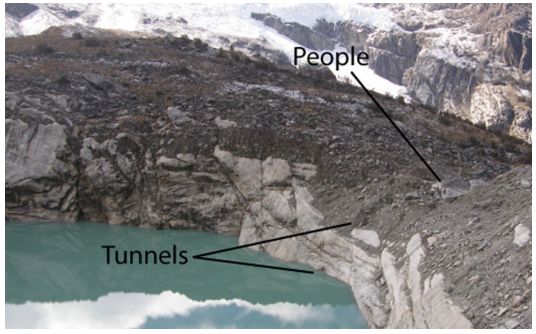

(e)

(f)

(g)

(h)

Figure 16.2: Examples of risk-reduction measures. (a) Siphoning, Lake Palcacocha, Peru (b) Excavation of spillway, Lake Weingarten, Switzerland (P. Teysseire), (c) Reinforcement of the dam, Lake Cuchillacocha, Peru, (d) Artificial dam and tunnels, Lake Llaca, Peru, (e) Permanent tunnels in the rock dam, Lake 513, Peru, (f) Evacuation routes, Carhuaz, Peru, (g) Barrier below the lake, Switzerland (C. Huggel), (h) Barrier with retention pond, Switzerland (C. Huggel)

Stirling (2007) distinguished between lack of knowledge about probabilities and about the negative consequences of an event, which are referred to as outcomes. Some examples of assessments and the corresponding methodological techniques are illustrated in Figure 16.1.
According to Figure 16.1a, strict quantitative risk assessment is only feasible for well-known systems, where knowledge is only slightly limited with regard to both probabilities and outcomes. Risk assessment as described in the previous section is not applicable under conditions of uncertainty, ambiguity or ignorance. The state of ignorance prevails where neither probabilities nor outcomes can be characterized. Ambiguity is related to problematic knowledge on the outcomes of an event only. In the case of risks related to natural hazards, knowledge of both hazard and damage potential must be assessed within these criteria. The condition of uncertainty prevails where knowledge about probabilities is limited (Stirling, 2007). With regard to risk management, Aven (2013); Cox (2012) suggest a more distinctive taxonomy of uncertainties, distinguishing among four categories ranging from determinism to deep uncertainties close to total ignorance.
Considering the current state of knowledge, strict risk assessment of high-mountain lake-outburst events is hardly possible even for current conditions because of the missing knowledge on probabilities. All management activities based on quantitative risk-assessments require definition of the probability of occurrence, which is difficult to derive for high-mountain lake-outburst events or for rock-slope failures triggering an impact wave. Some attempts will be presented in the following pages.

Probability of occurrence
Statistically-derived probability distributions for all type of landslide volumes (Brunetti et al., 2009) and magnitude-frequency relationships for very large rock avalanches (>10^6 m^3) in mountain topography (Korup and Clague, 2009) are established. Fundamental climate-induced changes in the environment (Beniston et al., 2007), however, imply changes in frequency, magnitude and interactions of processes (Fuchs et al., 2013; Kron, 2002), as already argued in Section 3.2.1. Probabilities derived from retrospective event analyses are therefore hardly applicable to paraglacial environments. Nevertheless, one attempt to quantify probabilities of occurrence of rock avalanches in paraglacial areas was done by Ballantyne and Stone (2013), by means of dating of timing and periodicity of slides in Scotland in relation to earlier deglaciation periods.
The application of fault- and event-trees was suggested, to relate the probability of occurrence to the effects of an event (Kappes et al., 2012). This strategy can be applied to relate the probability of a slope failure to the probability of a lake outburst triggered by the resulting impact wave. An example of an event tree for tsunami propagation and run up, given the occurrence of an earthquake-triggered rock slide, can be found in Lacasse et al. (2008). Recent research on assessment of cascading multi-hazards suggests Bayesian Networks as an evolution of event trees, because they allow for the inclusion of probability-density functions (to account for the inherent uncertainties) instead of one single probability value at each node (Marzocchi et al., 2012; Nadim and Liu, 2013). BNs further enable researchers to display the interactions and the causal relationships inherent to the processes being effective in the system of a high-mountain lake. The lake assessment scheme illustrated in Figure 4.2 in Chapter 4 was elaborated with regard to this purpose and offers the potential to be extended to a BN.

Replacing the probability of occurrence through the disposition is another approximation suggested (Delmonaco et al., 2006b). One example was given by Reynolds (2003) (closer explained in Section 4.3.3), who worked on the lake-outburst disposition and enhanced the assessment by a score rating system. The system of Reynolds (2003) does not explicitly take into account impacts through mass movements. The disposition is, however, an approximation of the probability of occurrence only. Lacasse et al. (2008) suggests generating artificial probabilities of occurrences by assigning quantitative probabilities to these qualitative descriptions. Virtually impossible, for example, would correspond to a probability of 0.001, completely uncertain to 0.5, likely to 0.9 and virtually certain to 0.999. The meaning of the verbal description of the uncertainty is given by Lacasse et al. (2008).
The application of the Monte Carlo simulation technique is another approach recommended for assessment of uncertainties of complex systems, to which multi-hazards belong (Nadim and Liu, 2013). Especially with regard to physically-based process simulations, this approach is, however, too laborious.

Despite all efforts, decision-making by means of probability-based quantitative risk assessments is at the moment hardly feasible for the case of high-mountain lake-outburst flows, because of the limited process understanding, constricted knowledge basis and other incertitudes.
Some authors, (e.g. Aven, 2010, 2012) therefore generally criticise probabilities as an imperfect concept for expressing uncertainties. As already mentioned in Section 3.1, a different set of risk definitions exists, which includes uncertainties rather than probabilities. Aven (2010, 2012) suggests basing decision-making on risk defined as a function of the uncertainty over the hazard and the consequences including the uncertainty about underlying factors. This approach is, however, not yet applied within the natural hazard community and will therefore hardly yet be considered a solution for decision makers.
Decisions with regard to high-mountain lake-outburst flows (triggered by rock/ice avalanche-induced impact waves) have therefore to be taken under uncertainties, especially with regard to the probability of occurrence.

With regard to future conditions, deep uncertainties close to ignorance often have to be assumed, because of the unknown development of both, hazards and damage potential.
Different science-based methods are, however, available to address problems under different incertitude conditions, as presented in Figure 16.1b. Recent scientific efforts – and the present thesis numbers amongst them – however, enhanced and contributed methodologies to improve knowledge on the outcomes, which reduces ambiguity and shifts the assessment of lake-outburst risks away from ignorance into the range of uncertainty, also for future conditions. Furthermore, several approaches, some of which were also elaborated in the present thesis, exist to approximate the probability of occurrence by means of disposition. All these achievements currently enable decision-making under conditions of low uncertainties only.

Decision strategies
Management strategies for risk problems involving uncertainties are based on principles rather than on risk thresholds. Two set of strategies are compiled in Table 16.2 and will be shortly summarized here. Another set of 10 tools which enable robust decisions even under deep uncertainties is further provided by Cox (2012).

Principles	Decision rules / tools
Six levels of treatment according to Paté-Cornell (1996)	
The detection of hazard and the identification of failure mode is a sufficient decision criterion.	0: zero-risk policy
The worst case has to be recognized and avoided, independent of probabilities	1: worst case approach
Prevention of the worst possible case that can be reasonably expected (e.g. maximum probable flood)	2: quasi-worst case
Prevention of the most probable mechanism given its maximum likelihood, by means of a central value of the outcome	3: best estimate
Decision based on the probability distribution of different system states, which are based on best estimates of the parameters (e.g. risk concept Switzerland)	4: Single probabilistic risk curve
Decision based on statistical analysis of existing data displaying all uncertainties	5: Multiple probabilistic risk curve
Two risk management strategies according to Aven and Renn (2009b)	
Risk informed and caution/precaution based	Risk as low as reasonably practicable (ALARP) Best available control technology (BACT)
Risk-informed and robustness and resilience-focused (risk-absorbing system)	Diversity of means to accomplish desired benefits Avoiding high vulnerability Allowing for flexible responses Preparedness for adaptation

Table 16.2: Risk-management strategies under uncertainties.

Aven and Renn (2009b) suggest two management strategies for uncertainty- introduced risk problems, which can be implemented by means of several tools. Risk management considering the caution or precaution principle is based on broad risk characterization and highlighted uncertainties. The precaution principle states, "Where there are threats of serious or irreversible damage, lack of full scientific certainty shall not be used as a reason for postponing cost-effective measures to prevent environmental degradation" (UN, 1992). The second approach suggested by Aven and Renn (2009b) aims at establishing a risk-absorbing system by improving the capability to cope with surprises through enhancing robustness and resilience.
Another set of policies behind decision rules was presented by Paté-Cornell (1996), also providing the corresponding assessment tools for decision-making. All these approaches require the definition of a risk management policy. For Switzerland, acceptance levels for quantitative risk assessments are available; policies for decision-making under uncertainties with regard to high-mountain lake-outburst events, however, have yet to be defined.

In cases of remaining deep uncertainties, Cox (2012) recommends applying adaptive risk management in order to enable "good" decisions. Adaptive learning in the sense of trial and error is certainly not a desirable risk-management strategy with regard to high-mountain lake-outburst events. His suggestions, however, go further than that. Cox (2012) proposes replacing the questions from Kaplan and Garrick (1981) to enable robust decision. The question of "What can

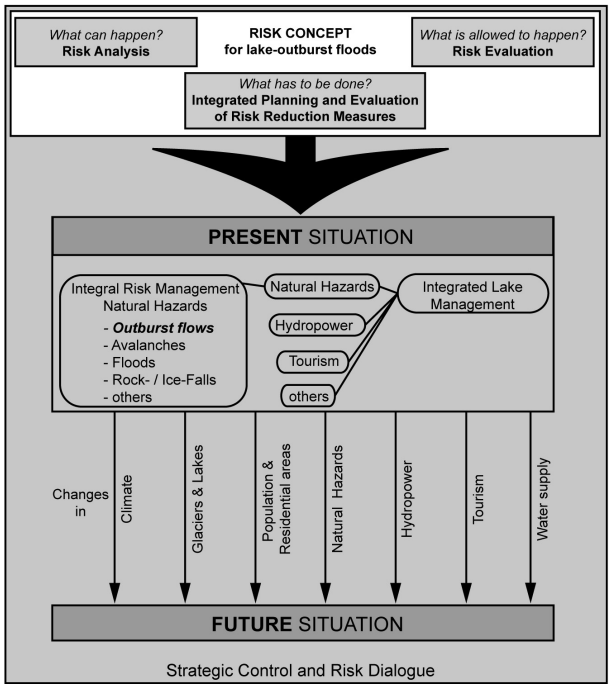

Figure 16.3: Integrated risk and lake management in the context of a changing environment.

happen?" for example, could be replaced by, "Is there a clearly better risk-management policy than the one I am using now?".

Integrating further lake uses into decision-making

Risk is not the only issue requiring management in the context of high-mountain lakes. The new lakes which are currently forming and those which, it is assumed, will form in future as a consequence of glacier recession, will be located in a changing environment. This context is illustrated in Figure 16.3. New high-mountain lakes have to compensate for the freshwater-storage function of the melting glaciers; they might feature the potential for generation of hydropower, or they might also attract tourists, because they could partly compensate for the inherent loss of fascinating glacierized landscapes (NELAK, 2013). These aspects should also be considered in decision-making.

Shifting the focus more towards integrated lake management rather than risk management only would allow for the use of synergies between the different stakeholders. Especially those among freshwater storage, energy production and risk-reduction measures could be included in the planning process, through consideration of multi-purpose solutions (NELAK, 2013). These risk-reduction measures could also be combined with water supply and hydropower generation by implementation of multi-purpose solutions.

These solutions would, on the one hand, provide the highest protection to lives and material assets from a long-term perspective, if the freeboard is planned and maintained adequately. On the other hand, these multi-purpose measures would also generate socio-economic benefits broader than risk reduction alone. This enhanced benefit is likely to raise the cost-effectiveness or even the cost-efficiency of a construction, which might simplify the fundraising (Haeberli et al., 2012). This management policy might reduce the urgent need for defining probabilities of occurrence of a hazardous event.

In this planning process, decision-making is very likely to take place under ambiguous points

of view, because of the participation of different stakeholders with various interests. Further conflicts with landscape protection laws (where available) have to be obviated by checking the regulatory framework in time, especially as constructions tend to open the terrain up for consecutive developments (Haeberli et al., 2012). This constellation requires an early and pronounced discourse on development options of deglaciating high-mountain areas between all stakeholders, which has to be based on profound knowledge and also start in good time.

CHAPTER 17

CONCLUSIONS AND OUTLOOK

This thesis contributes considerably to the knowledge base for dialogues and decision-making within integrated risk management of high-mountain lakes. Advancements were made regarding gaps in knowledge in multi-hazard assessment and risk analysis of cascading processes with high-mountain lakes integrating spatiotemporal aspects. Priority was given to outburst flows triggered by rock, ice or combined rock/ice avalanche-induced impact waves. This thesis explicitly addressed the relevance of the subject for Switzerland, and several methodological aspects for local-scale hazard and risk assessment on different temporal scales (summarized in Fig. 17.1).

Contributions to						Part	Chapter
		Method Advancement		Data generation			
Literature Review	Theoretical Framework	Swiss Alps	individual case	Swiss Alps	individual case		
							1 High-mountain lakes in a changing environment
x	x					I	2 Occurrence, consequences and terminologies
x	(x)						3 Embedding high-mountain lake-outburst events into the theoretical background of risk
x	(x)						4 Identifying and analysing high-mountain lake-outburst hazards
	x	x		(x)	(x)	II	5 Developing a model of rock-avalanche impact disposition into high-mountain lakes in Switzerland
				x			6 Spatially-explicit, deterministic assessment of the rock-avalanche impact disposition
		x		x			7 Probabilistic rock-avalanche impact disposition assessment considering parameter uncertainties
				x			8 Reliability and robustness assessment of the rock-avalanche impact disposition model (Appendix A)
				x			9 Relevance of rock-avalanche impact susceptibility of high-alpine lakes in Switzerland
x	(x)					III	10 Effect analysis of rapid mass movements triggering impact waves
(x)					x		11 2010 outburst event of Lake 513: Case-study and event descriptions (Appendix B)
			x		x		12 Uncertainty propagation in coupled impact-wave simulations (Appendices C, D, E)
			x		x		13 Hazard analysis of potential ice avalanches at Mount Hualcán
	x		(x)		x	IV	14 Cost assessment of a lake-outburst flow in Grindelwald with regard to touristic infrastructure
			x		x		15 Damage potential and risk estimation for future conditions with the example of Naters
x	x		(x)			V	16 Integrated risk management of high-mountain lakes
x	x	x	x	x	x		17 Conclusions and outlook
						VI	Appendices A-E

Figure 17.1: Contributions of this thesis to topics in the field of risk analysis of outburst flows from high-mountain lakes. x = Chapter contributes strongly to topic. (x) = Chapter contributes partly to topic.

The following conclusions can be drawn:

- A lake-outburst event triggered by a rock avalanche-induced impact wave is a relevant hazard in the Swiss Alps and the probability of an event is continuously rising. The reasons for the increasing probability are rooted in the formation of new lakes, which tend to be located and remain for long time periods close to walls featuring an increasing rock-avalanche disposition. Hotspots of rock-avalanche impact disposition into high-mountain lakes in Switzerland for current and future (at the moment of deglaciated Alps) conditions were identified in this study.
- Lake-outburst events due to impacts from ice avalanches are a serious but transient hazard. Ice-avalanche scenarios can be established by means of terrain analysis and aerial image interpretation, despite limited process understanding of ice break-off mechanisms.
- Methods for assessing the process chain triggered by a mass movement into a lake are available. The assessment requires extensive process understanding and knowledge of the location. The available model types were collected from the different disciplines involved, and a consistent definition of assessment methods was established to enable communication, exchange and collaboration between the different research fields. Hazard assessment of cascading processes can be done by means of coupled numerical simulations. This is, however, associated with considerable uncertainties.
- The definition of the probability of occurrence remains challenging for lake-outburst events as much as for rock-slope failure or ice break-off events. The disposition inherent in the respective environment resulted in a useful approximation, which can also be applied to hazard assessments under assessable future conditions. Prioritization of hazards and risk can be based on the respective disposition.
- Middle-term land-use changes can be modelled to derive the damage potential for future-oriented risk assessments on a local scale.
- Quantitative risk calculation remains hardly feasible even for present conditions, because of the unavailable quantification of probabilities and of data scarcity with regard to future conditions. Qualitative risk estimations, however, are useful for measurement planning or risk prioritization, since they can be applied in data-scarce assessments and also to future conditions.
- Risk-reduction activities are required in most cases, since damages from lake-outburst flows tend to be high due to the secondary and tertiary costs. Adequate and sustainable decisions can be made under uncertainties and corresponding decision strategies are available.
- A range of risk-reduction measures can be applied and experiences are available, especially in areas featuring a long history of lake-outburst events, such as the Cordillera Blanca, Peru. Organizational measures, such as early-warning systems, can prevent loss of lives. Engineering risk-reduction solutions have the advantage of providing long-term

protection to objects as well as to people, and further provide the opportunity for multi-purpose construction.

- Multi-purpose construction projects for risk reduction also benefit from the advantages provided by high-mountain lakes and might ensure a water supply. Switzerland could take a leading position in developing multi-purpose solutions, thanks to its experience in integrated risk management and in sustainable water resource management.

Summarizing these conclusions, the depiction of the possibilities for reducing ambiguity with regard to possible outcomes of lake-outburst events is perhaps the largest contribution of this thesis. This depiction is fundamental to integrated risk management and also to lake management, because decision-making under conditions of ambiguity is known to be highly problematic (Paté-Cornell, 1996). Many areas of work remain, requiring further efforts:

- In this study the slope failure hazard was mainly assessed by means of the disposition parameters. Knowledge regarding variable disposition and trigger parameters of large-scale slope failures is still limited and requires further investigations.
- The understanding of the complex flow behaviour of the resulting rapid mass movements is also fairly undeveloped and requires further investigations.
- Multi-hazards should be considered more systematically in hazard analyses. The relation and interaction between different processes needs to be integrated into assessment schemes, e.g. by means of Bayesian Networks, which also allow accounting for uncertainties.
- Efforts should be put into establishing fully physical simulations of cascading processes or in closer investigation and optimization of the interfaces between numerical process simulations to minimize uncertainties involved in the effect analysis of cascading processes.
- Detailed hazard analyses for future conditions based on the current knowledge are difficult. Therefore further extending the scientific basis for modelling future high-mountain landscapes without glaciers and corresponding process interactions is recommended (NELAK, 2013), as well as extensively observing snow and ice in high-mountains and continuously estimating the hazard.
- Similar to the hazard disposition assessment, areas of high damage potential have to be detected for future conditions. Hotspots of damage potential have to be defined and compared to the hotspots of hazard to allow prioritization of future risks and long-term planning. Corresponding approaches should be developed based on both spatial-planning scenarios on a national scale and local-scale land-use change assessments.
- A social discourse on risk acceptance and perception of such high-magnitude, low-frequency events should be started now, in order to adequately evaluate the risk estimates (also for future conditions) and to enable timely decisions.

- Further discussions should involve all stakeholders to evaluate benefits and risks emerging from new high-mountain lakes equally, and to consider multi-purpose constructions for risk reduction, and furthermore to find robust and broadly supported long-term solutions.

To summarize, high-magnitude, low-frequency cascading events pose challenges to risk managers. A knowledge base for first-order hazard assessments of high-mountain lakes and a range of risk assessment methodologies is available. It allows for localization and prioritization of risks in Switzerland, also with regard to future conditions. The direction and time scales of the changes in high mountains are known, and methodologies to assess causal relations and outcomes are available. Large uncertainties remain, especially regarding detailed hazard assessment of local cases. Decisions regarding risk management should nevertheless be taken promptly and with wide support, since many stakeholders are present and degrees of freedom in decision-making decrease with time.

REFERENCES

Abadie, S., Morichon, D., Grilli, S. and Glockner, S. (2010): Numerical simulation of waves generated by landslides using a multiple-fluid Navier–Stokes model, *Coastal Engineering*, 57(9), pp. 779–794.

Agliardi, F. and Crosta, G. (2003): High resolution three-dimensional numerical modelling of rockfalls, *International Journal of Rock Mechanics and Mining Sciences*, 40(4), pp. 455–471.

Aguilera, P., Fernandez, A., Fernandez, R., Rumi, R. and Salmeron, A. (2011): Bayesian networks in environmental modelling, *Environmental Modelling and Software*, 26(12), pp. 1376–1388.

Aksoy, H. and Kavvas, M.L. (2005): A review of hillslope and watershed scale erosion and sediment transport models, *CATENA*, 64(2–3), pp. 247–271.

Alean, J. (1985): Ice avalanches - some empirical information about their formation and reach, *Journal of Glaciology*, 31(109), pp. 324–333.

Allen, S., Cox, S. and Owens, I. (2011): Rock avalanches and other landslides in the central Southern Alps of New Zealand: a regional study considering possible climate change impacts, *Landslides*, 8(1), pp. 33–48.

Allen, S., Owens, I. and Huggel, C. (2008): A first estimate of mountain permafrost distribution in the Mount Cook region of New Zealand's Southern Alps., in *Ninth International Conference on Permafrost, Institute of Northern Engineering*, (edited by D. Kane and K. Hinkel), University of Alaska, Fairbanks, pp. 37–42.

Allen, S.K., Gruber, S. and Owens, I.F. (2009a): Exploring steep bedrock permafrost and its relationship with recent slope failures in the Southern Alps of New Zealand, *Permafrost and Periglacial Processes*, 20(4), pp. 345–356.

Allen, S.K., Schneider, D. and Owens, I.F. (2009b): First approaches towards modelling glacial hazards in the Mount Cook region of New Zealand's Southern Alps, *Natural Hazards and Earth System Sciences*, 9(2), pp. 481–499.

Ancey, C. (2007): Plasticity and geophysical flows: a review, *Journal of Non-Newtonian Fluid Mechanics*, 142(1–3), pp. 4–35.

Antunes do Carmo, J.S. and Carvalho, R.F. (2011): Large dam-reservoir systems: guidelines and tools to estimate loads resulting from natural hazards, *Natural Hazards*, 59(1), pp. 75–106.

Apostolakis, G. (1990): The concept of probability in safety assessments of technological systems, *Science*, 250(4986), pp. 1359–1364.

ARE (2008): *Raumkonzept Schweiz: Eine dynamische und solidarische Schweiz, Entwurf*, Bundesamt für Raumentwicklung (ARE), Bern, 72 pp.

Ashraf, A., Naz, R. and Roohi, R. (2012): Glacial lake outburst flood hazards in Hindukush, Karakoram and Himalayan Ranges of Pakistan: implications and risk analysis, *Geomatics, Natural Hazards and Risk*, 3(2), pp. 113–132.

Ashraf, A., Roohi, R., Naz, R. and Mustafa, N. (2014): Monitoring cryosphere and associated flood hazards in high mountain ranges of Pakistan using remote sensing technique, *Natural Hazards*, 73(2), pp. 933–949.

Ataie-Ashtiani, B. and Malek-Mohammadi, S. (2008): Mapping impulsive waves due to subaerial landslides into a dam reservoir: a case study of Shafa-Roud dam, *Dam Engineering*, 18(4), pp. 243–269.

Ataie-Ashtiani, B. and Najafi Jilani, A. (2006): Prediction of submerged landslide generated waves in dam reservoirs: an applied approach, *Dam Engineering*, 17(3), pp. 135–155.

Ataie-Ashtiani, B. and Najafi Jilani, A. (2007): A higher-order Boussinesq-type model with moving bottom boundary: applications to submarine landslide tsunami waves, *International Journal for Numerical Methods in Fluids*, 53(6), pp. 1019–1048.

Ataie-Ashtiani, B. and Nik-Khah, A. (2008): Impulsive waves caused by subaerial landslides, *Environmental Fluid Mechanics*, 8(3), pp. 263–280.

Ataie-Ashtiani, B. and Shobeyri, G. (2008): Numerical simulation of landslide impulsive waves by incompressible smoothed particle hydrodynamics, *International Journal for Numerical Methods in Fluids*, 56(2), pp. 209–232.

Ataie-Ashtiani, B. and Yavari-Ramshe, S. (2011): Numerical simulation of wave generated by landslide incidents in dam reservoirs, *Landslides*, 8(4), pp. 417–432.

Atallah, T.A. (2002): *A review on dams and breach parameters estimation*, Master's thesis, The Charles E Via, Jr. Department of Civil and Environmental Engineering, Virginia Polytechnic Institute and State University, 120 pp.

Aubrecht, C., Fuchs, S. and Neuhold, C. (2013): Spatio-temporal aspects and dimensions in integrated disaster risk management, *Natural Hazards*, 68(3), pp. 1205–1216.

Augustinus, P. (1995): Glacial valley cross-profile development: the influence of in situ rock stress and rock mass strength, with examples from the Southern Alps, New Zealand, *Geomorphology*, 14(2), pp. 87–97.

Aven, T. (2007): On the ethical justification for the use of risk acceptance criteria, *Risk Analysis*, 27(2), pp. 303–312.

Aven, T. (2010): On how to define, understand and describe risk, *Reliability Engineering & System Safety*, 95(6), pp. 623–631.

Aven, T. (2012): *Foundations of Risk Analysis*, 2nd edition, John Wiley & Sons, Ltd, Chichester, ISBN 9780470871249/ISSN, 228 pp.

Aven, T. (2013): On how to deal with deep uncertainties in a risk assessment and management context, *Risk Analysis*, 33(12), pp. 2082–2091.

Aven, T. and Kristensen, V. (2005): Perspectives on risk: review and discussion of the basis for establishing a unified and holistic approach, *Reliability Engineering & System Safety*, 90(1), pp. 1–14.

Aven, T. and Renn, O. (2009a): On risk defined as an event where the outcome is uncertain, *Journal of Risk Research*, 12(1), pp. 1–11.

Aven, T. and Renn, O. (2009b): The role of quantitative risk assessments for characterizing risk and uncertainty and delineating appropriate risk management options, with special Emphasis on terrorism risk, *Risk Analysis*, 29(4), pp. 587–600.

BABS (2003): *KATARISK - Katastrophen und Notlagen in der Schweiz, eine Risikobeurteilung aus der Sicht des Bevölkerungsschutzes*, Bundesamt für Bevölkerungsschutz (BABS), Bern, 24 pp.

BABS (2013): *Leitfaden KATAPLAN. Grundlage für kantonale Gefährungsanalysen und Massnahmenplanungen*, Bundesamt für Bevölkerungsschutz (BABS), Bern, 60 pp.

BABS and BAFU (2007): RiskPlan - Risiken erfassen, bewerten und Massnahmen planen, Bundesamt für Bevölkerungsschutz (BABS) and Bundesamt für Umwelt (BAFU) [Access: 31 August 2014], URL http://www.riskplan.admin.ch.

BABS and PLANAT (2008): *Risikoaversion. Entwicklung systematischer Instrumente zur Risiko- bzw. Sicherheitsbeurteilung. Zusammenfassender Bericht*, Bundesamt für Bevölkerungsschutz (BABS), Nationale Plattform Naturgefahren (PLANAT), Bern, 24 pp.

BAFU (2010): EconoMe 2.1. Wirtschaftlichkeit von Schutzmassnahmen gegen Naturgefahren, Bundesamt für Umwelt (BAFU) [Access: 01 June 2011], URL http://www.economе.admin.ch/index.php.

Bajracharya, S. and Mool, P. (2005): Growth of hazardous glacial lakes in Nepal, in *Proceedings of the JICA Regional Seminar on Natural Disaster Mitigation and Issues on Technology Transfer in South and Southeast Asia, 30 September – 13 October 2004, Kathmandu, Nepal*,

(edited by M. Yoshida, B. Upreti, T. Bhattarai and S. Dhakal), Tribhuvan University, Tri-Chandra Campus, Department of Geology with Japan International Cooperation Agency, pp. 131–148.

Bajracharya, S. and Mool, P. (2010): Glaciers, glacial lakes and glacial lake outburst floods in the Mount Everest region, Nepal, *Annals of Glaciology*, 50(53), pp. 81–86.

Bajracharya, S.R. (2009): Glacial lake outburst floods risk reduction activities in Nepal, in *Asia-Pacific Symposium on new technologies for prediction and mitigation of sediment disasters, 18 - 19 November, Tokyo, Japan*, Japan Society of Erosion Control Engineering (JSECE), pp. 11.

Ballantyne, C.K. (2002): A general model of paraglacial landscape response, *The Holocene*, 12(3), pp. 371–376.

Ballantyne, C.K. and Stone, J.O. (2013): Timing and periodicity of paraglacial rock-slope failures in the Scottish Highlands, *Geomorphology*, 186(0), pp. 150–161.

Ballantyne, C.K., Wilson, P., Gheorghiu, D. and Rodés, A. (2014): Enhanced rock-slope failure following ice-sheet deglaciation: timing and causes, *Earth Surface Processes and Landforms*, 39(7), pp. 900–913.

Bara, C. (2010): *Factsheet: social vulnerability to disasters, CRN Report*, Crisis and Risk Network (CRN), Center for Security Studies (CSS) and Swiss Federal Institute of Technology Zürich (ETH), 22 pp.

Barsch, D. and Caine, N. (1984): The nature of mountain geomorphology, *Mountain Research and Development*, 4(4), pp. 287–298.

Bartelt, P., Bühler, Y., Buser, O., Christen, M. and Meier, L. (2012): Modeling mass-dependent flow regime transitions to predict the stopping and depositional behavior of snow avalanches, *Journal of Geophysical Research: Earth Surface*, 117(F1), pp. F01015.

Bartelt, P., Buser, O. and Platzer, K. (2007): Starving avalanches: Frictional mechanisms at the tails of finite-sized mass movements, *Geophysical Research Letters*, 34(20), pp. L20407.

Bartelt, P., Salm, L.B. and Gruberl, U. (1999): Calculating dense-snow avalanche runout using a Voellmyfluid model with active/passive longitudinal straining, *Journal of Glaciology*, 45(150), pp. 242–254.

Becker, U., Dunwoody, S., Holzheu, F., Hunnius, G., Jungermann, H., Kemp, R., Kliemt, J., Lübbe, H., Peters, H.P., Rayner, S., Rohrmann, B., Sinn, H.W., Slovic, P., Somen, H.D., van den Daelen, W., Wiedemann, P.M., Weichenrieder, A.J. and Wildavsky, A. (1993): *Risiko ist ein Konstrukt. Wahrnehmungen zur Risikowahrnehmung*, *Reihe Gesellschaft und Unsicherheit*, vol. 2, Knesebeck, München, ISBN 3-926901-60-8 /ISSN, 362 pp.

Bell, R., Glade, T. and Danscheid, M. (2006): Challenges in defining acceptable risk levels, in *RISK21-Coping with Risks due to Natural Hazards in the 21st Century: Proceedings of the*

Risk21 Workshop, Monte Verita, Ascona, Switzerland, (edited by W.J. Ammann, S. Dannenmann and L. Vulliet), vol. 28, Taylor & Francis, pp. 77–87, doi:10.1201/9780203963562.ch8.

Bender, O., Borsdorf, A., Fischer, A. and Stötter, J. (2011): Mountains under climate and global change conditions - Research results in the Alps, in *Climate Change - Geophysical Foundations and Ecological Effects*, (edited by J. Blanco and H. Kheradmand), InTech, Rijeka, ISBN 978-953-307-419-1/ISSN, pp. 403–422.

Beniston, M., Stephenson, D., Christensen, O., Ferro, C., Frei, C., Goyette, S., Halsnaes, K., Holt, T., Jylha, K., Koffi, B., Palutikof, J., Scholl, R., Semmler, T. and Woth, K. (2007): Future extreme events in European climate: an exploration of regional climate model projections, *Climate Change*, 81(Supplement 1), pp. 71–95.

Benz, W. (1990): Smooth particle hydrodynamics: a review, in *The Numerical Modelling of Nonlinear Stellar Pulsations*, (edited by J.R. Buchler), *NATO ASI Series*, vol. 302, Springer Netherlands, ISBN 978-94-010-6720-1/ISSN, pp. 269–288.

Berger, M.J., George, D.L., LeVeque, R.J. and Mandli, K.T. (2011): The GeoClaw software for depth-averaged flows with adaptive refinement, *Advances in Water Resources*, 34(9), pp. 1195–1206.

BFE (2011a): *Energieszenarien für die Schweiz bis 2050. Erste Ergebnisse der angepassten Szenarien I und IV aus den Energieperspektiven 2007. Zwichenberichte I*, Bundesamt für Energie (BFE), Basel, 101 pp.

BFE (2011b): *Energieszenarien für die Schweiz bis 2050. Erste Ergebnisse der angepassten Szenarien I und IV aus den Energieperspektiven 2007. Zwischenbericht II*, Bundesamt für Energie (BFE), Basel, 122 pp.

BFL and SLF (1984): *Richtlinien zur Berücksichtigung der Lawinengefahren bei raumwirksamen Tätigkeiten*, Bundesamt für Forstwesen und Landschaftsschutz (BFL), Eidgenössisches Institut für Schnee- und Lawinenforschung (SLF), Bern, 42 pp.

BFS (1986): *GEOSTAT, Arealstatistik 1979/1985*, Bundesamt für Statistik (BFS), Neuchâtel.

BFS (1998): *GEOSTAT, Arealstatistik 1992/1997*, Bundesamt für Statistik (BFS), Neuchâtel.

BFS (2010): *Szenarien zur Bevölkerungsentwicklung der Schweiz 2010–2060*, Statistik der Schweiz, Bundesamt für Statistik (BFS), Neuchâtel, ISBN 978-3-303-01251-2/ISSN, 84 pp.

BFS (2011): Erhebungen, Quellen – Arealstatistik der Schweiz: Steckbrief, Bundesamt für Statistik (BFS) [Access: 27 February 2014], URL http://www.bfs.admin.ch/bfs/portal/de/index/infothek/erhebungen__quellen/blank/blank/arealstatistik/01.html.

Bühler, Y., Christen, M., Kowalski, J. and Bartelt, P. (2011): Sensitivity of snow avalanche simulations to digital elevation model quality and resolution, *Annals of Glaciology*, 52(58), pp. 72–80.

Biscarini, C. (2010): Computational fluid dynamics modelling of landslide generated water waves, *Landslides*, 7(2), pp. 117–124.

Bischof, N., Romang, H. and Bründl, M. (2008): Integral risk management of natural hazards - A system analysis of operational application to rapid mass movements, in *Safety, Reliability and Risk Analysis: Theory Methods and Applications*, (edited by S. Martorell, C.G. Soares and J. Barnett), Taylor and Francis, London, ISBN 978-0415485135 /ISSN, pp. 2789 – 2795.

Bland, J. and Altmann, D. (1986): Statistical methods for assessing agreement between two methods of clinical measurement., *The Lancet*, 1(8476), pp. 307–310.

Blaser, L., Ohrnberger, M., Riggelsen, C., Babeyko, A. and Scherbaum, F. (2011): Bayesian networks for tsunami early warning, *Geophysical Journal International*, 185(3), pp. 1431–1443.

Blown, I. and Church, M. (1985): Catastrophic lake drainage within the Homathko River basin, British Columbia, *Canadian Geotechnical Journal*, 22(1), pp. 551–563.

Boeckli, L., Brenning, A., Gruber, S. and Noetzli, J. (2012a): Permafrost distribution in the European Alps: calculation and evaluation of an index map and summary statistics, *The Cryosphere*, 6(4), pp. 807–820.

Boeckli, L., Brenning, A., Gruber, S. and Noetzli, J. (2012b): A statistical approach to modelling permafrost distribution in the European Alps or similar mountain ranges, *The Cryosphere*, 6(1), pp. 125–140.

Bohnenblust, H. and Slovic, P. (1998): Integrating technical analysis and public values in risk-based decision making, *Reliability Engineering & System Safety*, 59(1), pp. 151–159.

Bolch, T., Buchroithner, M., Peters, J., Baessler, M. and Bajracharya, S. (2008): Identification of glacier motion and potentially dangerous glacial lakes in the Mt. Everest region/Nepal using spaceborne imagery, *Natural Hazards and Earth System Sciences*, 8(6), pp. 1329–1340.

Bolch, T., Peters, J., Yegorov, A., Pradhan, B., Buchroithner, M. and Blagoveshchensky, V. (2012): Identification of potentially dangerous glacial lakes in the Northern Tian Shan, in *Terrigenous Mass Movements*, (edited by B. Pradhan and M. Buchroithner), Springer, Berlin, Heidelberg, ISBN 978-3-642-25494-9/ISSN, pp. 369–398.

Bornhold, B. and Thomson, R. (2012): Tsunami hazard assessment related to slope failures in coastal waters, in *Landslides: Types, Mechanisms and Modeling*, (edited by J.J. Clague and D. Stead), Cambridge University Press, Cambridge, ISBN 978-0521045896 /ISSN, pp. 108–120.

Bortz, J. and Döring, N. (2006): Qualitative Methoden, in *Forschungsmethoden und Evaluation*, Springer-Lehrbuch, Springer, Berlin, Heidelberg, ISBN 978-3-540-33305-0/ISSN, pp. 295–350.

Bossel, H. (2004): *Systeme, Dynamik, Simulation. Modellbildung, Analyse und Simulation komplexer Systeme*, Books on Demand, Norderstedt, ISBN 978-3-8334-0984-4/ISSN, 400 pp.

Bottino, G., Chiarle, M., Joly, A. and Mortara, G. (2002): Modelling rock avalanches and their relation to permafrost degradation in glacial environments, *Permafrost and Periglacial Processes*, 13(4), pp. 283–288.

Bouwer, L.M., Bubeck, P. and Aerts, J.C.J.H. (2010): Changes in future flood risk due to climate and development in a Dutch polder area, *Global Environmental Change*, 20(3), pp. 463–471.

Bründl, M. (2009): *Risikokonzept für Naturgefahren - Leitfaden*, Strategie Naturgefahren Schweiz, Nationale Plattform Naturgefahren (PLANAT), Bern, 420 pp.

Bründl, M. (2013): Dealing with natural hazard risks in Switzerland - the influence of hazard mapping on risk-based decision making, in *Dating Torrential Processes on Fans and Cones. Methods and Their Application for Hazard and Risk Assessment. Advances in Global Change Research*, (edited by M. Schneuwly-Bollschweiler, M. Stoffel and F. Rudolf-Miklau), vol. 47, Springer, Dordrecht, ISBN 978-94-007-4336-6/ISSN, pp. 355–365.

Bründl, M., Romang, H., Bischof, N. and Rheinberger, C.M. (2009): The risk concept and its application in natural hazard risk management in Switzerland, *Natural Hazards and Earth System Sciences*, 9(3), pp. 801–813.

Brunetti, M.T., Guzzetti, F. and Rossi, M. (2009): Probability distributions of landslide volumes, *Nonlinear Processes in Geophysics*, 16(2), pp. 179–188.

Brunner, G.W. (2010): *HEC-RAS, river analysis system hydraulic reference manual*, 4.1st edition, Computer Program Documentation, US Army Corps of Engineers,, Hydrologic Engineering Center, Davis, CA, 411 pp.

Burgerschaft (2011): Wälder, Burgerschaft Naters [Access: 13 June 2014], URL http://www.burgerschaft-naters.ch/.

BUWAL (2003): *Landschaft 2020 – Analysen und Trends, Grundlagen zum Leitbild des BUWAL für Natur und Landschaft*, *Schriftenreihe Umwelt*, vol. 352, Bundesamt für Umwelt, Wald und Landschaft (BUWAL), Bern, 154 pp.

BUWAL and BWG (1995): *Symbolbaukasten zur Kartierung der Phänomene*, *Mitteilungen des Bundesamtes für Wasser und Geologie*, vol. 6, Bundesamt für Umwelt, Wald und Landschaft (BUWAL), Bundesamt für Wasser und Geologie (BWG), Bern, 41 pp.

BWG and SGTK (2000): *Lithologisch-Petrographische GIS-Karte 1:500'000*, Schweizerische Geotechnische Kommission (SGTK), Bundesamt für Wasser und Geologie (BWG).

Byers, A., McKinney, D., Somos-Valenzuela, M., Watanabe, T. and Lamsal, D. (2013): Glacial lakes of the Hinku and Hongu valleys, Makalu Barun National Park and Buffer Zone, Nepal, *Natural Hazards*, 69(1), pp. 115–139.

Cammerer, H., Thieken, A. and Verburg, P. (2013): Spatio-temporal dynamics in the flood exposure due to land use changes in the Alpine Lech Valley in Tyrol (Austria), *Natural Hazards*, 68(3), pp. 1243–1270.

Cammerer, H. and Thieken, A.H. (2013): Historical development and future outlook of the flood damage potential of residential areas in the Alpine Lech Valley (Austria) between 1971 and 2030, *Regional Environmental Change*, 13(5), pp. 999–1012.

Cannata, M., Marzocchi, R. and Molinari, M.E. (2012): Modeling of landslide-generated tsunamis with GRASS, *Transactions in GIS*, 16(2), pp. 191–214.

Cannon, S.H. and Savage, W.Z. (1988): A mass-change model for the estimation of debris-flow runout, *The Journal of Geology*, 96(2), pp. 221–227.

Carey, M. (2005): Living and dying with glaciers: people's historical vulnerability to avalanches and outburst floods in Peru, *Global and Planetary Change*, 47(2-4), pp. 122–134.

Carey, M., Huggel, C., Bury, J., Portocarrero, C. and Haeberli, W. (2012): An integrated socio-environmental framework for glacier hazard management and climate change adaptation: lessons from Lake 513, Cordillera Blanca, Peru, *Climatic Change*, 112(3-4), pp. 733–767.

Carpignano, A., Golia, E., Di Mauro, C., Bouchon, S. and Nordvik, J.P. (2009): A methodological approach for the definition of multi-risk maps at regional level: first application, *Journal of Risk Research*, 12(3-4), pp. 513–534.

Carrivick, J.L. (2006): Application of 2D hydrodynamic modelling to high-magnitude outburst floods: an example from Kverkfjöll, Iceland, *Journal of Hydrology*, 321(1–4), pp. 187–199.

Carrivick, J.L. (2007): Modelling coupled hydraulics and sediment transport of a high-magnitude flood and associated landscape change, *Annals of Glaciology*, 45(1), pp. 143–154.

Carrivick, J.L. (2010): Dam break – Outburst flood propagation and transient hydraulics: a geosciences perspective, *Journal of Hydrology*, 380(3–4), pp. 338–355.

Carson, M.A. and Kirkby, M.J. (1972): *Hillslope form and process*, *Cambridge Geographical Studies*, vol. 3, Cambridge University Press, Cambridge, ISBN 9780521109116/ISSN, 476 pp.

Carter, T., la Rovere, E., Jones, R., Leemans, R., Mearns, L., Nakicenovic, N., Pittock, A., Semenov, S. and Skea, J. (2001): Developing and applying scenarios, climate change 2001: impacts, adaptation and vulnerability, in *contribution of Working Group II to the Fourth Assessment Report of the Intergovernmental Panel on Climate Change*, (edited by J. McCarthy, O. Canziani, N. Leary, D. Dokken and K. White), Cambridge, ISBN 0 521 80768 9 /ISSN, pp. 145–190.

Castellanos Abella, E. and Van Westen, C. (2007): Generation of a landslide risk index map for Cuba using spatial multi-criteria evaluation, *Landslides*, 4(4), pp. 311–325.

Cenderelli, D.A. (2000): Floods from natural and artificial dam failures, in *Inland Flood Hazards: Human, Riparian and Aquatic Communities*, (edited by E.E. Wohl), Cambridge University Press, Cambridge, ISBN 0521624193, 9780521624190/ISSN, pp. 73–103.

Cenderelli, D.A. and Wohl, E.E. (2001): Peak discharge estimates of glacial-lake outburst floods and "normal" climatic floods in the Mount Everest region, Nepal, *Geomorphology*, 40(1-2), pp. 57–90.

Chauhan, S.S., Bowles, D.S. and Anderson, L.R. (2004): Do current breach parameter estimation techniques provide reasonable estimates for use in breach modeling?, in *2004 Annual conference of the Association of State Dam Safety Officials, Phoenix, AZ*, pp. 15.

Chen, Y.M., Fan, K.S. and Chen, L.C. (2010): Requirements and functional analysis of a multihazard disaster-risk analysis system, *Human and Ecological Risk Assessment*, 16(2), pp. 413–428.

Chiarle, M., Iannotti, S., Mortara, G. and Deline, P. (2007): Recent debris flow occurrences associated with glaciers in the Alps, *Global and Planetary Change*, 56(1–2), pp. 123–136.

Chisolm, R., Somos-Valenzuela, M., McKinney, D. and Hodges, B. (2013): Using a hydrodynamic lake model to predict the impact of avalanche events at Lake Palcacocha, Peru, in *AGU Fall Meeting Abstracts, Poster*.

Chow, V. (1959): *Open Channel Hydraulics*, McGraw-Hill, New York.

Christen, M., Bartelt, P. and Gruber, U. (2007): RAMMS - a modeling system for snow avalanches, debris flows and rockfals based on IDL, *Photogrammetrie, Fernerkundung, Geoinformation*, 4, pp. 289–292.

Christen, M., Bartelt, P. and Kowalski, J. (2010a): Back calculation of the In den Arelen avalanche with RAMMS: interpretation of model results, *Annals of Glaciology*, 51(54), pp. 161–168.

Christen, M., Kowalski, J. and Bartelt, P. (2010b): RAMMS: Numerical simulation of dense snow avalanches in three-dimensional terrain, *Cold Regions Science and Technology*, 63(1-2), pp. 1–14.

Clague, J. and Mathews, W. (1973): The magnitude of Jökulhlaups, *Journal of Glaciology*, 12(66), pp. 501–504.

Clague, J.J. and Evans, S.G. (2000): A review of catastrophic drainage of moraine-dammed lakes in British Columbia, *Quaternary Science Reviews*, 19(17-18), pp. 1763–1783.

Clague, J.J. and Roberts, M.J. (2012): Landslide hazard and risk, in *Landslides: Types, Mechanisms and Modeling*, (edited by J. Clague and D. Stead), Cambridge University Press, Cambridge, ISBN 978-1-107-00206-7/ISSN, pp. 1–9.

Clarke, G.K. (1982): Glacier outburst floods from "Hazard Lake", Yukon Territory, and the problem of flood magnitude prediction, *Journal of Glaciology*, 28(98), pp. 3–21.

Cochachin, A. (2011): *Batimetría de la Laguna 513, estudio y monitoreo de las lagunas altoandinas*, Unidad de Glaciología y Recursos Hídricos, Autoridad Nacional del Perú, Huaraz, Peru.

Cohen, J.A.. (1960): A coefficient of agreement for nominal scales, *Journal of Educational and Psychological Measurement*, 20, pp. 37–46.

Corominas, J. (1996): The angle of reach as a mobility index for small and large landslides, *Canadian Geotechnical Journal*, 33(2), pp. 260–271.

Costa, J.E. (1994): Floods from dam failures, *Journal of Glaciology*, 40(134), pp. 439–462.

Costa, J.E. and Schuster, R.L. (1988): The formation and failure of natural dams, *Geological Society of America Bulletin*, 100(7), pp. 1054–1068.

Coussot, P. and Meunier, M. (1996): Recognition, classification and mechanical description of debris flows, *Earth-Science Reviews*, 40(3–4), pp. 209–227.

Cox, L.A. (2012): Confronting deep uncertainties in risk analysis, *Risk Analysis*, 32(10), pp. 1607–1629.

Cox, S. and Barrell, D. (2007): *Geology of the Aoraki Area, New Zealand*, Institute of Geological and Nuclear Sciences 1:250,000 geological map 15, GNS Science, Lower Hutt.

Cremonesi, M., Frangi, A. and Perego, U. (2011): A Lagrangian finite element approach for the simulation of water-waves induced by landslides, *Computers & Structures*, 89(11–12), pp. 1086–1093.

Crozier, M. and Glade, T. (2005): Landslide hazard and risk: issues, concepts and approach, in *Landslide Hazard and Risk*, (edited by T. Glade, M. Anderson and M. Crozier), John Wiley & Sons, Chichester, ISBN 978-0-471-48663-3/ISSN, pp. 1–40.

Cruden, D.M. and Varnes, D.J. (1996): Landslide types and processes, in *Landslides: investigation and mitigation, special report 247*, (edited by A. Turner and R. Schuster), Transportation Research Board, National Research Council, National Academy Press, Washington D. C, ISBN 0-309-06208-X/ISSN, pp. 36–75.

Cutter, S., Emrich, C., Webb, J. and Morath, D. (2009): *Social vulnerability to climate variability hazards: a review of the literature*, Final Report to Oxfam America, Hazards and Vulnerability Research Institute Department of Geography (HVRI), University of South Carolina, Columbia, 44 pp.

Dai, F.C., Lee, C.F. and Ngai, Y.Y. (2002): Landslide risk assessment and management: an overview, *Engineering Geology*, 64(1), pp. 65–87.

Dalban Cannassy, P., Bauder, A., Dost, M., Fäh, R., Funk, M., Margreth, S., Müller, B. and Sugiyama, S. (2011): Hazard assessment investigations due to recent changes in Triftgletscher, Bernese Alps, Switzerland, *Natural Hazards and Earth System Sciences*, 11, pp. 2149–2162.

Dao, M.H. and Tkalich, P. (2007): Tsunami propagation modelling - a sensitivity study, *Natural Hazards and Earth System Sciences*, 7(6), pp. 741–754.

Davies, M.C.R., Hamza, O. and Harris, C. (2001): The effect of rise in mean annual temperature on the stability of rock slopes containing ice-filled discontinuities, *Permafrost and Periglacial Processes*, 12(1), pp. 137–144.

Delis, A.I. and Kazolea, M. (2011): Finite volume simulation of waves formed by sliding masses, *International Journal for Numerical Methods in Biomedical Engineering*, 27(5), pp. 732–757.

Delmonaco, G., Margottini, C. and Spizzichino, D. (2006a): *ARMONIA methodology for multi-risk assessment and the harmonisation of different natural risk maps. Deliverable 3.1.1*, Applied multi-risk mapping of natural hazards for impact assessment, 21 pp.

Delmonaco, G., Margottini, C. and Spizzichino, D. (2006b): *Report on new methodology for multi-risk assessment and the harmonisation of didfferent natural risk maps. Deliverable 3.1*, ARMONIA. Applied multi-risk mapping of natural hazards for impact assessment, 21 pp.

Deltares (2011): *Delft3D-FLOW. Simulation of multi-dimensional hydrodynamic flows and transport phenomena, including sediments*, User Manual 3.15, Deltares, Delft, The Netherlands, 688 pp.

Deltares (2013): *SOBEK hydrodynamics, rainfall runoff and real time control*, User Manual 1.00.27425, Deltares, Delft, The Netherlands, 910 pp.

Denlinger, R.P. and Iverson, R.M. (2001): Flow of variably fluidized granular masses across three-dimensional terrain: 2. Numerical predictions and experimental tests, *Journal of Geophysical Research: Solid Earth*, 106(B1), pp. 553–566.

Denlinger, R.P. and Iverson, R.M. (2004): Granular avalanches across irregular three-dimensional terrain: 1. Theory and computation, *Journal of Geophysical Research: Earth Surface*, 109(F1), pp. F01014.

Di Risio, M., De Girolamo, P. and Beltrami, G. (2011): Forecasting landslide generated tsunamis: a review, in *The Tsunami Threat - Research and Technology*, (edited by N.A. Mörner), ISBN 978-953-307-552-5/ISSN, pp. 26.

Di Risio, M. and Sammarco, P. (2008): Analytical modeling of landslide-generated waves, *Journal of Waterway, Port, Coastal, and Ocean Engineering*, 134(1), pp. 53–60.

Domnik, B., Pudasaini, S.P., Katzenbach, R. and Miller, S.A. (2013): Coupling of full two-dimensional and depth-averaged models for granular flows, *Journal of Non-Newtonian Fluid Mechanics*, 201, pp. 56–68.

Dussaillant, A., Benito, G., Buytaert, W., Carling, P., Meier, C. and Espinoza, F. (2010): Repeated glacial-lake outburst floods in Patagonia: an increasing hazard?, *Natural Hazards*, 54(2), pp. 469–481.

Eisbacher, G. and Clague, J.J. (1984): *Destructive mass movements in high-mountains - hazard and management*, *Geological Survey of Canada*, vol. 84-16, Canadian Government Publishing Centre, Ottawa, ISBN 0-660-11729-0 /ISSN, 1-230 pp.

Elliott, J.R. and Pais, J. (2006): Race, class, and Hurricane Katrina: Social differences in human responses to disaster, *Social Science Research*, 35(2), pp. 295–321.

Emmer, A., Vilímek, V., Klimeš, J. and Cochachin, A. (2014): Glacier retreat, lakes development and associated natural hazards in Cordillera Blanca, Peru, in *Landslides in Cold Regions in the Context of Climate Change*, (edited by W. Shan, Y. Guo, F. Wang, H. Marui and A. Strom), Environmental Science and Engineering, Springer International Publishing, ISBN 978-3-319-00866-0/ISSN, pp. 231–252.

Epp, M. (2013): *Bathymetrie und Analyse von hochalpinen Seen mittels ferngesteuertem Echolot*, Master's thesis, Department of Geography, University of Zürich, 80 pp.

Ermini, L. and Casagli, N. (2003): Prediction of the behaviour of landslide dams using a geomorphological dimensionless index, *Earth Surface Processes and Landforms*, 28(1), pp. 31–47.

Evans, S. (1986): The maximum discharge of outburst floods caused by the breaching of man-made and natural dams, *Canadian Geotechnical Journal*, 23(3), pp. 385–387.

Evans, S. and Delaney, K. (2015): Catastrophic mass flows in the mountain glacial environment, in *Snow and Ice-Related Hazards, Risks and Disasters*, (edited by W. Haeberli and C. Whiteman), Elsevier, pp. 107–128.

Eymard, E., Gallou, T., Hilhorst, D. and Slimane, Y. (1998): Finite volumes and nonlinear diffusion equations, *RAIRO Mathematical Modelling and Numerical Analysis*, 32(6), pp. 747–761.

Faber, M. and Maes, M. (2005): Epistemic uncertainties and system choice in decision making, in *ICOSSAR'05 9th International Conference on Structural Safety and Reliability, 19 - 23 June 2005, Rome, Italy*, (edited by G. Augusti, G. Schuëller and M. Ciampoli), pp. 3519–3526.

Faeh, R. (2007): Numerical modeling of breach erosion of river embankments, *Journal of Hydraulic Engineering*, 133(9), pp. 1000–1009.

Faillettaz, J. and Funk, M. (2013): Glacier instabilities and prediction, *Mémoire de la Société vaudoise des Sciences naturelles*, 25, pp. 159–174.

Farinotti, D., Huss, M., Bauder, A. and Funk, M. (2009): An estimate of the glacier ice volume in the Swiss Alps, *Global and Planetary Change*, 68(3), pp. 225–231.

Feah, R., Mueller, R., Rousselot, P., Vetsch, D., Volz, C., Vonwiller, L., Veprek, R. and Farshi, D. (2011): *System Manuals of BASEMENT. Version 2.1*, Laboratory of Hydroulics, Glaciology and Hydrology (VAW). ETH Zürich. Available from URL http://www.basement.ethz.ch. [Access: 13 April 2014], 248 pp.

Fell, R., Ho, K., Lacasse, S. and Leroi, E. (2005): A framework for landslide risk assessment and management, in *Landslide Risk Management*, (edited by O. Hungr, R. Fell, R. Couture and E. Eberhardt), CRC Press, Vancouver, Canada, ISBN 9780415380430/ISSN, pp. 23.

Fischer, L., Amann, F., Moore, J.R. and Huggel, C. (2010): Assessment of periglacial slope stability for the 1988 Tschierva rock avalanche (Piz Morteratsch, Switzerland), *Engineering Geology*, 116(1–2), pp. 32–43.

Fischer, L., Kääb, A., Huggel, C. and Noetzli, J. (2006): Geology, glacier retreat and permafrost degradation as controlling factors of slope instabilities in a high-mountain rock wall: the Monte Rosa east face, *Natural Hazards and Earth System Sciences*, 6(5), pp. 761–772.

Fischer, L., Purves, R.S., Huggel, C., Noetzli, J. and Haeberli, W. (2012): On the influence of topographic, geological and cryospheric factors on rock avalanches and rockfalls in high-mountain areas, *Natural Hazards and Earth System Sciences*, 12(1), pp. 241–254.

FLO-2D (2014): FLO-2D, FLO-2D Software, INC, Nutrioso, AZ [Access: 05 April 2014], URL http://www.flo-2d.com/.

Flubacher, M., Huggel, C., Kääb, A. and Zemp, M. (2007): Web-based database on worldwide glacier and permafrost disasters, in *Geophysical Research Abstracts, European Geosciences Union*, vol. 9, pp. 2.

Fort, M., Cossart, E., Deline, P., Dzikowski, M., Nicoud, G., Ravanel, L., Schoeneich, P. and Wassmer, P. (2009): Geomorphic impacts of large and rapid mass movements: a review, *Géomorphologie : relief, processus, environnement*, 1, pp. 47–67.

Frattini, P., Crosta, G., Carrara, A. and Agliardi, F. (2008): Assessment of rockfall susceptibility by integrating statistical and physically-based approaches, *Geomorphology*, 94(3-4), pp. 419–437.

Fread, D.L. (1982): *DAMBRK: The NWS dam-break flood forecasting model*, Hydrologic Research Laboratory, National Weather Service, Silver Spring, Maryland, 56 pp.

Fread, D.L. (1991): *Breach: an erosion model for earthern dam failures*, Silver Spring, MD: Hydrological Research Laboratory, National Weather Service, National Oceanic and Atmospheric Administration, 39 pp.

Frey, H. (2007): *Identifikation und Analyse von Gletscherseen mit Fernerkundung und GIS*, Diploma thesis, Department of Geography, University of Zürich, 117 pp.

Frey, H., Haeberli, W., Linsbauer, A., Huggel, C. and Paul, F. (2010a): A multi-level strategy for anticipating future glacier lake formation and associated hazard potentials, *Natural Hazards and Earth System Sciences*, 10(2), pp. 339–352.

Frey, H., Huggel, C., Paul, F. and Haeberli, W. (2010b): Automated detection of glacier lakes based on remote sensing in view of assessing associated hazard potentials, *Grazer Schriften der Geographie und Raumforschung*, 45, pp. 206–216.

Fritz, H.M., Hager, W.H. and Minor, H.E. (2003a): Landslide generated impulse waves. 1. Instantaneous flow fields, *Experiments in Fluids*, 35(6), pp. 505–519.

Fritz, H.M., Hager, W.H. and Minor, H.E. (2003b): Landslide generated impulse waves. 2. Hydrodynamic impact craters, *Experiments in Fluids*, 35(6), pp. 520–532.

Fuchs, H., Pfister, M., Boes, R., Perzlmaier, S. and Reindl, R. (2011): Impulswellen infolge Lawineneinstoß in den Speicher Kühtai, *WasserWirtschaft*, Wasserbau 1-2, pp. 54–60.

Fuchs, S. (2013): Cost-benefit analysis of natural hazard mitigation, in *Encyclopedia of Natural Hazards*, (edited by P. Bobrowsky), Springer, Dordrecht, Heidelberg, New York, London, ISBN 9048186994/ISSN, pp. 121–125.

Fuchs, S., Keiler, M., Sokratov, S. and Shnyparkov, A. (2013): Spatiotemporal dynamics: the need for an innovative approach in mountain hazard risk management, *Natural Hazards*, 68(3), pp. 1217–1241.

Gardelle, J., Arnaud, Y. and Berthier, E. (2011): Contrasted evolution of glacial lakes along the Hindu Kush Himalaya mountain range between 1990 and 2009, *Global and Planetary Change*, 75(1-2), pp. 47–55.

Gądek, B. (2014): Climatic sensitivity of the non-glaciated mountains cryosphere (Tatra Mts., Poland and Slovakia), *Global and Planetary Change*, 121(0), pp. 1–8.

George, D.L. (2011): Adaptive finite volume methods with well-balanced Riemann solvers for modeling floods in rugged terrain: application to the Malpasset dam-break flood (France, 1959), *International Journal for Numerical Methods in Fluids*, 66(8), pp. 1000–1018.

Georges, C. (2004): 20th-century glacier fluctuations in the tropical Cordillera Blanca, Peru, *Arctic, Antarctic, and Alpine Research*, 36(1), pp. 100–107.

Gigli, G., Frodella, W., Garfagnoli, F., Morelli, S., Mugnai, F., Menna, F. and Casagli, N. (2014): 3-D geomechanical rock mass characterization for the evaluation of rockslide susceptibility scenarios, *Landslides*, 11(1), pp. 131–140.

Glaciorisk (2003): Gridabase - glacier risks data base. Glaciorisk European project. Survey and prevention of extreme glaciological hazards in European mountainous regions [Access: 25 May 2014], URL http://www.nimbus.it/glaciorisk/gridabasemainmenu.asp.

Glade, T. and Crozier, M.J. (2005): The nature of landslide hazard impact, in *Landslide Hazard and Risk*, (edited by T. Glade, M. Anderson and M. Crozier), John Wiley & Sons, Ltd, Chichester, ISBN 0-471-48663-9/ISSN, pp. 43–74.

Gletschersee (2012): Gletschersee Grindelwald, Oberingenieurkreis I Kanton Bern, Regierungsstatthalteramt Interlaken, Einwohnergemeinde Grindelwald, Schwellenkorporation Grindelwald [Access: 10 June 2012], URL www.gletschersee.ch.

GoC (2007): An emergency management framework for Canada, Government of Canada (GoC) Emergency Management Policy Directorate, Public Safety and Emergency Preparedness, Ottawa [Access: 23 May 2014], URL http://www.webcitation.org/5uKgDgagl.

Gomez-Gesteira, M., Crespo, A.J.C., Rogers, B.D., Dalrymple, R.A., Dominguez, J.M. and Barreiro, A. (2012a): SPHysics – development of a free-surface fluid solver – Part 2: Efficiency and test cases, *Computers & Geosciences*, 48(0), pp. 300–307.

Gomez-Gesteira, M., Rogers, B.D., Crespo, A.J.C., Dalrymple, R.A., Narayanaswamy, M. and Dominguez, J.M. (2012b): SPHysics – development of a free-surface fluid solver – Part 1: Theory and formulations, *Computers & Geosciences*, 48(0), pp. 289–299.

Grabs, W.E. and Hanisch, J. (1993): Objectives and prevention methods for glacier lake outburst floods (GLOFs), in *Snow and Glacier Hydrology (Proceedings of the Kathmandu Symposium, 16 – 21 November 1992)*, (edited by IAHS), International Association of Hydrological Sciences (IAHS), Great Yarmouth, pp. 341–352.

Grêt-Regamey, A., Brunner, S.H., Altwegg, J. and Bebi, P. (2013): Facing uncertainty in ecosystem services-based resource management, *Journal of Environmental Management*, 127(Supplement), pp. S145–S154.

Grêt-Regamey, A. and Straub, D. (2006): Spatially explicit avalanche risk assessment linking Bayesian networks to a GIS, *Natural Hazards and Earth System Sciences*, 6(6), pp. 911–926.

Gruber, F.E. and Mergili, M. (2013): Regional-scale analysis of high-mountain multi-hazard and risk indicators in the Pamir (Tajikistan) with GRASS GIS, *Natural Hazards and Earth System Sciences*, 13(11), pp. 2779–2796.

Gruber, S. (2012): Derivation and analysis of a high-resolution estimate of global permafrost zonation, *The Cryosphere*, 6(1), pp. 221–233.

Gruber, S. and Haeberli, W. (2007): Permafrost in steep bedrock slopes and its temperature-related destabilization following climate change, *Journal of Geophysical Research*, 112(F2), pp. 10.

Gruber, S., Hoelzle, M. and Haeberli, W. (2004): Permafrost thaw and destabilization of Alpine rock walls in the hot summer of 2003, *Geophysical Research Letters*, 31(13), pp. 4.

Guillén Ludeña, S., Schaub, Y., Mölg, N. and Schleiss, A. (2014): *Numerical simulation of ice-rock avalanche impacts over glacier lakes, unpublished report*, Laboratoire de Constructions Hydrauliques LCH-EPFL, Department of Geography University of Zürich.

GVB (n.y.): *Ihr Gebäude ist bei der GVB versichert - Wichtige Hinweise bei Schäden durch Hagel, Sturmwind und Überschwemmungen*, Gebäudeversicherung Bern, Bern.

Haeberli, W. (1976): Eistemperaturen in den Alpen, *Zeitschrift für Gletscherkunde und Glazialgeologie*, 11(2), pp. 203–220.

Haeberli, W. (1983): Frequency and characteristics of glacier floods in the Swiss Alps, *Annals of Glaciology*, 4, pp. 85–90.

Haeberli, W. (1992): Zur Stabilität von Moränenseen, *Wasser Energie Luft*, 84(11/12), pp. 361–364.

Haeberli, W., Alean, J., Müller, P. and Funk, M. (1989): Assessing risks from glacier hazards in high mountain regions: some experiences in the Swiss Alps, *Annals of Glaciology*, 13, pp. 96–102.

Haeberli, W., Clague, J.J., Huggel, C. and Kääb, A. (2010a): Hazards from lakes in high-mountain glacier and permafrost regions: climate change effects and process interactions, in *Advances de Geomorfología en España 2008 - 2010. XI Reunión Nacional de Geomorfología, Solsona*, pp. 439–446.

Haeberli, W., Hoelzle, M., Paul, F. and Zemp, M. (2007): Integrated monitoring of mountain glaciers as key indicators of global climate change: the European Alps, *Annals of Glaciology*, 46, pp. 150–160.

Haeberli, W., Kääb, A., Mühll, D.V. and Teysseire, P. (2001): Prevention of outburst floods from periglacial lakes at Grubengletscher, Valais, Swiss Alps, *Journal of Glaciology*, 47(156), pp. 111–122.

Haeberli, W. and Linsbauer, A. (2013): Brief communication 'Global glacier volumes and sea level - small but systematic effects of ice below the surface of the ocean and of new local lakes on land', *Cryosphere*, 7(3), pp. 817–821.

Haeberli, W., Portocarrero, C. and Evans, S.G. (2010b): *Nevado Hualcán, Laguna 513 y Carhuaz 2010 - observaciones, evaluación y recomendaciones.*, "Informe 513" un corto informe técnico luego de las reuniones y visita de campo en Julio 2010. On behalf of the Municipalidad de Carhuaz.

Haeberli, W., Schleiss, A., Linsbauer, A., Künzler, M. and Bütler, M. (2012): Gletscherschwund und neue Seen in den Schweizer Alpen: Perspektiven und Optionen im Bereich Naturgefahren und Wasserkraft, *Wasser Energie Luft*, 104(2), pp. 93–102.

Haeberli, W., Wegmann, M. and Vonder Mühll, D. (1997): Slope stability problems related to glacier shrinkage and permafrost degradation in the Alps, *Eclogae Geologicae Helvetiae*, 90, pp. 407–414.

Hancox, G., McSaveney, M.J., Manville, V.R. and Davies, T.R. (2005): The October 1999 Mt Adams rock avalanche and subsequent landslide dam-break flood and effects in Poerua River, Westland, New Zealand, *New Zealand Journal of Geology and Geophysics*, 48(4), pp. 683–705.

Harris, C., Arenson, L.U., Christiansen, H.H., Etzelmüller, B., Frauenfelder, R., Gruber, S., Haeberli, W., Hauck, C., Hölzle, M., Humlum, O., Isaksen, K., Kääb, A., Kern-Lütschg, M.A., Lehning, M., Matsuoka, N., Murton, J.B., Nötzli, J., Phillips, M., Ross, N., Seppälä, M., Springman, S.M. and Vonder Mühll, D. (2009): Permafrost and climate in Europe: monitoring and modelling thermal, geomorphological and geotechnical responses, *Earth-Science Reviews*, 92(3-4), pp. 117–171.

Harrison, S., Glasser, N., Winchester, V., Haresign, E., Warren, C. and Jansson, K. (2006): A glacial lake outburst flood associated with recent mountain glacier retreat, Patagonian Andes, *The Holocene*, 16(4), pp. 611–620.

Hasler, A. (2011): *Thermal conditions and kinematics of steep bedrock permafrost*, Doctoral thesis, Department of Geography, University of Zürich, 165 pp.

Hasler, A., Gruber, S. and Haeberli, W. (2011): Temperature variability and offset in steep alpine rock and ice faces, *The Cryosphere*, 5, pp. 977–988.

Hegglin, E. and Huggel, C. (2008): An integrated assessment of vulnerability to glacial hazards: a case study in the Cordillera Blanca, Peru, *Mountain Research and Development*, 28(3/4), pp. 299–309.

Heim, A. (1932): *Bergsturz und Menschenleben*, Fretz und Wasmuth, Zürich.

Heinimann, H.R., Hollenstein, K., Kienholz, H., Krummenacher, B. and Mani, P. (1998): *Methoden zur Analyse und Bewertung von Naturgefahren*, Bern, 200 pp.

Heller, V. and Hager, W.H. (2011): Wave types of landslide generated impulse waves, *Ocean Engineering*, 38(4), pp. 630–640.

Heller, V., Hager, W.H. and Minor, H.E. (2008): *Rutscherzeugte Impulswellen in Stauseen: Grundlagen und Berechnung*, Mitteilungen 206 der Versuchsanstalt für Wasserbau, Hydrologie und Glaziologie (VAW), ETH Zürich, 172 pp.

Hencher, S.R., Lee, S.G., Carter, T.G. and Richards, L.R. (2011): Sheeting Joints: characterisation, shear strength and engineering, *Rock Mechanics and Rock Engineering*, 44(1), pp. 1–22.

Henderson, M. (1966): *Open Channel Flow*, Macmillan series in civil engineering, New York, ISBN 0-02-353510-5 /ISSN, 522 pp.

Herget, J. (2005): *Reconstruction of Pleistocene ice-dammed lake outburst floods in the Altai Mountains, Siberia*, The Geological Society of America Special Paper 386, The Geological Society of America, Boulder, Colorado, ISBN 0-8137-2386-8/ISSN.

Hewitt, K. (1982): Natural dams and outburst floods of the Karakoram Himalaya, in *Hydrological Aspects of Alpine and High Mountain Areas (Proceedings of the Exeter Symposium, July 1982)*, vol. 138, International Association of Hydrological Sciences (IAHS), pp. 259–269.

Hewitt, K. (1983): *Interpretations of calamity from the viewpoint of human ecology*, Allen & Unwin, Boston, ISBN 0043011608/ISSN.

Hewitt, K. and Burton, I. (1971): *Hazardousness of a place: a regional ecology of damaging events.*, University of Toronto Press, Toronto, 154 pp.

Hählen, N. (2008): *Gletschersee Grindelwald - Abschätzung Schadenpotential*, Tiefbauamt des Kantons Bern Oberingenieurkreis I, Thun.

Hiess, H. (2010): *Spatial planning in climate change: a CIPRA background report*, *COMPACT*, vol. 02, International Commission for the Protection of the Alps (CIPRA), Schaan, 32 pp.

Hirt, C.W. and Nichols, B.D. (1981): Volume of fluid (VOF) method for the dynamics of free boundaries, *Journal of Computational Physics*, 39(1), pp. 201–225.

Hoek, E. and Brown, E. (1997): Practical estimates of rock mass strength, *International Journal of Rock Mechanics and Mining Sciences*, 34(8), pp. 1165–1186.

Holm, K., Bovis, M. and Jakob, M. (2004): The landslide response of alpine basins to post-Little Ice Age glacial thinning and retreat in southwestern British Columbia, *Geomorphology*, 57(3–4), pp. 201–216.

Holzer, M. (2011): Oral statements about land use development scenarios in Naters, interview (in German).

Hürlimann, M., Rickenmann, D., Medina, V. and Bateman, A. (2008): Evaluation of approaches to calculate debris-flow parameters for hazard assessment, *Engineering Geology*, 102(3-4), pp. 152–163.

Hubbard, B., Heald, A., Reynolds, J.M., Quincey, D., Richardson, S.D., Zapato, M., Santillan, N. and Hambrey, M.J. (2005): Impact of a rock avalanche on a moraine-dammed proglacial lake: Laguna Safuna Alta, Cordillera Blanca, Peru, *Earth Surface Processes and Landforms*, 30(10), pp. 1251–1264.

Huber, A. (1980): *Schwallwellen in Seen als Folge von Felsstürzen*, Mitteilungen der Versuchsanstalt für Wasserbau, Hydrologie und Glaziologie 47, ETH Zürich, Zürich, Switzerland.

Hufschmidt, G. (2011): A comparative analysis of several vulnerability concepts, *Natural Hazards*, 58(2), pp. 621–643.

Huggel, C. (2009): Recent extreme slope failures in glacial environments: effects of thermal perturbation, *Quaternary Science Reviews*, 28(11-12), pp. 1119–1130.

Huggel, C. (2010): *Dynamic controls on high-mountain risks - an integrated perspective*, Habilitation, Department of Geography, University of Zürich, 96 pp.

Huggel, C., Clague, J.J. and Korup, O. (2012): Is climate change responsible for changing landslide activity in high mountains?, *Earth Surface Processes and Landforms*, 37(1), pp. 77–91.

Huggel, C., Haeberli, W., Kääb, A., Bieri, D. and Richardson, S.D. (2004): An assessment procedure for glacial hazards in the Swiss Alps, *Canadian Geotechnical Journal*, 41(6), pp. 1068–1083.

Huggel, C., Kääb, A. and Haeberli, W. (2002a): Glacier hazards [Access: 03 June 2011], URL http://www.glacierhazards.ch.

Huggel, C., Kääb, A., Haeberli, W. and Krummenacher, B. (2003): Regional-scale GIS-models for assessment of hazards from glacier lake outbursts: evaluation and application in the Swiss Alps, *Natural Hazards and Earth System Sciences*, 3(6), pp. 647–662.

Huggel, C., Kääb, A., Haeberli, W., Teysseire, P. and Paul, F. (2002b): Remote sensing based assessment of hazards from glacier lake outbursts: a case study in the Swiss Alps, *Canadian Geotechnical Journal*, 39(2), pp. 316–330.

Huggel, C., Korup, O. and Gruber, S. (2013): Landslide hazards and climate change in high mountains, *Treatise on Geomophology. Elsevier Science*, 13(17), pp. 288–301.

Huggel, C., Zgraggen-Oswald, S., Haeberli, W., Kääb, A., Polkvoj, A., Galushkin, I. and Evans, S.G. (2005): The 2002 rock/ice avalanche at Kolka/Karmadon, Russian Caucasus: assessment of extraordinary avalanche formation and mobility, and application of QuickBird satellite imagery, *Natural Hazards and Earth System Sciences*, 5(2), pp. 173–187.

Hungr, O. (1995): A model for the runout analysis of rapid flow slides, debris flows, and avalanches, *Canadian Geotechnical Journal*, 32(4), pp. 610–623.

Hungr, O. (2008): Numerical modelling of the dynamics of debris flows and rock avalanches, *Geomechanik und Tunnelbau*, 1(2), pp. 112–119.

Hungr, O., Corominas, J. and Eberhardt, E. (2005): Estimating landslide motion mechanism, travel distance and velocity, in *Landslide Risk Management*, (edited by O. Hungr, R. Fell, R. Couture and E. Eberhardt), Taylor & Francis Group, London, ISBN 04-1538-043-X/ISSN, pp. 99–128.

Hungr, O., Evans, S.G., Bovis, M.J. and Hutchinson, J.N. (2001): A review of the classification of landslides of the flow type, *Environmental & Engineering Geoscience*, 7(3), pp. 221–238.

Hungr, O. and McDougall, S. (2009): Two numerical models for landslide dynamic analysis, *Computers & Geosciences*, 35(5), pp. 978–992.

Hunziker, M. (1995): The spontaneous reafforestation in abandoned agricultural lands: perception and aesthetic assessment by locals and tourists, *Landscape and Urban Planning*, 81(31), pp. 399–410.

Huss, M., Farinotti, D., Bauder, A. and Funk, M. (2008): Modelling runoff from highly glacierized alpine drainage basins in a changing climate, *Hydrological Processes*, 22(19), pp. 3888–3902.

Hutter, K., Wang, Y. and Pudasaini, S.P. (2005): The Savage–Hutter avalanche model: how far can it be pushed?, *Philosophical Transactions of the Royal Society A: Mathematical, Physical and Engineering Sciences*, 363(1832), pp. 1507–1528.

IBER (2010a): *IBER - Two-dimensional modelling of free surface shallow water flow. Hydraulic reference manual v1.0*, 56 pp.

IBER (2010b): *IBER - Two-dimensional modelling of free surface shallow water flow. Quick start guide v1.0*, 22 pp.

INAGGA (1997): *Estudios de vulnerabilidad de recursos hídricos de alta montaña*, Instituto Andino de Glaciología y Geo Ambiente (INAGGA), Huaraz.

INDECI (2006): *Manual basico para la estimación del riesgo*, 1st edition, Instituto Nacional de Defensa Civil (INDECI), Lima, Peru, 69 pp.

IPCC (2012): *Managing the risks of extreme events and disasters to advance climate change adaptation*, A special report of working groups I and II of the Intergovernmental Panel on Climate Change, Cambridge University Press, Cambridge, UK, and New York, NY, USA, ISBN 978-1-107-02506-6 /ISSN, 582 pp.

IPCC (2013): *Climate Change 2013. The Physical Science Basis. Summary for Policiymakers, Technical Summary and Frequently Asked Questions*, Part of the Working Group I Contribution to the Fifth Assessment Report of the Intergovernmental Panel on Climate Change, Intergovernmental Panel on Climate Change, ISBN 978-92-9269-138-8/ISSN, 203 pp.

Iribarren Anacona, P., Mackintosh, A. and Norton, K.P. (2014): Hazardous processes and events from glacier and permafrost areas: lessons from the Chilean and Argentinean Andes, *Earth Surface Processes and Landforms*, pp. 20.

Iverson, R., Schilling, S. and Vallance, J. (1998): Objective delineation of areas at risk from inundation by lahars, *Geological Society of America Bulletin*, 110(8), pp. 972–984.

Iverson, R.M., Logan, M. and Denlinger, R.P. (2004): Granular avalanches across irregular three-dimensional terrain: 2. Experimental tests, *Journal of Geophysical Research: Earth Surface*, 109(F1), pp. F01015.

Ives, J., Shrestha, R. and Mool, P. (2010): *Formation of glacial lakes in the Hindukush-Himalayas and GLOF risk assessment*, International Centre for Integrated Mountain Development (ICIMOD), Kathmandu, ISBN 978 92 9115 137 0 /ISSN, 66 pp.

Jaboyedoff, M., Baiffard, F., Couture, R., Locat, J. and Locat, P. (2004): Toward preliminary hazard assessment using DEM topographic analysis and simple mechanic modeling, in *Landslides Evaluation and Stabilization. Set of 2 Volumes: Proceedings of the Ninth International Symposium on Landslides, 28 June - 2 July , 2004 Rio de Janeiro, Brazil*, (edited by W. Lacerda, M. Ehrlich, A. Fontoura and A. Sayo), CRC Press, London, ISBN 9780415356657/ISSN, pp. 191–197.

Jaboyedoff, M., Baillifard, F., Bardou, E. and Girod, F. (2004b): The effect of weathering on Alpine rock instability, *Quarterly Journal of Engineering Geology and Hydrogeology*, 37(2), pp. 95–103.

Jaboyedoff, M., Baillifard, F., Philippossian, F. and Rouiller, J.D. (2004c): Assessing fracture occurrence using "weighted fracturing density": a step towards estimating rock instability hazard, *Natural Hazards and Earth System Sciences*, 4(1), pp. 83–93.

Jaboyedoff, M., Oppikofer, T., Abellán, A., Derron, M.H., Loye, A., Metzger, R. and Pedrazzini, A. (2012): Use of LIDAR in landslide investigations: a review, *Natural Hazards*, 61(1), pp. 5–28.

Jakob, M. (2005): A size classification for debris flows, *Engineering Geology*, 79(3–4), pp. 151–161.

Jensen, F. and Nielsen, T. (2007): *Bayesian Networks and Decision Graphs*, Information Science and Statistics, Springer Science and Business Media, New York, ISBN 0-387-68281-3/ISSN, 447 pp.

Jonkman, S.N., van Gelder, P.H.A.J.M. and Vrijling, J.K. (2003): An overview of quantitative risk measures for loss of life and economic damage, *Journal of Hazardous Materials*, 99(1), pp. 1–30.

Kabacoff, R. (2011): *R in Action. Data analysis and graphics with R*, Manning Publications Co., Shelter Island, NY, ISBN 1935182390/ISSN, 474 pp.

Kaibori, M., Sassa, K. and Tochiki, S. (1988): Betrachtung über die Bewegung von Absturzmaterialien, *International Symposium of INTERPRAEVENT*, 7(2), pp. 227–242.

Kantonsforstamt (2011): Waldeigentum, Kantonsforstamt St. Gallen [Access: 03 June 2014], URL http://www.wald.sg.ch/home/waldeigentum.html.

Kaplan, S. and Garrick, B.J. (1981): On the quantitative definition of risk, *Risk Analysis*, 1(1), pp. 11–27.

Kappes, M. (2011): *Multi-Hazard Risk Analyses: a Concept and its Implementation*, Doctoral thesis, Geography Department, University of Vienna, 375 pp.

Kappes, M., Keiler, M., Elverfeldt, K. and Glade, T. (2012): Challenges of analyzing multi-hazard risk: a review, *Natural Hazards*, 64(2), pp. 1925–1958.

Kappes, M., Keiler, M. and Glade, T. (2010): From single- to multi-hazard risk analyses: a concept addressing emerging challenges, in *Proceedings of Mountain Risks International conference, 24 - 26 November 2010, Firenze, Italy*, (edited by J.P. Malet, T. Glade and N. Casagli), CERG, pp. 24–26.

Kappes, M.S., Malet, J.P., Remaître, A., Horton, P., Jaboyedoff, M. and Bell, R. (2011): Assessment of debris-flow susceptibility at medium-scale in the Barcelonnette Basin, France, *Natural Hazards and Earth System Sciences*, 11(2), pp. 627–641.

Kattelmann, R. (2003): Glacial lake outburst floods in the Nepal Himalaya: a manageable hazard?, *Natural Hazards*, 28(1), pp. 145–154.

Kattelmann, R. and Watanabe, T. (1998): Approaches to reducing the hazard of an outburst flood of Imja glacier Lake, Khumbu Himalaya, in *Proceedings of International Conference on Ecohydrology of High Mountain Areas. 24 - 28 March 1996, Kathmandu, Nepal*, UNESCO, pp. 359–366.

Keiser, R. (2006): *Meshless Lagrangian Methods for Physics-Based Animations of Solids and Fluids*, Doctoral thesis, Swiss Federal Institute of Technology, ETH Zürich, 195 pp.

Kershaw, J.A., Clague, J.J. and Evans, S.G. (2005): Geomorphic and sedimentological signature of a two-phase outburst flood from moraine-dammed Queen Bess Lake, British Columbia, Canada, *Earth Surface Processes and Landforms*, 30(1), pp. 1–25.

Kim, J.H. and Pearl, J. (1983): A computational model for causal and diagnostic reasoning in inference systems, in *Proceedings of the Eighth International Joint Conference on Artificial Intelligence, 8-12 August 1983, Karlsruhe*, pp. 190–193.

Kirby, J.T., Wei, G., Chen, Q., Kennedy, A.B. and Dalrymple, R.A. (1998): *Funwave 1.0, fully nonlinear Boussinesq wave model documentation and user's manual*, *Res. Rep. CACR-98*, vol. 6, Center for Applied Coastal Research, Department of Civil Engineering, University of Delaware, Newark, 70 pp.

Kjærulff, U. and Madsen, A. (2013): *Bayesian Networks and Influence Diagrams: A Guide to Construction and Analysis*, *Information Science and Statistics*, vol. 22, 3rd edition, Springer, New York, ISBN 978-1-4614-5103-7/ISSN, 382 pp.

Klimeš, J., Benešová, M., Vilímek, V., Bouška, P. and Cochachin Rapre, A. (2014): The reconstruction of a glacial lake outburst flood using HEC-RAS and its significance for future hazard assessments: an example from Lake 513 in the Cordillera Blanca, Peru, *Natural Hazards*, 71(3), pp. 1617–1638.

Künzler, M., Huggel, C. and Ramírez, J. (2012): Rapid risk analysis for floods and volcanic debris flows – case study in Colombia, *Natural Hazards*, 1(64), pp. 767–796.

Korup, O. and Clague, J.J. (2009): Natural hazards, extreme events, and mountain topography, *Quaternary Science Reviews*, 28(11-12), pp. 977–990.

Korup, O. and Tweed, F. (2007): Ice, moraine, and landslide dams in mountainous terrain, *Quaternary Science Reviews*, 26(25–28), pp. 3406–3422.

Kothe, D., Williams, M., Lam, K., Korzekwa, D., Tubesing, P. and Puckett, E. (1999): A second-order accurate, linearity-preserving volume tracking algorithm for free surface flows on 3-D unstructured meshes, in *Proceedings of the 3rd ASME/JSME Joint Fluids Engineering Conference, San Francisco, CA*, Citeseer, pp. 1–6.

Kowalski, J. (2008): *Two-phase modeling of debris flows*, Doctoral thesis, Swiss Federal Institute of Technology, ETH Zürich, 136 pp.

Krautblatter, M., Funk, D. and Günzel, F.K. (2013): Why permafrost rocks become unstable: a rock–ice-mechanical model in time and space, *Earth Surface Processes and Landforms*, 38(8), pp. 876–887.

Körner, H. (1976): Reichweite und Geschwindigkeit von Bergstuerzen und Fliessschnee-Lawinen, *Rock Mechanics*, 8, pp. 225–256.

Kron, W. (2002): Flood risk=hazard * exposure * vulnerabiliy, in *Flood defence 2002*, (edited by B. Wu, Z.Y. Wang, G. Wang, G. Huang, H. Fang and J. Huang), vol. 1, Science Press New York Ltd, ISBN 9781880132548/ISSN, pp. 82–97.

Kunz, M. (2011): *Interactive visualizations of natural hazards data and associated uncertainties*, Doctoral thesis, Swiss Federal Institute of Technology, ETH Zürich.

Lacasse, S., Eidsvig, U., Nadim, F., Hoeg, K. and Blikra, L.H. (2008): Event tree analysis of Åknes rock slide hazard, in *Proceedings of the 4th Canadian Conference on Geohazards: From Causes to Management, Québec*, (edited by J. Locat, D. Perret, D. Turmel, D. Demers and S. Leroueil), Presse de l'Université Laval, pp. 8.

Lateltin, O. (1997): *Berücksichtigung der Massenbewegungsgefahren bei raumwirksamen Tätigkeiten*, Naturgefahren 1997. Empfehlungen, Bundesamt für Raumplanung (BRP), Bundesamt für Wasserwirtschaft (BWW) und Bundesamt für Umwelt, Wald und Landschaft (BUWAL), Bern, 42 pp.

Lavigne, F. and Suwa, H. (2004): Contrasts between debris flows, hyperconcentrated flows and stream flows at a channel of Mount Semeru, East Java, Indonesia, *Geomorphology*, 61(1–2), pp. 41–58.

Lavigne, F. and Thouret, J.C. (2003): Sediment transportation and deposition by rain-triggered lahars at Merapi Volcano, Central Java, Indonesia, *Geomorphology*, 49(1–2), pp. 45–69.

Lehmann Friedli, T. (2013): *Ökonomische Relevanz von Klimaanpassungen im Tourismus. Qualitative und quantitative Kosten-Nutzen-Bewertung von Anpassungsmassnahmen im Schweizer Alpenraum*, Doctoral thesis, Research Institute for Leisure and Tourism (CRED), University of Bern, 339 pp.

Lehmann Friedli, T. and Schaub, Y. (2013): Neue Gletscherseen im Alpenraum - Schaden- und Nutzenpotenzial für den Schweizer Tourismus, in *Nachhaltigkeit im alpinen Tourismus. Schweizer Jahrbuch für Tourismus 2012. St. Galler Schriften für Tourismus und Verkehr. Band 4*, (edited by T. Bieger, P. BeriteII and C. Laesser), Erich Schmidt Verlag GmbH & Co. KG, Berlin, ISBN 978 3 503 14423 5/ISSN, pp. 111–126.

Leiter, A.M. and Pruckner, G.J. (2009): Proportionality of willingness to pay to small changes in risk: the impact of attitudinal factors in scope tests, *Environmental and Resource Economics*, 42(2), pp. 169–186.

Leitungsgruppe des NFP 48 (2007): *Landschaften und Lebensräume der Alpen – Zwischen Wertschöpfung und Wertschätzung, Reflexionen zum Abschluss des Nationalen Forschungsprogramms 48. Schweizerischer Nationalfonds zur Förderung des wissenschaftlichen Forschung (FNSNF)*, vdf Hochschulverlag, Zürich, 110 pp.

Lentz, A. and Rackwitz, R. (2004): Loss-of-life modelling in risk acceptance criteria, in *Probabilistic Safety Assessment and Management*, (edited by C. Spitzer, U. Schmocker and V.N. Dang), Springer London, ISBN 978-1-4471-1057-6/ISSN, pp. 1924–1929.

Linsbauer, A., Paul, F. and Haeberli, W. (2012): Modeling glacier thickness distribution and bed topography over entire mountain ranges with GlabTop: application of a fast and robust approach, *Journal of Geophysical Research: Earth Surface*, 117(F3), pp. F03007.

Linsbauer, A., Paul, F., Machguth, H. and Haeberli, W. (2013): Comparing three different methods to model scenarios of future glacier change in the Swiss Alps, *Annals of Glaciology*, 54(63), pp. 241–253.

Liu, P.L.F., Wu, T.R., Raichlen, F., Synolakis, C.E. and Borrero, J.C. (2005): Runup and rundown generated by three-dimensional sliding masses, *Journal of Fluid Mechanics*, 536, pp. 107–144.

Lliboutry, L., Arnao, B. and Pautre, A. (1977): Glaciological problems set by the control of dangerous lakes in Cordillera Blanca, Peru. I-III, *Journal of Glaciology*, 18(78-80), pp. 239–290.

Loriaux, T. and Casassa, G. (2013): Evolution of glacial lakes from the Northern Patagonian Icefield and terrestrial water storage in a sea-level rise context, *Global and Planetary Change*, 102, pp. 33–40.

Lynett, P. and Liu, P.L.F. (2005): A numerical study of the run-up generated by three-dimensional landslides, *Journal of Geophysical Research: Oceans*, 110(C3), pp. C03006.

Maisch, M., Wipf, A., Denneler, B., Battaglia, J. and Benz, C. (1999): *Die Gletscher der Schweizer Alpen, Gletscherhochstand 1850, aktuelle Vergletscherung, Gletscherschwund-Szenarien*, Projektschlussbericht im Rahmen des Nationalen Forschungsprogrammes "Klimaänderungen und Naturkatastrophen", NFP 31, vdf Hochschulverlag AG, Zürich, 373 pp.

Malet, J., Delacourt, C., Maquaire, O. and Amitrano, D. (2007): Introduction to the thmatic volume: issues in landslide process monitoring and understanding, *Bulletin de la Societe Geologique de France*, 178(2), pp. 63–64.

Manville, V.R., Major, J. and Fagents, S. (2013): Modeling lahar behaviour and hazards, in *Modelling Volcanic Processes: The Physics and Mathematics of Volcanism*, (edited by F. S.A., T. Gregg and R. Lopes), Cambridge University Press, ISBN 9780521895439/ISSN, pp. 300–330.

Margreth, S., Faillettaz, J., Funk, M., Vagliasindi, M., Diotri, F. and Broccolato, M. (2011): Safety concept for hazards caused by ice avalanches from the Whymper hanging glacier in the Mont Blanc Massif, *Cold Regions Science and Technology*, 69(2–3), pp. 194–201.

Margreth, S. and Funk, M. (1999): Hazard mapping for ice and combined snow/ice avalanches – two case studies from the Swiss and Italian Alps, *Cold Regions Science and Technology*, 30(1-3), pp. 159–173.

Marinos, V., Marinos, P. and Hoek, E. (2005): The geological strength index: applications and limitations, *Bulletin of Engineering Geology and the Environment*, 64(1), pp. 55–65.

Marzocchi, W., Garcia-Aristizabal, A., Gasparini, P., Mastellone, M. and Di Ruocco, A. (2012): Basic principles of multi-risk assessment: a case study in Italy, *Natural Hazards*, 62(2), pp. 551–573.

Matambo, S.T. and Shrestha, A. (2011): Nepal: responding proactively to glacial hazards, *World Resources Report, Washington DC*, pp. 1–18.

MATRIX (2013): MATRIX - New Multi-Hazard and Multi-Risk Assessment Methods for Europe, EU Seventh framework programme [Access: 14 July 2014], URL http://matrix.gpi.kit.edu/index.php.

Matsuoka, N. (2008): Frost weathering and rockwall erosion in the southeastern Swiss Alps: Long-term (1994–2006) observations, *Geomorphology*, 99(1–4), pp. 353–368.

Mazzanti, P. and Bozzano, F. (2009): An equivalent fluid/equivalent medium approach for the numerical simulation of coastal landslides propagation: theory and case studies, *Natural Hazards and Earth System Sciences*, 9(6), pp. 1941–1952.

McColl, S., Davies, T. and McSaveney, M. (2010): Glacier retreat and rock-slope stability: debunking debuttressing, in *Geologically active: delegate papers of the 11th Congress of the International Association for Engineering Geology and the Environment, Auckland, Aotearoa, New Zealand*, (edited by A. Williams, G. Pinches, C. Chin, T. McMorran and C. Massey), Taylor & Francis Group, London, pp. 467–474.

McColl, S.T. (2012): Paraglacial rock-slope stability, *Geomorphology*, 153–154(0), pp. 1–16.

McDougall, S. (2006): *A new continuum dynamic model for the analysis of extremely rapid landslide motion accross complex 3D terrain*, Doctoral thesis, Geological Engineering, University of British Columbia, 268 pp.

McDougall, S. and Hungr, O. (2004): A model for the analysis of rapid landslide motion across three-dimensional terrain, *Canadian Geotechnical Journal*, 41(6), pp. 1084–1097.

McKillop, R. and Clague, J.J. (2007a): A procedure for making objective preliminary assessments of outburst flood hazard from moraine-dammed lakes in southwestern British Columbia, *Natural Hazards*, 41(1), pp. 131–157.

McKillop, R. and Clague, J.J. (2007b): Statistical, remote sensing-based approach for estimating the probability of catastrophic drainage from moraine-dammed lakes in Southwestern British Columbia, *Global and Planetary Change*, 56(1-2), pp. 153–171.

Medina-Cetina, Z. and Nadim, F. (2008): Stochastic design of an early warning system, *Georisk: Assessment and Management of Risk for Engineered Systems and Geohazards*, 2(4), pp. 223–236.

Mergili, M. and Schneider, J.F. (2011): Regional-scale analysis of lake outburst hazards in the southwestern Pamir, Tajikistan, based on remote sensing and GIS, *Natural Hazards and Earth System Sciences*, 11(5), pp. 1447–1462.

Merritt, W.S., Letcher, R.A. and Jakeman, A.J. (2003): A review of erosion and sediment transport models, *Environmental Modelling and Software*, 18(8–9), pp. 761–799.

Meyer, V., Becker, N., Markantonis, V., Schwarze, R., van den Bergh, J.C.J.M., Bouwer, L.M., Bubeck, P., Ciavola, P., Genovese, E., Green, C., Hallegatte, S., Kreibich, H., Lequeux, Q., Logar, I., Papyrakis, E., Pfurtscheller, C., Poussin, J., Przyluski, V., Thieken, A.H. and Viavattene, C. (2013): Review article: Assessing the costs of natural hazards – state of the art and knowledge gaps, *Natural Hazards and Earth System Sciences*, 13(5), pp. 1351–1373.

Meyer-Peter, E. and Müller, R. (1948): Formulas for bed-load transport, in *Proceedings of the 2nd Meeting of the International Association for Hydraulic Structures Research*, International Association of Hydraulic Research Delft, pp. 39–64.

Michlig, D. (2011): Oral statements about land-use development scenarios in Naters, interview (in German), 11 July 2011.

Mickey, R.M., Dunn, O.J. and Clark, V.A. (2004): *Applied statistics : analysis of variance and regression*, 3rd edition, Wiley, Hoboken, NJ, ISBN 0-471-37038-X/ISSN.

Müller, D. (1995): *Auflaufen und Überschwappen von Impulswellen an Talsperren*, Mitteilungen 137 der Versuchsanstalt für Wasserbau, Hydrologie und Glaziologie (VAW), ETH Zürich, 297 pp.

Molnia, B. (2009): Inventorying and monitoring the recent behavior of Afghanistan's glaciers, debriscovered glaciers, supraglacial lakes, and the potential for catastrophic flooding (jökulhlaups)., in *Geophysical Research Abstracts, European Geosciences Union General Assembly 2009, Vienna, Austria*, vol. 11, pp. EGU2009–13939.

Monaghan, J. (1992): Smoothed particle hydrodynamics, *Annual review in Astronomy and Astrophysics*, 30, pp. 543–574.

Monaghan, J. (2012): Smoothed particle hydrodynamics and its diverse applications, *Annual Review of Fluid Mechanics*, 44(1), pp. 323–346.

Monaghan, J.J. (2005): Smoothed particle hydrodynamics, *Reports on Progress in Physics*, 68(8), pp. 1703.

Mool, P. (1995): Glacier lake outburst floods in Nepal, *Journal of Nepal Geological Society*, 11, pp. 273–280.

Morris, M. (2000): *Concerted action on dambreak modelling - CADAM*, EU Environment and Climate Programme. Final Report SR 571, HR Wallingford Limited, 60 pp.

Morris, M., Hassan, M., Kortenhaus, A., Geisenhainer, P., Visser, P. and Zhu, Y. (2008): Modelling breach initiation and growth, in *Flood Risk Management: Research and Practice*, (edited by P. Samuels, S. Huntington, W. Allsop and J. Harrop), CRC Press, ISBN 978-0-415-48507-4/ISSN.

Morris, M., Hassan, M., Kortenhaus, A. and Visser, P. (2009): *Breaching Processes: A state of the art review*, Available from URL www.floodsite.net [Access: 01 September 2014], 70 pp.

Myers, E. and Baptista, A. (2001): Analysis of factors influencing simulations of the 1993 Hokkaido Nansei-Oki and 1964 Alaska tsunamis, *Natural Hazards*, 23(1), pp. 1–28.

Nadim, F. and Liu, Z. (2013): *D5.2 Framework for multi-risk assessment*, New methodologies for multi-hazard and multi-risk assessment methods for Europe MATRIX. Seventh framework programme, 78 pp.

Naef, D., Rickenmann, D., Rutschmann, P. and McArdell, B.W. (2006): Comparison of flow resistance relations for debris flows using a one-dimensional finite element simulation model, *Natural Hazards and Earth System Sciences*, 6(1), pp. 155–165.

Narama, C., Duishonakunov, M., Kääb, A., Daiyrov, M. and Abdrakhmatov, K. (2010): The 24 July 2008 outburst flood at the western Zyndan glacier lake and recent regional changes in glacier lakes of the Teskey Ala-Too range, Tien Shan, Kyrgyzstan, *Natural Hazards and Earth System Sciences*, 10(4), pp. 647–659.

NELAK (2013): *Neue Seen als Folge des Gletschwerschwundes im Hochgebirge - Chancen und Risiken. Formation des nouveaux lacs suite au recul des glaciers en haute montange -*

chances et risques, 1. edition, Forschungsbericht NFP 61, vdf Hochschulverlag AG an der ETH Zürich, Zürich, ISBN 978-3-7281-3533-9/ISSN, 300 pp.

Nilsen, T. and Aven, T. (2003): Models and model uncertainty in the context of risk analysis, *Reliability Engineering and System Safety*, 79(3), pp. 309–317.

Noetzli, J. and Gruber, S. (2009): Transient thermal effects in Alpine permafrost, *The Cryosphere*, 3, pp. 85–99.

Noetzli, J., Gruber, S., Kohl, T., Salzmann, N. and Haeberli, W. (2007): Three-dimensional distribution and evolution of permafrost temperatures in idealized high-mountain topography, *Journal of Geophysical Research*, 112, pp. 14.

Noetzli, J., Hoelzle, M. and Haeberli, W. (2003): Mountain permafrost and recent Alpine rockfall events: a GIS-based approach to determine critical factors, in *8th International Conference on Permafrost, Zurich, Switzerland*, vol. 2, pp. 827–832.

Norsys (2013): Netica, Norsys Software Corp [Access: 15 February 2014], URL https://www.norsys.com/.

Nöthiger, C. (2000): *Der Lawinenwinter 1999. Fallstudie Elm (Kanton Glarus). Indirekte Auswirkungen auf die lokale Wirtschaft*, Eidg. Institut für Schnee- und Lawinenforschung, SLF, Davos, 40 pp.

Nöthiger, C., Elsasser, H., Bründl, M. and Ammann, W. (2002): Indirekte Auswirkungen von Naturgefahren auf den Tourismus - Das Beispiel des Lawinenwinters 1999 in der Schweiz, *Geographica Helvetica*, 57(2), pp. 91–108.

Nöthiger, C.J. (2003): *Naturgefahren und Tourismus in den Alpen. Untersucht am Lawinenwinter 1999 in der Schweiz*, Eidg. Institut für Schnee- und Lawinenforschung, SLF, Davos, 245 (inkl CD-ROM) pp.

Nussbaumer, S., Schaub, Y., Huggel, C. and Walz, A. (2014): Risk estimation for future glacier lake outburst floods based on local land-use changes, *Natural Hazards and Earth System Sciences*, 14(6), pp. 1611–1624.

O'Brien, J.S. (2003): Reasonable assumptions in routing a dam break mudflow, in *Debris-Flows Hazard Mitigation: Mechanics, Predictions and Assessment*, (edited by D. Rickenmann and C. Chen), Millpress, Rotterdam, ISBN 978-90-5966-059-5/ISSN, pp. 683–693.

O'Brien, J.S., Julien, P.Y. and Fullerton, W.T. (1993): Two-dimensional water flood and mudflow simulation, *Jounal of Hydraulic Engineering*, 119(2), pp. 244–261.

OcCC (2007): *Klimaänderung und die Schweiz 2050 - erwartete Auswirkungen auf Umwelt, Gesellschaft und Wirtschaft*, OcCC and ProClim, Swiss Academy of Sciences, 167 pp.

O'Connor, J.E., Clague, J.J., Walder, J.S., Manville, V. and Beebee, R.A. (2013): Outburst floods, in *Treatise on Geomorphology*, (edited by J.F. Shroder), vol. 9, Academic Press, San Diego, ISBN 978-0-08-088522-3/ISSN, pp. 475–510.

O'Connor, J.E., Hardison, J.H. and Costa, J.E. (2001): *Debris flows from failures of Neoglacial-age moraine dams in the Three Sisters and Mount Jefferson wilderness areas, Orgeon*, US Geological Survey professional paper 1606, US Geological Suvey, Denver, 93 pp.

Oppikofer, T., Jaboyedoff, M. and Keusen, H.R. (2008): Collapse at the eastern Eiger flank in the Swiss Alps, *Nature Geoscience*, 1(8), pp. 531–535.

Osti, R. and Egashira, S. (2009): Hydodynamic characteristics of the TAM Pokhari glacier lake outburst flood in the Mt. Everest region, Nepal, *Hydrological Processes*, 23, pp. 2943–2955.

Panizzo, A., De Girolamo, P., Di Risio, M., Maistri, A. and Petaccia, A. (2005a): Great landslide events in Italian artificial reservoirs, *Natural Hazards and Earth System Sciences*, 5(5), pp. 733–740.

Panizzo, A., De Girolamo, P. and Petaccia, A. (2005b): Forecasting impulse waves generated by subaerial landslides, *Journal of Geophysical Research: Oceans*, 110(C12), pp. 23.

Pastor, M., Herreros, I., Fernández Merodo, J.A., Mira, P., Haddad, B., Quecedo, M., González, E., Alvarez-Cedrón, C. and Drempetic, V. (2009): Modelling of fast catastrophic landslides and impulse waves induced by them in fjords, lakes and reservoirs, *Engineering Geology*, 109(1–2), pp. 124–134.

Paté-Cornell, M.E. (1996): Uncertainties in risk analysis: six levels of treatment, *Reliability Engineering and System Safety*, 54(2–3), pp. 95–111.

Paul, F. (2007): *The New Swiss Glacier Inventory 2000 - Application of Remote Sensing and GIS*, Doctoral thesis, Schriftenreihe Physische Geographie 52, University of Zürich, 210 pp.

Paul, F. and Linsbauer, A. (2012): Modeling of glacier bed topography from glacier outlines, central branch lines, and a DEM, *International Journal of Geographical Information Science*, 26(7), pp. 1173–1190.

Pearl, J. (1988): *Probabilistic reasoning in intelligent systems. Networks of plausible inference*, 2nd edition, The Morgan Kaufmann Series in Representing an Reasoning, Morgan Kaufmann Publishers, Inc, San Francisco, California, ISBN 0-934613-73-7/ISSN, 75 pp.

Perlik, M., Wissen, U., Schuler, M., Hofschreuder, J., Jame, A., Keiner, M., Cavens, D. and Schmid, W.A. (2008): *Szenarien für die nachhaltige Siedlungs- und Infrastrukturentwicklung in der Schweiz (2005-2030)*, Nationales Forschungsprogramm NFP 54 „Nachhaltige Siedlungs- und Infrastrukturentwicklung", Zürich, 312 pp.

Petrascheck, A. and Loat, R. (1997): *Berücksichtigung der Hochwassergefahren bei raumwirksamen Tätigkeiten*, Natrugefahren 1997. Empfehlungen, Bundesamt für Raumplanung (BRP), Bundesamt für Wasserwirtschaft (BWW) und Bundesamt für Umwelt, Wald und Landschaft (BUWAL), Bern, 32 pp.

Pfeiffer, T. and Bowen, T.D. (1989): Computer simulation of rockfalls, *Bulletin of the Association of Engineering Geologists*, 26(1), pp. 135–146.

Pierce, M., Thornton, C. and Abt, S. (2010): Predicting peak outflow from breached embankment dams, *Journal of Hydrologic Engineering*, 15(5), pp. 338–349.

Pitman, E.B. and Le, L. (2005): A two-fluid model for avalanche and debris flows, *Philosophical Transactions of the Royal Society A: Mathematical, Physical and Engineering Sciences*, 363(1832), pp. 1573–1601.

Pitman, E.B., Patra, A.K., Kumar, D., Nishimura, K. and Komori, J. (2013): Two phase simulations of glacier lake outburst flows, *Journal of Computational Science*, 4(1–2), pp. 71–79.

PLANAT (2002): *Sicherheit vor Naturgefahren. Vision und Strategie*, PLANAT Reihe 1/2004, Nationale Plattform Naturgefahren (PLANAT), Biel, 42 pp.

PLANAT (2004): *Teilprojekt A: Gesamtübersicht*, Strategie Naturgefahren Schweiz, Nationale Plattform Naturgefahren (PLANAT), Bern, 45 pp.

PLANAT (2013): *Sicherheitsniveau für Naturgefahren*, Strategie Naturgefahren Schweiz, Nationale Plattform Naturgefahren (PLANAT), Bern, 15 pp.

Plattner, T.M. (2006): *Risikoaversion als relevanter Faktor der Risikobewertung von Naturgefahren*, Doctoral thesis, Environmental Systems Science, ETH Zürich, 160 pp.

Popinet, S. (2003): Gerris: a tree-based adaptive solver for the incompressible Euler equations in complex geometries, *Journal of Computational Physics*, 190(2), pp. 572–600.

Popinet, S. (2009): An accurate adaptive solver for surface-tension-driven interfacial flows, *Journal of Computational Physics*, 228(16), pp. 5838–5866.

Popov, N. (1991): Assessment of glacial debris flow hazard in the north Tien-Shan, in *Proceedings of the Soviet–China–Japan Symposium and Field Workshop on Natural Disasters, 2 – 17 September 1991*, pp. 384–391.

Portocarrero, C.A. (2013a): *Mapas de vulnerabilidad y riesgo de la sub cuenca Chucchún ante la posible ocurrencia de un proceso aluvión ico procedente de la Laguna 513*, Proyecto Glaciares, 107 pp.

Portocarrero, C.A. (2013b): *Reducing the risk of dangerous lakes in the Peruvian Andes: a handbook for glacial lake management*, US Agency for International Development, Washington, DC, 80 pp.

Post, A. and Mayo, I.R. (1971): *Glacier dammed lakes and outburst floods in Alaska: U.S. Geological Survey Hydrologic Investigations Atlas HA-455*.

Potter, D. (1973): *Computational physics*, Wiley & Sons, London, ISBN 0-471-69555-6 /ISSN, 315 pp.

Pralong, A., Birrer, C., Stahel, W.A. and Funk, M. (2005): On the predictability of ice avalanches, *Nonlinear Processes in Geophysics*, 12(6), pp. 849–861.

Preuth, T., Bartelt, P., Korup, O. and McArdell, B.W. (2010): A random kinetic energy model for rock avalanches: eight case studies, *Journal of Geophysical Research: Earth Surface*, 115(F3), pp. F03036.

Priest, S.D. (1993): *Discontinuity analysis for rock engineering*, Springer Science & Business Media, London, ISBN 0412476002/ISSN, 473 pp.

Pudasaini, S.P., Kattel, P., Kafle, J., Pokhrel, P.R. and Khattri, K.B. (2014): Two-phase and three-dimensional simulations of complex fluid-sediment transport down a slope and impacting water bodies, in *Geophysical Research Abstracts, Europen Geoscience Union, Vienna*, vol. 16.

Quincey, D.J., Lucas, R.M., Richardson, S.D., Glasser, N.F., Hambrey, M.J. and Reynolds, J.M. (2005): Optical remote sensing techniques in high-mountain environments: application to glacial hazards, *Progress in Physical Geography*, 29(4), pp. 475–505.

Rabatel, A., Francou, B., Soruco, A., Gomez, J., Cáceres, B., Ceballos, J.L., Basantes, R., Vuille, M., Sicart, J.E., Huggel, C., Scheel, M., Lejeune, Y., Arnaud, Y., Collet, M., Condom, T., Consoli, G., Favier, V., Jomelli, V., Galarraga, R., Ginot, P., Maisincho, L., Mendoza, J., Ménégoz, M., Ramirez, E., Ribstein, P., Suarez, W., Villacis, M. and Wagnon, P. (2013): Current state of glaciers in the tropical Andes: a multi-century perspective on glacier evolution and climate change, *The Cryosphere*, 7(1), pp. 81–102.

Racoviteanu, A.E., Arnaud, Y., Williams, M.W. and Ordoñez, J. (2008): Decadal changes in glacier parameters in the Cordillera Blanca, Peru, derived from remote sensing, *Journal of Glaciology*, 54(186), pp. 499–510.

Raymond, M., Wegmann, M. and Funk, M. (2003): *Inventar der gefährlichen Gletscher in der Schweiz*, Mitteilungen 182 der Versuchsanstalt für Wasserbau, Hydrologie und Glaziologie (VAW), ETH Zürich.

Reynolds, J., Dolecki, A. and Portocarrero, C. (1998): The construction of a drainage tunnel as part of glacial lake hazard mitigation at Hualcán, Cordillera Blanca, Peru, in *Geohazards in Engineering Geology*, (edited by J. Maund and M. Eddleston), Geological Society Engineering Group Special Publication 15, The Geological Society, London, ISBN 1-86239-012-6/ISSN, pp. 41–48.

Reynolds, J.M. (2003): *Development of glacial hazard and risk minimisation protocols in rural environments. Guidelines for the management of glacial hazards and risks*, Report No: R7816, Reynolds Geo-Science Ltd, Flintshire, UK, 68 pp.

Rheinberger, C.M. (2010): Experimental evidence against the paradigm of mortality risk aversion, *Risk Analysis*, 30(4), pp. 590–604.

Rheinberger, C.M. (2011): Entscheidungskriterien im Umgang mit Naturgefahren (Essay), *Schweizerische Zeitschrift fur Forstwesen*, 162(12), pp. 432–441.

Rheinberger, C.M., Romang, H.E. and Bründl, M. (2013): Proportional loss functions for debris flow events, *Natural Hazards and Earth System Sciences*, 13(8), pp. 2147–2156.

Richardson, S.D. and Reynolds, J.M. (2000): An overview of glacial hazards in the Himalayas, *Quaternary International*, 65-66, pp. 31–47.

Rickenmann, D. (1991): Hyperconcentrated flow and sediment transport at steep slopes, *Journal of Hydraulic Engineering*, 117(11), pp. 1419–1439.

Rickenmann, D. (1999): Empirical relationships for debris flows, *Natural Hazards*, 19(1), pp. 47–77.

Roberts, M.J. (2005): Jökulhlaups: a reassessment of floodwater flow through glaciers, *Reviews of Geophysics*, 43, pp. RG1002.

Romang, H. (2009): *Handbook with recommendations for IRM best practice, incl. a methodology for application to other European mountain regions*, Integral Risk Management of Extremely Rapid Mass Movements IRASMOS. Work package 5: Integral risk management. Deliverable D5.4. Best practice of integral risk management of snow avalanches, rock avalanches and debris flows in Europe, 148 pp.

Romstad, B., Harbitz, C. and Domaas, U. (2009): A GIS method for assessment of rock slide tsunami hazard in all Norwegion lakes and reservoirs, *Natural Hazards and Earth System Sciences*, 9(2), pp. 353–364.

Rosa, E. (2003): The logical strucutre of the social amplification of risk framework (SARF): metatheoretical foundation and policy implications, in *The social amplification of risk*, (edited by N. Pidegeon, R. Kaxpersen and P. Slovic), Cambridge University Press, Cambridge, ISBN 0-521-81728-5/ISSN, pp. 47–76.

Rosa, E.A. (1998): Metatheoretical foundations for post-normal risk, *Journal of Risk Research*, 1(1), pp. 15–44.

Rothenbuehler, C. (2006): *GISALP- raeumlich-zeitliche Modellierung der klimasensitiven Hochgebirgslandschaft des Oberengadins*, Doctoral thesis, Department of Geography, University of Zürich, 179 pp.

Röthlisberger, H. (1978): Eislawinen und Ausbrüche von Gletscherseen, *Gletscher und Klima-glaciers et climat, Jahrbuch der Schweizerischen Naturforschenden Gesellschaft, wissenschaftlicher Teil*, 1981, pp. 170–212.

Salm, B. (1993): Flow, flow transition and runout distances of flowing avalanches, *Annals of Glaciology*, 18, pp. 221–221.

Salzmann, N., Kääb, A., Huggel, C., Allgöwer, B. and Haeberli, W. (2004): Assessment of the hazard potential of ice avalanches using remote sensing and GIS-modelling, *Norsk Geografisk Tidsskrift - Norwegian Journal of Geography*, 58(2), pp. 74–84.

Santi, P.M., Russell, C.P., Higgins, J.D. and Spriet, J.I. (2009): Modification and statistical analysis of the Colorado rockfall hazard rating system, *Engineering Geology*, 104(1-2), pp. 55–65.

Savage, S.B. and Hutter, K. (1989): The motion of a finite mass of granular material down a rough incline, *Journal of Fluid Mechanics*, 199, pp. 177–215.

Schaub, Y., Haeberli, W., Huggel, C., Künzler, M. and Bründl, M. (2013): Landslides and new Lakes in deglaciating areas: a risk management framework, in *Landslide Science and Practice*, (edited by C. Margottini, P. Canuti and K. Sassa), Springer Berlin Heidelberg, ISBN 978-3-642-31312-7/ISSN, pp. 31–38.

Scheidegger, A.E. (1973): On the prediction of the reach and velocity of catastrophic landslides, *Rock mechanics*, 5(4), pp. 231–236.

Scheuner, T., Keusen, H., McArdell, B. and Huggel, C. (2009): Murgangmodellierung mit dynamisch-physikalischem und GIS-basiertem Fliessmodell, *Wasser Energie Luft*, 101(1), pp. 15–21.

Schilling, S. (1998): *LAHARZ: GIS programs for automated mapping of lahar-inundation hazard zones*, Open-File Report 98-638, U.S. Department of the Interior, U.S. Geological Survey, Vancouver, Washington, 84 pp.

Schimel, A.C.G., Healy, T.R., Johnson, D. and Immenga, D. (2010): Quantitative experimental comparison of single-beam, sidescan, and multibeam benthic habitat maps, *ICES Journal of Marine Science: Journal du Conseil*, 67(8), pp. 1766–1779.

Schneider, D., Bartelt, P., Caplan-Auerbach, J., Christen, M., Huggel, C. and McArdell, B.W. (2010): Insights into rock-ice avalanche dynamics by combined analysis of seismic recordings and a numerical avalanche model, *Journal of Geophysical Research: Earth Surface*, 115(F4), pp. F04026.

Schneider, D., Frey, H., García, J., Giráldez, C., Guillén Ludeña, S., Haeberli, W., Huggel, C., Rohrer, M., Salzmann, N. and Schleiss, A. (2013): *Río Chucchún catchment: Glacier and glacier lakes, and modeling and mapping of hazards related to glacier lake outburst floods*, Proyecto Glaciares. Scientific baseline Río Chucchún catchment. Local level (project component 1), 34 pp.

Schneider, D., Huggel, C., Cochachin, A., Guillén, S. and García, J. (2014): Mapping hazards from glacier lake outburst floods based on modelling of process cascades at Lake 513, Carhuaz, Peru, *Advances in Geosciences*, 35, pp. 145–155.

Schneider, D., Huggel, C., Haeberli, W. and Kaitna, R. (2011): Unraveling driving factors for large rock–ice avalanche mobility, *Earth Surface Processes and Landforms*, 36(14), pp. 1948–1966.

SECO (2005): Ein langfristiges Wachstumsszenario für die Schweizer Wirtschaft, *Volkswirtschaft. Konjunkturtendenzen Frühjahr 2005*, pp. 43–52.

Serraino, M. (2011): *Fels- und Eisstürze in Hochgebirgsseen der Schweizer Alpen. Eine GIS-basierte Analyse von Gefahrenpotentialen im 21. Jahrhundert*, Master's thesis, Department of Geography, University of Zürich, 107 pp.

Serrano-Pacheco, A., Murillo, J. and García-Navarro, P. (2009): A finite volume method for the simulation of the waves generated by landslides, *Journal of Hydrology*, 373(3–4), pp. 273–289.

Sheridan, M.F., Stinton, A.J., Patra, A., Pitman, E.B., Bauer, A. and Nichita, C.C. (2005): Evaluating Titan2D mass-flow model using the 1963 Little Tahoma Peak avalanches, Mount Rainier, Washington, *Journal of Volcanology and Geothermal Research*, 139(1–2), pp. 89–102.

Sim, J. and Wright, C. (2005): The Kappa statistic in reliability studies: use, interpretation, and sample size requirements, *Physical Therapy*, 85(3), pp. 257–268.

Singh, V. (1996): *Dam breach modelling technology*, *Water Science and Technology Library*, vol. 17, Kluwer Academic Publishers, Dordrecht, Boston, London, ISBN 978-0-7923-3925-0/ISSN, 242 pp.

Slaymaker, O. (2009): Proglacial, periglacial or paraglacial?, *Geological Society, London, Special Publications*, 320(1), pp. 71–84.

Slovic, P. (2000): *The Perception of Risk*, Risk, society and policy series, Earthscan Publications Ltd, London, ISBN 1-85383-527-7/ISSN, 473 pp.

Smart, G. (1984): Sediment transport formula for steep channels, *Journal of Hydraulic Engineering*, 110(3), pp. 267–276.

Smith, K. (2013): *Environmental Hazards: Assessing Risk and Reducing Disaster*, 6th edition, Routledge, New York, ISBN 9780415681059/ISSN, 478 pp.

Somos-Valenzuela, M., Chisolm, R., McKinney, D. and Rivas, D. (2013): Hazard map in Huaraz-Peru due to a glacial lake outburst flood from Palcacocha Lake, in *AGU Fall Meeting Abstracts, Poster*.

Sosio, R., Crosta, G.B., Chen, J.H. and Hungr, O. (2012): Modelling rock avalanche propagation onto glaciers, *Quaternary Science Reviews*, 47(0), pp. 23–40.

Sovilla, B., Burlando, P. and Bartelt, P. (2006): Field experiments and numerical modeling of mass entrainment in snow avalanches, *Journal of Geophysical Research: Earth Surface*, 111(F3), pp. F03007.

Sovilla, B., Margreth, S. and Bartelt, P. (2007): On snow entrainment in avalanche dynamics calculations, *Cold Regions Science and Technology*, 47(1–2), pp. 69–79.

Stirling, A. (2007): Risk, precaution and science: towards a more constructive policy debate, *EMBO Reports*, 8(4), pp. 309–315.

Stoffel, M. and Huggel, C. (2012): Effects of climate change on mass movements in mountain environments, *Progress in Physical Geography*, 36(3), pp. 421–439.

Stolz, A. and Huggel, C. (2008): Debris flows in the Swiss National Park: the influence of different flow models and varying DEM grid size on modeling results, *Landslides*, 5(3), pp. 311–319.

Straub, D. (2005): Natural hazards risk assessment using Bayesian networks, in *Proceedings of the 9th International Conference on Structural Safety and Reliability, ICOSSAR'05, 19-23 June 2005, Rome, Italy*, (edited by G. Augusti, G. Schuëller and M. Ciampoli), Millpress Rotterdam, pp. 2535–2542.

Stricker, B. (2010): *Murgänge im Torrente Riascio (TI): Ereignisanalyse, Auslösefaktoren und Simulation von Ereignissen mit RAMMS*, Master's thesis, Department of Geography, University of Zürich.

Strozzi, T., Delaloye, R., Kääb, A., Ambrosi, C., Perruchoud, E. and Wegmüller, U. (2010): Combined observations of rock mass movements using satellite SAR interferometry, differential GPS, airborne digital photogrammetry, and airborne photography interpretation, *Journal of Geophysical Research*, 115(F01014), pp. 11.

Strozzi, T., Wiesmann, A., Kääb, A., Joshi, S. and Mool, P. (2012): Glacial lake mapping with very high resolution satellite SAR data, *Natural Hazards and Earth System Sciences*, 12(8), pp. 2487–2498.

Swisstopo (2010): *DEM25 – The digital height model of Switzerland*, Federal Office of Topography (swisstopo), Wabern.

Takahashi, T. (1991): *Debris flow*, IAHR Monograph Series, Balkema, Rotterdam, ISBN 90-5410-104-0 /ISSN, 165 pp.

Tarvainen, T., Jarva, J. and Greiving, S. (2006): Spatial pattern of hazards and hazard interactions in Europe, in *Natural and Technological Hazards and Risks Affecting the Spatial Development of European Regions. Special Paper 42*, (edited by P. Schmidt-Thomé), Geological Survey of Finland, ISBN 951-690-944-2/ISSN, pp. 83–91.

Tedesco, M. and Steiner, N. (2011): In-situ multispectral and bathymetric measurements over a supraglacial lake in western Greenland using a remotely controlled watercraft, *The Cryosphere*, 5, pp. 445–452.

Teman, R. (1984): *Navier-Stokes equations: theory and numerical analysis*, vol. 343, AMS Chelsea Publishing, Providence, Rhode Island, ISBN 978-0-8218-2737-6/ISSN, 408 pp.

Thorarinsson, S. (1953): Some new aspects of the Grimsvota problem, *Journal of Glaciology*, 2(14), pp. 267–275.

Tingsanchali, T. and Chinnarasri, C. (2001): Numerical modelling of dam failure due to flow overtopping, *Hydrological Sciences Journal*, 46(1), pp. 113–130.

Totschnig, R. and Fuchs, S. (2013): Mountain torrents: quantifying vulnerability and assessing uncertainties, *Engineering Geology*, 155, pp. 31–44.

Ukita, J., Narama, C., Tadono, T., Yamanokuchi, T., Tomiyama, N., Kawamoto, S., Abe, C., Uda, T., Yabuki, H., Fujita, K. and Nishimura, K. (2011): Glacial lake inventory of Bhutan using ALOS data: methods and preliminary results, *Annals of Glaciology*, 52(58), pp. 65–71.

UN (1992): *Report on the United Nations Conference on Environment and Development*, *A/-CONF.151/26*, vol. 1, United Nations (UN), New York, NY, USA.

UNEP (2011): *UNEP chlimate change strategy*, for the UNEP programme of work 2010-2011, United Nations Environment Programme (UNEP), Kenya, ISBN 978-92-807-2985-3/ISSN, 32 pp.

UNISDR (2009): *UNISDR Terminology on Disaster Risk Reduction*, United Nations International Strategy for Disaster Reduction (UNISDR), Geneva, 35 pp.

Valderrama, P. and Vilca, O. (2012): Dinamica e implicancias del aluvión de la Laguna 513, Cordillera Blanca, Ancash Perú, *Revista de la Asociación Geológica Argentina*, 69(3), pp. 400–406.

Valiente, O.M. (2001): Sequía: Definiciones, tipologías y métodos de cuantificación, *Investigaciones Geográficas*, 26, pp. 59–80.

Varnes, D.J. (1978): Slope movement types and processes, in *Landslides: Analysis and Control. Special report 176*, (edited by R.L. Schuster and R. Krizek), Transportation Research Board (TRB), National Research Council, Washington, D.C., ISBN 978-0309028042/ISSN, pp. 11–33.

Vignjevic, R. and Campbell, J. (2009): Review of development of the smooth particle hydrodynamics (SPH) method, in *Predictive Modeling of Dynamic Processes*, (edited by S. Hiermaier), Springer US, ISBN 978-1-4419-0726-4/ISSN, pp. 367–396.

Vilímek, V., Emmer, A., Huggel, C., Schaub, Y. and Würmli, S. (2014): Database of glacial lake outburst floods (GLOFs)–IPL project No. 179, *Landslides*, 11(1), pp. 161–165.

Visser, P.J. (1988): A model for breach growth in a dike-burst, *Coastal Engineering Proceedings*, 1(21).

Voellmy, A. (1955): Über die Zerstörungskraft von Lawinen, *Schweiz. Bauzeitung*, 73(15), pp. 212–217.

Voigt, T., Füssel, H., Gärtner-Roer, I., Huggel, C., Marty, C. and Zemp, M. (2010): *Impacts of climate change on snow, ice, and permafrost in Europe: observed trends, future projections, and socio-economic relevance*, ETC/ACC Technical Paper 2010/2013, European Topic Centre on Air and Climate Change (ETC/ACC), Bilthoven, 117 pp.

Volkwein, A., Schellenberg, K., Labiouse, V., Agliardi, F., Berger, F., Bourrier, F., Dorren, L.K.A., Gerber, W. and Jaboyedoff, M. (2011): Rockfall characterisation and structural protection - a review, *Natural Hazards and Earth System Sciences*, 11, pp. 2617–2651.

Volz, C., Rousselot, P., Vetsch, D., Müller, R., Fäh, R. and Boes, R. (2010): Numerical modeling of dam breaching processes due to overtopping flow, in *Proceedings of 8th ICOLD European Club Symposium, 22 - 23 September 2010, Innsbruck*, pp. 691–696.

Vuichard, D. and Zimmermann, M. (1987): The 1985 catastrophic drainage of a moraine-dammed lake, Khumbu Himal, Nepal: cause and consequences, *Mountain Research and Development*, 7(2), pp. 91–110.

Wahl, T. (2004): Uncertainty of predictions of embankment dam breach parameters, *Journal of Hydraulic Engineering*, 130(5), pp. 389–397.

Wahl, T.L. (1998): *Prediction of embankment dam breach parameters: a literature review and needs assessment*, Dam Safety Rep. No. DSO-98-004, U.S. Dept. of the Interior, Bureau of Reclamation, Denver, 72 pp.

Walder, J. and O'Connor, J. (1997): Methods for predicting peak discharges of floods caused by failure of natural and constructed earthen dams, *Water Resources Research*, 33, pp. 2337–2348.

Walder, J.S. and Costa, J.E. (1996): Outburst floods from glaicer-dammed lakes: the effect of mode of lake drainage on flood magnitude, *Earth Surface Processes and Landforms*, 21(8), pp. 701–723.

Walder, J.S., Watts, P., Sorensen, O.E. and Janssen, K. (2003): Tsunamis generated by subaerial mass flows, *Journal of Geophysical Research: Solid Earth*, 108(B5), pp. 2236.

Walz, A., Lardelli, C., Behrendt, H., Lundstöm, C., Grêt-Regamey, A., S., K. and Bebi, P. (2007): Participatory scenario analysis for integrated regional modelling, *Landscape and Urban Planning*, 81(1), pp. 114–131.

Wang, J., Gu, X. and Huang, T. (2013): Using Bayesian networks in analyzing powerful earthquake disaster chains, *Natural Hazards*, 68(2), pp. 509–527.

Wang, W., Yao, T., Gao, Y., Yang, X. and Kattel, D.B. (2011): A first-order method to identify potentially dangerous glacial lakes in a region of the southeastern Tibetan Plateau, *Mountain Research and Development*, 31(2), pp. 122–130.

Wang, X., Liu, S., Ding, Y., Guo, W., Jiang, Z., Lin, J. and Han, Y. (2012): An approach for estimating the breach probabilities of moraine-dammed lakes in the Chinese Himalayas using remote-sensing data, *Natural Hazards and Earth System Sciences*, 12(10), pp. 3109–3122.

Wang, X., Liu, S., Guo, W. and Xu, J. (2008): Assessment and simulation of glacier lake outburst floods for Longbasaba and Pida Lakes, China, *Mountain Research and Development*, 28(3/4), pp. 310–317.

Wang, Z. and Bowles, D.S. (2006a): Dam breach simulations with multiple breach locations under wind and wave actions, *Advances in Water Resources*, 29(8), pp. 1222–1237.

Weber, F. (2007): *Naturerreignisse und Tourismus. Einfluss und Auswirkungen von Naturereignissen auf die Entwicklung des Tourismus im Alpenraum*, Serie: Berner Studien zu Freizeit und Tourismus; Heft 48, Bern.

Wegmann, M., Bruderer, A., Funk, M. and Keusen, H.R. (2004): Partizipatives Verfahren zum Risikomanagement bei Naturgefahren - Angewendet für Gletschergefahren, in *Interprävent 2004, Riva/Trient*, vol. 4, pp. 297–308.

Weinstein, N. (1980): Unrealistic optimism about future life events, *Journal of Personality and Social Psychology*, 39, pp. 806–820.

Werder, M., Bauder, A., Funk, M. and Keusen, H.R. (2010): Hazard assessment investigations in connection with the formation of a lake on the tongue of Unterer Grindelwaldgletscher, Bernese Alps, Switzerland, *Natural Hazards & Earth System Sciences*, 10(2), pp. 227–237.

Wessels, R.L., Kargel, J.S. and Kieffer, H.H. (2002): ASTER measurement of supraglacial lakes in the Mount Everest region of the Himalaya, *Annals of Glaciology*, 34(1), pp. 399–408.

Westoby, M.J., Glasser, N.F., Brasington, J., Hambrey, M.J., Quincey, D.J. and Reynolds, J.M. (2014): Modelling outburst floods from moraine-dammed glacial lakes, *Earth-Science Reviews*, 134(0), pp. 137–159.

Whitehouse, I. (1988): Geomorphology of the central Southern Alps, New Zealand: the interaction of plate collision and atmospheric circulation, *Zeitschrift für Geomorphology*, 69, pp. 105–116.

Wilhelm, C. (1997): Wirtschaftlichkeit im Lawinenschutz. Methodik und Erhebung zur Beurteilung von Schutzmassnahmen mittels quantitativer Risikoanalyse und ökonomischer Bewertung, Mitt. Eidgenöss. Inst. Schnee-Lawinenforsch., SLF, Davos, pp. 309.

Wissen Hayek, U., Jaeger, J., Schwick, C., Jarne, A. and Schuler, M. (2011): Measuring and assessing urban sprawl: what are the remaining options for future settlement development in Switzerland for 2030?, *Applied Spatial Analysis and Policy*, 4(4), pp. 249–279.

WMO (2014): Disaster Risk Reduction Definitions, Disaster Risk Reduction Programms, World Meteorological Organisation (WMO) [Access: 31 March 2014], URL http://www.wmo.int/pages/prog/drr/resourceDrrDefinitions_en.html.

Woodhead, S., Asselman, N., Zech, Y., Soares-Frazão, S., Bates, P. and Kortenhaus, A. (2007): *Evaluation of Inundation Models. Limits and Capabilites of Models*, Available from URL www.floodsite.net [Access: 01 September 2014], Delft, 34 pp.

Worni, R., Huggel, C., Clague, J.J., Schaub, Y. and Stoffel, M. (2014): Coupling glacial lake impact, dam breach, and flood processes: a modeling perspective, *Geomorphology*, 224(1), pp. 161–176.

Worni, R., Huggel, C. and Stoffel, M. (2013): Glacial lakes in the Indian Himalayas — From an area-wide glacial lake inventory to on-site and modeling based risk assessment of critical glacial lakes, *Science of the Total Environment*, 468–469, Supplement(0), pp. S71–S84.

Worni, R., Huggel, C., Stoffel, M. and Pulgarin, B. (2012a): Challenges of modelling recent, very large lahars at Nevado del Huila Volcano, Colombia, *Bulletin of Volcanology*, 74(2), pp. 309–324.

Worni, R., Stoffel, M., Huggel, C., Volz, C., Casteller, A. and Luckmann, B. (2012b): Analysis and dynamic modeling of a moraine failure and glacier lake outburst flood at Ventisquero Negro, Patagonian Andes (Argentina), *Journal of Hydrology*, 444-445, pp. 134–145.

Würmli, S. (2012): *Ausbruchsmechanismen von hochalpinen Seen—ein weltweites Inventar*, Master's thesis, Department of Geography, University of Zürich, 90 pp.

Würmli, S., Schaub, Y., Huggel, C. and Haeberli, W. (2013): A worldwide inventory of high-mountain lake outburst floods, in *Mountain under Watch, 21 - 22 February 2013, Poster Presentation, Aosta, Italy*.

Yamada, T. (1993): *Glacier lakes and their outburst floods in the Nepal, Himalaya*, Water and Energy Comission Secretariat, Kathmandu, 37 pp.

Yamada, T. and Sharma, C. (1993): Glacier lakes and outburst floods in the Nepal Himalaya, *Publications of the International Association of Hydrological Sciences (IAHS)*, 218, pp. 319–330.

Yao, X., Liu, S., Sun, M., Wei, J. and Guo, W. (2012): Volume calculation and analysis of the changes in moraine-dammed lakes in the north Himalaya: a case study of Longbasaba lake, *Journal of Glaciology*, 58(210), pp. 753–760.

Zapata Luyo, M. (2002): La dinámica glaciar en lagunas de la Cordillera Blanca, *ActaMontana (Czech Republic)*, 19(123), pp. 37–60.

Zemp, M., Haeberli, W., Hoelzle, M. and Paul, F. (2006): Alpine glaciers to disappear within decades?, *Geophysical Research Letters*, 33(13), pp. L13504.

Zemp, M., Roer, I., Kääb, A., Hoelzle, M., Paul, F. and Haeberli, W. (2008): *Global glacier changes: facts and figures*, United Nations Environment Programme (UNEP) and World Glacier Monitoring Service (WGMS), ISBN 978-92-807-2898-9/ISSN, 88 pp.

Zhu, Y., Visser, P. and Vrijling, J. (2004): Review on embankment dam breach modeling, in *New Developments in Dam Engineering. Proceedings of the 4th International Conference on Dam Engineering, 18 - 20 October, Nanjing, China*, (edited by M. Wieland, R. Qingwen and J.S.Y. Tan), Taylor & Francis Group, London, ISBN 978-0415362405 /ISSN, pp. 1189–1196.

Zimmermann, M., Mani, P. and Gamma, P. (1997): *Murganggefahr und Klimaänderung - ein GIS-basierter Ansatz. Schlussbericht NFP 31*, vdf Hochschulverlag AG der ETH Zürich, Zürich, 161 pp.

Zweifel, A. and Minor, H.E. (2004): *Impulswellen: Effekte der Rutschdichte und der Wassertiefe*, Mitteilungen 186 der Versuchsanstalt für Wasserbau, Hydrologie und Glaziologie (VAW), ETH Zürich, 208 pp.

CURRICULUM VITAE

SCHAUB
Yvonne
13.03.1984
Andelfingen ZH

Education

Jan 2011- Sept 2014	PhD in Geography, University of Zürich, Switzerland Thesis: "Outburst floods from high-mountain lakes: risk analysis of cascading processes under present and future conditions", supervision: PD Dr. Christian Huggel
Oct 2006 – Nov 2008	Studies in Geography (master's degree), University of Zürich, Switzerland Minor subject: Glaciology, Key aspects: Physical Geography and GIS Thesis: „Risk management of natural hazards: sensitivity of the risk in relation to the input parameters and its relevance to the action planning", supervision: Dr. Michael Bründl, SLF.
Oct 2003 – Oct 2006	Studies in Geography (bachelor's degree), University of Zürich, Switzerland Minor subject: Geology Thesis: " Glacial and Holocene geomorphodynamics: on the theory of genesis and the distribution of kettle basins", supervision: Prof. Dr. Max Maisch.
Aug 1998 – Sept 2002	Swiss high school Zürcher Unterland, Bülach Switzerland Modern language side, Key aspects: Spanish and Geography

Work experiences

Aug 2010 - Dec 2011	Academic staff Vice President's office Medicine and Science, University of Zürich, Switzerland
Apr 2009 – Nov 2009	Project collaborator Instituto de Montaña, Huaraz, Peru
Nov 2008 - Feb 2009	Internship for young professionals WSL-Institut for Snow and Avalanche Research, SLF, Davos
Mar 2007 – June 2007, Sept 2006 – Oct 2006	Internship Forest Department of the Canton Graubünden Division Countermeasures for Natural Hazards, Chur Switzerland.

PERSONAL BIBLIOGRAPHY

Peer-reviewed publications

Worni, R., Huggel, C., Clague, J.J., Schaub, Y. and Stoffel, M. (2014): Coupling glacial lake impact, dam breach, and flood processes: a modeling perspective, *Geomorphology*, 224(1), pp. 161–176.

Vilímek, V., Emmer, A., Huggel, C., Schaub, Y. and Würmli, S. (2014): Database of glacial lake outburst floods (GLOFs)–IPL project No. 179, *Landslides*, 11(1), pp. 161–165.

Nussbaumer, S., Schaub, Y., Huggel, C. and Walz, A. (2014): Risk estimation for future glacier lake outburst floods based on local land-use changes, *Natural Hazards and Earth System Sciences*, 14(6), pp. 1611–1624.

Lehmann Friedli, T. and Schaub, Y. (2013): Neue Gletscherseen im Alpenraum - Schaden- und Nutzenpotenzial für den Schweizer Tourismus, in Nachhaltigkeit im alpinen Tourismus. *Schweizer Jahrbuch für Tourismus 2012. St. Galler* Schriften für Tourismus und Verkehr. Band 4, (edited by T. Bieger, P. BeriteII and C. Laesser), Erich Schmidt Verlag GmbH & Co. KG, Berlin, ISBN 978 3 503 14423 5/ISSN, pp. 111–126.

Schaub, Y., Haeberli, W., Huggel, C., Künzler, M. and Bründl, M. (2013): Landslides and new Lakes in deglaciating areas: a risk management framework, in *Landslide Science and Practice*, (edited by C. Margottini, P. Canuti and K. Sassa), Springer Berlin Heidelberg, ISBN 978-3-642-31312-7/ISSN, pp. 31–38.

Schaub, Y. und Bründl, M., 2010. Zur Sensitivität der Risikoberechnung und Massnahmenbewertung von Naturgefahren. *Schweizerische Zeitschrift für Forstwesen*, 161(2): pp. 27-35.

Publications without peer review

Guillén Ludeña, S., Schaub, Y., Mölg, N. and Schleiss, A. (2014): Numerical simulation of ice-rock avalanche impacts over glacier lakes, unpublished report, Laboratoire de Constructions Hydrauliques LCH-EPFL, Department of Geography University of Zürich.

NELAK (2013): *Neue Seen als Folge des Gletschwerschwundes im Hochgebirge - Chancen und Risiken. Formation des nouveaux lacs suite au recul des glaciers en haute montange - chances et risques.* vdf Hochschulverlag AG an der ETH Zürich, Zürich, 1. Edition, Forschungsbericht NFP 61, pp.300.

Bründl, M. (2009): *Risikokonzept für Naturgefahren - Leitfaden*, Strategie Naturgefahren Schweiz, Nationale Plattform Naturgefahren (PLANAT), Bern, 420 pp.

Schaub, Y. (2008): *Risikomanagement von Naturgefahren – Sensitivität der Risikoberechnung in Bezug auf die Eingabefaktoren und deren Bedeutung für die Massnahmenbewertung*. Master's thesis, Universtiy of Zürich and WSL Institute for Snow and Avalanche Research SLF. November 2008, p. 111.

Conference presentations (first or presenting author only)

Schaub, Y. and Huggel, C. (2014): *Modelling rock-/ice-avalanche induced impact waves: sensitivity of the model chain to model parameters* (Poster). EGU General Assembly, Vienna, 27 April - 02 May 2014.

NELAK (2013): *Neue Seen als Folge des Gletscherschwundes im Hochgebirge - Chancen und Risiken* (Oral Presentation). NFP61 - Progress Report Meeting 2013, Thun, 14 November 2013.

Schaub, Y., Schneider, D., Guillén Ludeña, S., Cochachin Rapre, A. and Huggel, C. (2013): *Modeling outburst floods at Laguna 513, Cordillera Blanca, Peru: Evaluation of rock-/ice-avalanche scenarios* (Poster). Foro Glaciares - Huaraz, 1 - 4 July 2013 and HMGWP-Conference - Huaraz, 13 - 22 July 2013 and Swiss Geoscience Meeting, Lausanne, 14 November 2013.

Schaub, Y., Cochachin Rapre, A., Torres Castillo, J.E., Salazar Checa, C.J., Huggel, C. (2013): *Rock-/ice-avalanches on Hualcán: Mapping of changes in glaciations and estimation of future ice-detachment scenarios in the Chucchún subbasin, Cordillera Blanca, Perú* (Poster). Foro Glaciares - Huaraz, 1 - 4 July 2013.

Haeberli, W., Huggel, C., Schaub, Y., Künzler, M., Mölg, N., Schleiss, A., Jordan, F., Terrier, S., Müller, H.R., Lehmann, T. and Bütler, M. (2013): *New lakes in deglaciating high-mountain areas (NELAK): managing chances and risks* (Poster), CH-AT Mountain Days - Mittersill, 12 - 13 June 2013.

Schaub, Y., Huggel, C. and Haeberli, W. (2013): *Glacier lake outburst floods - modelling process chains* (Poster). EGU General Assembly, Vienna, 04 - 07 April 2013.

Würmli, S., Schaub, Y., Huggel, C. and Haeberli, W. (2013): *A worldwide inventory of high-mountain lake outburst floods* (Poster). Mountain under Watch - Aosta, 21 - 22 February 2013.

Schaub, Y., Huggel, C., Allen, S. and Haeberli, W. (2012): *Present and future lake outburst potential due to impacts of rock-avalanches in the Swiss Alps: A multi-criteria analysis* (Oral Presentation). 8th Alexander von Humboldt International Conference, Cusco, Peru, 14 November 2012.

Schaub, Y., Huggel, C., Serraino, M. and Haeberli, W. (2012): *New lakes in deglaciating high-mountain areas: Regional intercomparison of current and future risks from impact waves due to rock/ice avalanches in the Swiss Alps* (Poster). EGU General Assembly, Vienna, 22 - 27 April 2012.

Schaub, Y., Haeberli, W., Huggel, C., Künzler, M. and Bründl, M. (2011): *Landslides and new lakes in deglaciating areas: a risk management framework* (Poster). The Second World Landslide Forum, Rome, 03 - 09 October 2011.

Schaub, Y., Haeberli, W., Huggel, C., Künzler, M. and Bründel, M. (2011): *New lakes in deglaciating Alpine areas: Addressing current and future risks from impulse waves due to rock/ice avalanches* (Poster). EGU General Assembly, Vienna, 04 - 08 April 2011.

Schaub, Y., Haeberli, W., Künzler, M. and Huggel, C. (2011): *NELAK- New Lakes in the Swiss Alps: Location, geometry, damming material, formation time, hazard potential and risks* (Poster). NFP61 - Progress Report Meeting 2011, Murten, 31 March - 01 April 2011.

Part VI

Appendix

APPENDIX A

RAID-MODEL: AGREEMENT PLOTS OF THE SENSITIVITY ANALYSIS

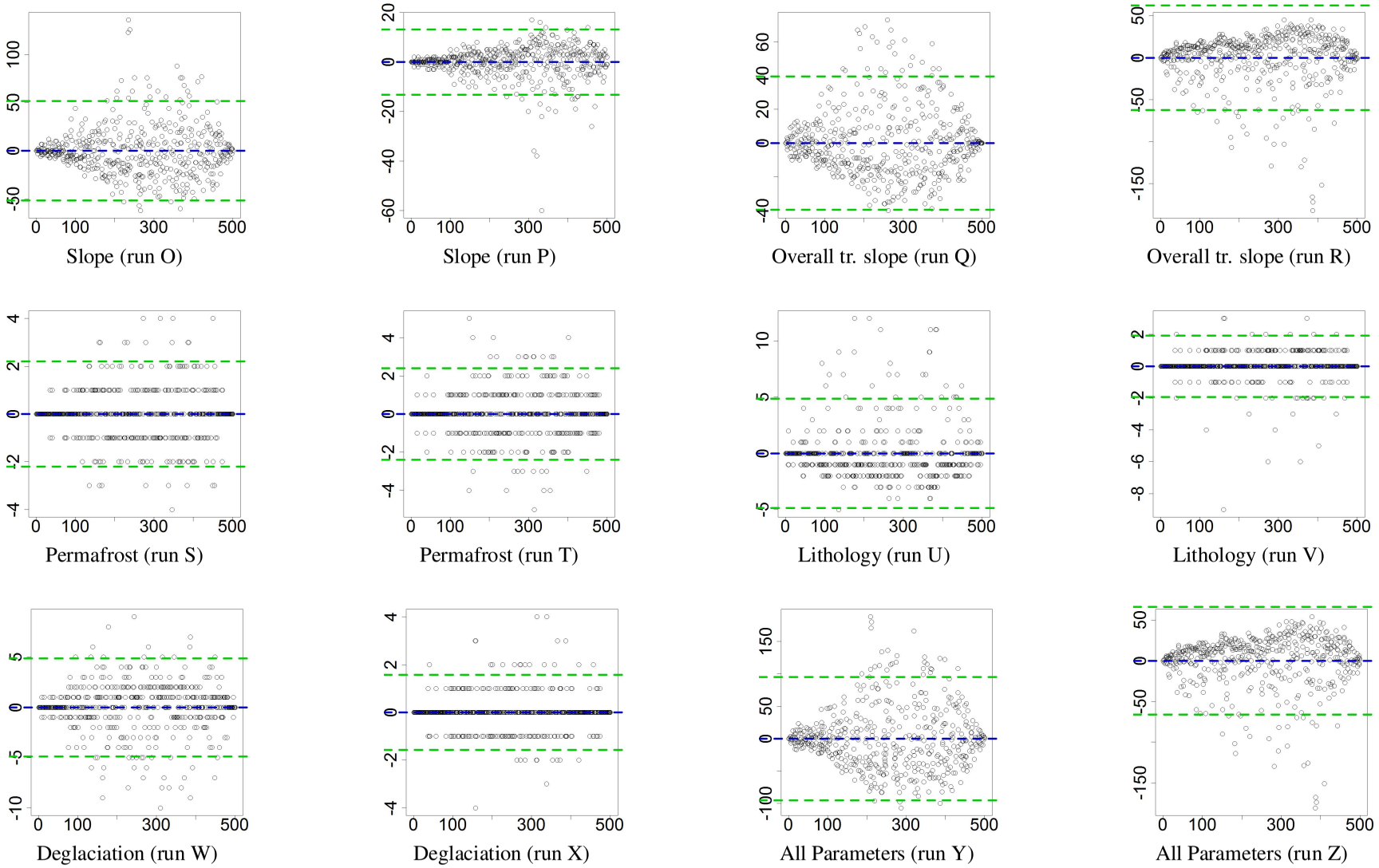

Figure A.1: Results of the sensitivity analysis of the ranking of the impact indexes. Agreement of rankings by (ii) the parameter uncertainty definition for present conditions with the default run Np. The x-axes represents the mean between the assessed and the default rank (each entry represents one lake). The y-axes indicates the deviation of the varied rank from the mean (zero) in number of ranks. Entries along the blue line did not feature any variation in the rank. The dashed green lines represent the standard deviation, which delineates the confidence-levels. These confidence levels (in number of ranks) were transferred into Table 8.3 and evaluated to define the sensitivity of the ranking against variation of the respective factor.

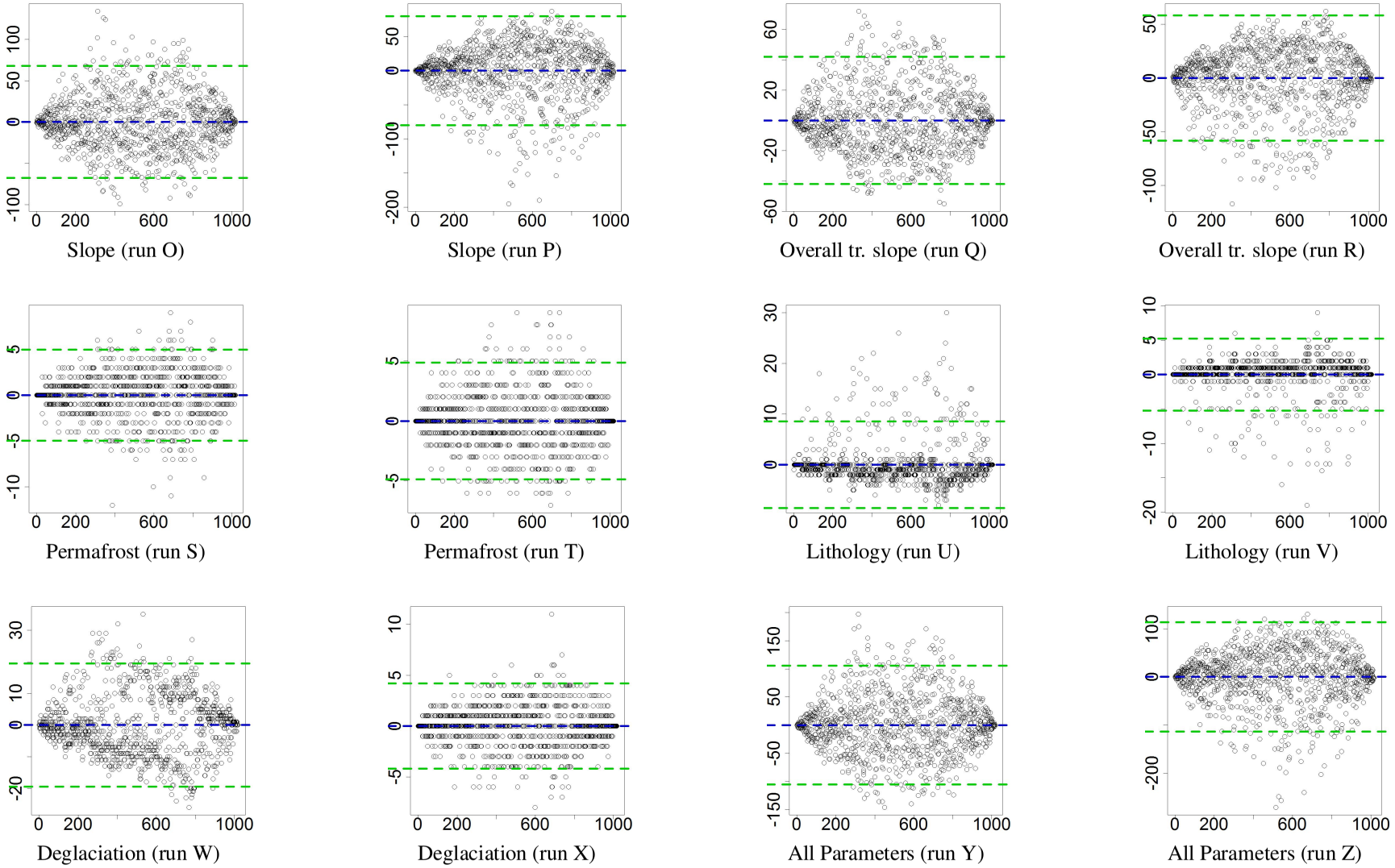

Figure A.2: Results of the sensitivity analysis of the ranking of the impact indexes. Agreement of rankings by (ii) the parameter uncertainty definition for future conditions with the default run Np. The x-axes represents the mean between the assessed and the default rank (each entry represents one lake). The y-axes indicates the deviation of the varied rank from the mean (zero) in number of ranks. Entries along the blue line did not feature any variation in the rank. The dashed green lines represent the standard deviation, which delineates the confidence-levels. These confidence levels (in number of ranks) were transferred into Table 8.3 and evaluated to define the sensitivity of the ranking against variation of the respective factor.

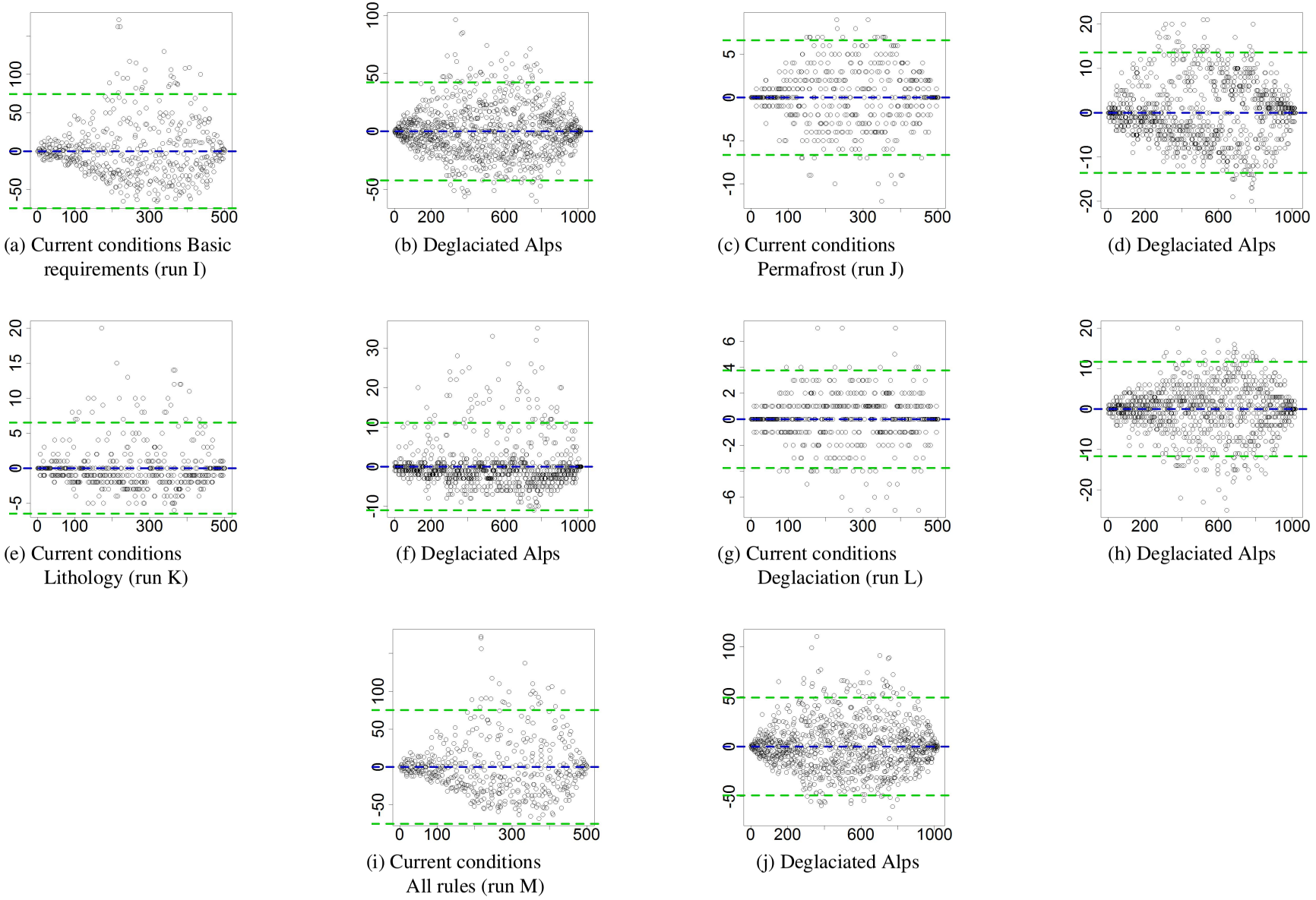

Figure A.3: Results of the sensitivity analysis of the ranking of the impact indexes. Agreement of rankings by (iii) the classification of disposition parameters into disposition elements for present and future conditions with the default run Np. The x-axes represents the mean between the assessed and the default rank (each entry represents one lake). The y-axes indicates the deviation of the varied rank from the mean (in number of ranks). Entries along the blue line did not feature any variation in the rank. The dashed green lines represent the standard deviation, which delineates the confidence-levels. These confidence levels (in number of ranks) were transferred into Table 8.3 and evaluated to define the sensitivity of the ranking against variation of the respective factor.

APPENDIX B

RAMMS AND IBER: SETTINGS OF THE SIMULATIONS

Simulation Parameters		Further parameters	
Grid resolution	8m	Release	Block release
Dumb step	5	Erosion law	Velocity square driven
Density	1000	Total momentum	5
Lambda	1		
Numerical scheme	second order		

Table B.1: Settings of RAMMS ice-avalanche simulations.

Simulation Parameters		Further parameters	
Grid resolution	8m	Release	Hydrograph
Dumb step	60	Erosion law	Velocity square driven
Density	1900	Total momentum	5
Lambda	1		
Numerical scheme	second order		

Table B.2: Settings of RAMMS outburst-flow simulations.

General Parameters		Hydrodynamics		Roughness	
Number of Threads	8	Inlet	Total Discharge	Land-use class	River
Numerical Scheme	First order	Inlet conditions	Critical/Subcr.	Manning-nr.	0.025
CFL	0.45	Outlet flow conditions	Supercr./Subcr.		
Wet-Dry-Limit	0.01m				
Numerical scheme	second order				

Table B.3: Settings of IBER impact wave simulations. The additional modules for turbulence, sediment transport, encroachments and breaching were disabled.

APPENDIX C

RAMMS AND IBER: RESULTS OF THE 54 IMPACT-WAVE SIMULATIONS

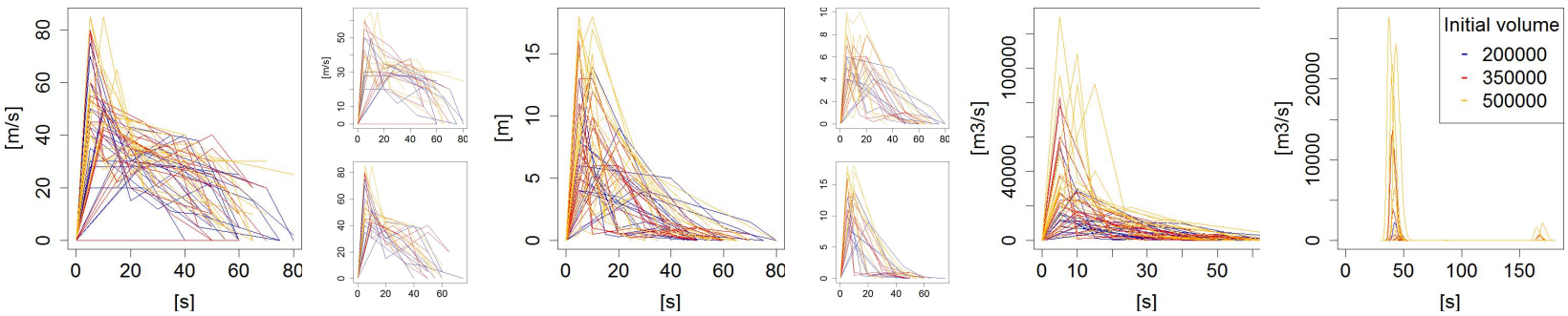

(a) Flow velocity (b) (c) Flow height (d) (e) Impact hydrograph (f) Overtopping hydrograph

Figure C.1: The (a-d) RAMMS avalanche-simulation results on the lake shoreline were converted into the (e) impacting hydrographs (the transformation methods are described in Section 12.1), which leaded to overtopping simulations by IBER (f). Influence of the initial volume on the model results: The x-axes represent the duration of the respective process. The small graphs illustrate the flow velocity (b) and the flow height (d) as a function of the transformation methods mean (upper plot) and max (lower plot).

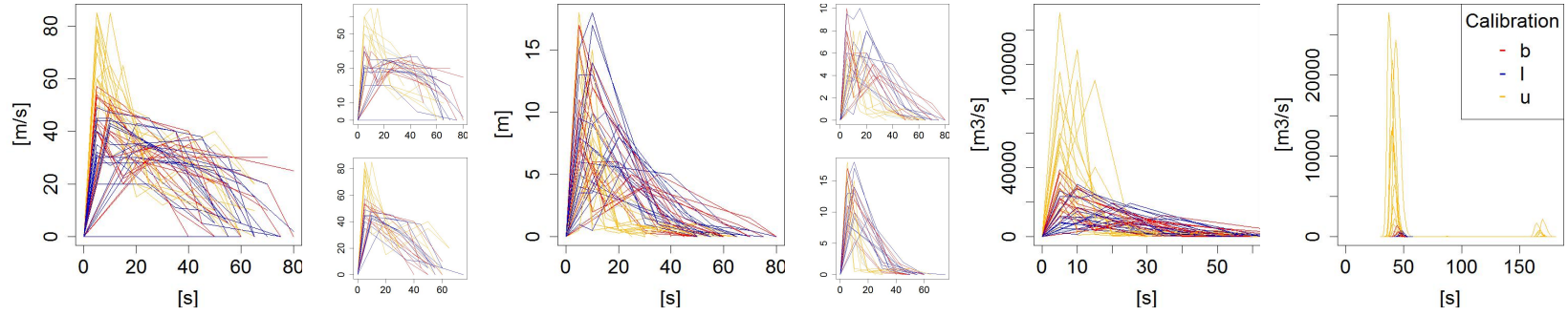

(a) Flow velocity (b) (c) Flow height (d) (e) Impact hydrograph (f) Overtopping hydrograph

Figure C.2: The (a-d) RAMMS avalanche-simulation results on the lake shoreline were converted into the (e) impacting hydrographs (the transformation methods are described in Section 12.1), which leaded to overtopping simulations by IBER (f). Influence of the calibration on the model results: The x-axes represent the duration of the respective process. The small graphs illustrate the flow velocity (b) and the flow height (d) as a function of the transformation methods mean (upper plot) and max (lower plot).

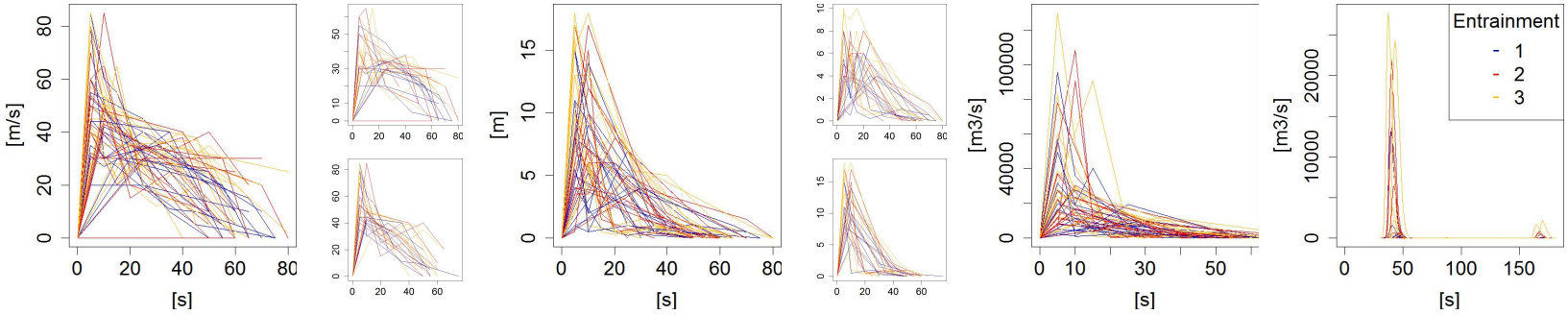

(a) Flow velocity (b) (c) Flow height (d) (e) Impact hydrograph (f) Overtopping hydrograph

Figure C.3: The (a-d) RAMMS avalanche-simulation results on the lake shoreline were converted into the (e) impacting hydrographs (the transformation methods are described in Section 12.1), which leaded to overtopping simulations by IBER (f). Influence of entrainment on the model results. The x-axes represent the duration of the respective process. The small graphs illustrate the flow velocity (b) and the flow height (d) as a function of the transformation methods mean (upper plot) and max (lower plot).

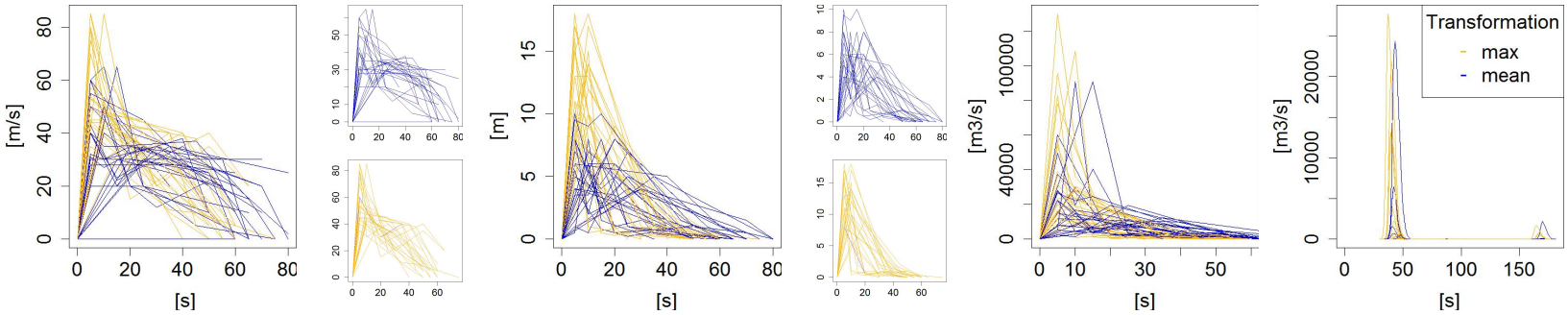

(a) Flow velocity (b) (c) Flow height (d) (e) Impact hydrograph (f) Overtopping hydrograph

Figure C.4: The (a-d) RAMMS avalanche-simulation results on the lake shoreline were converted into the (e) impacting hydrographs (the transformation methods are described in Section 12.1), which leaded to overtopping simulations by IBER (f). Influence of the transformation on the model results. The x-axes represent the duration of the respective process. The small graphs illustrate the flow velocity (b) and the flow height (d) as a function of the transformation methods mean (upper plot) and max (lower plot).

APPENDIX D

ANOVA OF THE 54 IMPACT-WAVE SIMULATIONS: RESULTS AND STATISTICAL EVALUATION

	Overtopping time					Overtopping volume				Maximum discharge				Mean discharge				Overtopping height			
	Nr.	min.	med.	max.	outl.	min.	med.	max.	outl.	min.	med.	max.	outl.	min.	med.	max.	outl.	min.	med.	max.	outl.
Initial volume																					
small		0	0	0	14	0	0	0	10,273	0	0	0	2,229	0	0	0	685	0	0	0	4
	4	*5*	*10*	*14*		*63*	*1,667*	*10,273*		*19*	*363*	*2,229*		*10*	*143*	*685*		*0.1*	*1.9*	*3.8*	
medium		0	4	17		0	0	3,425	76,748	0	0	656	34,257	0	0	285	1,903	0	0.3	6.8	
	9	*8*	*12*	*17*		*235*	*2,564*	*34,257*	*79,572*	*61*	*558*	*6,431*	*13,582*	*13*	*256*	*1,903*	*4,421*	*0.7*	*2.7*	*6.8*	
large		0	12	21		0	3,310	76,748	171,368	0	660	13,156	27,731	0	265	4,263	8,160	0	3.1	9.2	
	13	*9*	*14*	*21*		*554*	*9,626*	*171,368*		*146*	*1,563*	*27,731*		*55*	*566*	*8,160*		*1.1*	*3.9*	*8*	*9.2*
Calibration																					
lower		0	0	14		0	0	656		0	0	155	2,904	0	0	60	730	0	0	2.5	4.6
	5	*10*	*11*	*14*		*656*	*3,630*	*3,630*	*10,215*	*155*	*709*	*709*	*2,034*	*60*	*239*	*239*	*730*	*1.2*	*2.5*	*4.6*	
best-fit		0	0	14		0	0	2,329	2,989	0	0	611	1,377	0	0	271	467	0	0	3.6	
	7	*8*	*10*	*14*		*235*	*2,990*	*2,990*	*7,007*	*62*	*611*	*611*	*1,377*	*13*	*232*	*467*		*0.7*	*2.7*	*3.6*	
upper		0	14	21		0	9,950	171,369		0	1,897	27,732		0	626	8,160		0	3.9	9.2	
	14	*5*	*15*	*21*		*63*	*26,829*	*171,368*		*19*	*5,112*	*27,731*		*10*	*1,636*	*8,160*		*0.2*	*4.5*	*9.2*	
Entrainment																					
no		0	0	17		0	0	2,323	76,748	0	0	516	13,156	0	0	154	4,263	0	0	3.9	5.3
	6	*9*	*14*	*17*		*354*	*2,671*	*9,626*	*76,748*	*146*	*469*	*1,564*	*13,156*	*55*	*153*	*566*	*4,263*	*1.1*	*2.5*	*5.3*	
little		0	0	20		0	0	3,630	131,549	0	0	708	21,842	0	0	285	6,264	0	0	66.8	8.1
	8	*5*	*12*	*20*		*63*	*3,528*	*131,549*		*19*	*682*	*21,842*		*10*	*279*	*6,264*		*0.2*	*3.1*	*8.1*	
double		0	1	21		0	2,350	17,800	171,369	0	508	3,792	27,731	0	205	1,369	8,160	0	2.6	9.2	
	12	*9*	*13*	*21*		*849*	*8,611*	*34,256*	*171,369*	*137*	*1,706*	*6,431*	*27,731*	*55*	*576*	*1,903*	*8,160*	*1.1*	*3.7*	*9.2*	
Transformation																					
max		0	10	20		0	1,820	17,800	171,369	0	421	3,792	27,732	0	0	1,369	8,160	0	2.2	8.9	
	19	*5*	*13*	*20*		*63*	*2,990*	*17,801*	*171,369*	*19*	*384*	*3,792*	*27,732*	*10*	*259*	*1,369*	*8,160*	*0.1*	*3*	*8.9*	
mean		0	0	11	21	0	0	549	171,369	0	137	137	24,351	0	0	55	7,743	0	0	1	9.2
	7	*9*	*15*	*21*		*550*	*9,626*	*34,732*	*170,398*	*137*	*1,564*	*6,447*	*24,351*	*137*	*1,564*	*6,447*	*24,351*	*1.1*	*3.9*	*6.3*	*9.2*

Table D.1: Descriptive statistics on the ANOVA-results per dependent variable. Minimum, medium, maximum values and outliers. "Nr." refers to the number of overtopping waves caused, the corresponding rows are marked in italic. For abbreviations see Table 12.1.

	Overtopping time			Overtopping volume			Maximum discharge			Mean discharge			Overtopping height		
	%	Importance		%	Importance		%	Importance		%	Importance		%	Importance	
Main Effects															
Initial volume	24.6	1.4E-06	***	14.4	7.9E-05	***	14.6	2.7E-05	***	15.0	2.0E-05	***	22.3	4.9E-08	***
medium - small		0.009	***		0.558			0.426			0.369			0.005	**
large - small		1.0E-05	***		9.7E-05	***		3.1E-05	***		2.1E-05	***		0	***
large - medium		0.004	***		0.002	**		9.3E-04	***		8.7E-04	***		2.3E-04	***
Calibration	27.2	3.9E-07	***	24.3	1.3E-06	***	26.0	2.1E-07	***	26.8	1.4E-07	***	29.2	3.2E-09	***
lower - best-fit		0.758			1.0			0.999			0.999			0.911	
upper - best-fit		7.3E-06	***		8.0E-06	***		1.5E-06	***		1.0E-06	***		1.0E-07	***
upper - lower		1.1E-07	***		8.0E-06	***		1.5E-06	***		1.0E-06	***		0	***
Entrainment	7.4	0.003	**	4	0.037	*	4.0	0.023	*	4.1	0.020	*	10.1	4.4E-05	***
little - no		0.709			0.393			0.297			0.296			0.199	
double - no		0.004	**		0.028	*		0.02	*		0.02	*		3.4E-05	***
double - little		0.025	*		0.352			0.345			0.318			0.004	**
Transformation	13.7	1.9E-05	***	1.7	0.087		2.3	0.034	*	2.3	0.035	*	7.8	4.9E-05	***
Interactions	13.7			40.9			40.2			39.1			21		
Vol:Er	0.5	0.912		4.9	0.082		4	0.104		4	0.099		1.2	0.489	
Vol:Cal	6.5	0.029	*	25.1	9.6E-06	***	24.6	3.6E-06	***	24.4	3.3E-06	***	12.1	9.4E-05	***
Vol:Trans	2.2	0.139		1.1	0.357		1.6	0.204		1.3	0.266		1.8	0.088	
Er:Trans	0.01	0.991		1	0.413		0.8	0.449		0.7	0.471		0.3	0.646	
Cal:Er	2.1	4.2E-01		6.6	0.032	*	6.3	0.022	*	6.1	0.024	*	5.1	0.015	*
Cal:Trans	2.4	1.2E-01		2.2	0.141		2.9	0.058		2.6	0.078		0.5	0.502	
Residuals	14.5			14.9			13.0			12.8			9.6		

*Table D.2: Variances in the dependent variables in all model runs caused by the main effects of the independent factors or the interactions between them. The percentages refer to the sum of the square, indicating the absolute variance introduced by the factor/interaction. The importance of the differences between the factors/interactions' means was calculated with the Wilcoxon test. The importance of the differences between the independent factors' groups means were calculated according to the TukeyHSD test. These importances were classified in "strong" (p<0.001; ***), "considerable" (p<0.01; **) and "noticeable" (p<0.05; *). For abbreviations see Table 12.1.*

	Overtopping time			Overtopping volume			Maximum discharge			Mean discharge			Overtopping height		
	%	Importance		%	Importance		%	Importance		%	Importance		%	Importance	
Main Effects															
Initial volume	20.6	0.032	*	13.0	0.069		12.7	0.051		12.9	0.046		16.2	0.074	
medium - small		0.159			0.707			0.588			0.584			0.314	
large - small		0.032	*		0.099			0.069			0.078			0.075	
large - medium		0.115			0.111			0.087			0.104			0.212	
Calibration	32.5	0.017	*	33.0	0.020	*	35.0	0.013	*	35.9	0.015	*	31.1	0.031	*
lower - best-fit		0.987			0.687			0.638			0.674			0.940	
upper - best-fit		0.026	*		0.041	*		0.025	*		0.029	*		0.052	
upper - lower		0.033	*		0.031	*		0.020	*		0.023	*		0.054	
Entrainment	8.3	0.102		10.1	0.095		9.8	0.070		9.9	0.082		18.9	0.060	
little - no		0.717			0.425			0.321			0.365			0.508	
double - no		0.291			0.104			0.075			0.089			0.073	
double - little		0.111			0.341			0.308			0.331			0.173	
Transformation	2.2	0.193		6.7	0.071		8.4	0.038	*	7.8	0.050	*	3.3	0.120	
Interactions	34.1			34.7			32.0			30.7			24.9		
Vol:Er	13.0	0.095		3.6	0.406		3	0.375		3.1	0.404		3.3	0.514	
Vol:Cal	6.4	0.214		12.9	0.114		12.1	0.087		12.0	0.105		7.3	0.276	
Vol:Trans	2.9	0.294		1.5	0.507		1.8	0.378		1.2	0.526		1.4	0.595	
Er:Trans	5.3	0.167		11.2	0.084		10.0	0.068		10.2	0.079		5.7	0.225	
Cal:Er	4.8	0.370		5.5	0.377		5.1	0.313		4.2	0.384		6.1	0.425	
Cal:Trans	1.7	0.239		0.0	0.870		0.0	0.913		0.0	0.867		1.1	0.405	
Residuals	2.3			2.7			2.0			2.3			3.4		

*Table D.3: Variances in the dependent variables in the overtopping model runs caused by the main effects of the independent factors or the interactions between them. The percentages refer to the sum of the square, indicating the absolute variance introduced by the factor/interaction. The importance of the differences between the factors/interactions' means was calculated with the Wilcoxon test. The importance of the differences between the independent factors' groups means were calculated according to the TukeyHSD test. These importances were classified in "strong" ($p<0.001$; ***), "considerable" ($p<0.01$; **) and "noticeable" ($p<0.05$; *). For abbreviations see Table 12.1.*

APPENDIX E

ANOVA OF THE 54 IMPACT-WAVE SIMULATIONS: INTERACTION PLOTS

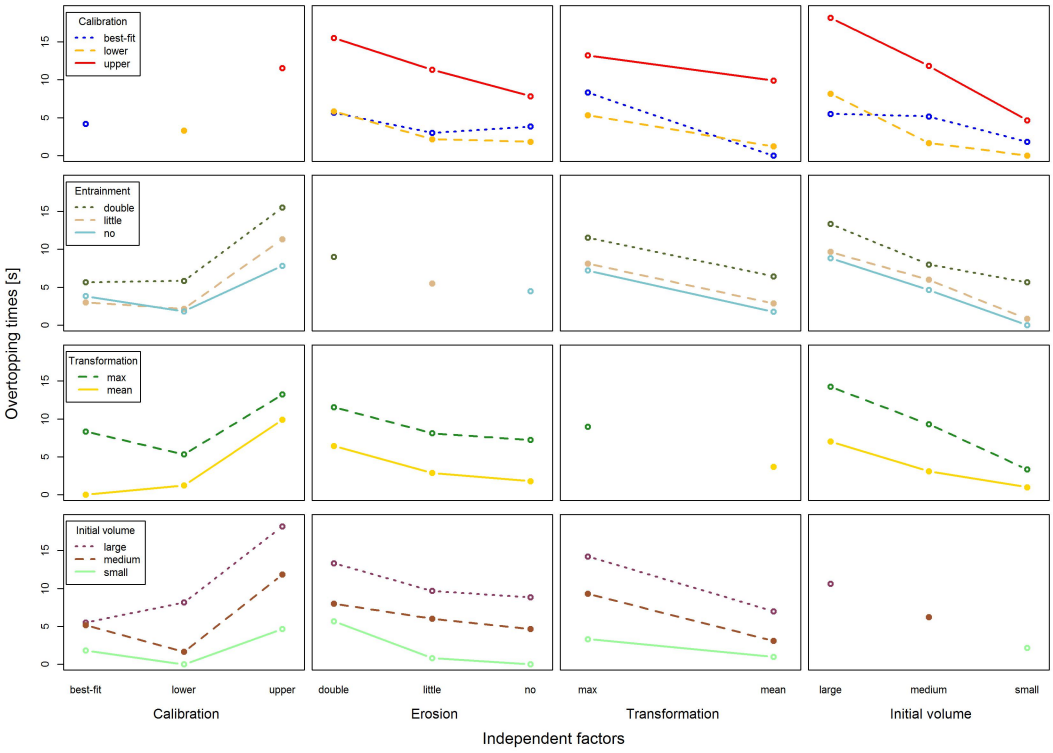

Figure E.1: Interactions amongst the independent factors' groups for the overtopping times in all runs. For abbreviations see Table 12.1.

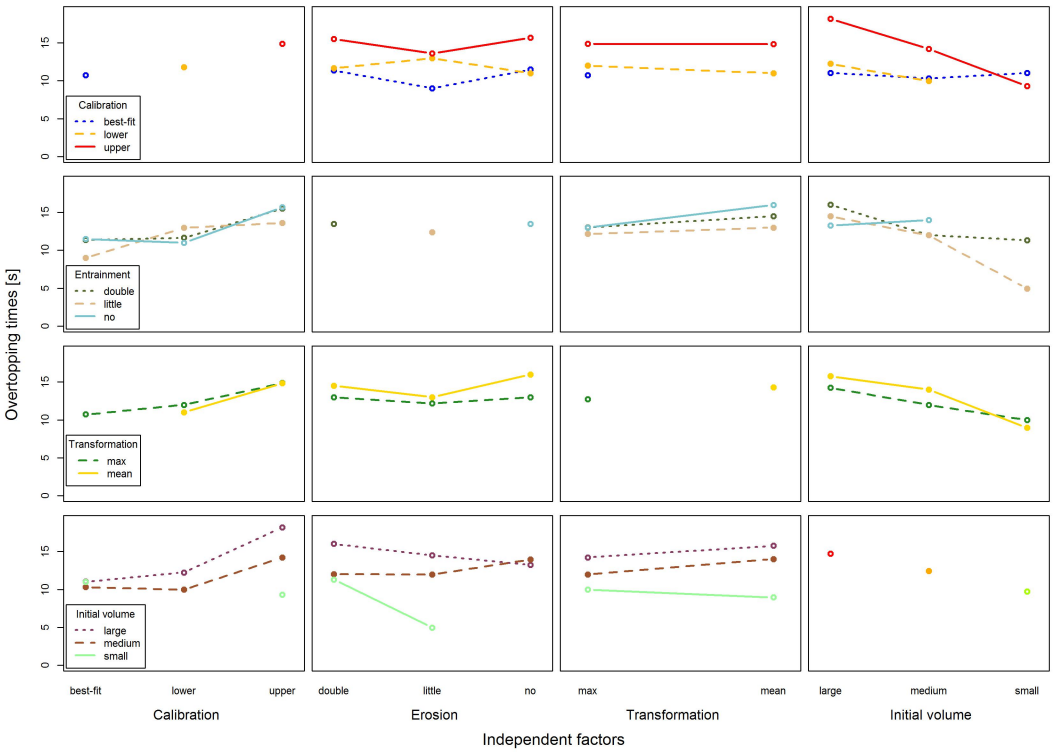

Figure E.2: Interactions amongst the independent factors' groups for the overtopping times in the overtopping runs. For abbreviations see Table 12.1.

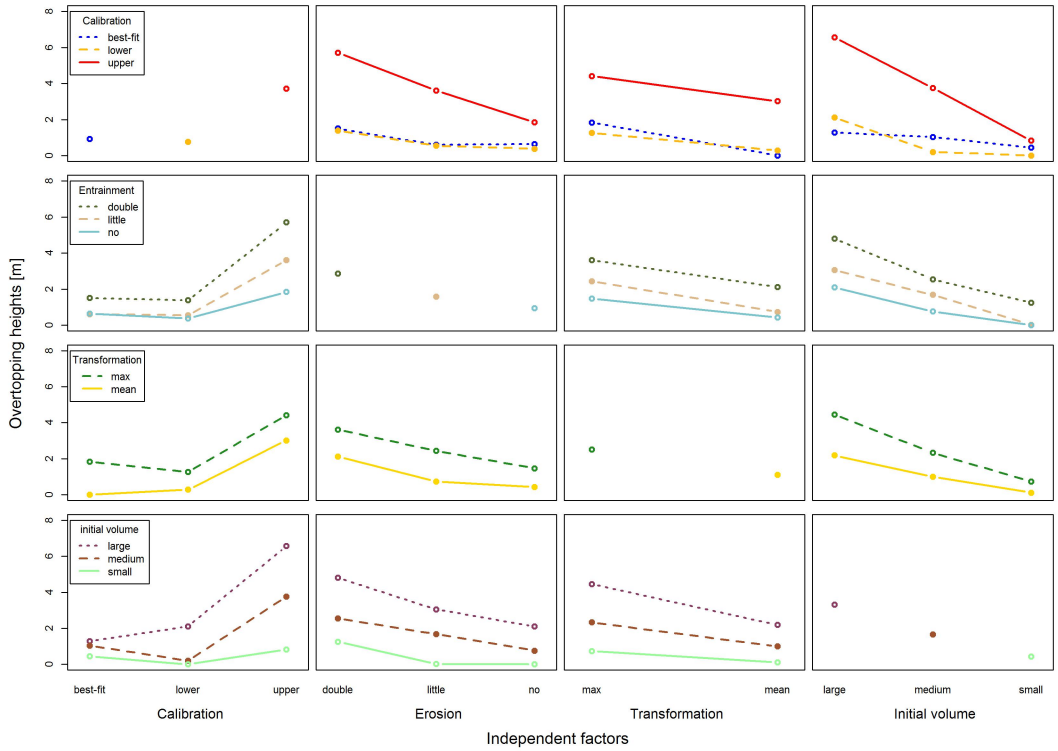

Figure E.3: Interactions amongst the independent factors' groups for the overtopping heights in all runs. For abbreviations see Table 12.1.

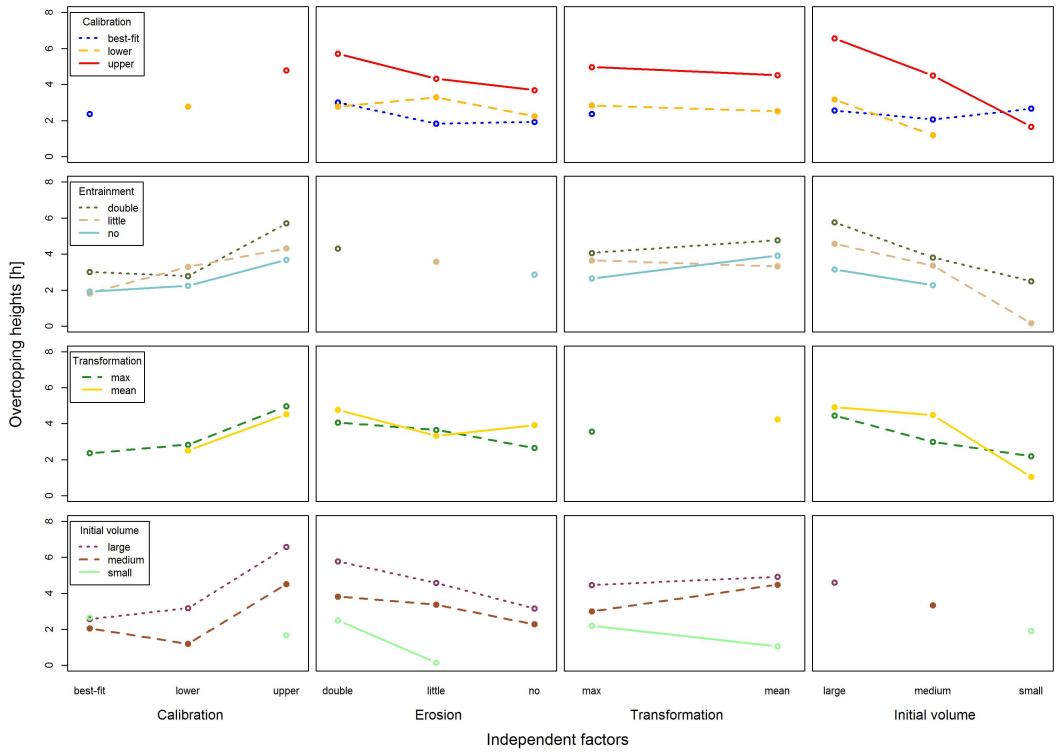

Figure E.4: Interactions amongst the independent factors' groups for the overtopping heights in the overtopping runs. For abbreviations see Table 12.1.

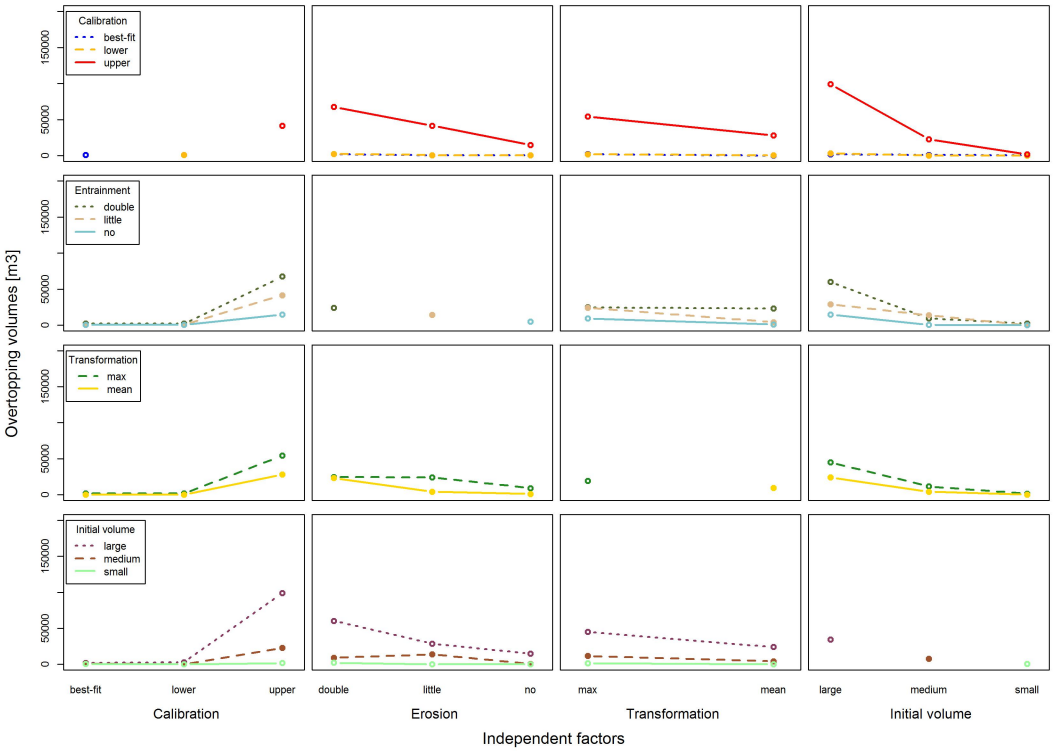

Figure E.5: Interactions amongst the independent factors' groups for the overtopping volumes in all runs. For abbreviations see Table 12.1.

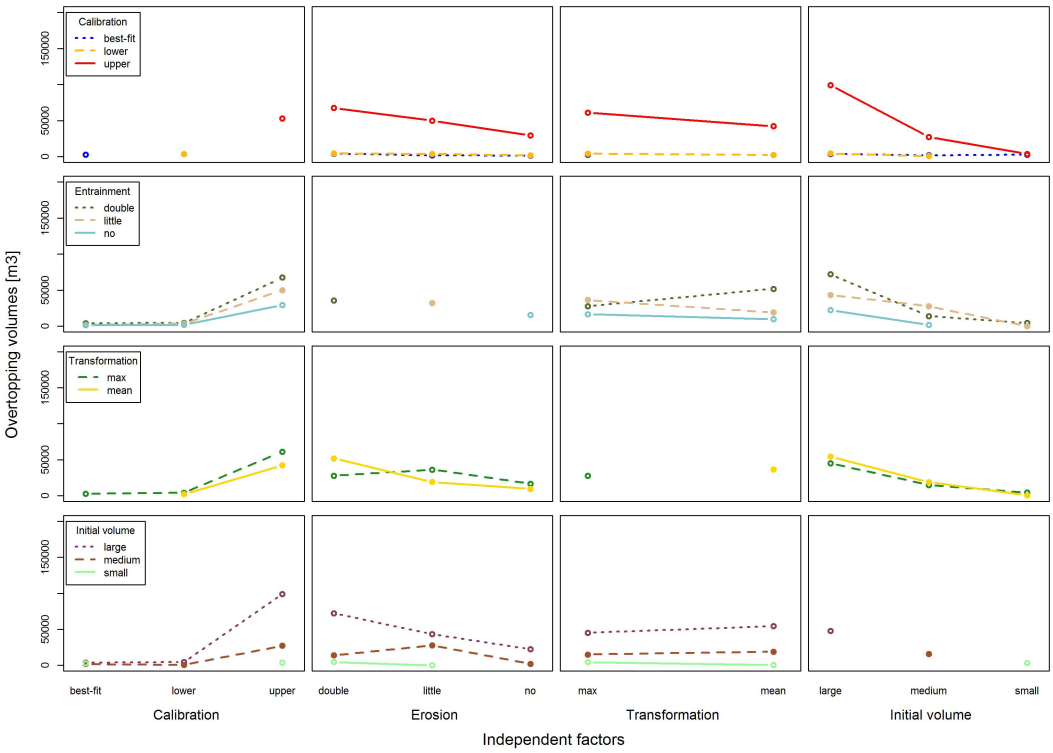

Figure E.6: Interactions amongst the independent factors' groups for the overtopping volumes in the overtopping runs. For abbreviations see Table 12.1.

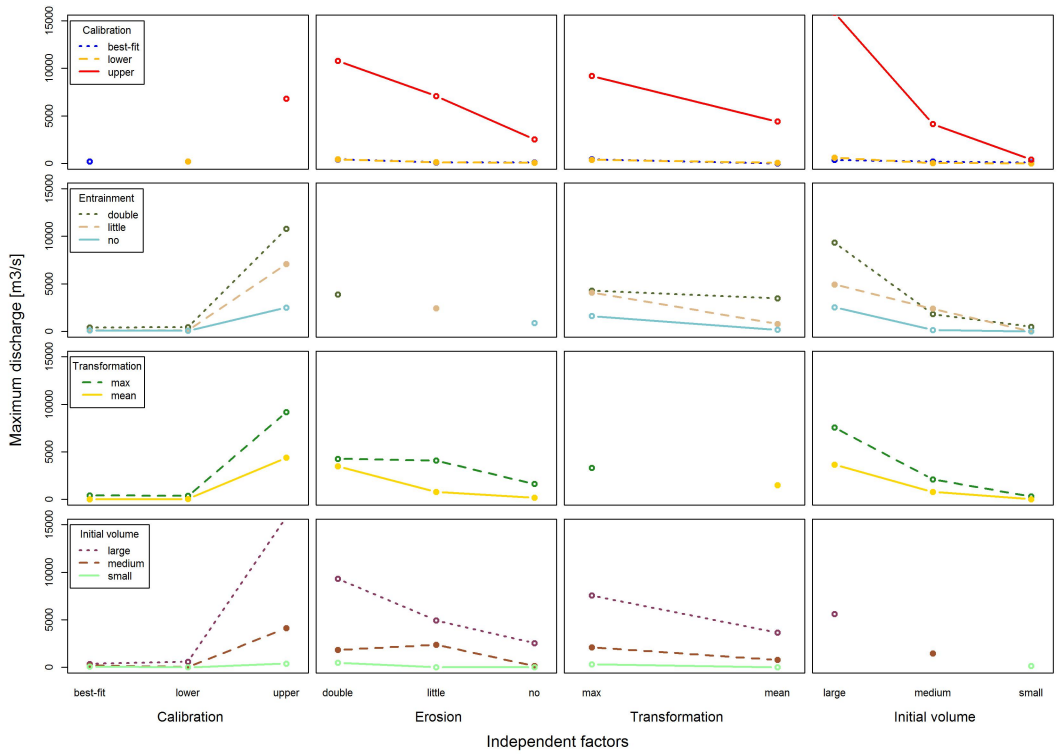

Figure E.7: Interactions amongst the independent factors' groups for the maximum discharge in all runs. For abbreviations see Table 12.1.

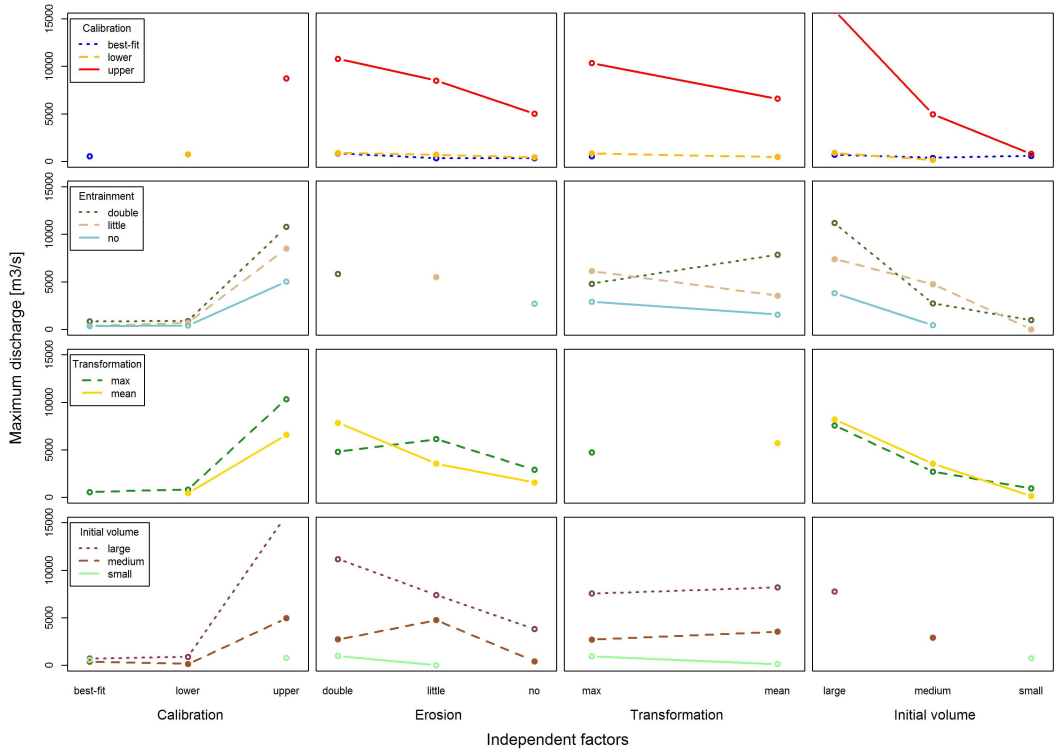

Figure E.8: Interactions amongst the independent factors' groups for the maximum discharge in the overtopping runs. For abbreviations see Table 12.1.

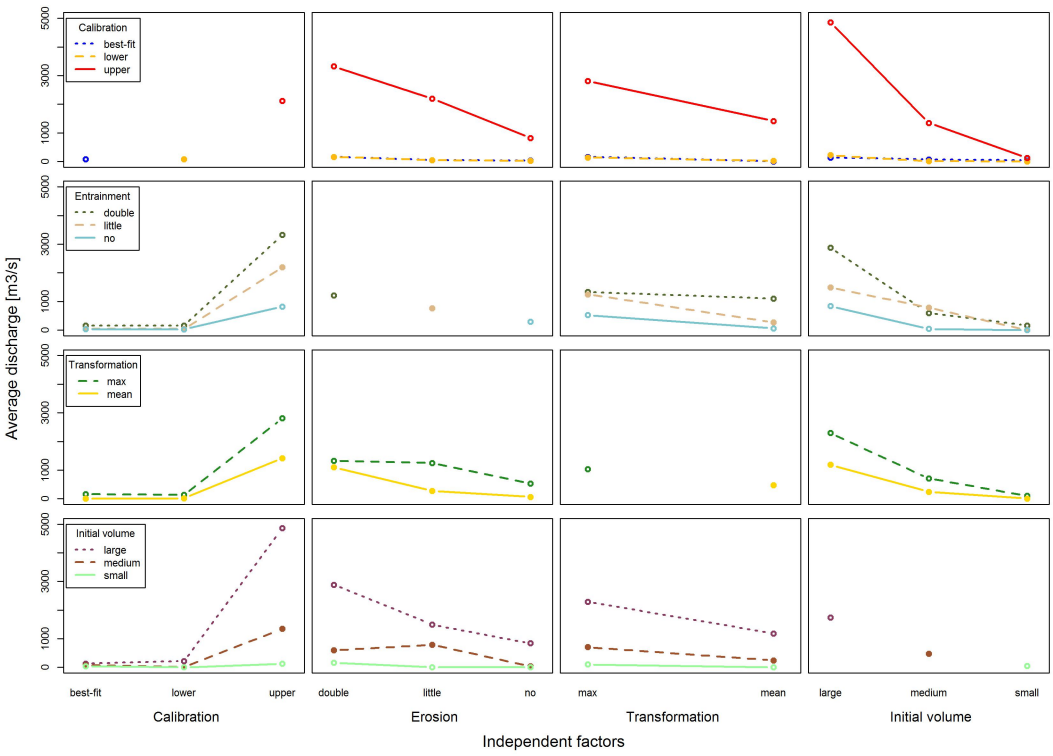

Figure E.9: Interactions amongst the independent factors' groups for the average discharge in all runs. For abbreviations see Table 12.1.

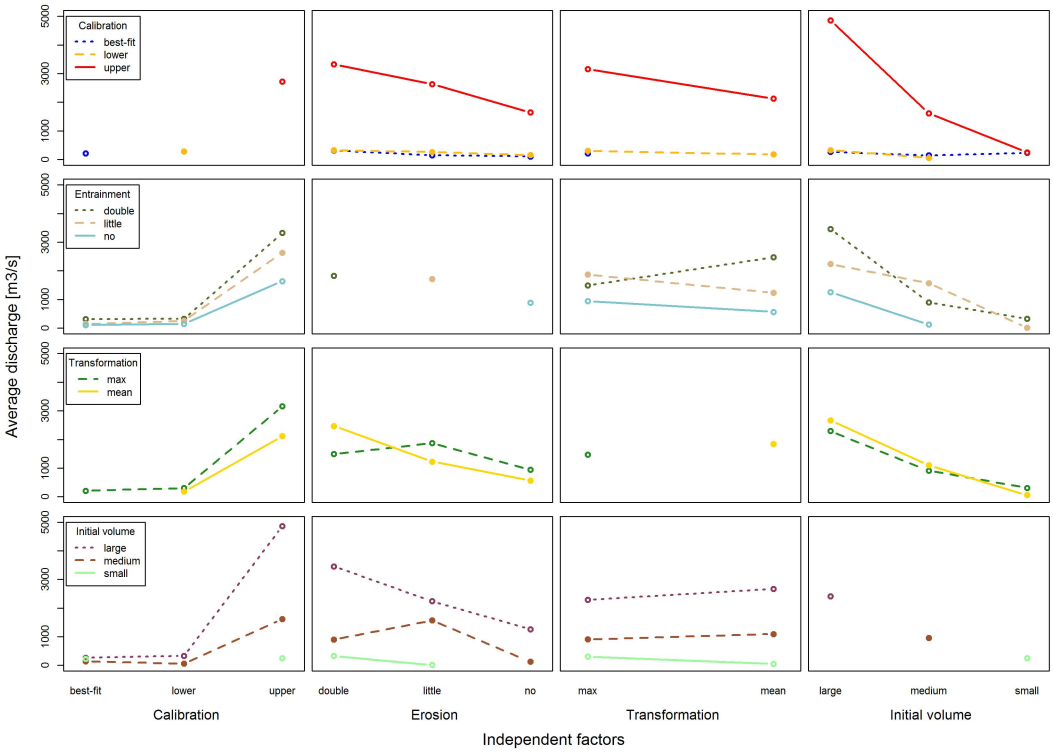

Figure E.10: Interactions amongst the independent factors' groups for the average discharge in the overtopping runs. For abbreviations see Table 12.1.